deposition it is thought that they formed by similar processes, e.g. the mass wasting of steep slopes ultimately generated by tectonic movement. Table 5.6 lists the differences between the two breccias. It is suggested that the limestone breccia is better sorted and far more laterally continuous because it represents more distal talus deposition within a subaqueous environment permitting transport of finer material over larger distances.

Table 5.6 The differences between the limestone breccia at Kesme and the mega-breccia at Kapikaya.

Limestone breccia	**Mega-breccia**
monomict	polymict
moderately sorted	poorly sorted
white matrix	no matrix
subaqueous environment of deposition	subaerial environment of deposition

5.4.2.6 Interpretation of sub-facies association B

A summary of the description and interpretation of the sub-facies discussed above is given in table 5.7. The sub-facies in group B have all been interpreted as having been deposited in subaqueous lacustrine or lagoonal environments, but in close association with sub-facies interpreted as alluvial deposits. This suggests that lakes and lagoons were at least episodically present during both Lower (Kizildag Formation) and Upper Miocene (Aksu Formation) accumulation of conglomerate-rich successions. In general these facies represent low-energy environments with variable salinities and oxygen contents. The fauna, where present is specific to this sort of environment although there is evidence of periodic marine influence in some of the localities and general close proximity to marine facies (Figs. 5.11 and 5.13,). Figure 5.18 is a generalised model of how these facies may have accumulated between pulses of coarse clastic sedimentation and an ever encroaching sea.

Table 5.7 Summary of the features of sub-facies association B.

Name	Lower boundary	Upper boundary	Lateral variation	Thickness	Sorting/ composition	Structures	Matrix	Interpretation
Organic-rich horizons	planar	planar/eroded into by overlying sediments	continuous >0.5km (Bozburun Dag) 10-15m (Yaylaalan)	0.6-1m	poorly sorted fragments, also contains gastropods and terrigenous material			immature coal
Green clays	non-erosive	planar/eroded into by overlying sediments	not laterally persistent over 100's meters	0.05-3m	Potamid gastropods, Orbulina	structureless		lagoonal clay
Laminated limestone and lime mud	unconformity (Kepezbelenli), flat (Yaylaalan)	eroded into by overlying conglomerates (Kepezbelenli), flat (Yaylaalan)	laterally persistent <300m	2-5m	charophytes, algae, plant stems (Kepezbelenli)	burrowing, folded (Yaylaalan)		lacustrine limestone
Gastropod siltstones	not observed	gradational	<0.5km	5-10cm	moderately sorted, Viviparus-like gastropods, mammal bones		silt	lacustrine silts
Limestone breccia	unconformable	planar	laterally persistent	0.3-1.5m	entirely Mesozoic limestone clasts	angular, clast-supported fabric	white carbonate silt	slope talus deposited in a lake

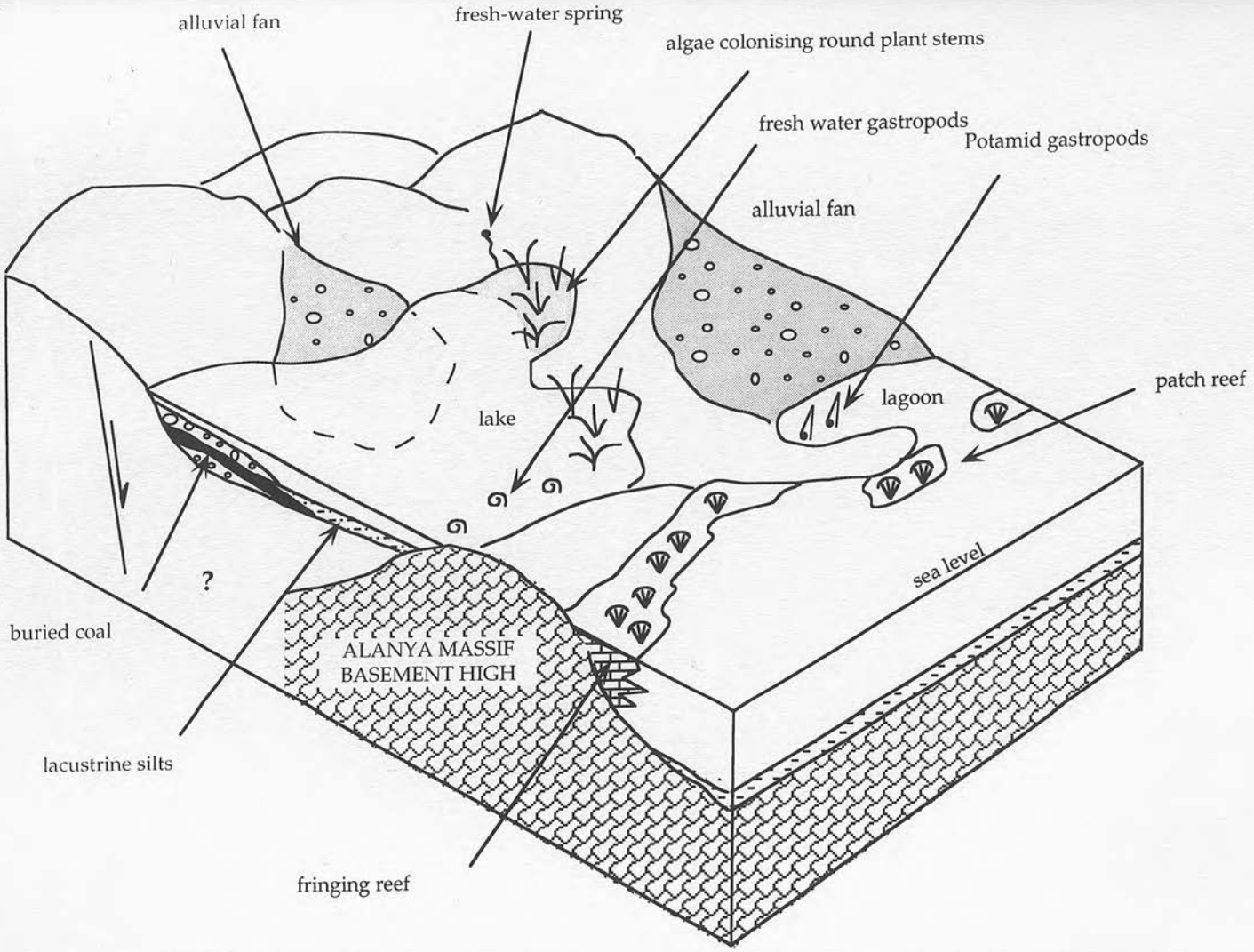

Figure 5.18 Generalised model of the depostional environments and processes active in the formation of the lagoonal and lacustrine sediments observed in the study area. No precise scale or orientation is intended.

5.5.3 Sub-facies association C

A list of the sub-facies discussed in this section, their localities with reference to figure 5.1 and the formations in which they are found is given in table 5.8.

Table 5.8 List of the sub-facies in sub-facies association C, their localities and formations.

Sub-facies	Localities	Formation
Echinoid-scaphopod facies	Yesilbag Aspendos Deniztepesi	Tepekli
Porites bafflestones	S. Kargi Alarahan Kesme	Tepekli
High-angle cross-bedded conglomerates	S. Kargi Alarahan Bozburun Kargi baraj	Tepekli

5.5.3.1 Echinoid-scaphopod facies

Description

This facies has been described in detail in chapter 3 section 3.6.3.1 from the view of its large biogenic carbonate component. It is discussed again here because of its implications for the interaction between terrigenous detritus, the formation of biogenic carbonate, fresh water input and marine generated wave action. To save repetition only a brief review is given here.

This facies occurs either just below reef limestone and just above continental red beds as at Aspendos (Figs. 5.1 and 5.6), or in lateral continuity with a framework reef structure as seen at Yesilbag and South Kargi. It consists of coarse micro-conglomerate with abundant whole and fragmented scaphopods, echinoids, large benthic foraminifera and algal rhodoliths up to 5cm in diameter. These rhodoliths encrust rounded pebbles, most commonly veined grey Mesozoic limestone (Fig. 3.17).

They are irregular in shape and individual layers do not encircle the clast, but can be traced out to their terminations, which are abrupt and often ragged. Although algal encrustation is visible on many of the micro-conglomerate clasts, the largest rhodoliths are developed on clasts significantly larger than average.

Random orientation of scaphopods is the norm in this facies, but millimetre scale, graded laminations with scaphopods parallel to these are occasionally seen (Fig. 3.18). The scaphopod most commonly found here is *Dentalium* (Upper Cretaceous-Recent) with its prominent longitudinal ribs. Most of the specimens found were fragments.

Interpretation

This facies is vitally important in terms of interpreting these shoreface facies because it is the closest facies to a true beach. The environment envisaged is a very shallow water one (probably only a few meters deep) indicated by the intimate association with reef framestones (e.g. at Yesilbag), and an environment of high-energy (Orzag-Sperber *et al.* 1977), where constant movement, probably wave action, shift and roll over the sands allowing the formation of rhodoliths. Deposition of coarse material is by periodic fluvial input rather than a constant rain of sediment and this may have generated laminations. Algal rhodoliths encrust the free surfaces of clasts protruding from sediment, colonising other surfaces when currents reorientated the pebbles.

5.5.3.2 Porites bafflestones

Description

The best examples of this facies occur at South Kargi, Kesme and Yesilbag (Fig. 5.1) and have already been described in chapter 3 (section 3.6.1.2). They are discussed again here in the light of the interactive nature of their deposition between fluvially sourced terrigenous detritus and marine influences on the biogenic building of the bafflestone itself. Again, to avoid repetition only a brief summary of the description is given here.

These rocks are interbedded with coral framestones, coarse conglomerates with high angle cross-sets and minor amounts of unstructured clastics including fine-grained siltstones and sandstones with caliche development. At South Kargi for instance, five separate reef horizons are interbedded with coarse alluvial clastics (Fig. 5.19). As shown by Fig. 5.20 they do not persist laterally over 100m. Vertical coral sticks of *Porites sp.* can be seen to have produced a well spaced framework in which terrigenous sediment is deposited. Planar changes in grainsize of the terrigenous components can be seen (e.g. bedding planes), but there is no apparent effect on the coral sticks, which pass through these boundaries uninterrupted.

Interpretation

In the geological record it is not possible to specify which of the many non-preserved environmental controls may have influenced the monospecific colonisation of *Porites*. However, it has been observed that *Porites* is a coral which is able to thrive in conditions of low salinity, low temperature and reduced water circulation (Marshall and Orr 1931, Manton 1935, Wells 1954 and Scoffin and Stoddart 1978). It is also associated with higher sediment flux than most other corals in the Miocene (e.g. Martin *et al.*, 1989). The presence of these bafflestones at the boundary between continental and marine sediments bears out the hypothesis that these may have been fluvially influenced. The nature of the sedimentary beds through which the coral sticks pass uninterrupted indicates that these boundaries were formed while the coral heads protrude from them. This has three important implications:

- Sea level was higher than sedimentary boundaries at the time of bed deposition suggesting that accommodation space remained (Fig. 5.21).
- The ongoing input of terrigenous material and the continued uninterrupted growth of coral sticks suggests that relative sea level was rising at the time of deposition (section 3.8.1 for discussion of rate of relative sea level rise deduced from this).
- The coral framework may well have behaved firstly as a sediment trap and later as a barrier to further fluvially generated sediment basinward of the reef. Evidence for this can be seen at South Kargi where basinward of the Porites bafflestones (as determined from the palaeocurrents) Tarbellastrea framestones, which are essentially sediment free and finer-grained echinoid-scaphopod facies are deposited (Fig. 5.20).

Figure 5.19 Photomontage showing the five reef-horizons at South Kargi, central Aksu basin (Fig. 5.1), interbedded with coarse red alluvial clastics.

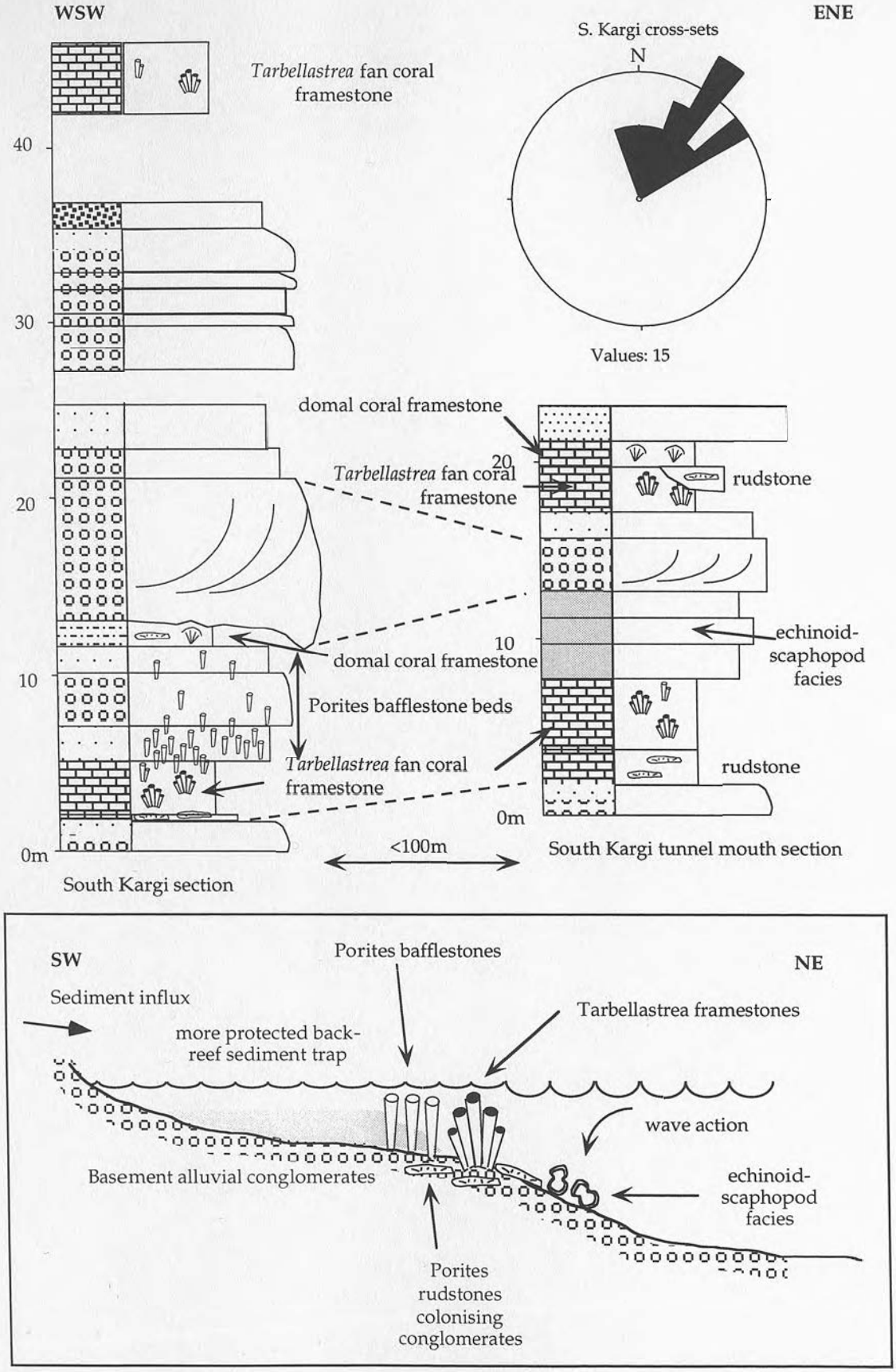

Figure 5.20 Correlation of the logged sections at South Kargi, central Aksu basin, and a model showing the sub-facies relationships deduced from these logs and palaeocurrent data, with reference to basinal and alluvial processes. (Key to symbols can be found on Fig. 3.7.)

Corals colonise and grow up to sea level

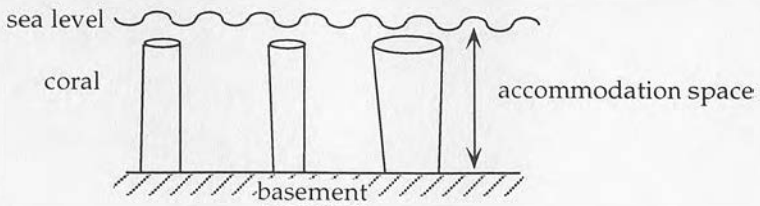

Sand input into reef, but insufficient to drown corals

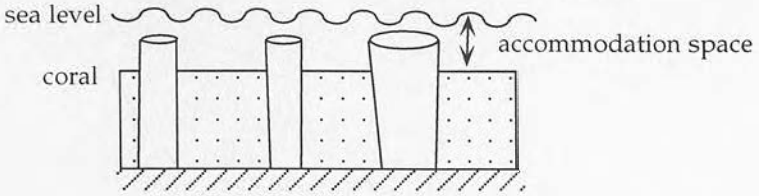

Sea level rise allows corals to grow vertically using sand to support them

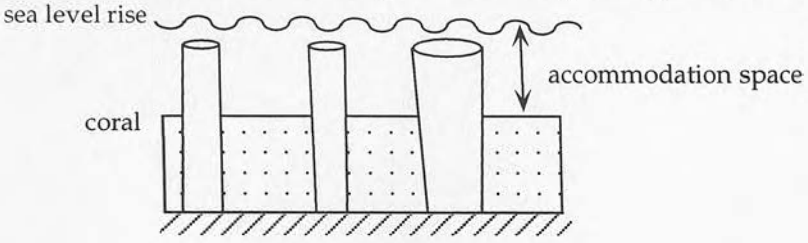

Conglomerate input into reef, but insufficient to drown coral

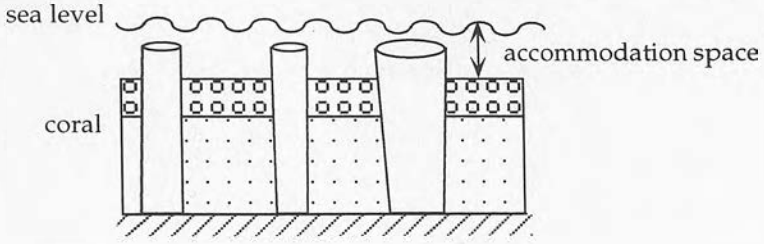

Sand input fills accommodation space and drowns coral

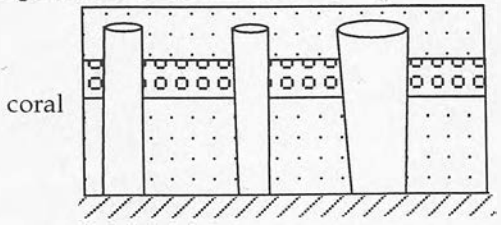

Figure 5.21 Cartoon of rising sea level versus sediment input in Porites baffestone environments.

5.5.3.3 High angle, cross-bedded conglomerates

Description

High-angle (~25°) cross-bedded conglomerates are preserved at Alarahan and South Kargi (Fig. 5.20) and are interbedded with reef framestones. At Bozburun Dag they are interbedded with the lagoonal clays and organic-rich horizons (Fig. 5.10) and the angle of repose of the cross-sets is distinctly lower than it is at the other two localities (Fig. 5.22). Periodic interbedded red, caliche-rich, fine sandstones can also be seen in close vertical proximity to these conglomerates at South Kargi.

Lateral thickness variations are common in this sub-facies. Figure 5.20 shows two logged sections taken from the South Kargi locality which are spaced approximately 100m apart, but which document the same stratigraphic level. The difference in thickness between the cross-bedded units of each section at comparable levels is apparent. A similar feature can be seen on the two walls of the river gorge at Alarahan, separated by approximately 50m.

These conglomerates are coarse-grained and clast-supported. Their thickness ranges from up to 2-10m and they are often associated with erosive channel scours. A few are also imbricated with well-rounded recrystallised carbonate clasts dominating over angular cherts. In general these conglomerates are well sorted although a clear bimodal size distribution exists between the clasts and the micro-conglomerate-grade matrix which has a similar composition. Occasionally biogenic material is found within the conglomerates. These are most commonly coral clasts, but they can include oysters, gastropods, and bivalves of various types.

Interpretation

The association of these conglomerates with both fully marine reef framestones and red beds containing caliche, as can be seen at South Kargi (Figs. 5.19 and 5.20) suggests that these high-angle cross-bedded conglomerates formed at the boundary between continental and marine environments. There are two possible modes of deposition for these conglomerates, Gilbert-type delta foresets and channel mouth bars.

Figure 5.22 Photograph of high-angle cross-bedded conglomerates at the Bozburun Dag pass, north west Kopru basin.

According to Nemec (1990a) these two depositional environments can be distinguished using the criteria displayed in table 5.9.

Table 5.9 Distinguishing features of Gilbert-type delta foresets and channel mouth bars (Nemec, 1990a).

Gilbert-type delta foresets	Channel mouth bars
Very thick stratification, generally up to 100s m	Much thinner stratification
Foresets consist of alternating high and low density turbidites and debris flows (10-100cm)	Thick laminae (0.4-3cm) that are generally inversely graded and resemble grain-flow layers
Topsets are multiple channel fills	Topsets are parallel-laminated and ripple cross-laminated

Postma (1990) suggests that the control over which of these two delta front systems develops is dependent on stability, spacing, discharge and width of the distributary channels. He maintains that in shallow-water fan-delta system mouth bars will develop on moderate to low gradients which are generally well vegetated braid and coastal plains whilst the classic Gilbert-type delta front develops on steeper gradients characterised by ephemeral discharge. Figure 5.23 shows the 12 major prototype deltas suggested by Postma (1990).

The criteria outlined above suggest that the cross-bedded conglomerates described above may represent more than one delta-type. At Bozburun, the facies relations with organic-rich deposits suggests a well vegetated area, albeit locally, with periods of little coarse clastic input. This points to a relatively shallow gradient and the conglomerates here have been interpreted as having been deposited as mouth-bar-type foresets with a Gilbert-type profile (e.g. number 9; Fig. 5.23). These are similar to those documented by McCallum and Robertson (in press) in the Pliocene of Cyprus. Alarahan and South Kargi, with their higher angle cross-sets and association with immature soils, overbank fines and coarse conglomeratic channels are thought to have been deposited at small scale Gilbert-type delta fronts (e.g. number 3; Fig. 5.23). As in Cyprus (McCallum, 1989), there is little evidence that any of these cross-bedded

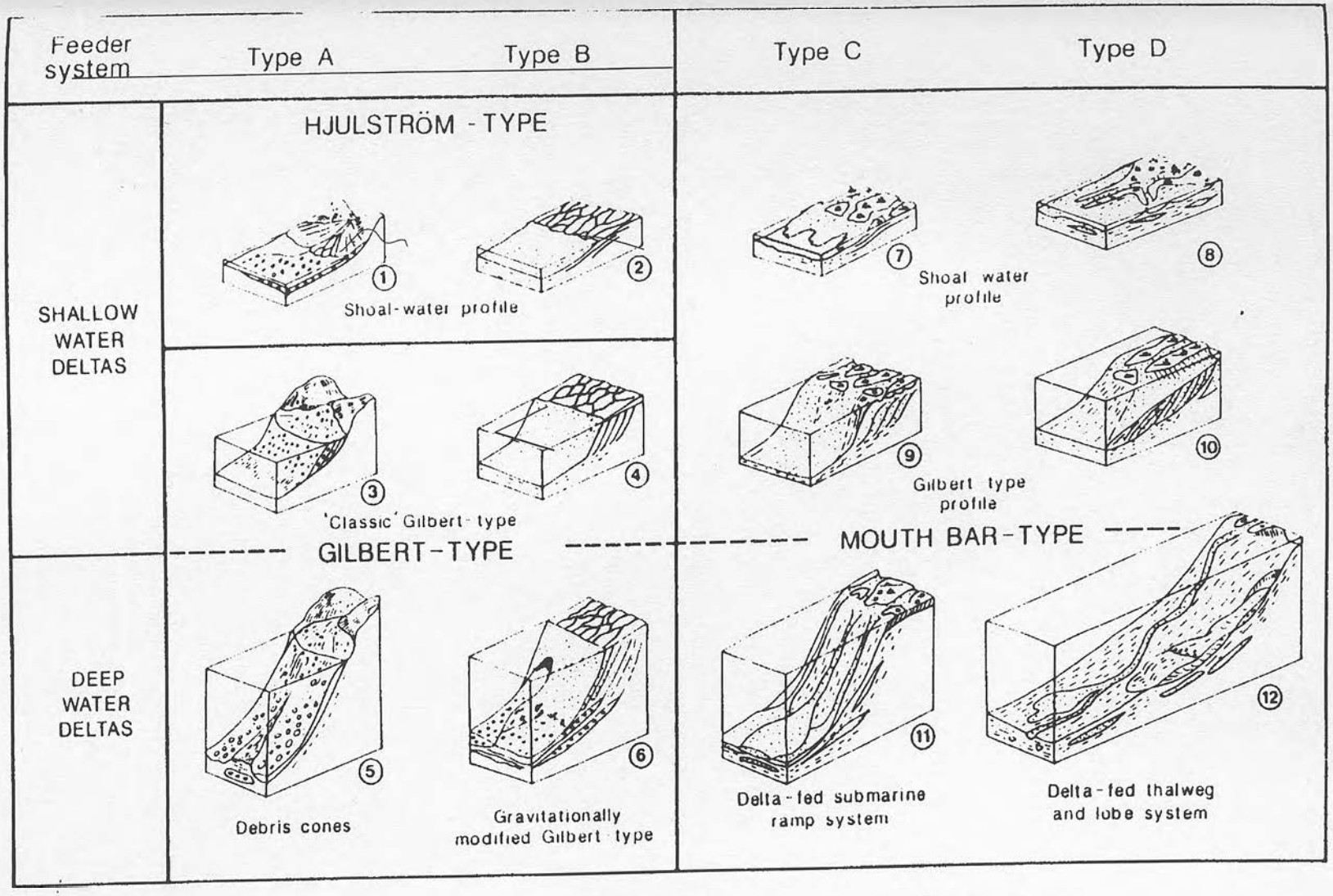

Figure 5.23 The twelve major prototype deltas suggested by Postma (1990).

conglomerates formed a single, unified delta front as is required by the strict definition of Gilbert-type deltas. Instead, the cross-bedded units are thinner and highly localised.

Dunne and Hempton (1984) suggested that the development of Gilbert-type or mouth-bar-type deltas was dependent on the slope of the basin floor. This was later challenged by Nemec (1990a) who suggested that distributory channel variables outlined above controlled the delta type. On a smaller scale however, it has been shown that the angle of the basin slope is an important factor in determining the structures of the deposits developed and their process of deposition.

In a subaqueous environment, gravity induced processes dominate. Influx of particles to a subaqueous delta slope leads to steepening of the slope because the rate of deposition by fallout from suspension and bedload dumping decreases down slope. Above a certain angle (ϕ_i, the angle of initial yield) however, the slope surface becomes unstable and this leads to mass failure, transporting material down the slope face and leaving the previously steepened slope at a more gentle inclination. This angle (ϕ_r) is commonly referred to as the angle of repose (Van Burkalow, 1945). Allen (1970) argued that avalanching down slope will occur if the slope (with angle ϕ), is subjected to a sufficiently large downslope acceleration (a) where:

$$a = a_{max} \times (\phi_i - \phi)/(\phi i - \phi_r)$$

in which:

$\phi_i > \phi > \phi_r$

$a_{max} = g\,(\tan\phi i - \tan\phi_r)$ = maximum possible downslope acceleration that will initiate a free-running avalanche.

Allen (op. cit.) shows that the angle of repose (ϕ_r) is nearly constant for a given material despite differing avalanche conditions. This suggests the reason for the progradation of constant slope foresets at the front of delta systems as pictured in figure 5.24 (Nemec 1990b, p32).

CONICAL SUBAQUEOUS DELTA

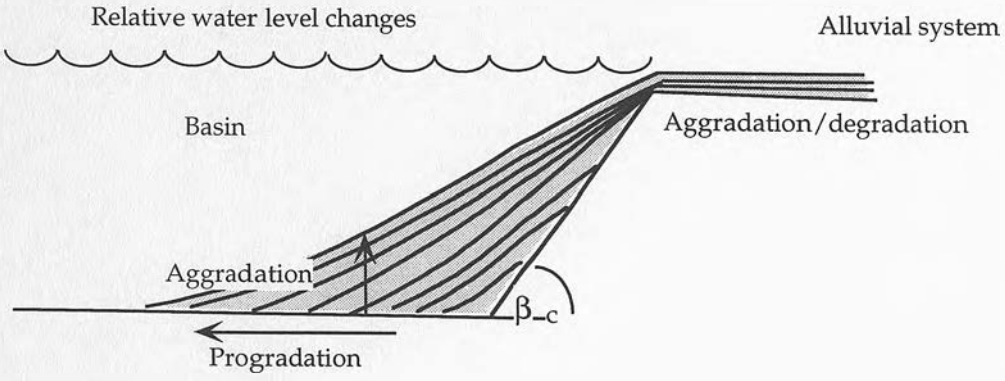

GILBERT-TYPE DELTA

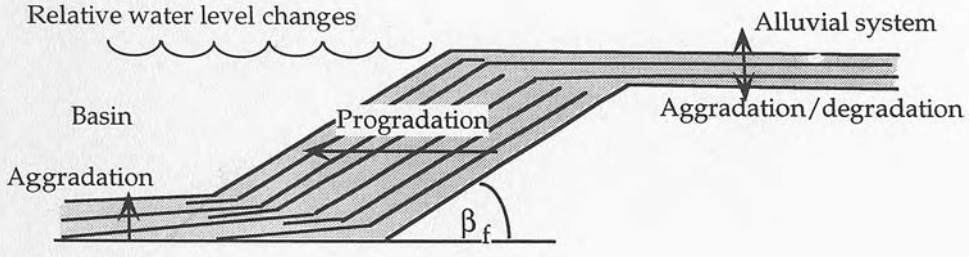

Figure 5.24 Schematic diagrams of conical and Gilbert type deltas, where $\beta_f < \beta_c$. (After Nemec, 1990b)

In the study area however, with the exception of the Kargi baraj site, the high-angle cross-bedded conglomerates are not directly associated with basement changes in slope, such as a basin margin or fault. Instead, these conglomerates (e.g. at Alarahan and South Kargi) are associated with reef-framestones. It is possible that the topographic structures produced by coral growth may have been sufficient to produce a gradient change at sea level able to initiate avalanching, from which progradational foresets could develop. Evidence of reef talus is abundant at Alarahan suggesting that basinward steep slopes were already active producing conical aggradational patterns (Fig. 5.24) and though probably too steep for parallel foreset development, these slopes were probably exploited and either reduced in inclination by constant avalanching (Allen, 1970) or by wave action (Nemec, 1990b) of which there is evidence in the form of echinoid-scaphopod facies deposits at South Kargi (Fig. 5.20) until they attained the critical slope. Subsequently, cascading sedimentation down the front of the slope produced prograding cross-sets similar to those described by Postma and Roep (1985) and Colella *et al.* (1987).

As has already been discussed above in section 5.5.3.2 concerning Porites bafflestones, the controls on this sort of clastic-carbonate interaction seems to be dependent on both sediment flux and relative sea level change. As is shown at Alarahan in figure 5.25, for example, following deposition of cross-bedded conglomerates, relative sea level rise and low sediment influx allowed the colonisation of the frontal foreset by Poritid reefs. This sort of interrelationship contains a potential problem. Reef colonisation enhances the preservation potential of alluvial/delta front sediments and it would be easy to exaggerate their importance in terms of the depositional system.

Lack of transition facies in any one section may be due to avulsion and rapid colonisation by reefs which protect underlying sediments from wave erosion thus increasing preservation potential. Thus, the best section preserved are those which were not active clastic channel systems at the time of the rapid relative sea level rise.

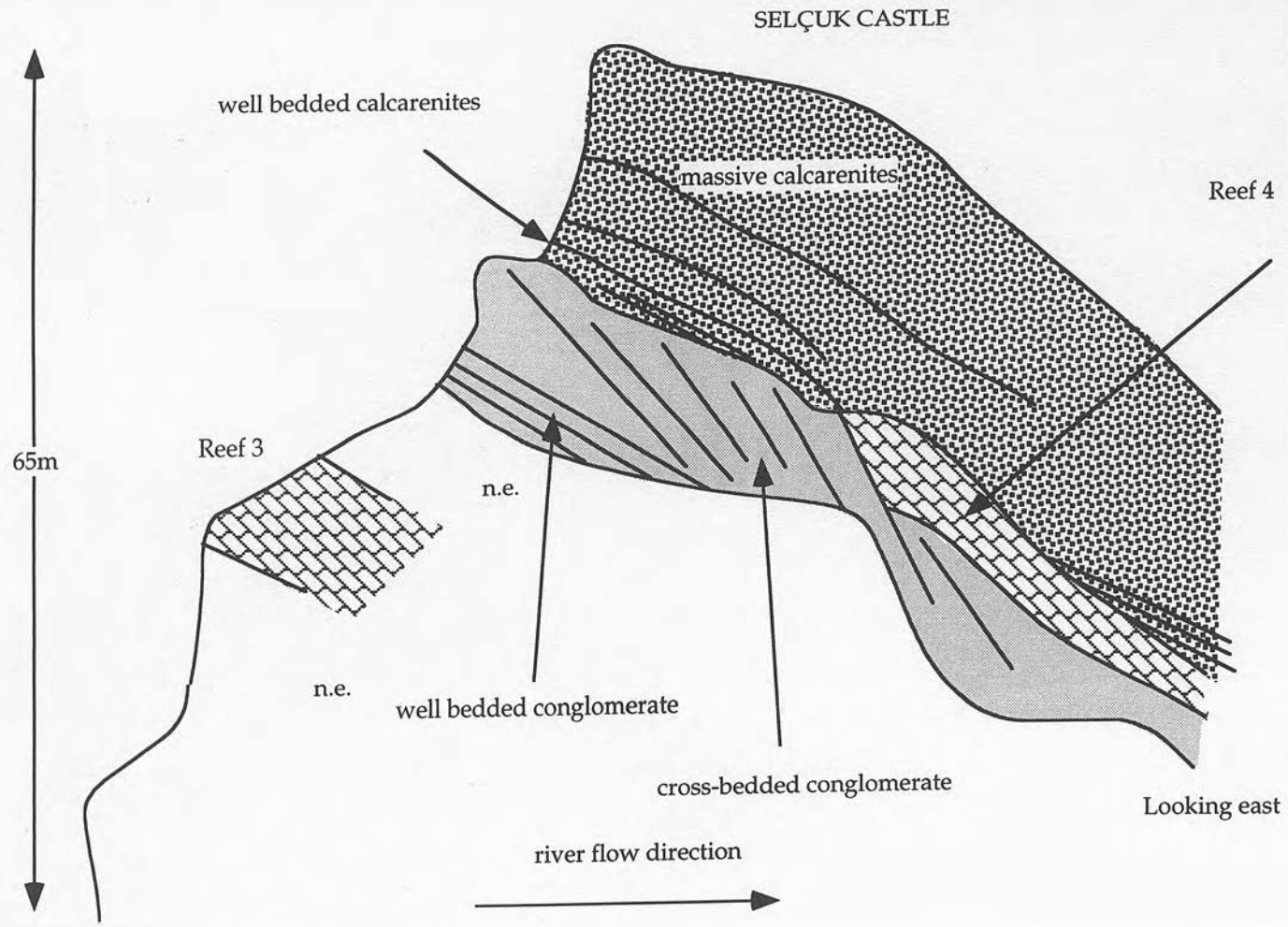

Figure 5.25 Field sketch of high-angle cross-bedded conglomerates and reef limestones at Alarahan. The cliff drawn here is exposed on the left bank of the river (Alara Çay) beneath the Selçuk castle. Reef numbers are with reference to the section logged at this locality (Fig. 3.4).

Table 5.10 Summary of the features of sub-facies association C.

Name	Lower boundary	Upper boundary	Lateral variation	Thickness	Sorting/ composition	Structures	Matrix	Interpretation
Echinoid-scaphopod facies	faintly erosive?	channelised/ planar	changes to domal coral framestone/ Porites bafflestone	0.01-2m	rhodoliths, scaphopods, echinoids, grit and pebbles	alignment of scaphopods	grit-siltstone	wave-reworked beach gravel.
Porites bafflestones	gradational	sharply erosive	varies to echinoid-scaphopod facies	~3-5m	Porites sticks, with horizons of conglomerate and gritstone		silt-grit	fluvial sediment trap at the marine-fresh-water interface
High-angle cross-bedded conglomerates	planar-erosive and channel shaped	sometimes convex up	lateral thickness variations common on a scale of 50m	2-10m	well sorted, rare biogenic clasts	high angle (~25°) cross-sets, imbrication	grit	Gilbert-type delta foresets

5.5.3.4 Interpretation of sub-facies association C.

A summary of the description and interpretation of the sub-facies discussed above is given in table 5.10. All the sub-facies in group C have been interpreted as having been deposited at the continental-marine interface. Shoreline sediments are the most sensitive recorders of relative sea level change. Throughout the study area, where ever these sediments are preserved they record a rise in relative sea level. They also record basinal processes and the presence of the echinoid-scaphopod facies suggests that wave action was an important processes in reworking delta front sediments. Note that overall there is a transition from a continental environment of deposition to a marine environment (Oymapinar Limestone and Karpuzçay Formation at the Kargi baraj locality, Fig. 5.1). In detail however, there is abundant evidence of the small-scale prograding nature of the shoreline at least in vertical section. Figure 5.26 is a generalised model for the formation of the shoreline facies described above.

5.5.4 Sub-facies association D

Table 5.11 List of the sub-facies in sub-facies association C, their localities and formations.

Sub-facies	Localities	Formation
Clast-supported conglomerates	Bucakkoyu Altinkaya Ballibucak Kesme	Tepekli Kesme
Matrix-supported conglomerates	Kargi baraj	Taskesigi
Fossiliferous and cross-bedded sandstones	Deniztepesi Saburlar Kesme	Tepekli Kesme

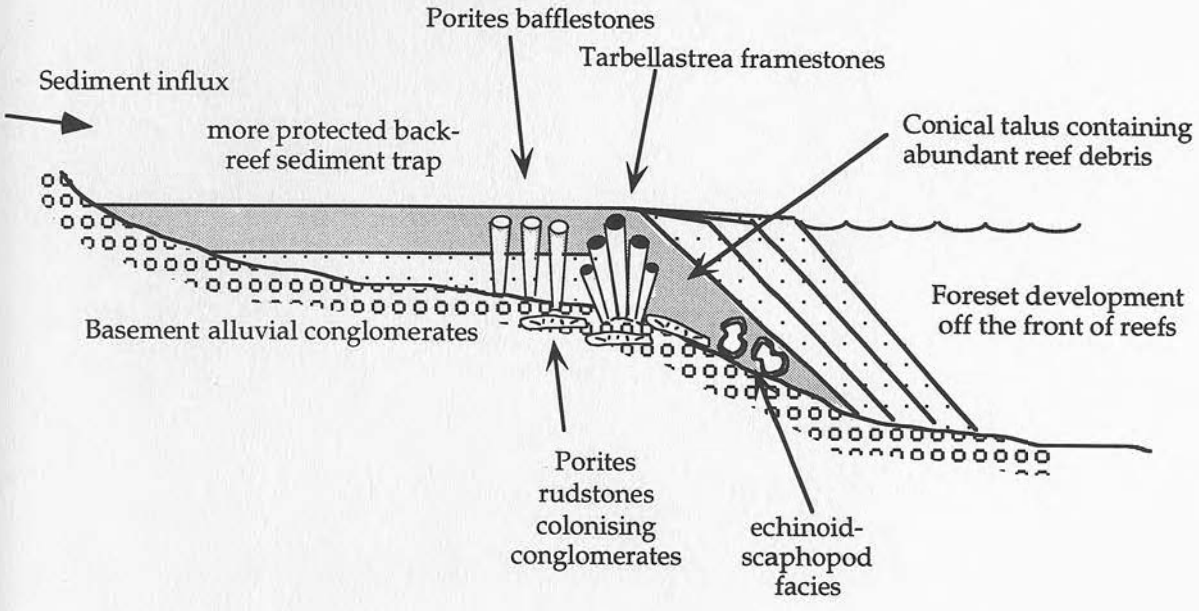

Figure 5.26 Model of the fan-delta shoreline facies preserved in the study area.

5.5.4.1 Clast-supported conglomerates

Description

These conglomerates constitute a thick succession (i.e. ~500-1000m) of laterally continuous conglomerates and sandstones. In two places (e.g. at Altinkaya and Bucakköyü; Fig. 5.1) they pass up into shallow-water carbonate successions consisting of small patches of reef framestones and calcarenites. At Altinkaya, they are interbedded with these carbonates on a scale of 10-50cm.

The interbedded conglomerates and sandstones of this facies are well bedded and parallel sided (Fig. 5.27). Clasts are generally rounded and they are distinctively well sorted. Clast fabrics such as imbrication are rare, but do occur. Matrix for the conglomerates is compositionally similar to that of the interbedded sandstones and is generally fine sand grade or coarser. The cement is the ubiquitous carbonate which characterises the cements of all the rocks under study, but in these rocks, perhaps because of the overwhelming predominance of carbonate, this results in "fairy chimney" weathering patterns of palaeokarstic origin (e.g. columnar structures up to 7m in height) between the Köprü Bridge and Ballibucak.

Interpretation

Both the association of these successions with shallow-marine carbonates and the absence of any evidence of subaerial deposition suggest that these conglomerates and sandstones were deposited subaqueously. There is no evidence of the bathymetry, but as the sequence passes up into shallow-marine carbonates, this suggests that they were deposited in an inner-shelf environment. The fairy chimneys are one of the many palaeo-karst features that proliferate in the Köprü basin and are making building the hydro-electric dam planned for the Beskonak area impossible (Degirmenci, 1992).

Figure 5.27 Photograph of the parallel bedded conglomerates at Bucakkoyu, west Kopru basin.

Figure 5.29 Cross-bedded sandstones and conglomerates north of Yesilbag, north-east Kopru basin (Fig. 5.1), Aksu Formation.

5.5.4.2 Matrix-supported conglomerates

Description

The most spectacular exmplw of these lithotypes occur in the Taskesigi Member (Karpuzçay Formation) of the Manavgat basin (Table 2.6) and have already been described in chapter 4 (section 4.5.3.1). At the Kargi baraj site (Aksu basin, Fig. 5.1) a similar matrix-supported conglomerate directly onlaps an undulating and now steeply dipping unconformity in Jurassic limestone. This horizon is both localised and varies greatly in thickness. Towards the road tunnel (at present under construction), a sequence of matrix supported conglomerates between 15 and 20m thick is visible. This decreases to a single flow <1m thick just to the north of the dam itself and passes laterally into oyster and coral-rich Lower-Middle Miocene limestones (section 3.6.3.4). Overlying these matrix-supported conglomerates is a series of cross-bedded, imbricated, clast-supported conglomerates (described above), which are localised above the matrix-supported conglomerates.

The Jurassic basement onto which this succession onlaps is bored and encrusted. Bored pebbles of this same limestone are found plentifully within the conglomerate itself along with abundant *Porites* corals and oysters. The sequence is made up of layers with varying amounts of grey silty matrix from a fully matrix-supported texture, to angular micro-conglomerates which are clast-supported. All are markedly poorly sorted

Interpretation

The shallow-marine bioclastic debris, the bored and encrusted basement and the lateral facies change to shallow-water reef environments indicates a submarine environment of deposition. The present, nearly vertical angle of dip of the basement has, almost certainly, been exaggerated by later east-west tectonic shortening during the Aksu Phase at the end of the Miocene (chapter 7), but the interbedded angular clast-supported micro-conglomerates resemble talus deposits and suggest that the slope on this basement was also steep during deposition. The sequence as a whole, including the overlying cross-bedded conglomerates and lateral facies change to reef framestones is remarkably similar to that described by Barrier (1984) from the palaeofault scarp of the Capo

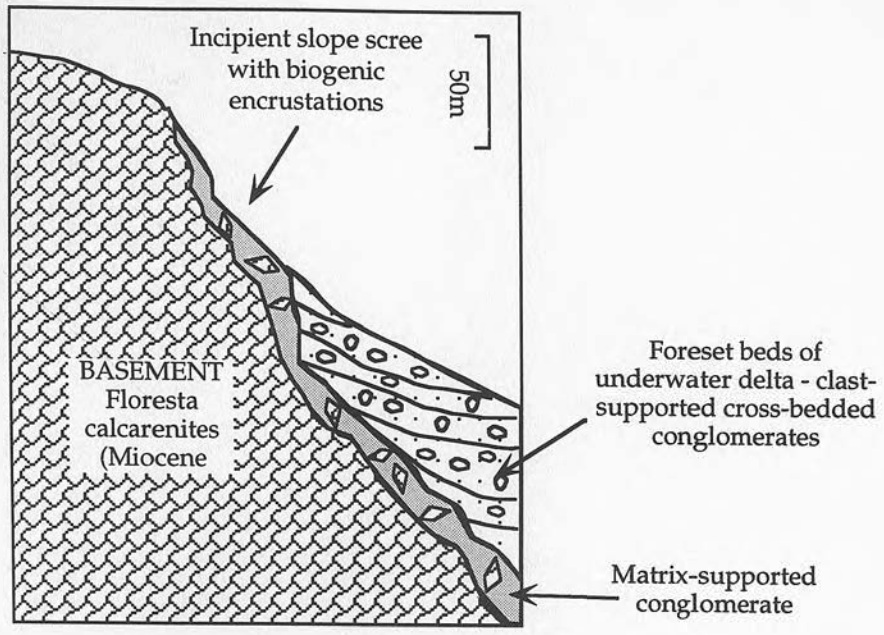

Figure 5.28 Outcrop sketch of the most proximal (back-edge) part of an underwater conical delta abutting against a paleofault scarp of the Capo dell'Armi horst, Messinian Strait, Italy. (Modified from Nemec, 1990; originally from Barrier, 1984). The facies associations shown here closely resemble those observed in the Kargi baraj area, Aksu basin.

dell'Armi horst, Messinian Strait, Italy, which he interpreted as the most proximal 'back-edge' of an underwater conical delta (Fig. 5.28). There is however no evidence of a fault along this margin of the Aksu basin.

5.5.4.3 Fossiliferous and cross-bedded sandstones

Description

Because of their high biogenic carbonate content, these sediments have been described in detail in chapter 3, and only a brief summary of the salient points is given here. Fossiliferous sandstones are common throughout the study area although they vary greatly from place to place. At Deniztepesi they are interbedded with medium to coarse conglomerates, and *in situ* coralline limestone. At Kesme by contrast gastropod-rich sandstones are interbedded with cross-bedded sandstones, conglomerates and *Montastrea* framestones. Well developed cross-bedded sandstones also occur in the lower part of the section at Saburlar, associated with oyster-rich beds and conglomerate horizons.

This sub-facies resembles the echinoid-scaphopod facies rocks in some instances although large algal rhodoliths are generally absent (e.g. Deniztepesi). Also the fossil assemblage tends to be much higher diversity including coral, bivalves, gastropods and oysters as well as abundant algal fragments and proportionally fewer scaphopods and echinoids. Almost all fossil specimens located in these sediments were fragmented. In some more rare cases however, the fossil content may be monospecific constituting a gastropod or oyster lag. These can be seen in the north of the Köprü basin near Yesilbag and Kasimlar and are described in more detail in chapter 3 (section 3.6.3.3) under gastropod grainstone/wackestones. Beds are generally 10-20cm in thickness, with cross-bedding being rather trough-shaped (Fig. 5.29). Rare water escape structure were also observed in this section.

Interpretation

These fossiliferous sandstones are thought to represent sediments which through gravity-driven processes (possibly triggered by storm induced flooding) swept up shells from shallow marine settings, depositing them further off-shore. These were later winnowed by currents to produce the rather concentrated biogenic lags now preserved. Similar sediments have

been documented by McCallum (1989) in the Athalassa Formation of southern Cyprus. It is thought that this sub-facies is of slightly deeper water origin than scaphopod-echinoid facies because they do not show any obvious signs of wave reworking. Neither would storm flooding of continental areas produce the later winnowing. The association of these sediments with cross-bedded sandstones could indicate constant working by unidirectional currents, sweeping the shelf.

5.5.4.4 Interpretation of sub-facies association D

A summary of the description and interpretation of the sub-facies discussed above is given in table 5.12. Water depths are not clearly indicated by the sub-facies in group D although they were certainly all deposited in a marine environment (Table 5.12). There is little evidence to suggest very deep water and the lateral and vertical facies transitions to shallow-water reef carbonates which can be observed for all three of the sub-facies described here, strongly indicates relatively shallow water, at least periodically. It is suggested therefore that these sub-facies were deposited in a shallow-marine shelf environment fed by rivers and reworked by wave and storm processes.

5.6 Provenance and Palaeocurrent data

Interpretation of the abundances of clast types in the conglomerates within the study area is difficult, mainly because so much of the hinterland is dominated by similar successions of Mesozoic carbonate, radiolarian chert and sandstones. A more detailed study involving detailed work in the hinterland itself might have produced a more informative interpretation of the 53 conglomerate analyses measured in Aksu conglomerate successions and displayed in Appendix 4a. This was beyond the scope of this project however. A few simple trends have been deduced from manipulation of conglomerate analysis data and these are discussed below.

Table 5.12 Summary of the features of sub-facies association D.

Name	Lower boundary	Upper boundary	Lateral variation	Thickness	Sorting/ composition	Structures	Matrix	Interpretation
Clast-supported conglomerates and sandstones	planar	planar	laterally persistent	0.3-1m	well sorted	rare imbrication	fine sandstone-micro-conglom'	upper shelf sands and conglomerates
matrix-supported conglomerates	unconformity	planar-slightly undulating	thickness changes from 30m to 0m over 1km. Changes to reef carbonates	0-30m	very poorly sorted, coral oysters, Mesozoic limestone clasts (bored)	chaotic	siltstone	debris flow
Fossiliferous and cross-bedded sandstones	planar- faintly scoured	planar	?	10-20cm	generally well sorted, bioclasts may be significantly larger	rare monospecific oyster/ gastropod lags	coarse-fine sandstone	redeposited, winnowed shelf sands

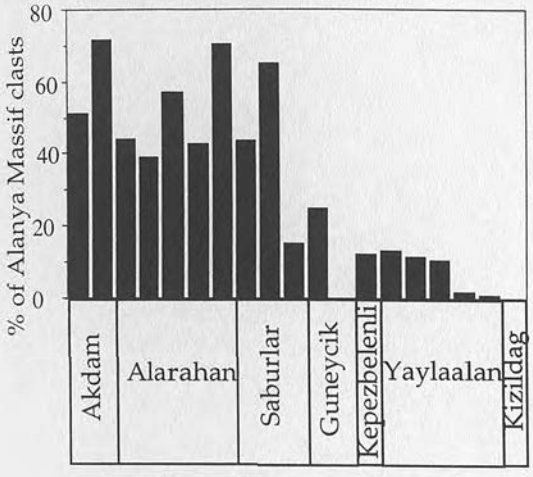

Bar chart of Alanya Massif clasts in the Kizildag Formation conglomerates

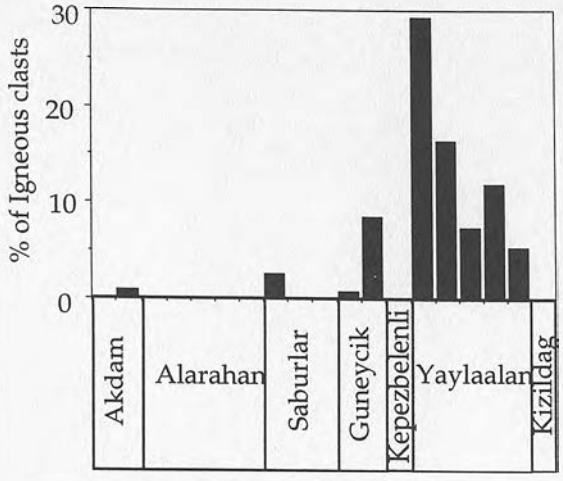

Bar chart of igneous clasts in the Kizildag Formation conglomerates

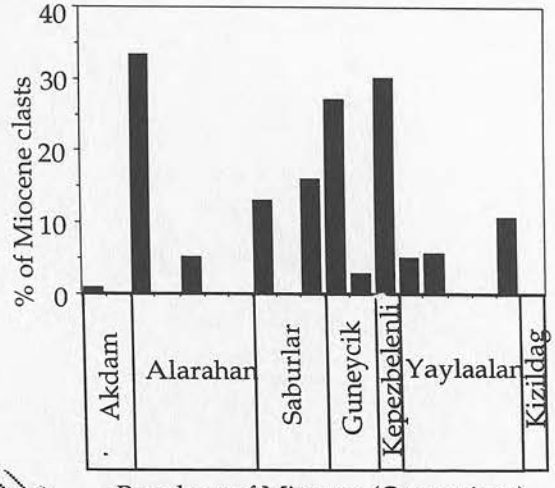

Bar chart of Miocene (Oymapinar) limestone clasts in the Kizildag Formation conglomerates

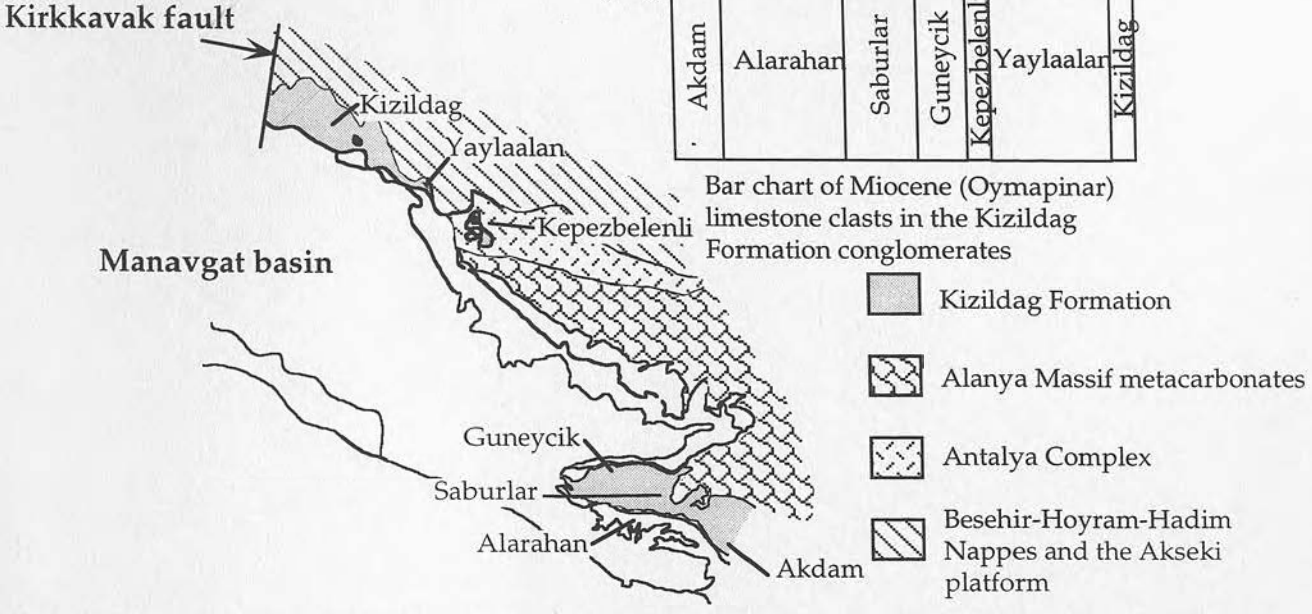

Figure 5.30 Provenance data from the basal conglomerates in the Manavgat basin (Appendix 4a). The location of conglomerates containing Alanya Massif clasts are all closely associated with present day exposure. Alanya Massif material is not present in the more northerly conglomerates indicating localised derivation. Igneous clasts derived from the Antalya Complex show a similar, but inverse relationship. Miocene limestone clasts do not appear to be geogaphically controlled suggesting that shallow-water carbonate was abundant throughout the area at this time.

5.6.1 The Manavgat basin

Figure 5.30 shows the location of conglomerates analysed in the Manavgat basin, excluding those that are part of the Middle and Upper Miocene sequence described in chapter 4. This diagram shows that reworking of basement was extremely localised. For instance, the abundance of igneous clasts in the southern part of the basin, where conglomerates overlie Alanya Massif is limited, whilst clasts of the Alanya massif limestone and schist are much less abundant in the north western part of the basin, where the conglomerates overlie Mesozoic limestone and Antalya Complex (primarily limestone, basalt and radiolarite).

In conjunction with the palaeocurrent data displayed in figure 5.31, the following interpretations can be made:

- Very little material from the Alanya Massif, Beysehir-Hoyran-Hadim Nappes and Anamas-Akseki Platform (Fig. 1.3) was transported over the Alanya Massif to the area near Alarahan and Saburlar in the south of the basin. The source for these conglomerates was probably east of the basin;
- Remarkably little Alanya Massif material was transported westwards towards Yaylaalan and Kizildag. These conglomerates were obviously sourced to some extent from the east, north of the Alanya Massif, but also from the north.

Put together, these conclusions indicate that the Alanya Massif formed a palaeo-high during the Lower Miocene, around which conglomerate-dominated successions were deposited. This is confirmed, by the absence of lower Miocene conglomerates overlying the Alanya Massif in the north of the basin (Fig. 4.29) and the direct colonisation of Burdigalian-Langhian reefs. The identification of Miocene algal limestone clasts throughout the Lower Miocene of the basin is somewhat problematic. Their presence indicates that shallow-water marine limestones were forming before those preserved (e.g. earlier in the Burdigalian). Almost all the conglomerates observed in the Manavgat basin below the Burdigalian-Langhian reefs (Oymapinar Limestone) have been interpreted as continental deposits, the exception being at Saburlar. The presence of Miocene marine clasts in these essentially continental

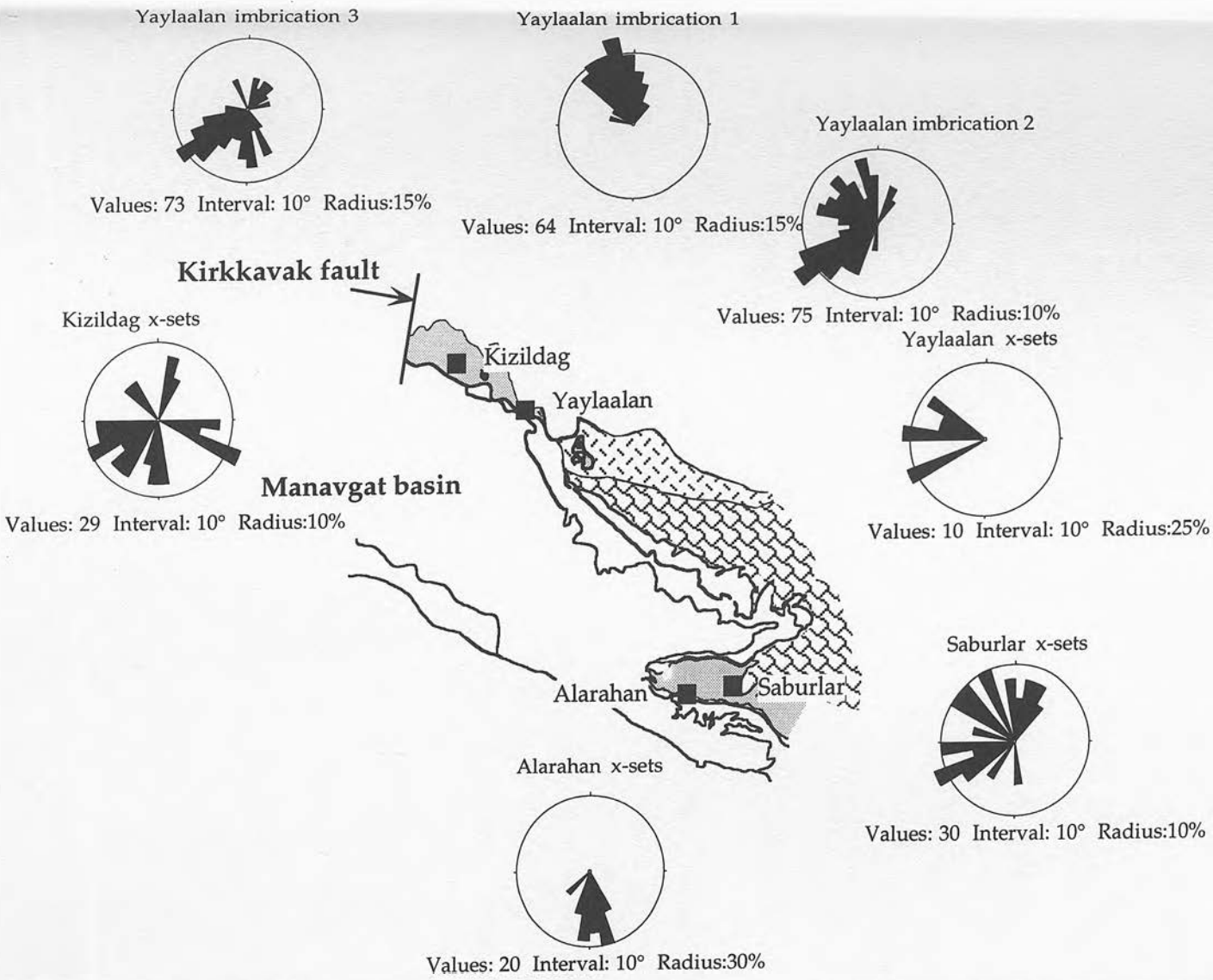

Figure 5.31 Palaeocurrent data from the Lower conglomerate succession in the Manavgat basin. The variety of directions is typical of fan-delta palaeocurrents. However, a few important trends can be discerned. First, the majority of the data from the northern margin of the basin indicates that it was sourced from the east and not directly from the north. In the south of the basin the palaeocurrents indicate that there was both a southerly and westerly component to the flow direction.

Burdigalian (or older) conglomerates indicates that there must have been at least one "transgression" over parts of this area of which these clasts are the only remaining remnant.

5.6.2 The Aksu and Köprü basins

Much less can be deduced from conglomerates analysed in the Aksu and Köprü basins. In both basins, Miocene algal limestone clasts are only found in conglomerates closely associated with preserved reef structures (Fig. 5.32), e.g. at Altinkaya, Dumanli and Bucakköyü in the Köprü basin and in the Bucak junction conglomerates in the Aksu basin. Figure 5.33 shows the distribution of radiolarian chert clasts in the Köprü basin. The abundance difference between the north east Köprü basin conglomerates and the rest of the Köprü basin conglomerates is mirrored in other clast types (e.g. grey limestone clasts, appendix 4a). This suggests that the north Köprü conglomerates were deposited by a different system from the west Köprü conglomerates and eroded a hinterland with different proportions of similar components e.g. radiolarian chert and grey limestone.

Figure 5.34 shows palaeocurrent data collected for the Aksu conglomerates in the Aksu and Köprü basins. In the west of the Köprü basin and including the sub-basins located on the Mesozoic carbonate "promontory" between the Köprü and Aksu basins (section 5.5.1.2), the broad flow direction seems to have been to the south. Variations in flow direction are not uncommon in alluvial fans, due to avulsion (e.g. Postma, 1990) and the palaeocurrents from the north east of the Köprü basin appear to have a bimodal direction distribution: broadly to the south and east-west. The location of the "breach" in the Kirkkavak fault, now filled with these conglomerates (Fig. 5.16) in the far north west of the Köprü basin and its associated southerly palaeocurrents (Fig. 5.34) suggests that part of the source of material was through this conduit although it is not at all clear what palaeogeographic role the Kirkkavak fault played at this time. East-west directed currents to the south west of this "breach" between Kasimlar and Kesme may indicate an interplay between material derived from the breach and material derived from the west. This seems particularly likely since the conglomerates in the Kasimlar-Kesme area are interbedded with shallow-water carbonates

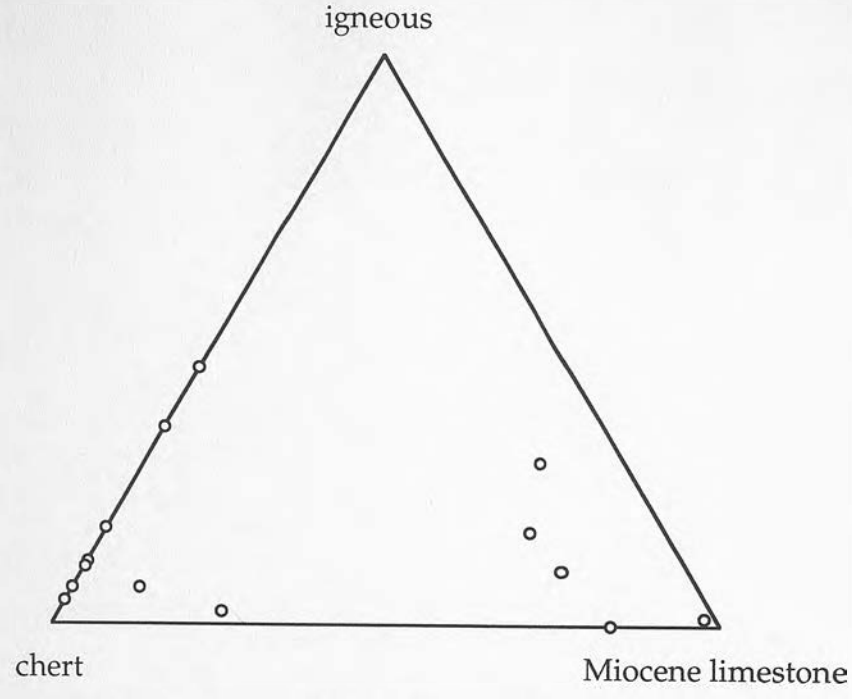

Figure 5.32 Triangular diagram of typical conglomerates from the Köprü and Aksu basins. All the Miocene clasts come from conglomerates associated with *in situ* Miocene reefs.

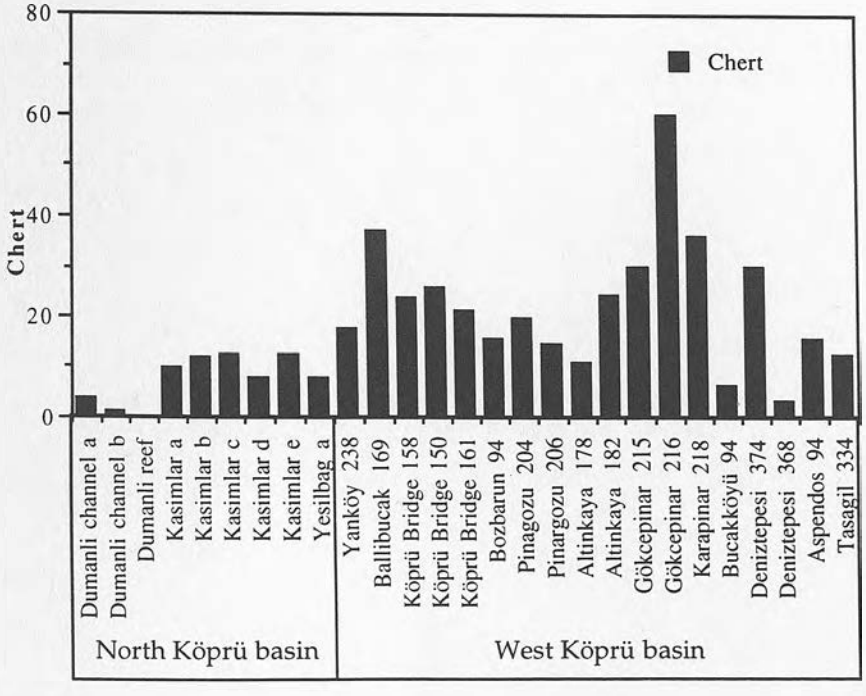

Figure 5.33 Bar chart of radiolarian chert distribution through out the Köprü basin. This distribution is mirrored by other clast types and suggests that the north eastern fan-delta system was a separate system from that along the western margin.

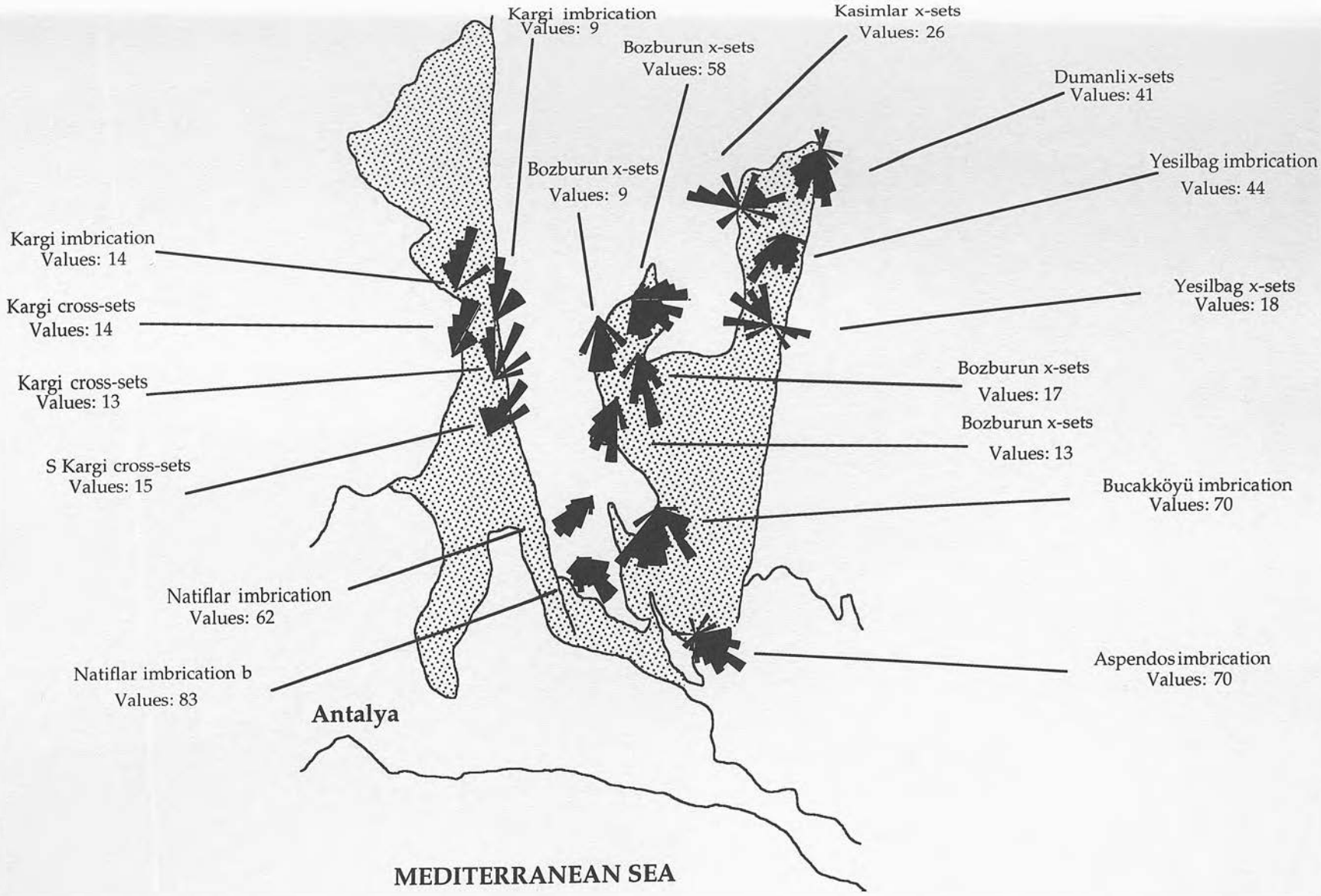

Fig 5.34 Palaeocurrent data from the Aksu conglomerates in the Aksu and Köprü basins.

including reef framestones, suggesting close proximity to subaerial conditions and alluvial sedimentation.

The Aksu basin palaeocurrents were all measured in a small area around village of Kargi and the new dam site (Fig 5.1). Much of the outcrop from which these measurements were made is now submerged or only accessible by boat! The overwhelming indication is of north east directed flow, away from the passive basin margin to the west.

5.7 General interpretation of the sedimentary system.

Table 5.13 summarises the interpretation of individual sub-facies and the sub-facies associations as a whole. The close spatial and temporal association of alluvial, lacustrine, lagoonal, coastal and shelf facies within these conglomerate dominated successions suggests that they represent deposition and preservation of the products of a fan delta system. The Aksu and Kizildag Formations have been sub-divided into formation groups as a result of the sub-facies associations described above. The sum-division is shown in table 5.14.

The study of clastic sediments within the framework of the fan-delta concept is a relatively recent one. Defined as alluvial fans that prograde into a standing body of water from an adjacent highland by Holmes (1965) and McGowen (1970) the impetus for studying fan-deltas began primarily in 1975 when Walker first proposed four models for deep water conglomerates. Rust (1979) suggested that there was little significant difference between the internal structures of fan delta facies deposited in a marine environment and their terrestrial counterparts, alluvial fans, save for minor reworking by waves. It is now widely accepted however that fan-deltas are distinct depositional systems (Nemec and Steel, 1988) and that even single subaerial flows are considerably transformed when passing into water (Nemec and Steel, 1984). Coarse fan-deltas have become the focus of increasing interest and research over the last few years because they are sensitive recorders of tectonic, climatic and base level conditions as well as being excellent potential reservoirs for hydrocarbons and coal (Colella and Prior, 1990).

Table 5.13 Summary of the interpretation of sub-facies and sub-facies associations

Sub-facies association	Sub-facies	Interpretation of sub-facies	Interpretation of sub-facies association
A	Clast-supported angular conglomerate	fault talus	ALLUVIAL
	Clast-supported conglomerates and coarse sandstones	sheet flood and channelised braided stream deposits.	
	Matrix-supported conglomerates	debris flow	
	Laminated sandstones	braided stream bars, over bank flows, sheet floods	
	Calcretes and associated fine sediments	palaeosol	
B	Organic-rich facies	immature coal	LAGOONAL / LACUSTRINE
	Green clays	lagoonal clay	
	Laminated limestone and lime mud	lacustrine limestone	
	Gastropod siltstones	lacustrine silts	
	Limestone breccia	slope talus deposited in a lake	
C	Echinoid-scaphopod facies	wave-reworked beach gravel.	SHORELINE
	Porites bafflestones	fluvial sediment trap at the marine-fresh-water interface	
	High-angle cross-bedded conglomerates	mouth-bar-type foresets	
D	Clast-supported conglomerates	upper shelf sands and conglomerates	SHELF
	Matrix-supported conglomerates	debris flow	
	Fossiliferous and cross-bedded sandstones	redeposited, winnowed shelf sandstones	

Table 5.14 Sub-division of the Aksu and Kizildag Formations (Akay and Uysal, 1985; Akay et al., 1985) into formation Members.

Environment	Sub-environment	Aksu Formation	Kizildag Formation
Continental	Alluvial	Kapikaya	Kargi
	Lagoonal and Lacustrine		Calcaire de Kepez
Marine	Shoreline	Kesme	Tepekli
	Shelf		

5.8 Classification of the fan delta systems

The extensive development of shelf facies indicates that, contrary to the original model of fan-deltas as fans passing directly into deep water (e.g. in fjords), the subaqueous parts of the fan-deltas studied were developed in relatively shallow water (Etheridge and Westcott, 1984; Elliott, 1986; Fraser and Suttner, 1986; Postma, 1990). They can therefore be classified as shallow-water deltas (Postma, 1990), which includes both marine and lacustrine environments, unlike the exclusively marine classification of shelf-type deltas (Etheridge and Westcott, 1984). Corner's classification (in Nemec, 1990) "steep general slope fan-deltas" suggests Gilbert-type foresets on a scale an order of magnitude larger than those seen here. The difficulty in classifying these fans may be the result of the restricted geographical space (i.e. the narrow shape of the basin) preventing full morphological development.

Figure 5.35 shows the geographic areas covered by the different Formation Members. From the palaeocurrent (Figs. 5.31 and 5.34) and provenance data discussed above 7 separate fan-delta systems can be tentatively identified. Not all of these were active at the same time and no single fan-delta system persisted throughout the Miocene.

5.9 Controls on fan-delta development

Relative sea level changes are hugely more important in the development of the shelf facies of a fan-delta

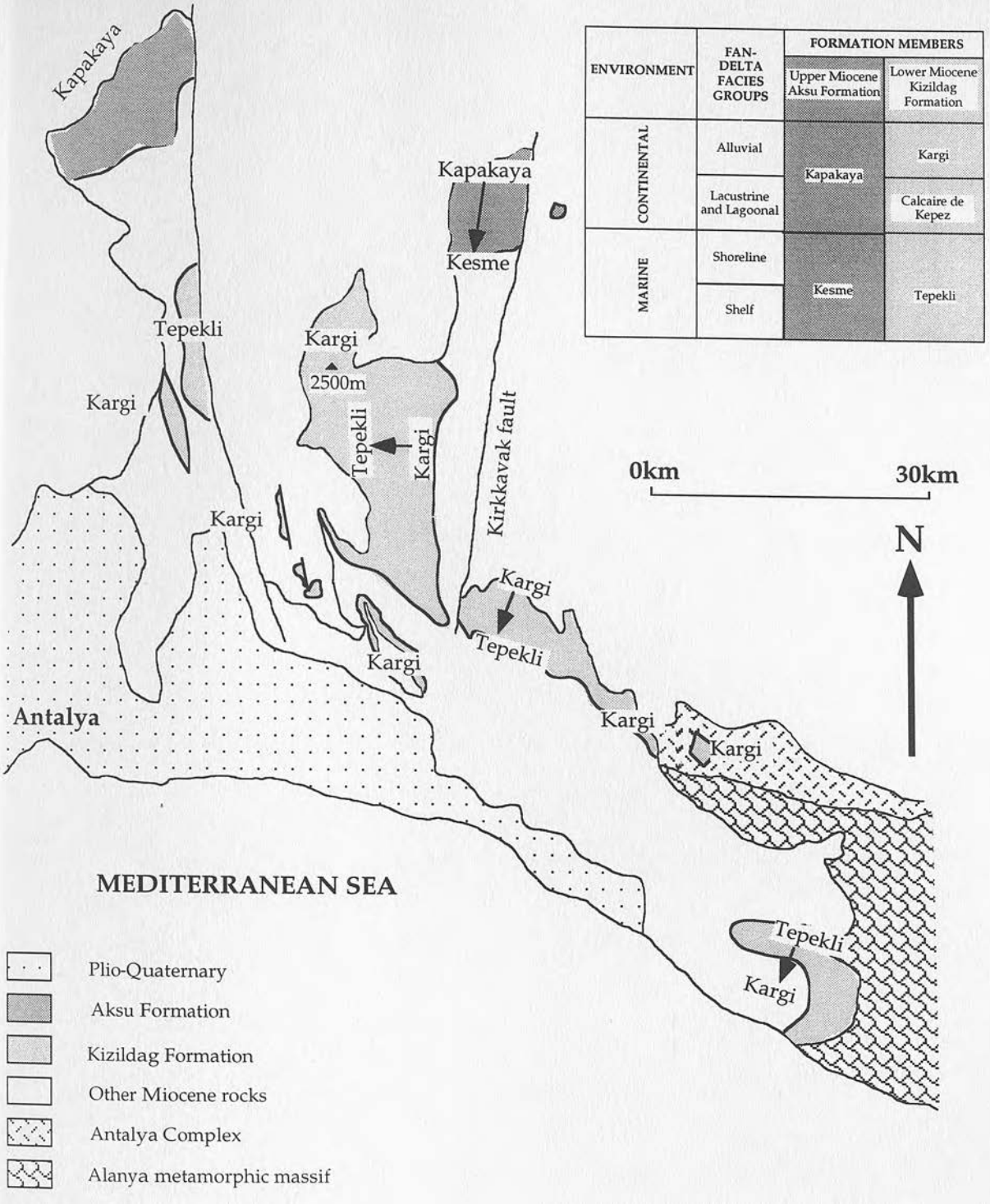

Figure 5.35 Geographic areas covered by the different formation members in the Aksu Conglomerate Formation.

level change and basinal controls such as wave reworking produces the wide range of environmentally informative deposits described above.

A modified version of the conceptual framework for delta systems suggested by Elliott (1986) is presented in Figure 5.36a. The arrows indicate the direction of thought required for the study of modern deltas. In studying ancient deltas this process is reversed in order to deduce information on the climate, tectonic activity and sea level change. Figure 5.36b shows this conceptual framework with the information gained from study of the facies inserted. These three extra-basinal controls are discussed below.

5.9.1 Climate

The following information from the sub-facies discussed above has palaeoclimatic implications:

- The abundance of calcrete in finer-grained alluvial sediments;
- The paucity of preserved plant debris except in exceptional cases (e.g. coal at Bozburun Dag);
- Some of the conglomerate and sandstone geometries and structures (e.g. channel-mouth-bars) have been interpreted as indicating flashy, ephemeral flow (section 5.5.1.2);
- The alluvial facies described here resembles modern sequences from the Red Sea area (Hayward, 1982);
- Ancient successions of alluvial facies are also similar to those studied here (e.g. Quaternary of Cyprus, Poole, 1992).

A semi-arid climate during the Miocene has been interpreted, not dissimilar from the current climatic regime affecting south coastal Turkey. This is in agreement with Maizels and McBean (1990) who suggested that a humid environment is unlikely to have generated many of the features listed above (section 5.5.1.6).

a)

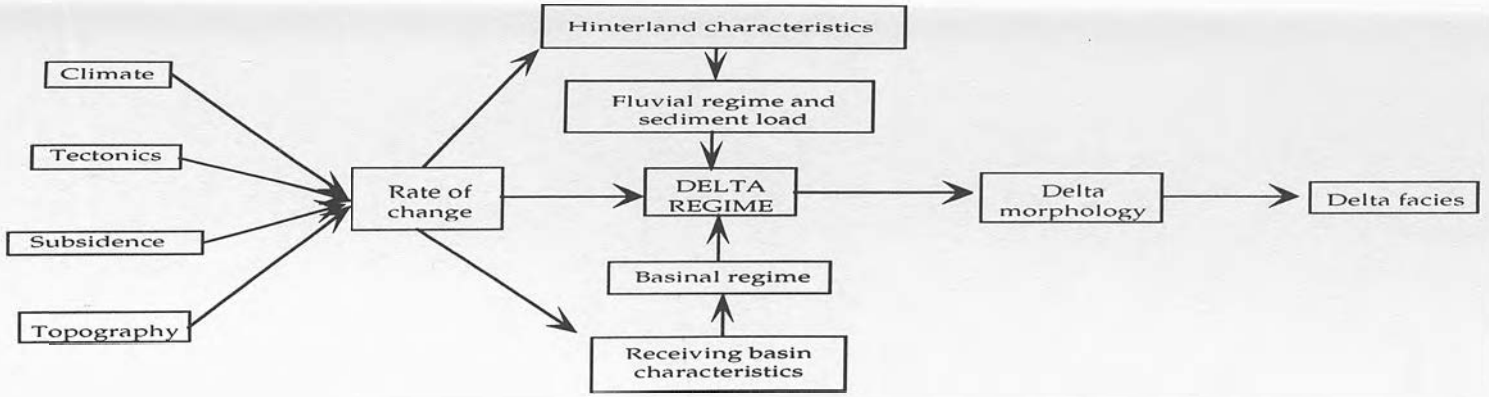

b)

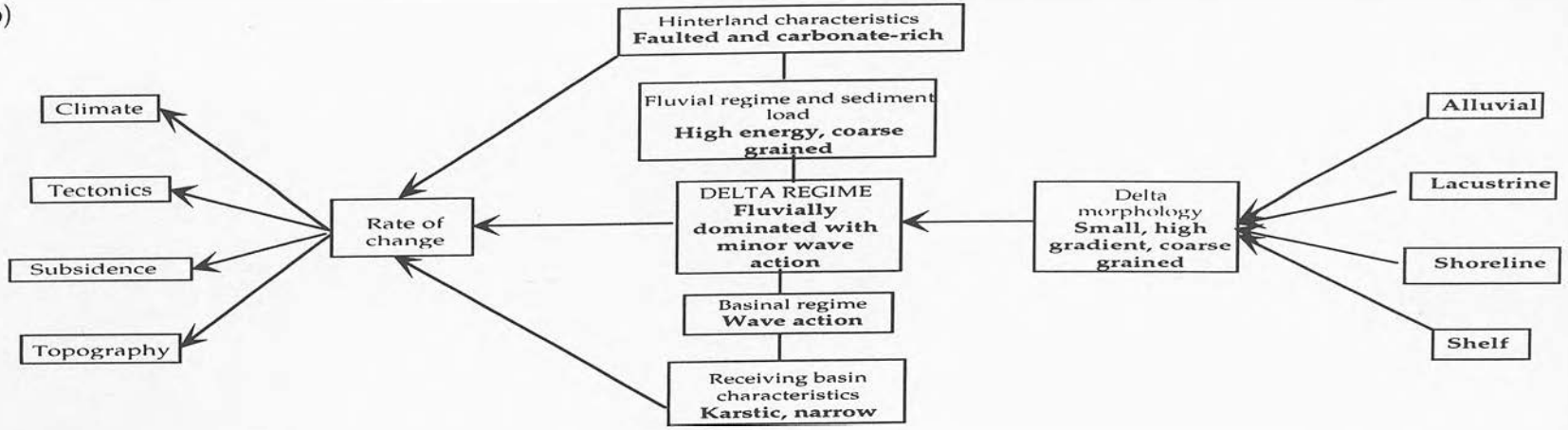

Figure 5.36 a) The conceptual framework for the comparative study of both modern and ancient delta systems (modified from Postma, 1990; originally from Elliot, 1986). b) The reversed framework showing the evidence gained from facies analysis of the fan-delta deposits in the study area.

5.9.2 *Tectonics*

The most two most important pieces of evidence of tectonic activity displayed by the Aksu Formation Conglomerates are firstly, the thickness of the preserved succession, and secondly, the consistently very coarse grainsize.

Wescott and Etheridge (1980) suggested that the thickness of fan-delta deposits depends upon a complex interaction of mountain-front uplift, sediment supply and basin subsidence. It is suggested here that relative sea level change can also play a vital role. Degirmenci (1992) estimated a minimum thickness of 440m for the west Köprü basin conglomerates from borehole data which did not hit basement in the centre of the Köprü basin. The altitude of the basin rises sharply towards the west however, being roughly 1000m higher near Altinkaya (Fig. 5.1) than it was in the centre of the basin close to the contact with the Karpuzçay turbidites. The tortuous track that climbs up to this village with its isolated Lycian remains is lined from bottom to top with continuous, horizontally bedded continental and then marine conglomerates (Fig. 5.27). A slightly more accurate estimate of the minimum thickness of this conglomerate succession is therefore in the order of 1.5km.

All the successions described above, whatever the environment of deposition, are dominated by cobble conglomerates rather than micro-conglomerate or sandstone. Such continual coarse conglomerate sedimentation suggests the sustaining of a high gradient of deposition. There are three potential processes which could maintain high gradients:

- uplift of the basin margins;
- subsidence of the basin itself;
- relative sea-level fall.

Given that these three processes are all interdependent, the discussion below attempts to isolate the relative activity of each.

There are two main pieces of evidence for relative sea level rise during the deposition of both the Lower and Upper Miocene conglomerate

successions. On a local scale, sea level can be demonstrated to be rising during clastic accumulation by the Porites bafflestone sub-facies where coral sticks pass undisturbed through clastic boundaries (section 5.5.3.2; Fig. 5.21). On a more regional scale, where transitions from one environment of deposition to another are visible, all the successions go from being subaerially deposited to being deposited in a marine environment (Fig. 5.35). This suggests that overall, relative sea level rise was more dominant that the prograding of fan-delta sequences. Bearing in mind the constantly coarse material deposited in these thick sequences (e.g. >1500m), this indicates that relative sea level rise was very rapid.

A conservative estimate for the minimum sedimentation rate for the Lower Miocene conglomerates in the west of the Köprü basin is 20cm/1000yrs. Bearing in mind that many of the cobbles in the conglomerates are roughly 20cm in diameter this suggests that 20cm/1000yrs may be heavily underestimated, possibly by an order of magnitude. Discounting subsidence, this minimum sedimentation rate computes to 200m/Ma sea level rise, which is already twice that of the quickest eustatic sea level change during the Miocene (Haq *et al.*, 1988; Fig. 5.38). Given that this estimate may also be an order of magnitude too low, and that relative sea level rise eventually outpaces delta progradation, relative sea level rise must be accepted as a major control in the development of the fan-deltas studied.

How much of this relative sea level rise can be accounted for by subsidence (tectonic or compaction driven) and how much by eustatic processes? The thickness of the sequences once again holds a key to understanding this problem. It seems highly unlikely that a coarse conglomerate succession over 1500m thick could be filling accommodation space entirely generated by pre-existing palaeotopography. It is therefore safe to assume that some of this accommodation space was generated by subsidence of the basin relative to the margins during deposition. Clearly some of this subsidence is likely to have been driven by compaction of those sediments and the ones beneath as a result of the deposition of 1500m of conglomerate. Note however that the grainsize remains coarse throughout the succession. Thus, this is no generally subsiding area which passes from subaerial to

submarine environment becoming more distal to the source in the process. This is an area where the hinterland is continuing to rise, constantly generating topographic highs susceptible to erosion, over and above a relatively rising sea level.

5.9.3 *Eustacy*

From the above discussion it can be seen therefore that some of the relative sea-level rise can be attributed to subsidence due to compaction and it seems likely that if there is evidence of a rising hinterland, the basins themselves may also have been subjected to active tectonic subsidence. The component of sea level rise contributed by eustacy is difficult to assess in detail. The curve produced by Haq *et al.* (1988; Fig. 5.37) indicates several periods of sharp sea level rise in the order of 100m. These periods may account for the formation of those sequences where sea level rise is so clearly documented (e.g. Porites bafflestones, section 5.5.3.2). The gentle eustatic sea level rise suggested by Haq's curve for the Burdigalian may have contributed to the relative sea level rise deduced for the Lower Miocene Aksu conglomerates, but it cannot have been the only component. The same is true for the Upper Miocene conglomerates, though the gradient on the eustatic curve for the Tortonian is somewhat steeper here. The sudden drowning of the reef carbonates and conglomerates at the Burdigalian-Langhian boundary (Fig. 4.32) across the Isparta Angle may have been caused in part by a eustatic sea level rise. A sea level high stand has been documented elsewhere in the Mediterranean at this time (e.g. south-east Turkey, Gürbüz, 1993; Sardinia, Cocozza and Jacobacci, 1975; southern Cyprus, Robertson *et al.*, 1991).

In terms of the larger scale stratigraphy, nannoplankton dating across the basin by C. Müller (pers. comm., 1992 and 1994) suggests that deposition of the Karpuzçay Formation turbidites began in the Serravallian (Fig. 4.24). There is evidence of interbedding of the Lower Miocene Aksu Formation conglomerates and the Karpuzçay Formation in the centre of the Köprü basin where boreholes have been drilled (Degirmenci, 1992). In general however the Serravallian is conglomerate poor, the exception being the cone of coarse conglomerates in the centre of the Aksu basin reported by

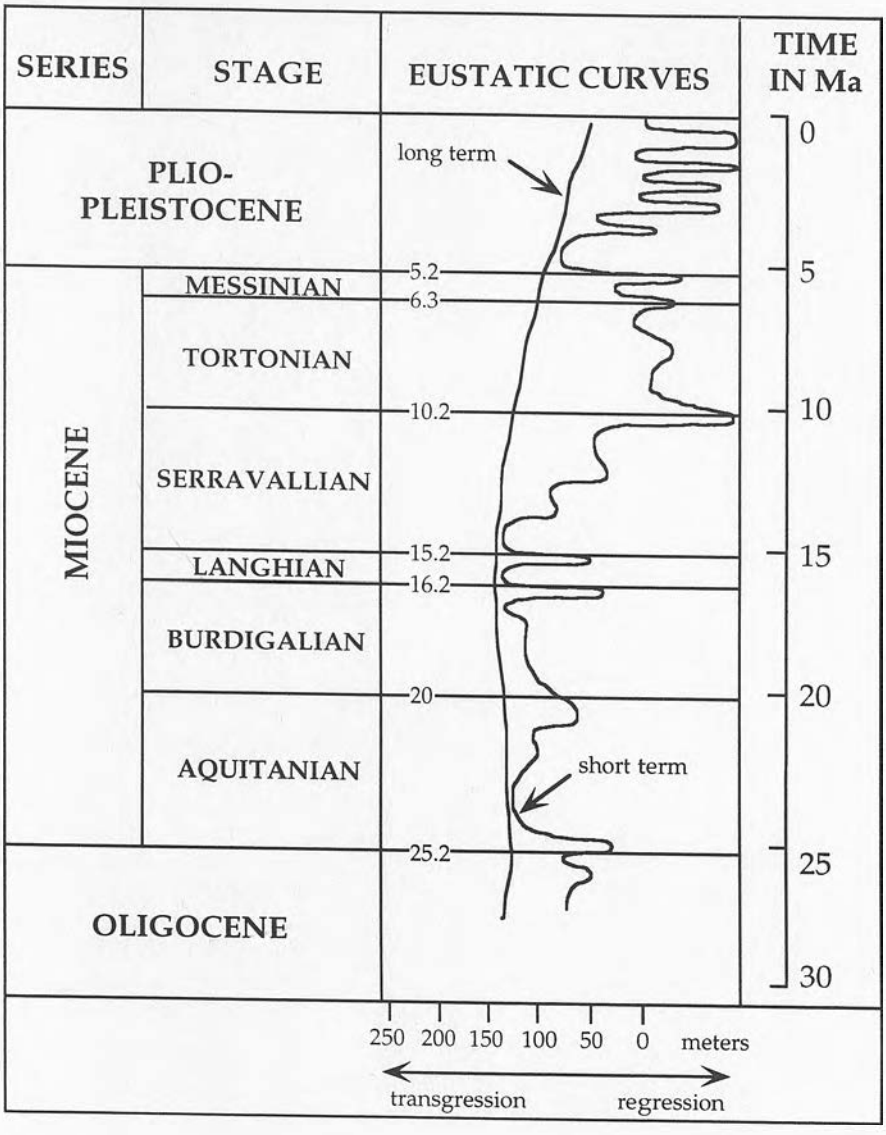

Figure 5.37 Eustatic sea level curve for the Miocene (Haq *et al.*, 1988).

Poisson (1977a). Relative to the conglomerates the turbidites are very fine -grained. The most obvious cause of this sudden dearth of conglomerate would seem to be either a cessation of tectonic uplift or a very rapid sea level rise that cuts off coarse clastic supply and allows more distal systems to feed the basin. Given that the palaeocurrents in both the Aksu and Köprü basins indicate axially derived turbidites (Figs. 4.10 and 4.16) and marginally-derived Lower Miocene conglomerates (Fig. 5.34), rapid relative sea level rise producing a new, more distal sediment source seems the more likely of the two options. The eustatic sea level curve (Haq *et al.* 1988) indicates a gradual sea level drop throughout the Serravallian.

5.10 Conclusions

- The Kizildag and Aksu Formations can be interpreted mainly as deposits of fan-delta systems.

- Alluvial, lacustrine, lagoonal, coastal and shallow-marine shelf environments have been identified.

- 7 separate fan-delta systems can be tentatively identified as having been active during two distinct time periods, the Lower-Middle Miocene (Burdigalian-Early Serravallian) and Upper Miocene (Tortonian-Lower Messinian).

- These are all shallow-shelf type fan-deltas either with well developed mouth-bar units or with small Gilbert-type foresets.

- The nature of the facies preserved suggest that these fan-deltas were fluvially dominated. There is clear evidence of wave action however, suggesting that this process was also important in reworking shoreline facies.

- The development of reef frameworks may have influenced clastic deposition. High angle foresets in coarse conglomerates are associated with reef buildups and this topography may have produced gradient changes which initiated foreset formation.

- A semi-arid climate subject to flash floods and ephemeral flow can be deduced from the alluvial facies.

- There is clear evidence of rapid relative sea level rise throughout both the Lower Miocene and Upper Miocene in the shoreline facies.

- Relative sea level rise seems to have been the most important control on fan-delta evolution, overprinting the prograding fan-delta signature despite the rapid sedimentation rate.

- Some of the relative sea level rise can probably be attributed to compaction, but the majority is thought to be tectonically induced.

- Active tectonic uplift of the hinterland caused continual coarse sedimentation.

- Eustatic processes, though potentially active are not thought to have had complete control over any of the changes in sedimentary facies seen throughout the Miocene.

Chapter 6

STRONTIUM ISOTOPE DATING

6.1 Context

Lack of good marker fossils in neritic sediments is a common dating problem which can be addressed by the use of isotopic dating methods. Consequently, $^{87}Sr/^{86}Sr$ analysis was attempted with a view to dating the deposition of the shallow water carbonates, particularly those at the base of the Miocene section in the study area (Oymapinar Limestone). Dating of these sediments permits correlation of the neritic sediments, discussion of relative sea level change and ultimately a more detailed interpretation of basin history. This study contributes to the biostratigraphic database on Miocene rocks in providing ages for previously undated key sections.

6.2 Introduction to Strontium dating

Because the residence time of Sr in the oceans is long (2.5-5Ma) relative to ocean mixing time (500-1000 yrs, e.g. Beets, 1992; Richter and Turekian, 1993; McArthur, 1994) both the Sr concentration and the Sr isotopic ratio can be assumed to be constant throughout the oceans at any given time. Sr-isotope ratios have been generally increasing with a step-like pattern since the Jurassic (Hodell, 1994) and studies over the last decade have concerned the accurate documentation of these variations particularly in the Cenozoic (DePaolo, 1986; DePaolo and Ingram, 1985; Hess *et al.*, 1986; and Koepnick *et al.*, 1985; Koepnick *et al.*, 1988). More recently workers have increasingly focused on narrower segments of the curve using independent dating methods such as biostratigraphy and magnetostratigraphy, so that the technique can be used for solving stratigraphic problems.

Originally the $^{87}Sr/^{86}Sr$ of the oceans was predicted as increasing monotonically through time due to the decay of ^{87}Rb to ^{87}Sr (Wickman, 1948). Early workers attempting to document this change (Peterman *et al.*, 1970; Veizer and Compston, 1974; Burke *et al.*, 1982) quickly realised that Sr

evolution was not monotonic, but developed irregularly with both positive and negative gradients. Causes for the shape of the oceanic Sr ratio curve have subsequently been studied in considerable detail and the following hypotheses have been put forward:

- ^{87}Sr supplied to the oceans by weathering of continental crust via rivers (Brass, 1976);
- ^{87}Sr subtracted from the ocean budget due to hydrothermal exchange of ^{87}Sr depleted basalts at mid-ocean ridges (Brass, 1976);
- Dissolution of carbonates on the sea floor adds old marine Sr whose $^{87}Sr/^{86}Sr$ is not very different from that of sea water and generally acts as a buffer (Elderfield and Geiskes, 1982; Palmer and Edmond, 1989; Richter and Liang, 1993).

6.3 Application of $^{87}Sr/^{86}Sr$ dating technique to the Miocene of the study area and the correction for radiogenic Sr

The main sink for Sr in the oceans is biogenic carbonate (Brass, 1976; Palmer and Elderfield, 1985). As organisms precipitating carbonate shells or tests do not appear to discriminate between the various isotopes of Sr (e.g. 88, 87, 86, and 84) the $^{87}Sr/^{86}Sr$ ratio can be assumed to represent the ratio in sea water at the time of formation. Radiogenic ^{87}Sr derived from the decay of ^{87}Rb can be largely ignored in the study of biogenic carbonates as they generally contain relatively low concentrations of Rb relative to Sr providing diagenetic alteration has not occurred (Elderfield, 1986). For example, uncleaned planktic foraminifera contain 6± 2 ppm of Rb, whilst their Sr concentration is in the order of 1150 ± 50 ppm (Beets, 1992) making the $Rb/Sr < 0.01$.

The sediments discussed in this chapter have been described in chapter 3. They include the shallow-water reef limestones and deeper water planktic foraminiferal marls which overlie them.

6.4 Methodology

6.4.1 Sample selection

The use of bulk samples for Sr analysis comprehends the risk of including unknown components within the sample such as clay and silt-sized detrital calcite (Beets, 1992) and, because bulk carbonates are more susceptible to diagenesis (Richter and DePaolo, 1988; Garrison, 1981) it also increases the risk of using altered samples. For this reason a variety of micro- and macro-fauna rather than bulk sediment were selected for $^{87}Sr/^{86}Sr$ analysis and these are listed in table 6.1. As not all these fauna construct their shells/tests of carbonate in its most stable form (e.g. low Mg calcite, see Table 6.1) it was essential to carry out careful screening of selected samples for evidence of diagenetic alteration from the less stable forms of carbonate (e.g. aragonite and high Mg-calcite). Even those samples composed of low Mg-calcite fauna were inspected, for visible cementation either on or in the structure of the shell/test.

Screening was undertaken in a number of ways depending on sample preservation. For instance, foraminifera were hand picked from washed and sieved (63μ) marl samples and inspected under a reflected light microscope. Those specimens showing signs of considerable abrasion or whose tests were infilled with a dark mineral thought to be pyrite, or encrusted with specks of a grey mineral thought to be manganese oxide were discarded. Some foraminiferal samples were also inspected using SEM photography. This indicated that the preservation of both benthic and planktic foraminifera was in general quite good (Fig. 6.1), although rare cases of calcite rhombs infilling chambers were observed, (Fig. 6.2). Hodell and Woodruff (1994) point out however that even though conspicuous evidence of diagenetic alteration is lacking, it is often difficult to demonstrate unambiguously that foraminiferal calcite has been completely unaffected by diagenesis.

This problem was clearly illustrated during the cleaning process. Most authors using foraminifera for Sr analysis do not indicate what method of disaggregation of the marl sample was used prior to hand-picking of the foraminifera. After picking the foraminifera however, Miller *et al.* (1991)

Figure 6.1 SEM photograph of a benthic formainifera (Florilous bonneam, C. Glover pers. com. 1995) showing excellent preservation of skeletal structure from the Ahmetler section, Manavgat basin.

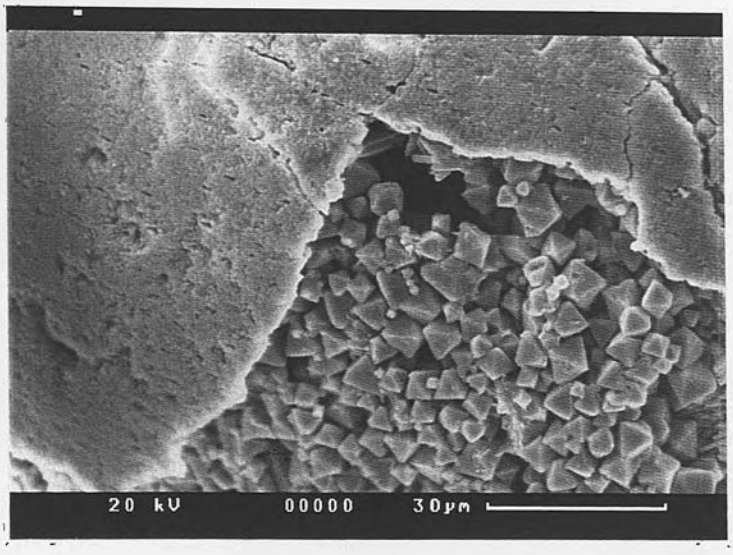

Figure 6.2 SEM photograph of a foraminifera which has been filled with diagenetic calcite rhombs.

Table 6.1 Table showing the type of carbonates found in samples used for $^{87}Sr/^{86}Sr$ analysis and the sediment in which they were preserved.

Fauna	original carbonate	Sediment	Preservation of structure	carbonate at time of analysis
Planktic foraminifera	Low Mg calcite	in marls	good	Low Mg calcite
Benthic foraminifera	Low Mg calcite	in marls	good	Low Mg calcite
Oyster	Low Mg calcite	in marls and siltstones	generally good	Low Mg calcite
Echinoid	Low Mg calcite	in calcarenites	good	Low Mg calcite
Algae	High Mg calcite	in calcarenites	good	? high/low Mg calcite
Coral	Aragonite	in marl,	good	Aragonite and low Mg calcite
		in sandstones or in reef framework interbedded with sandstones	good	Low Mg calcite
		in sandstones or in reef framework interbedded with sandstones	poor	Low Mg calcite
Gastropod	Aragonite	in marl	good	Aragonite

report cleaning their foraminifera using an ultrasound bath for 2-10s, whilst Oslick *et al.* (1994) used approximately 3s of ultrasound treatment. Müller (1990) crushed planktic foraminifera prior to washing them several times in an ultrasonic bath. Hodell *et al* (1991) in contrast do not report cleaning foraminifera using ultrasound at all. None of these authors report the amplitude and frequency of the vibrations of the ultrasound used. The rapidity with which present-day foraminifera explode when placed in an ultra sound bath depends on the frequency and amplitude of the vibrations used. In general however, they explode within a few seconds (K. Darling pers. com., 1994).

Due to lithification, marl samples containing abundant foraminifera collected for this study were initially disaggregated using an ultrasound bath (FS400b with a frequency of 35-40Khz) for 2 x 3 minutes. Hand-picked foraminifera from these samples had therefore already received ultrasound

treatment in excess of that which destroys recent foraminifera. It proved possible to expose these foraminifera to further ultrasound treatment without causing widespread disaggregation of individuals and this poses the question of why these foraminifera behaved differently from recent samples. The obvious explanation is that diagenetic alteration has filled voids in the structure and transformed the test itself, thus rendering the specimen more resistant to destruction by ultrasound vibrations. As pointed out earlier however it has proved difficult to unequivocally identify diagenetic alteration in foraminifera using light microscope or SEM techniques (Hodell and Woodruff, 1991). By not testing the resistance of their foraminiferal samples to ultrasound, other authors (e.g. Hodell and Woodruff, 1994; Miller *et al.*, 1991; Beets, 1992; Oslick *et al.*, 1994) have perhaps not explored this problem or used its implications as a method of identifying diagenetic alteration in foraminifera.

Carpenter *et al.* (1991) suggest that early marine diagenesis does not significantly alter the $^{87}Sr/^{86}Sr$, because the cements formed in this environment are in isotopic equilibrium with ambient sea water. Making the assumption that the diagenetic alteration of the foraminifera took place soon after formation and in the absence of guidance from previous workers it was decided that foraminiferal samples resistant to ultrasound treatment would be used and this issue is discussed further in the light of the results obtained (section 6.5.1.2).

Most workers using foraminifera for Sr analysis sampled planktic foraminifera (e.g. Palmer and Elderfield, 1985; Hess *et al.*, 1986; Hodell *et al.*, 1991; Miller and Feigenson, 1991). However Beets (1992) showed that there is no significant difference in the Sr-isotope ratios of benthic and planktic foraminifera. For this reason samples of mixed benthic and planktic foraminifera were used as well as samples containing only planktic foraminifera and samples of the large benthic foraminifera *Operculina*. Table 6.2 lists the samples selected, the name of their section and the type of fauna chosen.

Coral samples were inspected in a number of different ways. The majority of the corals initially selected as potential samples for Sr analysis were *Porites sp.* reflecting the relative abundance of this type of coral. Poritids have small

corallites making species distinctions difficult in all samples. In the samples recovered from the study area it was found to be almost impossible to classify *Porites sp.* corals to species level because almost without exception thin sections revealed that the finely ornamented structure on which distinctions are made, were replaced with secondary calcite. A few of these corals were selected for Sr analysis despite the knowledge that they were diagenetically altered as it was hoped that information concerning the timing of diagenesis might be gained. Where other types of coral were selected and identified, thin section study sometimes revealed that only partial diagenetic alteration appeared to have taken place. Some of these samples were subsequently analysed by x-ray diffraction methods (XRD) to ascertain what minerals were present and by comparing the size of the peaks to standards of known aragonite:calcite composition an estimate of the ratio of the two minerals was ascertained. If the quantity of sample was sufficient the calcite and aragonite were then separated using heavy liquids (Appendix 1). Two coral samples were inspected using an energy dispersive spectroscopic microprobe (LINK system). The mean Sr values for these two samples were 0.7% and 0.65% values far closer to the percentages found in living Scleractinid aragonite (approximately 0.8%) than they are for diagenetic low magnesium calcite (0.02%), although this latter figure does depend to some extent on the Sr concentration of the fluids involved. SEM photographs taken of these same samples reveal good preservation of skeletal fibres (Fig. 3.11). There has been some preferential dissolution along organic-rich growth lines, but there is no evidence of general calcitization (C. Cuif pers. com., 1994).

Screening the algae for diagenetic alteration proved to be very difficult. In thin section evidence of widespread replacement by spar was absent and the preservation of the detailed structure of the algae was generally good. Samples were subsequently drilled from algal crusts as in Beets (1992), but no attempt was made to determine whether diagenetic alteration had taken place to low Mg calcite. Rare gastropod samples that were selected for Sr analysis were first analysed using XRD to determine if aragonite was still present. In hand specimen samples retaining primary carbonate were relatively easy to identify since they had a very fragile structure and were faintly pink in colour. This sort of preservation was exclusively associated with fine-grained, clay-rich marl rather than calcarenites or sandstones.

Table 6.2 List of the fauna used for $^{87}Sr/^{86}Sr$ analysis.

Section name	Basin/area	Sample no	Fauna
Alarahan	S Manavgat	4j.Alarahan.1	*Porites sp.*
		4j.Alarahan.2	*Porites sp.*
		4j.Alarahan.3	*Porites sp.*
		4j.Alarahan.4	*Porites sp.*
		10j. Alarahan.5	*Operculina*
		8O.Alarahan.1	planktic foraminifera
		8O. Alarahan.2	planktic foraminifera
		8O. Alarahan.3	planktic foraminifera
Ahmetler	N Manavgat	12j.Ahmetler.1	algae
		16S.313.6	algae
		12j.Ahmetler.2	algae
		16S.313.7	algae
		16S.341.6	planktic foraminifera
Yaylaalan	N Manavgat	14j.290.2	echinoid
		14j.290.5	algae
		14j.290.6	mixed foraminifera
		14j.290.7	mixed foraminifera
Oymapinar	N Manavgat	13j.Oymapinar.4	echinoid
		13j.Oymapinar.7	mixed foraminifera
		13j.Oymapinar.8	mixed foraminifera
Saburlar	central Manavgat	11j.295-6.1	*Operculina*
		11j.295-6.2	algae
		11j.295-6.3	Porites
		30A.296.3	mixed foraminifera
Deniztepesi	south Köprü	25S.373.6	algae
		25S.373.3	oyster
		16J.373.2	mixed foraminifera
		16j.373.1	mixed foraminifera
Bucakkoyu	south Köprü	17J.416.6	mixed foraminifera
		18j.417.4	algae
		18j.417.2	algae
		18J.417.5	mixed foraminifera
		18J.417.6	mixed foraminifera
Aspendos	south Köprü	17j.415.1	echinoid
		17j.415.2	gastropod
		17j.415.3a-c	gastropod
		17j.415.4	mixed foraminifera
Altinkaya	Central Köprü	19J.181.2	oyster
		"19J.181,1a"	oyster
		19J.180.2	algae
Ballibucak	Central Köprü	16J.163.3	algae
		16J.164.2	oyster
Kesme	NE Köprü	26j.399.1b	oyster
Yesilbag	NE Köprü	27j.Yesil.3	algae
		27j.Yesil.9	oyster
Dumanli	NE Köprü	22m.407.1	mixed foraminifera
Çetmi	NE Köprü	22m.404.3	oyster
		20j.421.1	algae
Kargi baraj	Central Aksu	15M.1	oyster
		15M.3	oyster
		15M.5	oyster
Sipahiler	NW Köprü	30J.236.8	algae

Oysters from the Kargi baraj section were studied in thin section before being drilled from remaining sample blocks. Good shell structure was apparent in all thin sections and Jones *et al* (1994) report that they successfully used oysters from the Jurassic to document Sr ratios.

Two samples drilled from well preserved echinoid tests were included amongst those selected for Sr analysis. Although echinoid shells are made of low Mg calcite, their structure is a porous one and easily altered by diagenesis (S. Hesselbo pers. com., 1994).

6.4.2 Cleaning methods

All samples were cleaned in pure ethanol in an ultrasound bath for up to 40 minutes. Foraminiferal samples were inspected regularly and removed from the ultrasound bath once disaggregation of individual foraminifera began. The foraminifera were rinsed with clean ethanol and removed using a pipette and dried in the oven. Other samples were rinsed in clean ethanol and dried on filter paper. Samples were then ground down to powder using a pestle and mortar and weighed to an accuracy of 5 decimal places.

6.4.3 Chemistry

Weighed samples were placed in teflon beakers and 10ml of 2.5M HCL was added to dissolve the sample. After several hours the sample was inspected to ensure that complete dissolution had occurred and centrifuged for about 5 minutes to remove any particulate matter remaining undissolved. The sample was then loaded into a pre-conditioned cation exchange column containing Bio-Rad AG50W-X8, 200-400 mesh resin. 2 x 1ml of 2.5M HCL was used to rinse the sample down into the column, and it was then eluted with 42ml of 2.5M HCL. The Sr was subsequently collected using 10ml of 2.5M HCL in a cleaned teflon beaker and evaporated under a lamp for several hours. When dry, a single drop of concentrated nitric acid was added and left to evaporate. This converts the Sr-chlorides to Sr-nitrates which give better ion yields. A total procedure blank run through this chemistry was found to contain 0.6 ng of Sr. Relative to the Sr content in the samples studied, this is negligible.

6.4.4 *Mass Spectrometry*

Re and Ta single filaments were constructed using filament supports that had been boiled in RO water and outgassed for 10 minutes at 4.5A in a vacuum $<1x10^{-5}$ torr. Due to the small size of some the samples two methods of loading were used. The larger samples were dissolved in 1 µl of 1M phosphoric acid (H_3PO_4) and loaded on to a Ta filament. Small samples were loaded in the same way onto Re filaments which had already been loaded with 1 µl or less of H_3PO_4 and 1 µl of a tantalum activator which is prepared by dissolving Ta_2O_5 powder in dilute HF. This method is similar to that of Brick (1986). The tantalum activator enhances the ionisation potential of Sr allowing the analysis of smaller samples to a comparable precision to the H_3PO_4 method. All loaded filaments were dried gradually by passing a small current (1-1.5A approx.) through them. This current was then increased until white fumes of phosphoric acid could be seen and the filament glowed dull red. Loaded filaments were then fixed into a 20 sample turret head.

A VG Sector 54-30 mass spectrometer in dynamic multicollection mode was used to measure the Sr isotope abundances. A beam intensity for mass 88 of 1V (±10%) and a filament current of around 2.5A were selected. The measuring cycle used was 84.5, 86, 87, 88 axial masses with the following collector spacings from axial: L3-4 amu; L2-2 amu; L1-1 amu; H1 + 1 amu and H2 + 2 amu. Peak intensities were corrected for zero and Rb interference where necessary. The $^{87}Sr/^{86}Sr$ ratios were corrected for instrumental mass fractionation to a $^{86}Sr/^{88}Sr = 0.1194$ using an exponential fractionation law. Isotope ratios were collected in 15 blocks of ten cycles and the mean and standard error for each block and the whole population were calculated. Up to 10% of the values falling outside 2σ were rejected and post-rejection means and standard errors were calculated. If necessary the beam was refocused and the aiming intensity restored between blocks. Typical in-run precision of ± 0.00012% is achieved for 150 ratios. Repeat analyses of the NBS 987 standard during and prior to this study give an $^{87}Sr/^{86}Sr = 0.710237 \pm 26$ (2S.D.).

6.4.5 *Calculations*

Two recently published Miocene $^{87}Sr/^{86}Sr$ sea water curves (Hodell and Woodruff, 1994; Miller *et al.*, 1991) were used to provide the geochronological reference. Although other curves have been published recently, these two were selected because they used different methods to link data points.

Miller *et al.* (1991) interpreted the spread of Sr ratios for the Miocene on a plot of $^{87}Sr/^{86}Sr$ versus age and deduced a linear evolution with a change in gradient at 14.5-14.7 Ma (Fig. 6.3). These two relationships are described as:

<u>For 25.1-14.7 Ma</u>

Age (Ma) = $11906.91 - [16777.17 \times (^{87}Sr/^{86}Sr)]$

with a correlation coefficient, $r^2 = 0.984$, $n = 38$

<u>For 14.5-8.3 Ma</u>

Age (Ma) = $56239.94-[79319.75 \times (^{87}Sr/^{86}Sr)]$

with a correlation coefficient, $r^2 = 0.603$, $n = 30$

An NIST 987 Strontium standard value of 0.710252 is reported.

Hodell and Woodruff (1994) pursue a different line. They claimed that the entire Miocene sea water curve could be best described using a high order polynomial function. They specified a ninth order polynomial best fit, but did not report either the equation or the regression coefficient used. Plotting up their data and fitting the highest order polynomial function (5th order) available on the software package (Cricket Graph 1.3.2, see Fig. 6.3), the following relationship was derived.

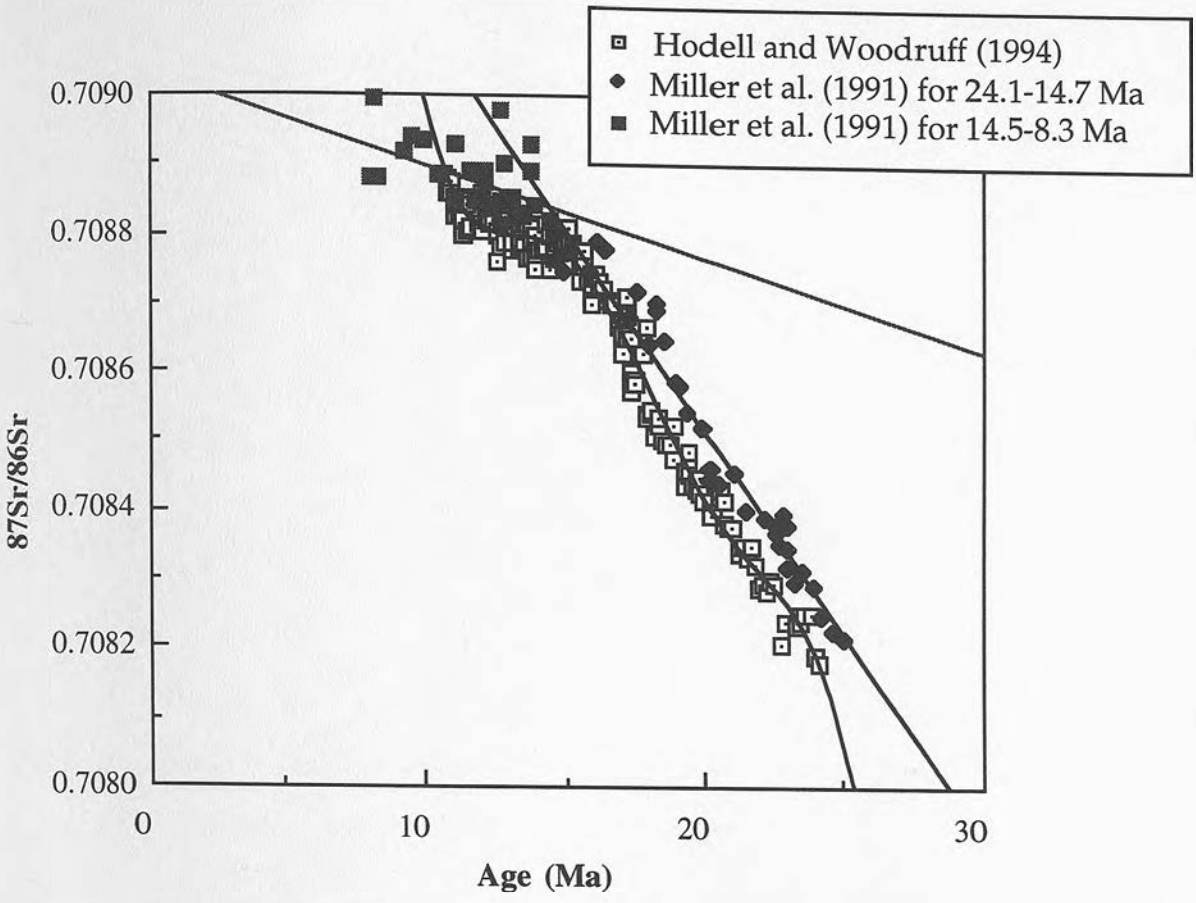

Figure 6.3 Graph of Sr ratio versus Age showing the two linear regressions relating the data of Miller et al. (1991) and a 5th order polynomial best fit through the data reported by Hodell and Woodruff (1994).

For 10.74-24.14 (Ma)

$$^{87}Sr/^{86}Sr = 0.75044 - 1.2802\times10^{-2} \times [\text{Age (Ma)}] + 1.5413\times10^{-3} \times [\text{Age (Ma)}]^2 - 9.0592\times10^{-5} \times [\text{Age (Ma)}]^3 + 2.5960\times10^{-6} \times [\text{Age (Ma)}]^4 - 2.9104\times10^{-8} \times [\text{Age (Ma)}]^5$$

with a correlation coefficient, $r^2 = 0.985$, $n = 171$

Data was normalised to a constant standard reference material NIST-987 = 0.710235.

Because polynomial equations higher than 4th order are algebraically insoluble, the roots of this 5th order equation were calculated for the measured $^{87}Sr/^{86}Sr$ values by iteration.

For calculation purposes all $^{87}Sr/^{86}Sr$ were normalised to the relevant standard by the addition/subtraction of the difference between the measured values of NBS-987 reported (e.g. Miller *et al.*, 1991 and Hodell and Woodruff, 1994 respectively) and those measured during and prior to Sr analysis in East Kilbride (NBS-987 = 0.710237 and 2 S.D. = 0.000026, see for instance Miller *et al.*, 1991).

6.5 Results

Appendix 2 lists all the $^{87}Sr/^{86}Sr$ values measured and the ages calculated using the equations derived from both Miller *et al.* (1991) and Hodell and Woodruff (1994). Errors for these ages were also generated using the analytical error.

6.5.1 Assessment of the validity of the ages

6.5.1.1 Comparison of the two Sr sea water curves

Figure 6.4 is a chart showing the ages and errors derived from $^{87}Sr/^{86}Sr$ analysis for those samples for which independent nannoplankton zones were available (C. Müller pers. com., 1992 and 1994) and using the boundaries defined by Berggren *et al.* (1985, Fig. 2.2). All these samples were either planktic foraminiferal samples or mixed benthic and planktic foraminiferal samples, picked from marls overlying shallow water

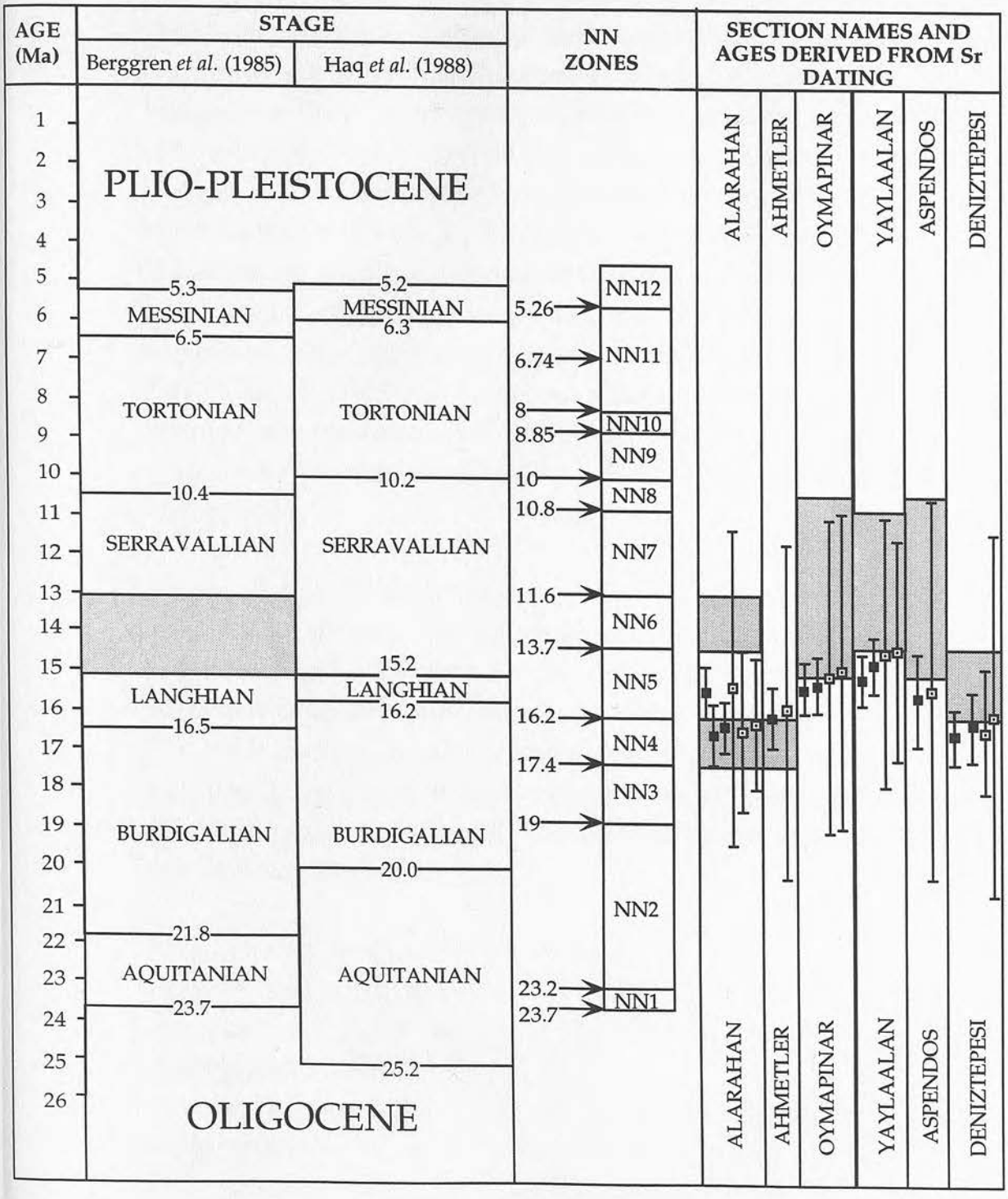

Figure 6.4 Chart showing the ages derived for foraminiferal samples by Sr analysis and their NN zones (C. Müller pers. com., 1992 and 1994). Black squares are derived using the straight line fit from Miller et al. 1991. White squares are derived using a 5th order polynomial fit through Hodell and Woodruff's (1994) data. Shaded areas are the biostratigraphic ages from nannoplankton analysis of the same samples (C. Müller pers. com., 1993; 1994). See text for more details.

carbonates (Table 6.2). Figure 6.4 shows ages calculated using the equations and $^{87}Sr/^{86}Sr$ curves from both the Lower Miocene of Miller *et al* (1991) and Hodell and Woodruff (1994) and these vary systematically depending on the regression equation used (Appendix 2) with the ages from Hodell and Woodruff (1994) always being slightly younger than those of Miller *et al.* (1991) This is due to the difference in the data sets used to define each curve (see Fig. 6.3). Much more spectacular than the variation in age however is the variation in the error bars for the two models (Fig. 6.4; Appendix 2). Those calculated using Hodell and Woodruff's polynomial best fit are up to 5 times larger than those calculated using Miller *et al.*'s simple linear regression. This discrepancy is due to the coincidental proximity of the foraminiferal $^{87}Sr/^{86}Sr$ values to a pronounced inflection point on the polynomial curve (Fig. 6.5). Thus, even relatively small errors on the data span a nearly horizontal part of the curve and result in 1 σs for age of up to 4 million years.

Assessment of which of these two curves is the more valid is beyond the scope of this project. The data reported here merely serve to illustrate the large discrepancies between the results generated by each model in particular regions of the Miocene. A better constraint on how the global $^{87}Sr/^{86}Sr$ changes with time during the Miocene will only be gained by producing more independently generated curves from different regions, correlating them and attempting to understand what controls the changes in gradient (e.g. Hodell, 1994).

Because the majority of the $^{87}Sr/^{86}Sr$ measured lie within error of this point of inflection on the Hodell and Woodruff (1994) polynomial curve, ages calculated using this curve were discounted and only those calculated using the regression line according to Miller *et al.* (1991) will be discussed further. It should be noted however that the problem really lies in the data sets on which these curves are based. Both papers document a change in slope in this region of the graph (see Fig. 6.3), but the combination of Millers *et al.*'s apparently older data set and their chosen point of inflection (in an area of no data!) allows the Sr ratios for this study to be calculated using Miller's Lower Miocene curve with the high correlation coefficient rather than his Upper Miocene curve with its very poor correlation coefficient (sections 6.4.5 and 6.5.2.2). Because of this and the assumption that a polynomial

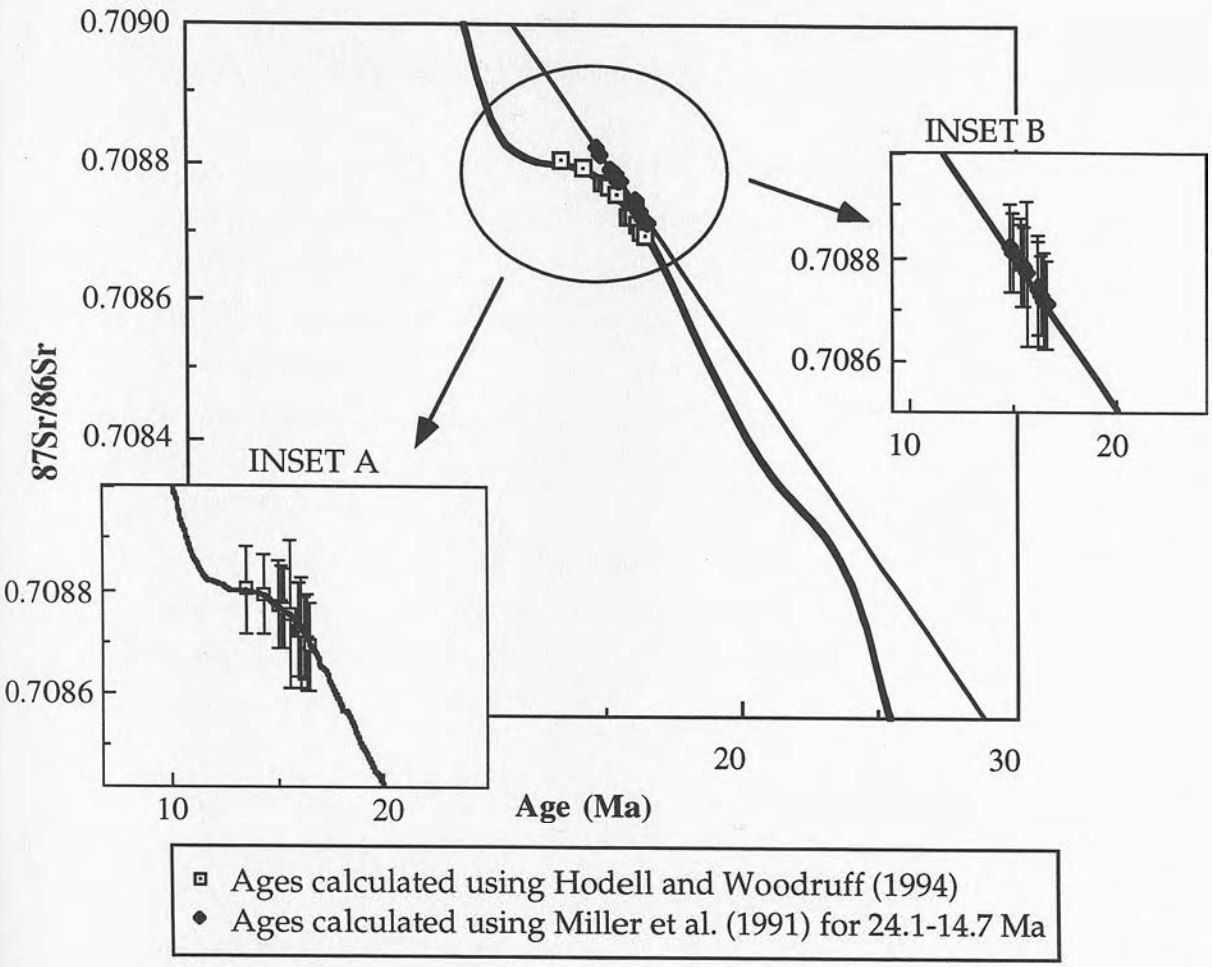

Figure 6.5 Graph of Sr ratio versus Age (Ma) with the two regression lines relating to the Lower Miocene linear best fit of Miller et al. (1991) and the 5th order polynomial fit of Hodell and Woodruff (1994). Sr isotope ratios for foraminiferal samples shown in Fig 6.5 are plotted using the two regressions to calculate the age. Note that the ages calculated using the polynomial best fit are systematically younger than those of the simple linear regression. Insets A and B are details of the area circled showing the error bars calculated using the two regression equations. Note that the equivalent age errors for the polynomial regression will be much larger than those for the simple linear regression.

relationship does not describe the evolution of $^{87}Sr/^{86}Sr$ with time, all the age data presented here should be treated with caution.

6.5.1.2 Foraminiferal samples

The stratigraphic positions of the foraminiferal samples in individual sections generally correlates with the ages generated using Miller *et al.* 's (1991) method and are within error of the nannoplankton zones identified for these samples. This suggests that late diagenetic processes did not significantly alter the original Sr sea water ratio incorporated into the foraminiferal test (Beets and De Ruig, 1992). Carpenter *et al.* (1991) showed that early diagenetic cementation, if active, may not have altered the $^{87}Sr/^{86}Sr$ to any great extent as secondary calcite and aragonite are in isotopic equilibrium with ambient sea water. It seems likely therefore that the resistance of some foraminiferal samples to ultrasound treatment is due to early diagenetic alteration, which has not significantly altered their Sr composition.

Loss of the primary Sr isotopic signature does occur however, when sediments are subject to open-system behaviour (Quinn *et al.*, 1991; Scoffin 1987) i.e. input of extrinsic Sr with a different $^{87}Sr/^{86}Sr$ from that of the sediments. This may have occurred in the two sections where the ages do not match stratigraphic positions i.e. at Deniztepesi and Yaylaalan (Fig. 6.4 and Appendix 2). This is discussed further in section 6.6.

6.5.1.3 Macrofossil samples

The lack of correlation between the ages generated by $^{87}Sr/^{86}Sr$ dating and the relative stratigraphic positions of the Poritid coral samples in the Alarahan section (see Table 6.4) illustrates the alteration of the Sr isotopic composition on transformation from aragonite to low Mg-calcite (Appendix 1, XRD data).

The algal samples from the Ahmetler section show a similar lack of correlation (table 6.5) also suggesting a diagenetic influence and that transformation from high Mg-calcite to low Mg-calcite has occurred despite there being no visual evidence for it.

Table 6.4 Measured values of $^{87}Sr/^{86}Sr$ and the ages calculated using the Lower Miocene regression from Miller et al. (1991) for the Porites sp. samples in the Alarahan section. The results are arranged in stratigraphic order, e.g. lowest sample at the bottom of the table.

Sample number	2 S.E. (ppm)	Dynamic $^{87}Sr/^{86}Sr$ measured	Dynamic $^{87}Sr/^{86}Sr$ normalised to Miller *et al.* (1991)	Age (Ma) for 25.1-14.7 Ma from Miller *et al.* (1991)
4j.Alarahan.4	24	0.708613	0.708628	18.13
4j.Alarahan.3	24	0.708365	0.708380	22.30
4j.Alarahan.2	26	0.708350	0.708365	22.55
4j.Alarahan.1	26	0.708357	0.708372	22.43

Table 6.5 Measured values of $^{87}Sr/^{86}Sr$ and the ages calculated using the Lower Miocene regression from Miller et al. (1991) for algal samples in the Ahmetler section. The results are arranged in stratigraphic order, e.g. lowest sample at the bottom of the table.

Sample number	2(S.D.)	Dynamic $^{87}Sr/^{86}Sr$ measured	Dynamic $^{87}Sr/^{86}Sr$ normalised to Miller *et al.* (1991)	Age (Ma) for 25.1-14.7 Ma from Miller *et al.* (1991)
16S.313.7	26	0.708688	0.708703	16.879
12j.Ahmetler.2	22	0.708728	0.708743	16.208
16S.313.6	26	0.708662	0.708677	17.315
12j.Ahmetler.1	26	0.708736	0.708751	16.074

Sr ages generated for the three oysters samples from the Kargi baraj section (Table 6.6) also failed to show systematic correlation with stratigraphic position. Of the other 7 oyster samples loaded, 4 aborted before completing all 15 blocks and two of these samples showed anomalously high Rb contents as inferred from the Rb interference measured during Sr analysis.

In this case then it seems that the assumption that radiogenic ^{87}Sr from the decay of ^{87}Rb can be ignored due to the relatively low concentrations of Rb in biogenic carbonates (Elderfield, 1986) cannot be sustained probably due to diagenetic alteration and the $^{87}Sr/^{86}Sr$ measured should be treated with caution (section 6.3). Jones *et al.* (1994) report successfully using oysters from the Jurassic for Sr dating.

It was not possible to assess the correlation of Sr ages with stratigraphic position for echinoids, operculinids, or gastropods independently as no section had sampled a series of each of these fossils. However, in relation to other fossils, the Sr ages for operculinids and gastropods where XRD showed that primary aragonite had been retained (Appendix 1), indicated that they correlated well with stratigraphic position. Echinoids have a more ambiguous record.

Table 6.6 Measured values of $^{87}Sr/^{86}Sr$ and the ages calculated using the Lower Miocene regression from Miller et al. (1991) for oyster samples in the Kargi section. The results are arranged in stratigraphic order, e.g. lowest sample at the bottom of the table.

Sample number	2(S.D.)	Dynamic $^{87}Sr/^{86}Sr$ measured	Dynamic $^{87}Sr/^{86}Sr$ normalised to Miller *et al.* (1991)	Age (Ma) for 25.1-14.7 Ma from Miller *et al.* (1991)	Age (Ma) for 14.5-8.3 Ma from Miller *et al.* (1991)
15M.1	26	0.708727	0.708742	16.225	
15M.3	20	0.708848	0.708863		13.104
15M.5	24	0.708722	0.708737	16.309	

6.5.2 *Ages of the shallow water carbonates and the transgression surface*

Prior to this work, only one of the shallow-water carbonate successions had been directly dated (Oymapinar section; Poisson, pers. com. 1992). The ages produced by $^{87}Sr/^{86}Sr$ analysis for these neritic sediments therefore provide valuable information about the timing of transgression (i.e. the lower surface of the shallow-water carbonates) rather than the age of the transition to

planktic foraminiferal marls (chapter 4). $^{87}Sr/^{86}Sr$ ratios from these marls were used to confirm the validity of the results by comparison with biostratigraphic ages. Furthermore, this work has allowed the study of previously undated sections. Particularly important is the Bucakköyü section in the west of the Köprü basin, where shallow-water carbonates are found within a thick succession (~1.5km) of conglomerates. The results of this study are discussed in the light of their structural implications in chapter 7.

6.5.2.1 Lower-Middle Miocene

The ages derived from Sr dating of the shallow water carbonates, where not automatically discounted due to evidence of diagenetic alteration, are shown in figure 6.6. The samples from the Manavgat basin show a younging trend from south east to north west spanning the Burdigalian to Earliest Langhian (Berggren *et al.*, 1985) or NN2 - NN5. In accordance with the log correlation shown in figure 4.24 this suggests that the Mesozoic basement was transgressed from the south and that this transgression took place during the Burdigalian. Samples from the western side of the Köprü basin, though located further north than those of the Manavgat basin span a similar time (NN2-NN4; Fig. 6.6). This has been interpreted as indicating that the Köprü basin already had significant basinal topography during the Early Miocene allowing an earlier marine influence than on the more peneplaned Manavgat area. This is in agreement with sedimentological data discussed in chapter 5.

The Sr ages for the foraminiferal samples show a similar, though less exaggerated pattern of diachroneity to that of the shallow water carbonate samples, such that sections where early shallow water carbonate has been preserved also contain early evidence of deeper water marls. Although no sections which did not contain shallow water carbonate were sampled and analysed, it seems probable that deposition outside the Manavgat basin was controlled by local structure and tectonics. This is discussed further in chapter 7.

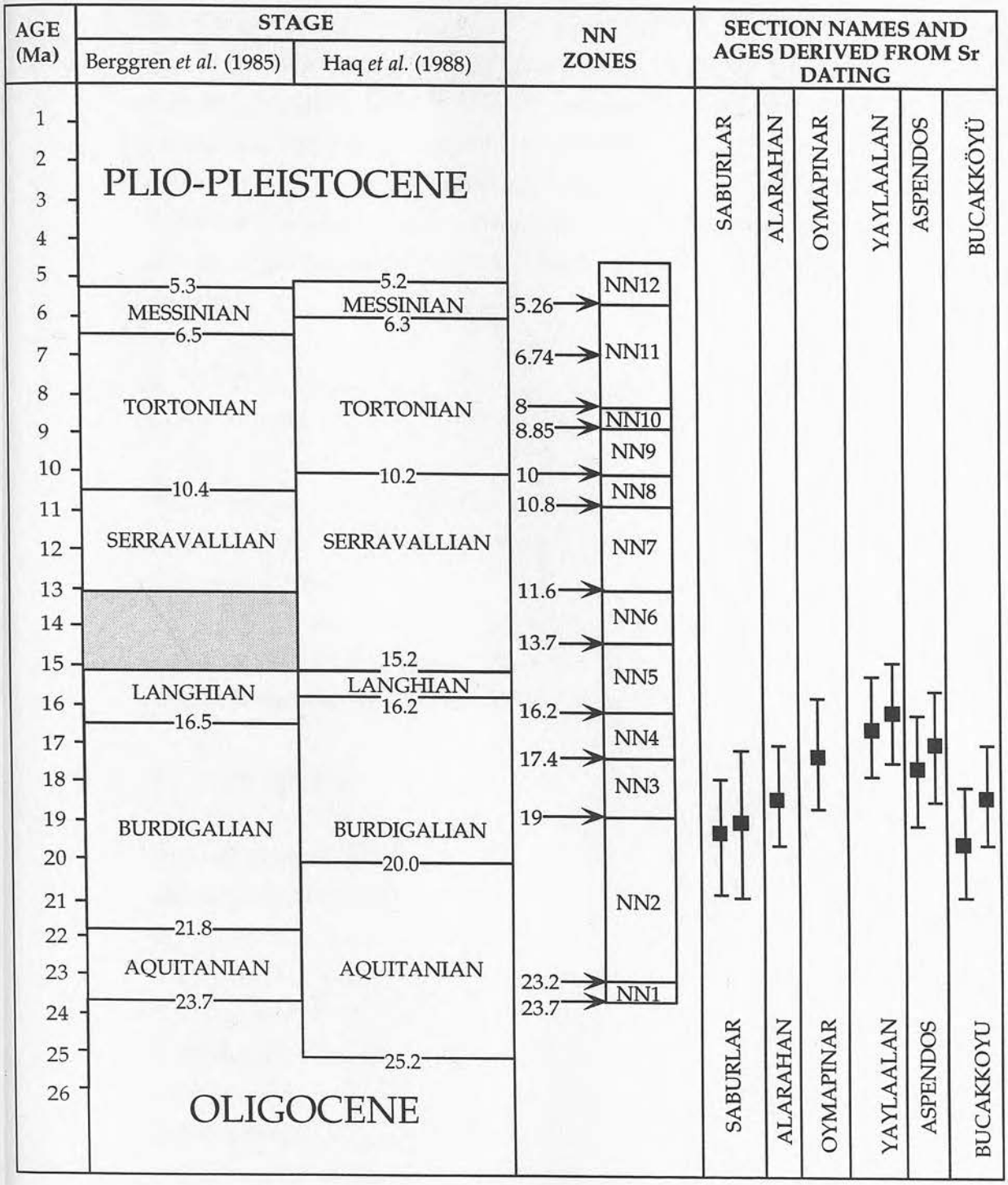

Figure 6.6 Chart showing the ages derived from non-foraminiferal samples by Sr analysis using the linear fit from Miller *et al.* 1991.

6.5.2.2 Upper Miocene

Only three of the 54 samples measured had a $^{87}Sr/^{86}Sr$ equivalent to Upper Serravallian or younger. The imbalance is partially due to a sampling bias in that the Lower Miocene reefs are not only more abundant but also better preserved than the Upper Miocene reefs in the study area. It is possible however that diagenetic alteration resulted in lower $^{87}Sr/^{86}Sr$ in some Upper Miocene samples (see discussion below). Calculating the equivalent ages of the younger samples in some cases proved problematic for the following reasons.

- The regression coefficient for the Upper Miocene given by Miller *et al.* (1991) is very low ($r^2 = 0.603$). There is little confidence therefore that this evolution line fits the data points.
- The polynomial fit of Hodell and Woodruff (1994) is not valid beyond the influence of their data points. Thus samples with $^{87}Sr/^{86}Sr > 0.708884$ (i.e. younger than 10.74 Ma) cannot be calculated.
- The convergence of Africa and Eurasia resulted in the isolation and desiccation of the Mediterranean at the end of the Miocene. It is not clear when global Sr curves become invalid for the Mediterranean (Müller *et al.*, 1990).

6.6 Diagenesis

In seven out of the 11 foraminiferal samples where independent nannoplankton zones were identified, the Sr ages obtained, though within error, are on the old side (Fig. 6.4). The Sr values of diagenetically altered corals in the Alarahan section produced ages of between 22.5 and 18.1 using the regression of Miller et al. (1991) or 21-17.5 according to Hodell and Woodruff (1994) (table 6.4), significantly older than expected (e.g. Upper Burdigalian). All Sr curves for the Lower-Middle Miocene (e.g. Miller *et al.*, 1991; Hodell *et al.*, 1991; Oslick *et al.*, 1994; Hodell and Woodruff, 1994) predict that diagenetic alteration in a marine environment occurring substantially later than formation would result in a higher $^{87}Sr/^{86}Sr$ value (see Fig. 6.3). It would seem reasonable to infer therefore that the low $^{87}Sr/^{86}Sr$ values of the Alarahan coral samples are not entirely the product of diagenetic alteration in a fully marine environment.

Rapid stabilisation of primary aragonite and high Mg-calcite to low Mg-calcite occurs in the freshwater phreatic (5000 yrs) and vadose (100000-200000 yrs) zones whilst stabilisation in marine phreatic environments where minerals have stayed in contact with trapped formation waters can take up to 3 million years (Scoffin, 1987). Freshwater $^{87}Sr/^{86}Sr$ ratios are influenced by the geology of the basement through and over which it passes. When looking at the $^{87}Sr/^{86}Sr$ of Messinian evaporites in the Mediterranean, Müller *et al.* (1990) assumed that the $^{87}Sr/^{86}Sr$ composition of the rivers emptying into the Mediterranean is the same today as it was during the Miocene because the source area has not changed much since then (Albarede and Michard, 1987). Today, the mean $^{87}Sr/^{86}Sr$ value of river water from the Nile is 0.7060 (Brass, 1976; Albarede and Michard, 1987) much lower than both the present day sea water $^{87}Sr/^{86}Sr$ value and the range of values for the Miocene (0.708-0.709) and this is attributed to the hinterland basement being largely Mesozoic carbonate and mafic rocks. A hinterland dominated by heavily karstified Mesozoic limestone (Degirmenci, 1992) and mafic rocks surrounds the study area (Fig. 1.4) suggesting that run off in this region is also likely to have low $^{87}Sr/^{86}Sr$ values. Thus, diagenetic alteration influenced by freshwater may account for the anomalously low $^{87}Sr/^{86}Sr$ of the coral samples.

The ratio of Sr in fresh water to sea water is 1:10 (Müller, 1990). Thus high concentrations of fresh water would be required to influence the Sr ratios in a marine environment. Even in very marginal reef carbonate settings with high, but variable volumes of run-off, the $^{87}Sr/^{86}Sr$ does not appear to be influenced by freshwater $^{87}Sr/^{86}Sr$ values (S. Tudhope and R. Ellam pers. com., 1994) although it is possible that in this case the run-off had a similar $^{87}Sr/^{86}Sr$ to sea water. It therefore seems likely that the diagenetic event that led to the changing of the Sr signature occurred in a non-marine environment e.g. in an open system (Quinn *et al.*, 1991; Scoffin, 1987)

Although it is possible that the entire $^{87}Sr/^{86}Sr$ signature preserved in these corals is due to the most recent period of exposure to an open fresh water system (e.g. ~Middle Pliocene, C. Glover pers. com., 1994) it is possible that it occurred during the Late Miocene when a combination of the Messinian draw down (Hsü *et al.*, 1973) and the Aksu phase compressional event

(Poisson, 1977) is likely to have left most, if not all of the study area above sea level.

6.8 Conclusions

- A diachronous transgression from south to north identified using nannoplankton biostratigraphy of planktic foraminiferal marls (Geceleme Formation) affected the Manavgat basin during the Burdigalian (chapter 4). This is confirmed by $^{87}Sr/^{86}Sr$ dating of the neritic sediments (Oymapinar Limestone).

- A Lower-Middle Burdigalian age was produced for a previously undated key section in the west of the Köprü basin.

- Deposition of shallow-water carbonates occurred earlier in the western central part of the Köprü basin than in the north of the Manavgat basin.

- Fresh water diagenetic alteration of samples may result in significantly lowering the $^{87}Sr/^{86}Sr$ due to the domination of the hinterland by Mesozoic carbonate and mafic rocks.

- The accuracy of calculated ages for the Mid Miocene are difficult to assess due to a change in the gradient of the $^{87}Sr/^{86}Sr$ curve. Further detailed study of the global Sr curve at this time is needed both to aid the use of this technique as a chronological tool and in understanding the controls over such changes in gradient.

- The low gradient of the global $^{87}Sr/^{86}Sr$ curve in the Upper Miocene means that error bars on the ages for this time period are large. In the Mediterranean however Late Miocene isolation from the global oceans means that the Sr curve is not valid. Further Sr analysis on mid-Mediterranean samples is needed to pin down when fluvial input to the Mediterranean first began to affect the $^{87}Sr/^{86}Sr$. Comparison between the east and west Mediterranean would add to the understanding of the relative independence of intra-Mediterranean basins during the Messinian.

- Foraminifera which are resistant to ultrasound treatment have probably suffered diagenetic alteration.

Chapter 7

STRUCTURE AND TECTONIC CONTEXT

7.1 Context

Brittle and ductile structures measured in the field area are considered along with inferred structural information from sedimentary facies and thickness variations. Observations of this kind have been used by other authors to support various models for the evolution of the Isparta Angle during the Miocene. Stress-field analysis from this information is not possible however without taking into account the strong N-S structural grain of basement rocks (e.g. Antalya Complex, section 1.4). Development of Miocene basins must also be seen in terms of the wider picture of tectonic processes active in the Eastern Mediterranean at the time, e.g. westward expulsion of the Anatolian block and subduction along the Hellenic trench.

7.2 Organisation of this chapter

Section 7.3 is a brief summary of the structural setting of the Isparta Angle which has been discussed at greater length in chapter 1 (section 1.4). This is followed by a résumé of the previous work which focused on the structural development of the area. Section 7.5 presents the data collected during field seasons as part of this study. Deformational structures, both from direct observation, and inferred indirectly from other field evidence, are discussed and interpreted. This section has been divided into two parts in order to treat the Manavgat basin separately from the Aksu and Köprü basins. This was thought necessary because of the difference in orientation, both of the present-day basin margins, and the structures within them. Published models of the evolution of the Isparta Angle during the Miocene and Plio-Quaternary are considered in section 7.6 in the light of the data presented here, and a new model is proposed.

7.3 Introduction

The Miocene sedimentary basins under study here are contained within in a zone known as the Isparta Angle ("Coubure d'Isparta"; Blumenthal, 1963) which sits at the junction between the Hellenide and Tauride arcuate orogenic belts and is bounded on either side by Mesozoic allochthonous units (e.g. Lycian Nappes, Beysehir-Hoyran-Hadim Nappes; Fig. 7.1). Tightening of this angle occurred during the Miocene and at the Miocene-Pliocene boundary producing compressive deformational structures in Miocene sediments. Within this compressional context, very few extensional features obviously relating to the formation of the Aksu, Köprü and Manavgat basins are apparent. Extension can be inferred however, from sedimentary thickness variations in the Manavgat basin and small micro-faults, at, or near, the base of Miocene sections (see below). Reactivation of Miocene and older structures is a constant source of complexity in an area which has suffered multiple tectonic events dating back to the Triassic (Robertson and Woodcock, 1982; Senel, 1984). It is within this historical framework that structures observed and measured in Miocene sediments from the study area are considered and discussed in terms of the basin evolution.

7.4 Previous work

The Palaeozoic-Recent history of the study area has been the subject of research over the last 20 years and has in some instances occasioned vigorous debate (for synthesis see Robertson and Dixon, 1984). Much of this centres on the origin and emplacement (mode and direction) of the Antalya Complex, which forms part of the basement to the Miocene basins within the Isparta Angle (Figs. 7.1 and 7.2, e.g. Lefevre, 1967; Brunn *et al.*, 1971; Dumont *et al.*, 1972; Brunn, 1974; Poisson, 1977; Monod, 1977; Ricou *et al.*, 1979; Hayward, 1984; Robertson and Woodcock, 1980; 1982; 1984; Poisson, 1984; Ricou *et al.*, 1984; Waldron, 1984; Marcoux *et al.*, 1989; Robertson, 1993). A more detailed outline of the debate surrounding the Antalya Complex is given in chapter 1 (section 1.4), but for the purposes of this chapter, a brief summary is provided here.

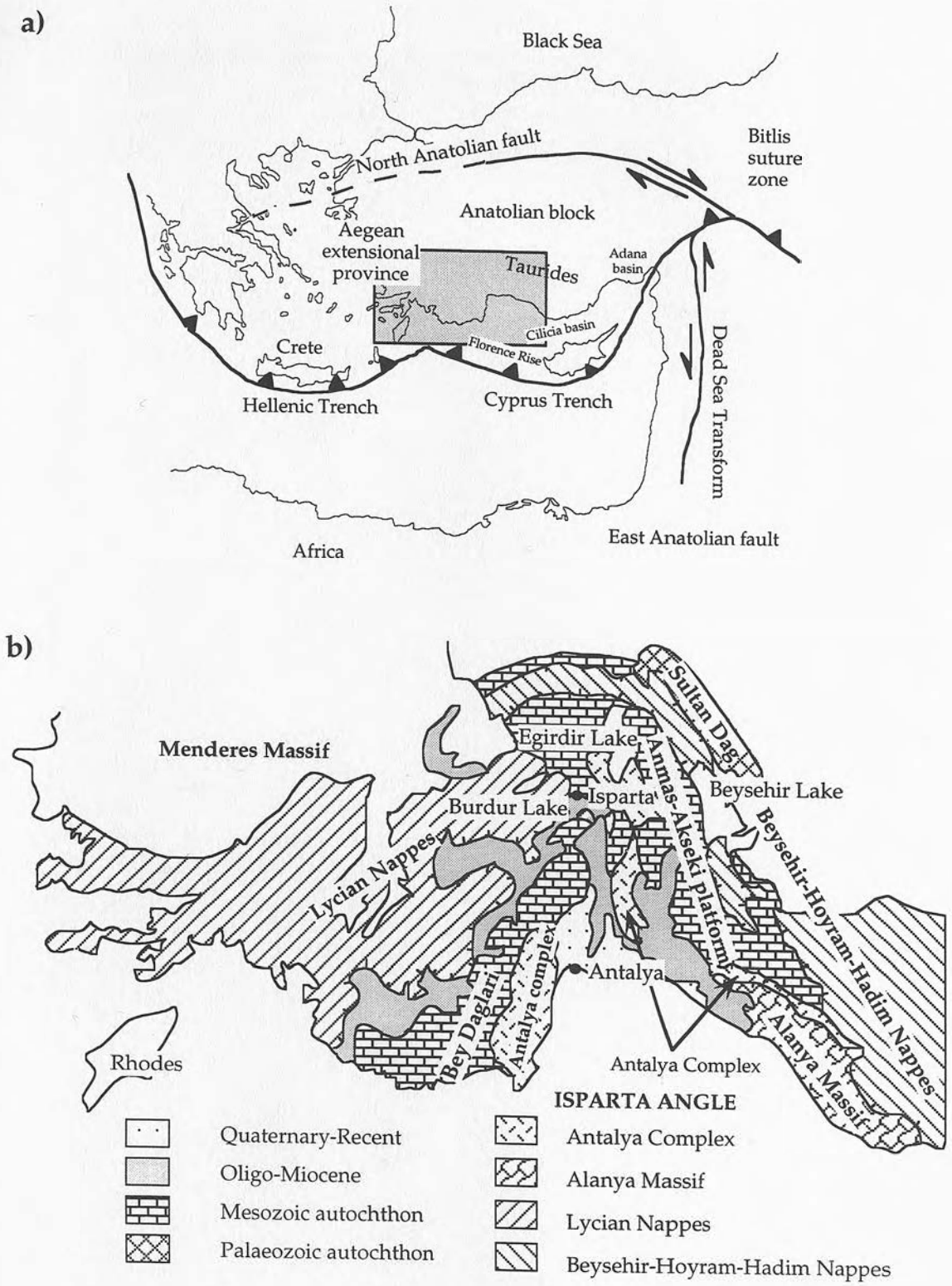

Figure 7.1 Map of a) the north-eastern Mediterranean showing the tectonic units mentioned in the text and b) the Isparta Angle region and surrounding units

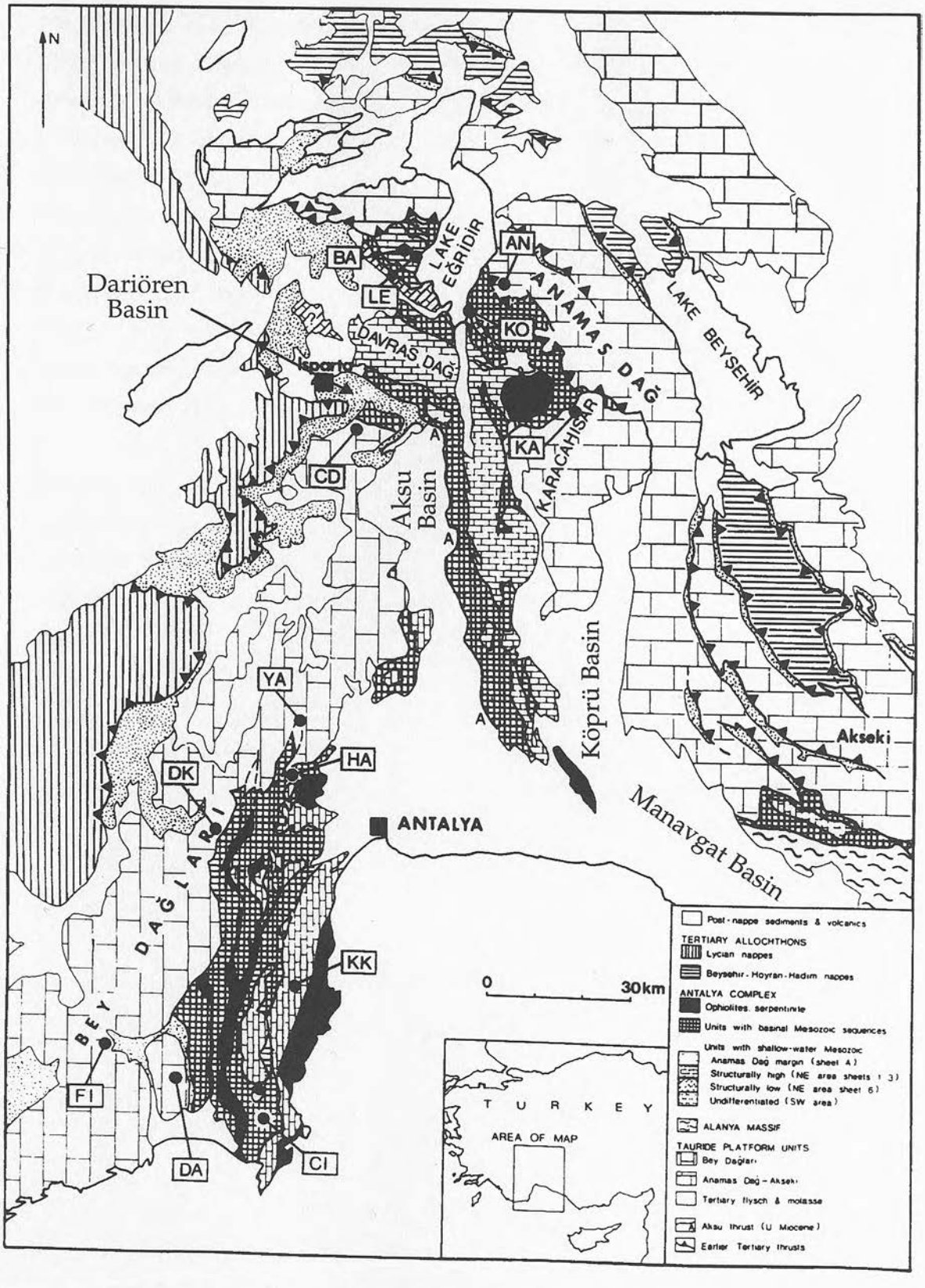

Figure 7.2 A more detailed map of the Isparta Angle showing the north-south structural lineaments within the Antalya Complex and the location of the palaeomagnetic sites of Morris and Robertson (1993). Modified from Waldron (1984).

The Antalya Complex is divided into five north-south trending tectonic zones (Fig. 7.2; Woodcock and Robertson, 1981a; b) which, taken as a whole, record the initiation, construction and later disruption of part of a small Mesozoic-Cainozoic oceanic basin by a combination of thrust and strike-slip tectonics (Robertson and Woodcock, 1980b; Woodcock and Robertson, 1981). Poisson *et al.* (1983) showed that the Antalya Complex was emplaced prior to the Oligocene in the central part of the study area (south-west of the Köprü basin). By contrast, Hayward (1982) demonstrated that the Antalya Complex in the south-west of the Isparta Angle was an uplifted landmass shedding sediments in the Early Miocene and was thrust westward, near to its present position, onto the Bey Daglari (Fig. 7.2) during the Mid-Miocene.

Extensive palaeomagnetic studies of both eastern and western arms of the Isparta Angle and the Miocene sediment between them, have been carried out over the last decade. These show that the eastern limb, consisting of the Beysehir-Hoyran-Hadim (BHH) nappes and part of the Anamas-Akseki platform (Fig. 7.1) has rotated clockwise by 40° during the Late Eocene-Oligocene (Kissel *et al.*, 1993). The western limb of the Isparta Angle (e.g. the Bey Daglari; Kissel and Poisson, 1987), the south western segment of the Antalya Complex and the northern part of the Anamas-Akseki platform (Morris and Robertson, 1993; Figs. 7.1 and 7.2) was rotated anticlockwise by 30°, after Burdigalian-Langhian times (Morris and Robertson). Kissel and Poisson (1986) stated that there is no evidence for the rotation of Neogene sediments within the Isparta Angle during the last 15 Ma (e.g. since Langhian). They interpreted this apparent paradox by decoupling the Lycian Nappe system from the Akseki-Beysehir Taurides using a décollement horizon at the base of the Antalya Complex to take up the rotation of the Bey Daglari. Their model, shown in figure 7.3, indicates that the formation of the Bey Daglari anticline was caused during anticlockwise rotation, by the movement of the Lycian Nappes towards the SE (Kissel *et al.*, 1993). A 30° anticlockwise rotation of the Bey Daglari is supported by Morris and Robertson (1993). Their data from the south-western segment of the Antalya Complex however, indicated that this area was rotated along with the Bey Daglari. This implies that a décollement horizon at the base of the Antalya Complex is unlikely to have taken up all the rotation. One possibility is that rotation

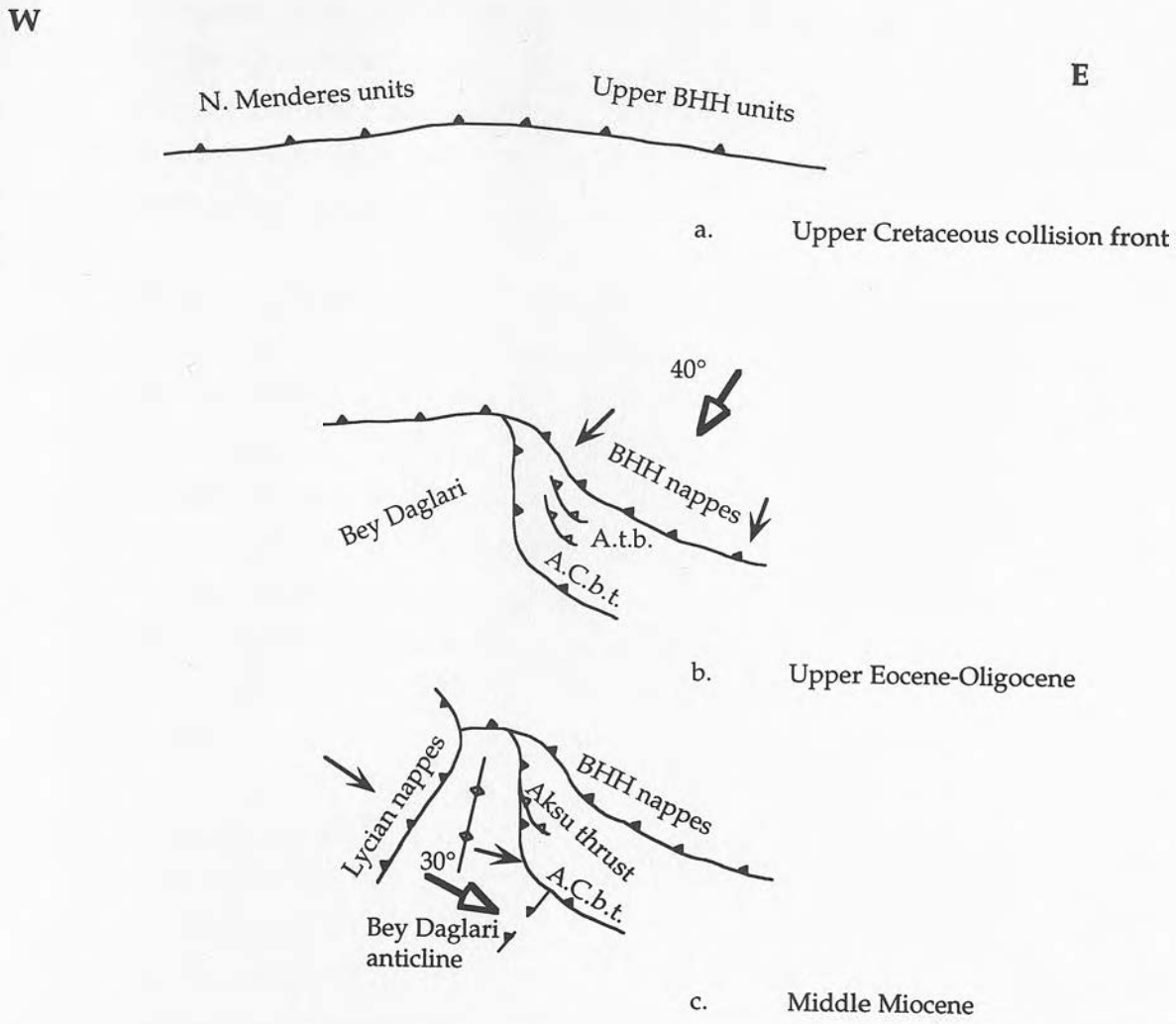

Figure 7.3 Schematic model for the formation of the Isparta Angle from Kissel *et al.* (1993). BHH nappes = Beysehir-Hoyran-Hadim nappes; A.C.t.b. = Antalya Complex basal thrust; A. t.b. = Akseki thrust belt; A.t. = Aksu thrust.

was accommodated across a more diffuse zone within the Antalya Complex, potentially utilising the older north-south tectonic lineaments. Morris and Robertson (1993) document a remagnetisation event which occurred during the Early-Middle Miocene and suggest that this is likely to have resulted from the migration of orogenic fluids ahead of the advancing Lycian Nappes.

Studies of field evidence within Neogene sediments of the Isparta Angle have also occupied various authors. Hayward (1982; 1984) followed up earlier work (e.g. Gutnic and Poisson, 1970; Poisson, 1977; Woodcock and Robertson, 1977a; 1977b) on the NE-SW trending Miocene basin to the west of the Bey Daglari (Figs. 7.1 and 7.2). This basin was interpreted as a foreland basin succession related to the south-eastward thrusting of the Lycian Nappes (Hayward, 1982; 1984). Hayward (1982) also studied the small Miocene basin on the south-eastern margin of the Bey Daglari (Fig. 7.2), which he similarly interpreted as having been formed by load induced flexure.

The N-S orientation of the Bey Daglari anticline and the prominent high angle N-S striking reverse faults in the centre of the Isparta Angle (e.g. the Kirkkavak fault, Pinargözü fault zone, Aksu thrust; Figs. 7.5 and 7.22) led Poisson (1977a and b) to define an east-west compressional event which he named the Aksu Phase, and dated as Latest Miocene. The front of this west-vergent system was considered to be situated in the middle of the Bey Daglari (Poisson, 1977; Ricou *et al.*, 1977; Marcoux *et al.*, 1989). The cause of the west vergence of this event has long been thought (e.g. Dumont *et al.*, 1979) to be closely related to the westward expulsion of the Anatolian block (McKenzie, 1972; 1978; Sengör and Yilmaz, 1981; Sengör *et al.*, 1985) which began with the collision at the Bitlis Suture zone (Sengör and Yilmaz, 1981; Dewey *et al.*, 1986) at around 13 Ma (Le Pichon and Angelier, 1979; Le Pichon *et al.*, 1993).

Dupoux (1983) examined the field evidence for the Aksu Phase in the Köprü basin and noted that populations of micro-faults were orientated both NNW-SSE and NE-SW. He interpreted the NW-SE trends as the products of rotation from an original N-S orientation due to strong sinistral shear along NNW-SSE orientated faults. Dupoux (1983)

considered that the Aksu Phase was the last compressive phase to have affected the Isparta Angle.

More recently, this compressional phase has been re-examined by Frizon de Lamotte *et al.* (1995). These authors compiled previously published data (Dumont, 1979; Dumont *et al.*, 1979; Dupoux, 1983, Akay and Uysal, 1985; Marcoux *et al.*, 1989, Auboug *et al.*, unpublished data) and presented new generational slickenside data from the study area suggesting that contrary to Dupoux's (1983) conclusion, the Latest Miocene deformation can be divided into two distinct events with different orientations:

- First, E-W compression resulting in broadly N-S striking reverse faults in the centre of the Isparta Angle (the Aksu Phase);
- Later, south-directed transport (the Susuz Dag Phase).

Frizon de Lamotte *et al.* (1995) propose that rather than forming either due to movement of the Lycian Nappes (Kissel, 1993), or as a result of the Aksu Phase east-west compression (Poisson, 1977), the Bey Daglari anticline developed as a regional lateral culmination on a south-vergent blind thrust (Fig. 7.4), parallel to the thrust front visible off-shore along the Florence Rise (Fig. 7.1; Sage and Letouzey, 1990). Investigation of the Florence Rise was undertaken by a "Training through Research" Cruise in 1991. Results from this study, suggest that the interpretation of the structures visible along the Florence Rise may be more complicated (Woodside *et al.*, 1992) than initially suggested by Sage and Letouzey (1990).

The Dariören basin is the north-eastern extension of the Lycian flexural basin at the apex of the Isparta Angle (Fig. 7.2) Here, an Aquitanian-Burdigalian succession was thought to have been terminated by south-westward thrusting and folding of the Davras Dag carbonate platform to the north (Poisson, 1977; Akbulut, 1977). The age of this deformation is thought to be prior to the Aksu Phase (i.e. pre-Messinian).

Much interest has been concentrated on the active N-S extension along the coast of western Turkey (McKenzie, 1972; 1978; Jackson *et al.*, 1982; Jackson and McKenzie, 1984, 1988; Papadopoulos *et al.*, 1986; Lyon Caen *et*

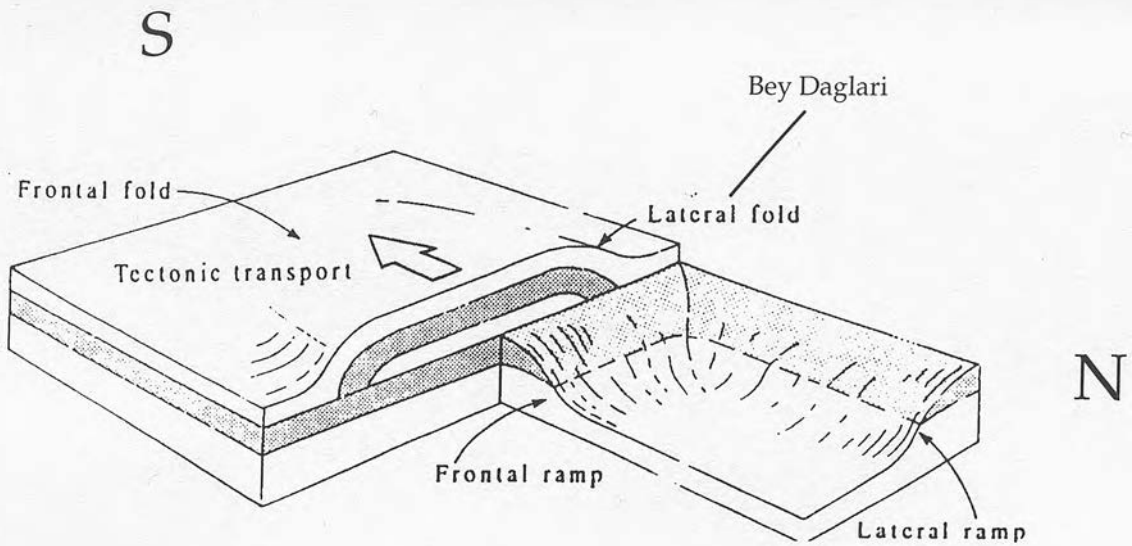

Figure 7.4 Block diagram illustrating the geometry of a lateral culmination fold on a south-vergent blind thrust as envisaged by Frizon de Lamotte *et al.* (1995). Diagram modified from Frizon de Lamotte *et al.* (in press). Originally from Schirmer (1988); Frizon de Lamotte *et al.* (1991).

al., 1988; Eyidogan, 1988). Berckemer (1977), Le Pichon and Angelier (1979), Le Pichon (1981) and Angelier *et al.* (1982) have suggested that the extension may be governed mainly by extensional forces acting on the leading edge of the upper plate along the Hellenic subduction zone. This extensional system has also been modelled, taking into account the dextral strike-slip movement related to the North Anatolian Fault (NAF) and the westward escape of the Anatolian block (McKenzie, 1978; Jackson and McKenzie, 1984; 1988; Ekström and England, 1989; Taymaz *et al.*, 1991; Zanchi *et al.*, 1993). The Isparta Angle lies at the boundary between the zone dominated by extension behind the Hellenic Arc and that governed by expulsion-driven compression (Dumont *et al.*, 1979). Neotectonic studies of the area have therefore focused on the formation of the Plio-Quaternary graben systems in the northern lakeland area of the region (e.g. the Aci area, Angelier *et al.*, 1981; Burdur, Price and Scott, 1994) and in assessing the mechanics and implications of formation of these structures (Jolivet *et al.*, 1994).

7.5 Deformational structures

7.5.1 The Manavgat basin

7.5.1.1 Basement and basal Miocene structures

The basement of the eastern part of the Manavgat basin is entirely composed of the Alanya Massif (Fig 7.1). This consists of Permian meta-carbonate, micaceous schists and blueschists (Ozgül, 1983; Okay and Ozgül, 1984). It is thought to have been emplaced onto the Antalya Complex to the north before the Early Eocene (Monod, 1977; Okay and Ozgül, 1984). Outcrops of the Alanya Massif are highly fractured and veined, but unless faults penetrating the Alanya Massif also offset the overlying Miocene sediment, identification and dating of fault groups within the basement could not be attempted. Faults affecting both the Alanya Massif and the Miocene succession were occasionally found along the northern margin of the basin, e.g. 1km from the Akseki road locality, but it was in all cases impossible to be sure whether all overlying Miocene sediment was affected, or just the Lower and Middle Miocene successions.

No Miocene sediment overlies the fault along which the Alanya Massif was emplaced onto the Antalya Complex.

The Antalya Complex forms the boundary of the Manavgat basin for less than 2km. Its relationship with Miocene sediment can be observed along the road north from Yaylaalan (Fig. 7.5) where it is unconformably overlain by a thick succession of Kargi Member conglomerates (see chapter 5, table 5.1). Palaeocurrent evidence from these conglomerates and the absence of Miocene sediments prior to reef formation in the Late Burdigalian-Langhian on the northern part of the Alanya Massif, indicates that during the Lower Miocene the Anatalya Complex was palaeogeographically low relative to the Alanya Massif to the south (see Chapter 5 section 5.3.3). Although there is no clear evidence for fault-generated palaeotopography between the Antalya Complex and Alanya Massif, this possibility cannot be ignored.

The most northern section of the margin of the Manavgat basin is composed of part of the Anamas-Akseki platform carbonates (Fig. 7.1). Access to this part of the northern margin of the basin is extremely difficult, and although the boundary was observed from a distance (e.g. Kizildag and Karabucak; Fig. 7.5), it was not studied in detail. Here again, the basement is overlain by a thick succession of fan-delta conglomerates (see chapter 5) and it is probable that active faulting along, or close to, the present-day margin helped generate the large volume of conglomerate preserved.

7.5.1.2 Evidence of brittle fracture in Miocene sediments

Faulting

Micro-faults within the Miocene sediments of the Manavgat basins are prolific. In the poorly lithified sediments of the Karpuzçay and Geceleme formations however, fault surfaces are generally not well preserved. The better lithified Lower Miocene formations including the Oymapinar limestone and Çakallar Formation contain well exposed micro-scale faults, often with both striations and crystal lineations developed on fault planes.

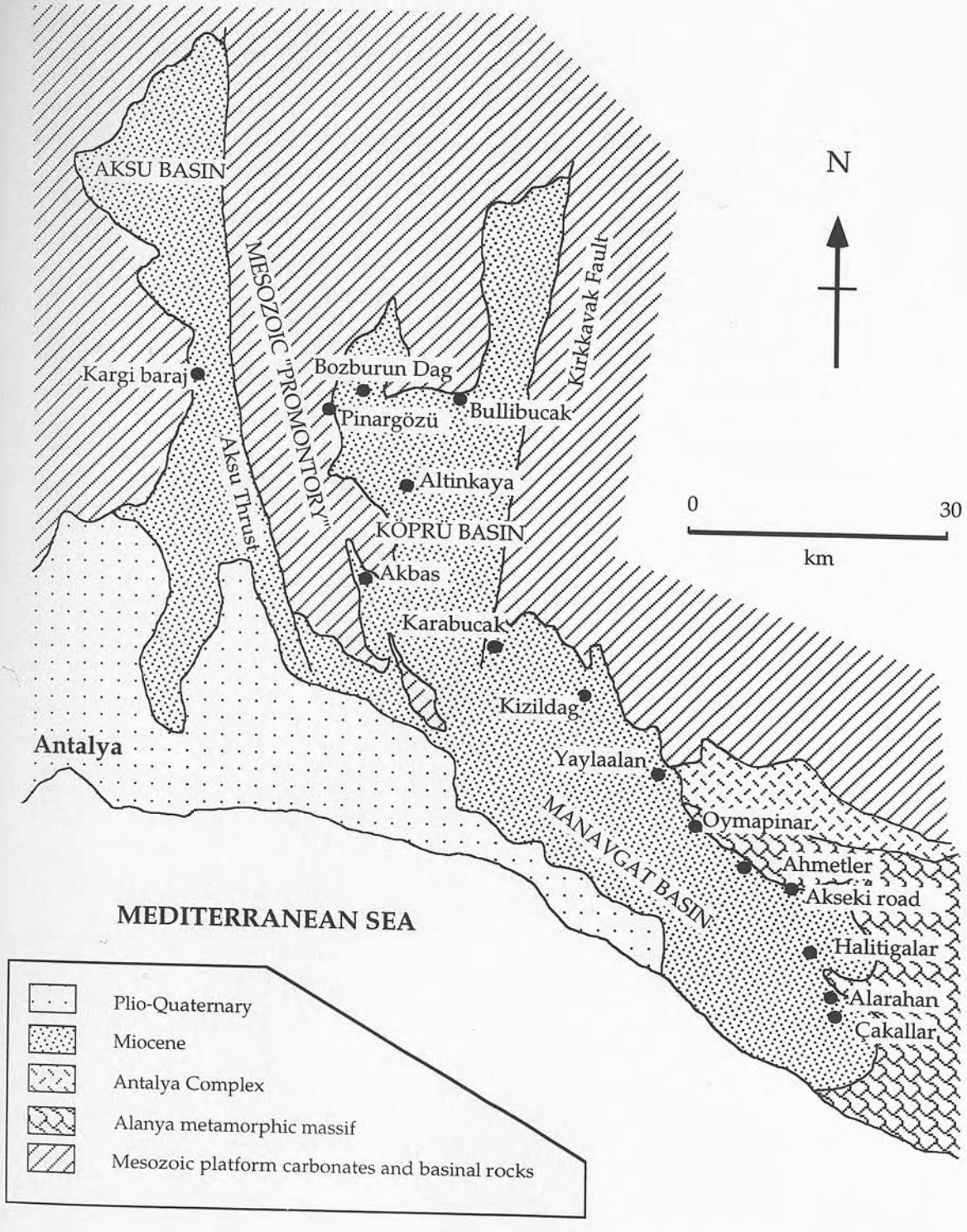

Figure 7.5 Localities referred to in the text of chapter 7.

The fault populations collected from this area can be divided into two groups based on their stratigraphic position and orientational characteristics. Figure 7.6 is a map of the Manavgat basin with stereonets of fault data measured in the Oymapinar limestone at the Akseki road locality and the Geceleme and Karpuzçay Formations long the road to Akseki from the coast. The normal faults measured from the Oymapinar limestone are well clustered and have slightly lower dips to the planes than those from the overlying softer formations (e.g. Geceleme and Karpuzçay; Fig. 7.6b).

This angular difference may be the result of more than one period of extensional faulting (Fig. 7.7), although lithological control over the angle of faulting cannot be ruled out. There is however sedimentary evidence to support an early faulting event affecting the Lower-Mid Miocene successions i.e. the Oymapinar limestone, in the form of fault talus at the Akseki road locality (see chapter 3 section 3.6.2.3). The rapid transition from shallow-water carbonate formation to deeper water planktic foraminiferal marls and its correlation with talus and coarse calcirudite deposits (the Çakallar Formation) also suggest active tectonics at the Burdigalian-Langhian boundary (sections 3.6.2.3, 4.8, 5.9). Further evidence for a Burdigalian-Langhian extensional event is presented below (see fractures and sedimentary evidence for faulting).

In detail, however, the faults measured from the Oymapinar limestone at the Akseki road locality have a more complicated history than simple normal faulting. Although all the faults measured here had normal offsets, where slickensides were preserved they indicated movement with reverse and sinistral components (Fig. 7.8). Similar faults are seen in the central part of the Manavgat basin in the Oymapinar limestone near the village of Halitigalar (Fig. 7.5). As with the normal-offset faults in the Karpuzçay and Geceleme Formations, reverse-offset faults in these less well-lithified formations generally have poorly preserved fault surfaces and very few slickensides. Reverse-offset faults are more rare than normal offset faults however, but when they are seen they have the same NW-SE strike and high angle associated with normal faults in these formations (Fig. 7.6). Strike slip components on these faults are

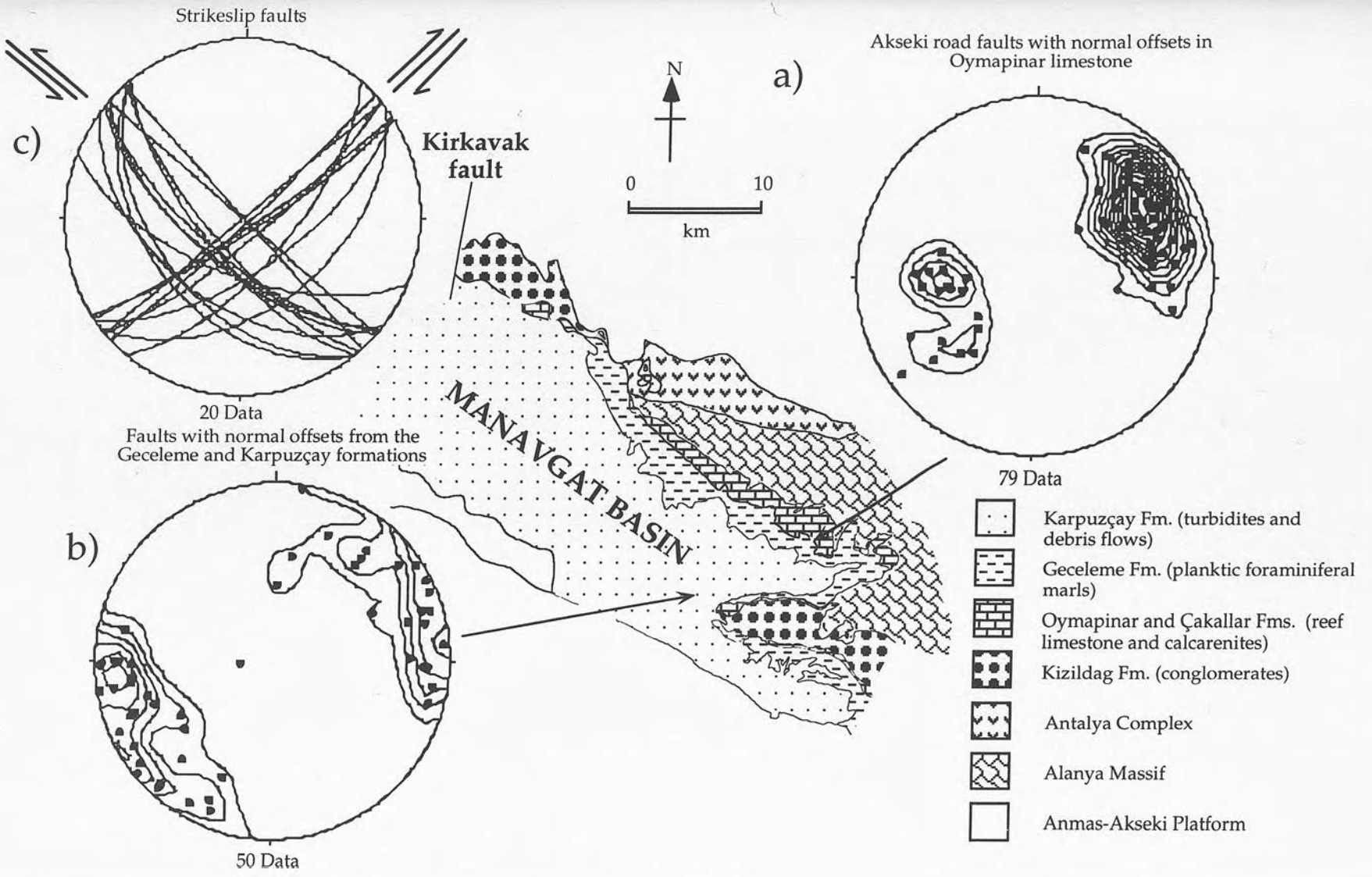

Figure 7.6 Stereoplots of the poles to the planes of faults in the Manavgat basin: a) faults with normal offsets in the Omapinar limestone at the Akseki road locality; b) faults with normal offsets in the Geceleme and Karpuzçay Formations along the road to Akseki; c) planes of faults with strikeslip slickensides showing the orientations of faults with sinistral and dextral displacements.

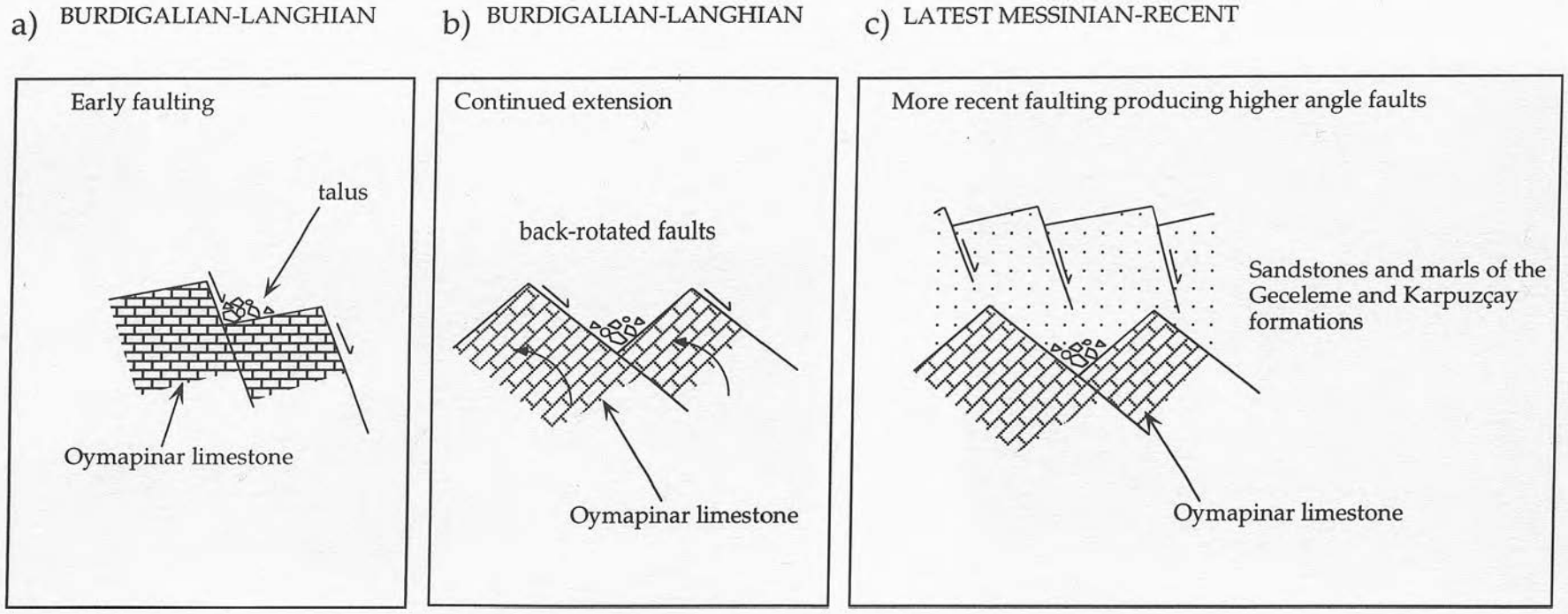

Figure 7.7 a) Nomal faulting event in the Early Miocene leads to talus formation and forms high-angle normal faults. b) Continued extension on these fault causes back-rotation producing a shallower angle. c) Subsequent faulting forms new higher angle faults in the overlying sandstones and marls.

7.8 Photographs showing the normal offsets and transpressional slickensides on the faults at the Akseki Road locality.

occasionally possible to recognise, but are impossible to assess or measure without slickenside information. Given that there is no evidence of pure reverse faulting however, it is assumed that most of the reverse faults observed in the Middle to Late Miocene sediments were transpressional. Figure 7.9 shows a 2-d model of the changing fault-types through time from the Lower Miocene to Plio-Quaternary.

Figure 7.6C shows strike-slip faults measured largely from Oymapinar limestone exposures around the basin. A clear pattern of NW-SE striking faults associated with sinistral movement and NE-SW striking faults associated with dextral displacement can be discerned. The similarity of strike between the normal offset faults and sinistral strike-slip faults produces an explanation for the reactivation seen on faults at the Akseki road locality.

The youngest sediments affected by this transpressional faulting are those at the top of the Karpuzçay Formation. The youngest so far documented occur in the Ahmetler section and have been dated as nannofossil zone 11b (Flecker *et al.*, 1995). Overlying the Karpuzçay Formation is an erosional unconformity at the base of the Pliocene succession the oldest of which are thought to be N19 (Akay and Uysal, 1985; Akay *et al.*, 1985; C. Glover, pers. com., 1995). It is therefore assumed that the age of the transpressional faulting is Latest Messinian to Early Pliocene (e.g. Poisson, 1977; Frizon de Lamotte *et al.*, 1995). The unconformity can therefore be assumed to have formed between the Latest Messinian and the Early Pliocene and this confirms Poisson's (1977a) age for the Aksu Phase of compression. There is no evidence to suggest conclusively however, that reverse faulting only occurred at the Mio-Pliocene boundary.

Normal faults affecting Upper Miocene sediments are of higher angle than those in the older Miocene strata (Fig. 7.6). Similarly orientated faults also affect Pliocene sediments (C. Glover, pers. com., 1995), but it is not clear when, in the Plio-Quaternary they were formed. The three possibilities are as follows:

- Shortly after the compressional phase at the end of the Messinian when the Pliocene basin was formed;

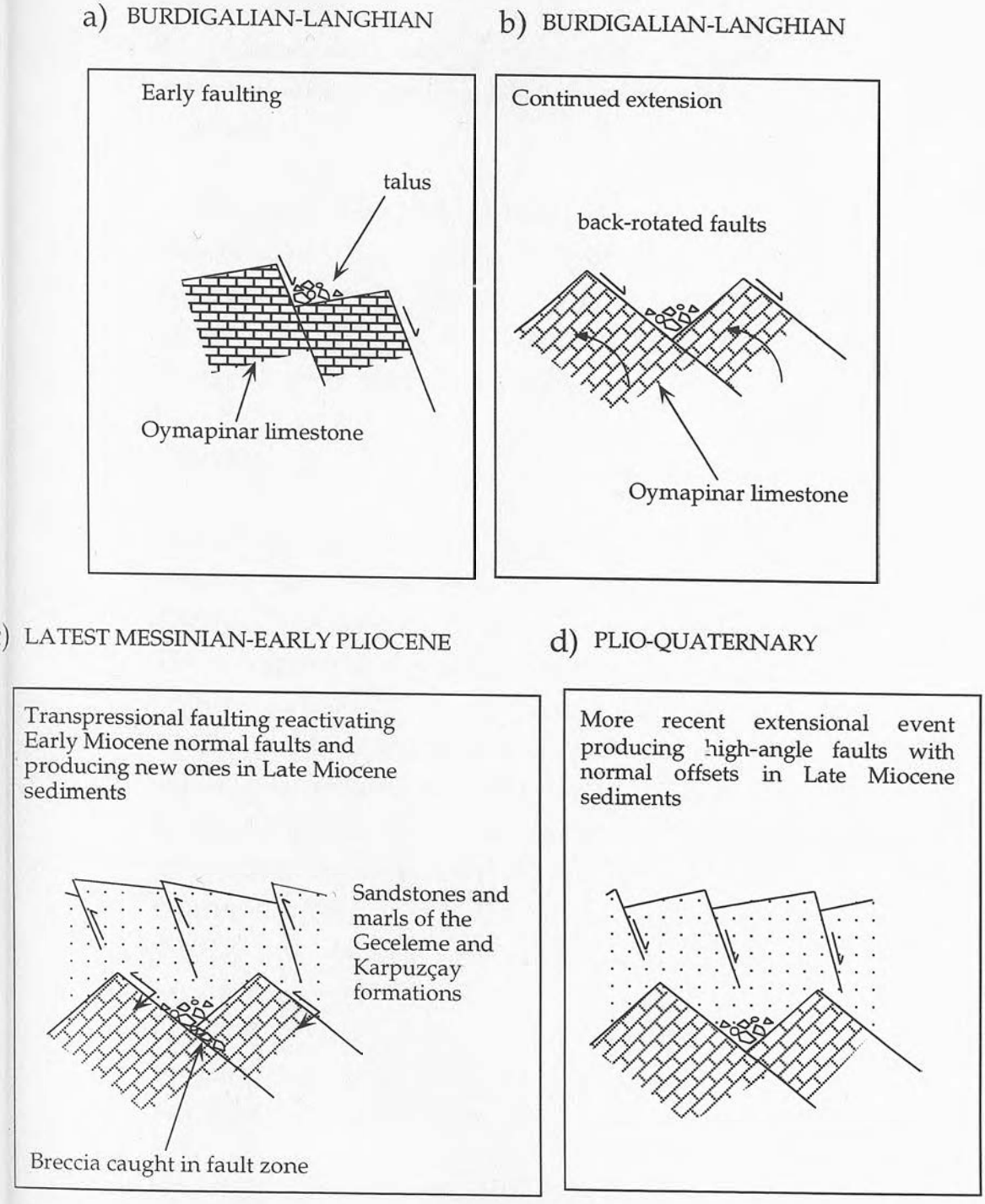

Figure 7.9 a) Normal faulting event in the Early Miocene leads to talus formation and forms high-angle normal faults. b) Continued extension on these faults causes back-rotation producing a shallower angle. c) The Aksu phase at the end of the Miocene causes reactivation of normal faults with transpressional displacements, but this is not sufficient to completely reverse the previous normal displacement. High-angle reverse faults are formed in Middle to Late Miocene sediment. d) Subsequent extension results in the formations of new higher angle faults in the overlying sandstones and marls. It is not clear whether many of these are reactivated transpressional faults. There is no evidence that the Early Miocene faults are reactivated during the Plio-Quaternary extensional phase.

- During the Late Pliocene, when tilting of Pliocene sediments occurred (C. Glover pers. com., 1995);
- During an extensional event thought to have taken place during the Quaternary which formed the graben structures in the north of the area, (e.g. Burdur Graben; Price and Scott, 1994).

It is beyond the scope of this project to speculate as to which of these events may have caused the high angle normal faults in the Upper Miocene sediments, but the reader is referred to a Ph.D. thesis currently being undertaken by C. Glover for further information on the evolution of the Pliocene basin in this area.

Fractures

On the southern limb of the anticline (Fig. 7.10), along the road from the coast to the Selçuk castle of Alarahan a fairly extensive exposure of Çakallar Formation can be seen containing abundant small fractures. These fractures are well developed in the better lithified fine- to medium-grained sandstone horizons and bound small (i.e. 1-2 cm) tilted blocks, similar to extensional fault blocks (Fig. 7.11). The coarser debris flows and calcarenites interbedded with these horizons however, are not fractured in any systematic way at all and the less well lithified marls show weakly developed, non-penetrative fracturing. At the boundary between fractured sandstone and largely non-fractured calcarenite layers the tilted blocks, in rotating backwards, have impinged upon the overlying sandstone layer. Instead of the fracture persisting across the boundary into the overlying calcarenite, there is generally no sign of the fracture, but the relief on the base of the calcarenite mirrors the offset pattern of the fractures, resembling a cast of asymmetrical ripples (Fig. 7.11).

One method of producing this fracture pattern is to invoke early extensional joint formation prior to complete lithification of the calcarenite which therefore behaves in a more ductile-like fashion. At a larger scale, soft sediment deformation in relation to active faulting would suggest syn-sedimentary deformation. In this case the calcarenite would have been deposited as a drape to a normal-fault structure. Here, however, because of the multiple layers of fractured and non-fractured

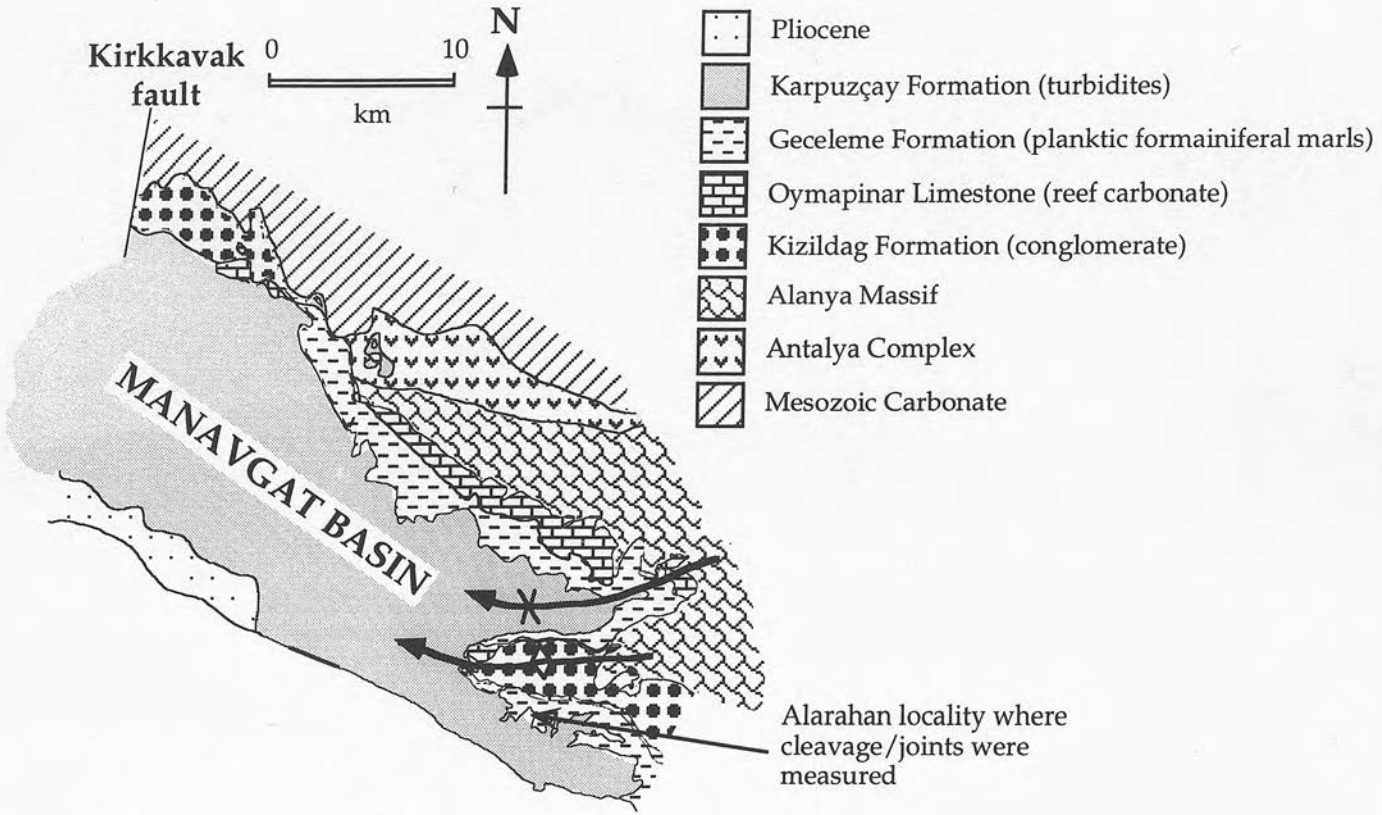

Figure 7.10 Geological map showing the broadly east-west orientation of the west-vergent folds in the east of the basin.

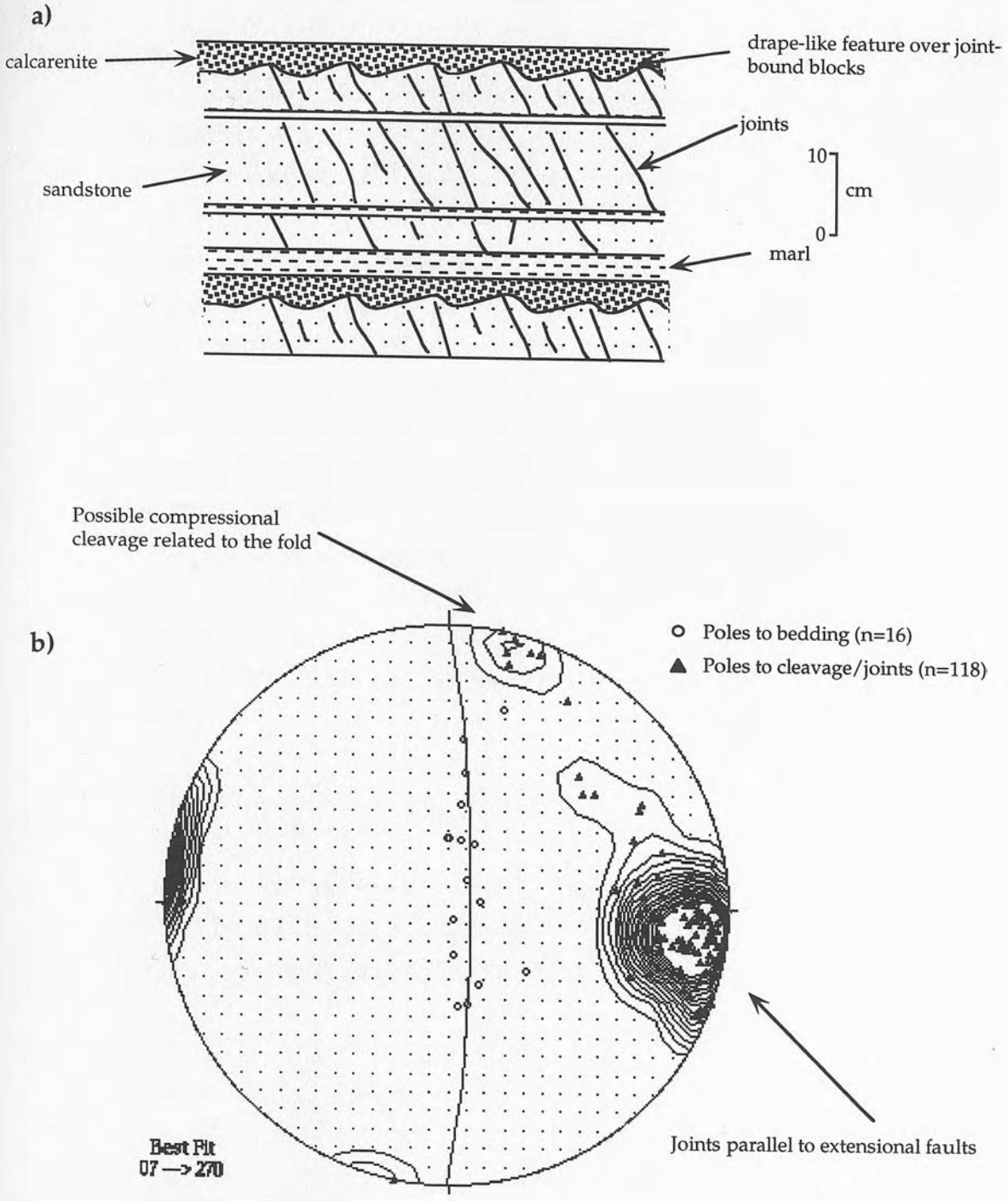

Figure 7.11 a) Schematic sketch of the fractured and non-fractured layers in the Çakallar Formation at Alarahan; b) Stereonet projection of these fractures showing that they have a bipartate distribution. Those with planes parallel to the π-girdle of the fold (N-S) all have small normal offsets on them and are almost certainly unrelated to the formation of the fold. The similarity between the orientations of these fractures and the normal faults seen in the Lower Miocene Oymapinar Limestone (Fig. 7.6) suggest that these are joints and may have formed at a similar time. However, later Plio-Quaternary extension cannot be ruled out. The small number of fractures whose planes are orientated east-west could theoretically be related to the folding event in the form of axial planar cleavage. However, it is also possible that they are conjugate sets to the extensional joint system.

beds and the clear relationship between jointing and lithological type/grainsize, it is suggested that fracture formation occurred after deposition of the entire sequence and lithification of the sandstones, but prior to complete lithification of the calcarenites and marls.

Figure 7.11 is a stereonet projection of the poles to the planes of the fractures measured at the Alarahan locality. It shows that the fractures have a bipartite distribution. The majority of the fractures including all those which had a noticeable normal offset have planes orientated N-S parallel to the π-girdle of the main west-verging anticline. From their orientation these joints seem unlikely to be related to the formation of the fold. The second much smaller group of fractures which cluster close to the π-girdle in areas where poles to bedding of the fold are absent is much more likely to be related to fold generation. No normal offsets were observed on these fractures and it is possible that they represent axial planar cleavage formed during fold formation (section 7.5.1.3 below).

Sedimentary evidence for faulting

Evidence for Miocene faulting has been deduced from the study of Manavgat basin sediments and discussed mainly in chapter 3 (section 3.8.1). It can be summarised as follows:

- There is an abrupt transition from shallow-water carbonates to deeper-water planktic foraminiferal marls at the Burdigalian-Langhian boundary;
- This boundary is also marked in many sections by coarse angular conglomerate horizons which have been interpreted as fault talus.

Akay's (1985) NE-SW cross-section across the syncline and anticline in the Manavgat basin (Fig. 7.14a) shows the following features of interest:

- The points of inflection at the sides of the folds are all rather steeper than would be predicted from dips elsewhere on the fold (i.e. rather box-fold-like in shape;
- The thickness of almost all of the formations varies across the fold.

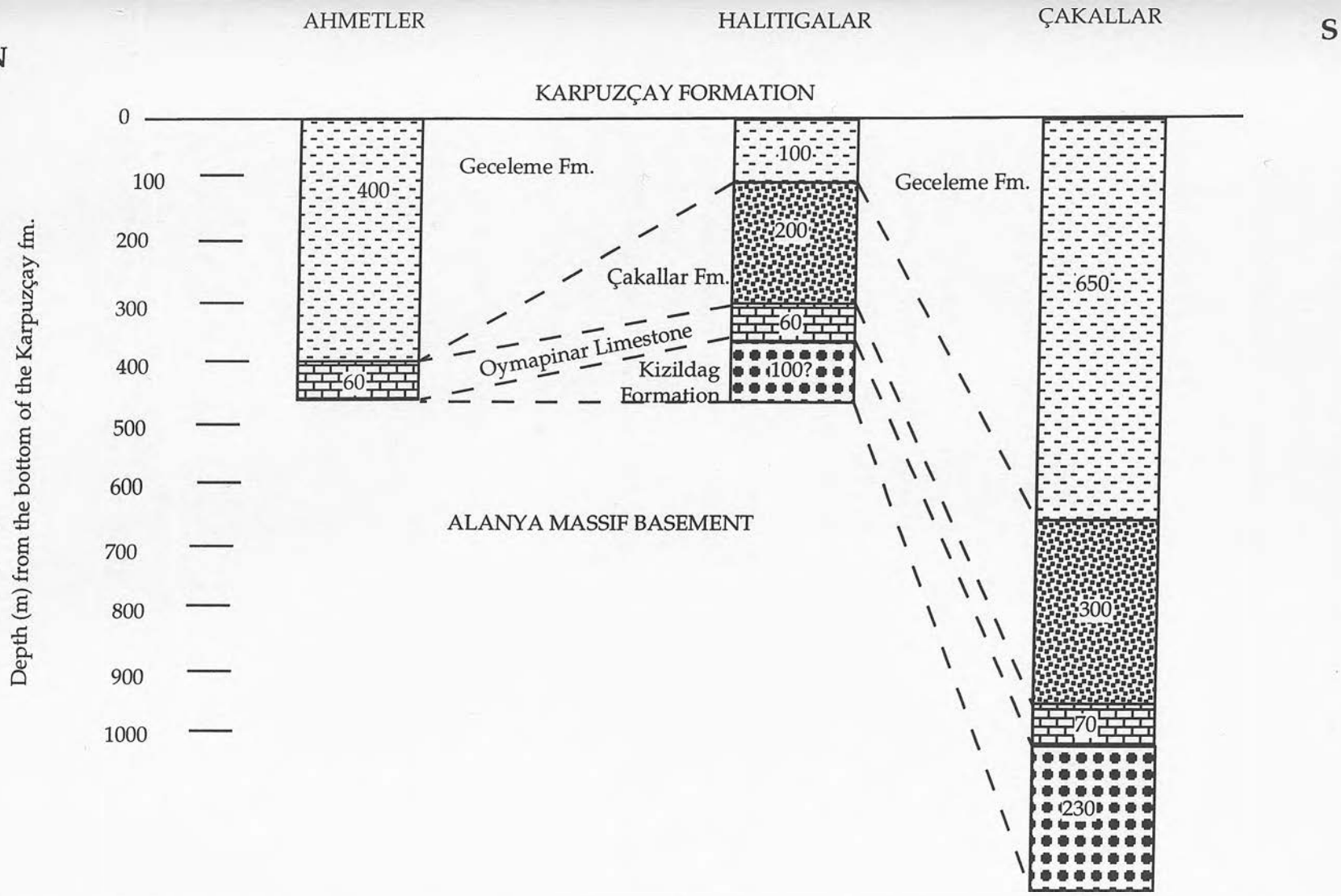

Figure 7.12 A structural cross section across the Manavgat basin, hung off the top of the Geceleme Formation. Note that the largest thickness differences are in the Geceleme Formation. This, and the association of the Çakallar Formation which is thought to be at least partly fault derived, indicate that there was a post-reef faulting event which led to the deepening of the basin in two distinct localities, the far north and the far south.

Figure 7.12 shows sections measured in the field during this study at the three inflection points on the sides of the folds (Ahmetler in the extreme north, Halitigalar on the northern margin of the anticline and Çakallar on the southern limb of the anticline) exposed in the basin. These sections are hung from the boundary between the bottom of the Karpuzçay Formation and the top of the Geceleme Formation. The thickness changes become apparent at once and can be seen in table 7.1.

Interpretation

The distribution of the Kargi conglomerates suggests that alluvial depositional processes infilled a Pre-Lower Miocene palaeotopography on top of the Alanya Massif. In the north of the basin, the Alanya Massif formed a "high" on top of which no conglomerates were deposited (see chapter 5, section 5.7.1, Fig. 5.3). The altitude of this "high" cannot be estimated, but there is little evidence of it being a source of material for deposition in the basin and it is therefore not thought to have had extensive relief. In central parts of the basin the accumulation of 60-70m of *in situ* reef carbonate in the Burdigalian and the absence of any deeper-water sediment suggests that, in this region at least, little of the accommodation space generated by the previous palaeotopography remained. The diachroneity of the reefs indicates that there was still a south-dipping slope from the Alanya Massif "high", such that a rising sea level resulted in northward transgression (chapter 4 section 4.7 for discussion; section 6.5.2).

The Çakallar Formation has been interpreted as having been generated largely by faulting of nearby reef carbonates and Alanya Massif basement (see chapter 3). In this context their patchy distribution around the basin would reflect the localised faulting at the time. It is interesting to note that the localisation of Çakallar Formation along the limbs of the folds, albeit unevenly, suggest that they were the focus for faulting prior to formation of the fold. This distribution pattern is similar to that documented by Follows and Robertson (1990) in the Miocene of southern Cyprus. The suggestion that the limbs of the fold were also the location of faulting is borne out by the thickness variation of the Geceleme Formation. Here, the far thicker successions on the southern limbs of the

Table 7.1 Thickness variations and a summary of the main rock types making up the Miocene formations folded in the east of the Manavgat basin.

Formation	Rock type	Thickness variation
Karpuzçay Formation	Sandstones, conglomerates, siltstones and marls	Top of the formation not seen in the north of the basin and overlain by an erosional unconformity at the base of the Pliocene in the south. At least 4-600m thick
Geceleme Formation	Planktic foraminiferal marls (100-200m water depth)	Thick successions on the south-facing limbs of the folds. A much thinner succession is seen at Halitigalar on the north facing limb of the fold
Çakallar Formation	Calcarenites and debris flows containing clasts of shallow water reefal material and Alanya Massif basement, interbedded with sandstones and marls	Patchy distribution e.g. not at Ahmetler, but 5km to the east several hundred meters is exposed. Distributions is concentrated along the limbs of the folds, not at fold noses
Oymapinar Limestone	Shallow water *in situ* coral and algal reefs	Relatively constant thickness across the area. Diachronous from south to north (Bizon *et al.*, 1974; Akay and Uysal, 1985; Akay *et al.*, 1985; Flecker *et al.*, 1995)
Kizildag Formation	Mainly continental conglomerates and sandstones	Pinch out towards the north. Not found at all on the part of the northern margin of the Manavgat basin which is bounded by the Alanya Massif

folds relative to the northern limb of the anticline indicates that the extensional faulting which resulted in the deposition of the Çakallar Formation produced an asymmetrical half-graben feature in the north of

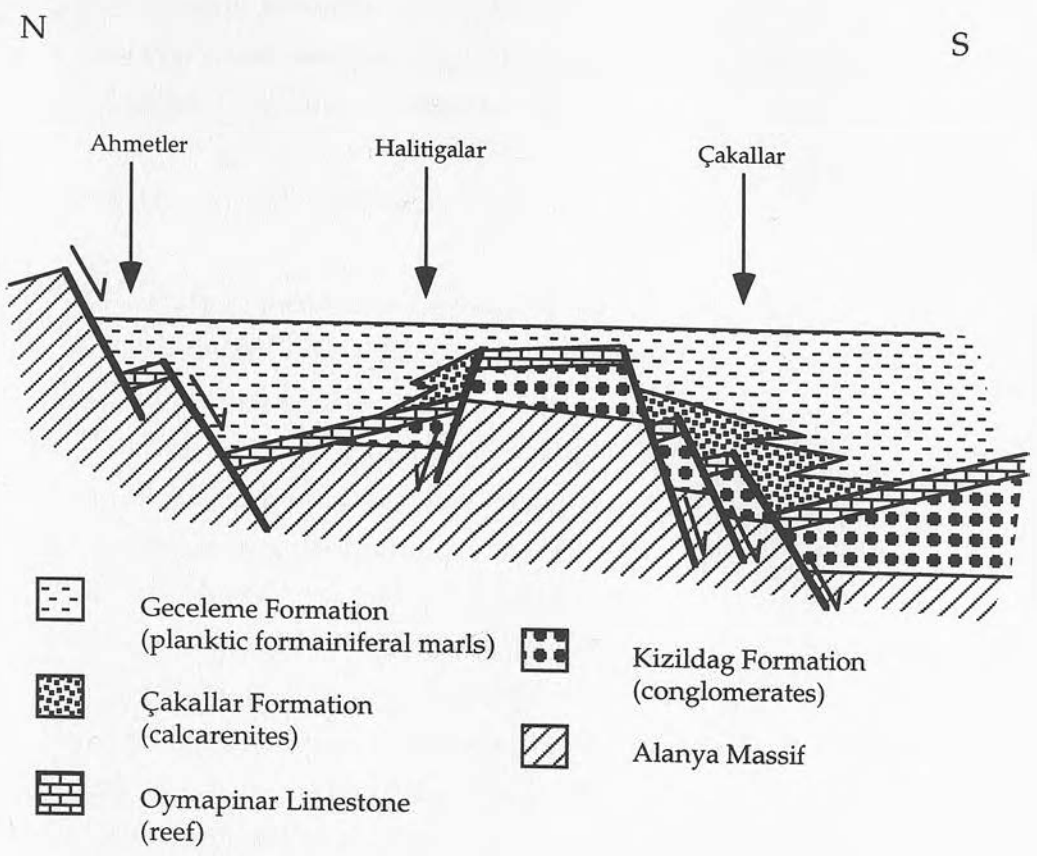

Figure 7.13 Schematic cross-section across the Manavgat basin at the end of deposition of the Geceleme Formation. The basically asymmetric fault geometries shown here are inferred from the variations in thickness of the Geceleme Formation across the area (see Fig. 7.12).

the basin and another fault-generated deep in the south. Figure 7.13 is a schematic cross-section suggesting the structure of the Manavgat basin at the end of Geceleme Formation deposition.

Summary of the conclusions drawn from the evidence for faulting

- There is substantial evidence to suggest that a broadly NNW-SSE extensional faulting event occurred in Late Burdigalian-Langhian time, prior to the deposition of the Geceleme Formation;
- This probably resulted in the formation of an asymmetrical half-graben in the north of the basin and a fault-generated depocentre in the south;
- Reactivated Early Miocene normal faults with obliquely (sinistral) orientated reverse slickensides, and reverse and strike-slip faults in Upper Miocene sediments suggest that a transpressional event occurred at some point before the Lower Pliocene.
- Higher angle normal faults than those seen in the Oymapinar limestone affect Upper Miocene sediments. Similarly orientated faults also affect Pliocene sediments. It is not clear however which of the three possible post-Miocene extensional faulting events may have generated these faults (C. Glover, pers. com., 1995).

7.5.1.3 Folding of Miocene sediments

Folding in the east of the Manavgat basin is dominated by the open-style, west verging anticline-syncline system shown in Figure 7.10. This exposes Alanya Massif basement at the eastern end of the core of the anticline. Akay and Uysal (1985) indicates that this folding affected all the Miocene strata equally (Fig. 7.14a) and that there was no previous faulting event. Reconstruction of his cross section to its pre-folding dimensions shows however, that this cannot have been the case. Only very pronounced and patchy subsidence with perhaps dramatic lateral variations in compaction could produce the thickness variations required if no faulting had occurred. Figure 7.14b shows the thickness variations of sections on the limbs of the folds, measured from Akay's (1985) cross-section across the area illustrating the improbable depositional patterns of this model. The reef carbonates in this diagram were used as a horizontal marker on top of which the overlying thicknesses were constructed, because it is possible to assume that the reefs were deposited at or very near sea level, an effectively horizontal plane. The diachroneity of the

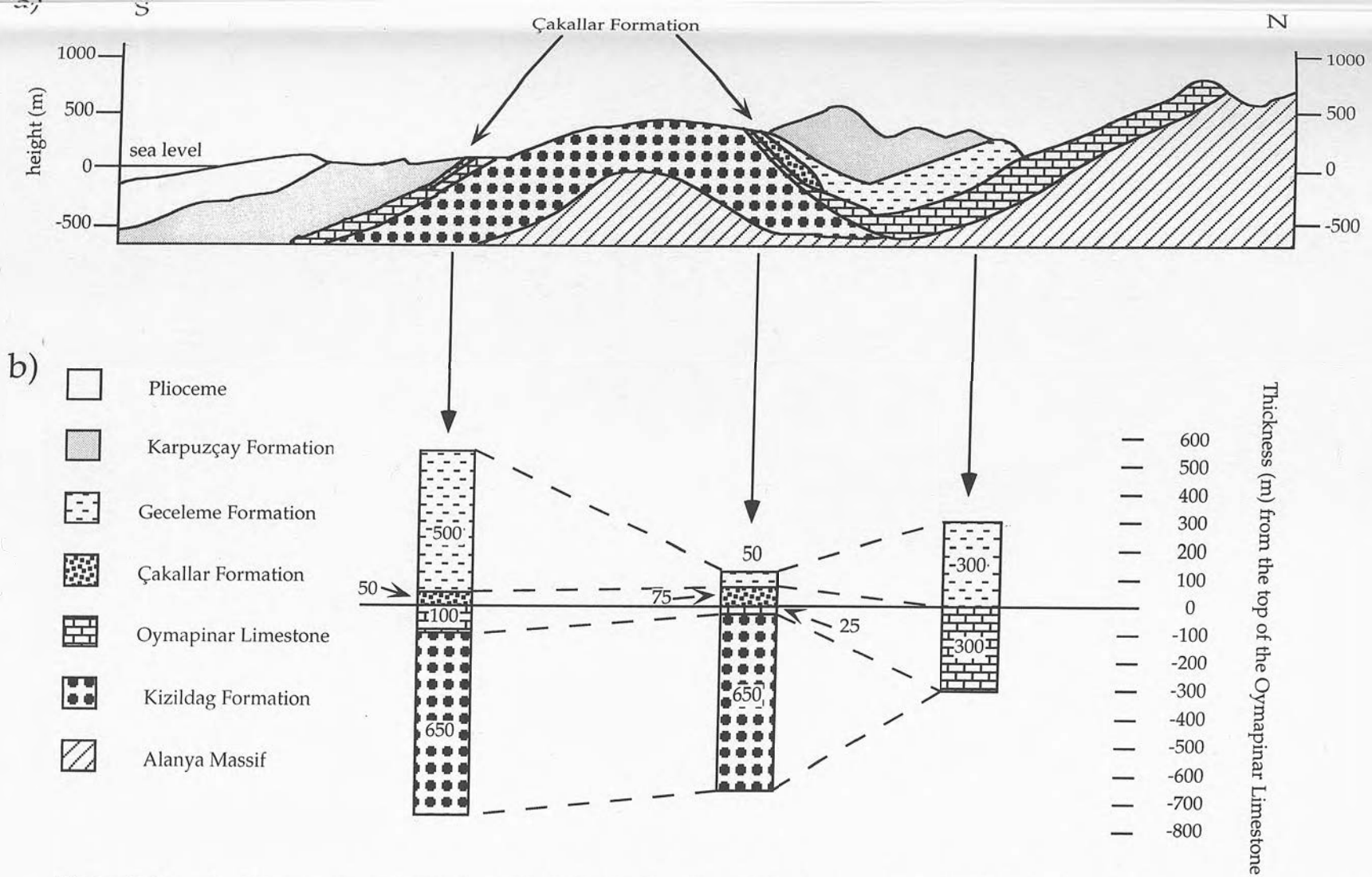

Figure 7.14 a) Cross-section across the Manavgat basin taken from Akay and Uysal (1985). This model assumes that no extensional faulting has occurred during deposition of the Miocene succession. b) Schematic reconstruction of the cross-section showing the improbable thickness distributions of the Upper Miocene sediments. It has been assumed that the reef horizon was effectively horizontal at the time of deposition (i.e. at or near the surface of the sea) indicating that the underlying conglomerates filled pre-existing palaeotopgraphy. The diachroneity of the reefs from south to north has not been taken into account. Neither subsidence, nor compaction has been accounted for in the estimation of the thickness variations of the overlying succession, but it is not thought that these processes could entirely account for the distribution pattern seen.

reefs has not been taken into account and would tilt the diagram towards the south, but would not significantly affect the thickness patterns of the overlying sediments.

Although the thickness variations across the area require faulting of the Lower-Middle Miocene sediments, it is not clear what rôle these faults played during the phase of compression which folded the overlying strata. The largest population of faults collected in the Lower Miocene succession (Fig. 7.6) is found on the northern margin of the basin and indicates that the faults are orientated with a NW-SE strike, not directly parallel to the symmetry of the fold which strikes E-W. As discussed above, the extension direction deduced from the joint pattern on the southern limb of the anticline may only represent a snapshot of the distribution of stresses in one small geographical area at a fraction of the total time of faulting. It does however, provide a measure of the extension direction without direct reference to underlying weaknesses in the Alanya Massif, something which can never be precluded when considering larger faults, where the tips are not seen. The joints strike N-S, perpendicular to the fold (Fig. 7.11), but it can be assumed that if the orientation of the faults bounding the inferred horst-graben system was parallel to this, then the thickness variations shown in figure 7.12 would change from east to west rather than north to south. Thus, the constraints imposed by the geometry of the sediments require that at least a component of the fault strike orientation, was E-W and it seems reasonable to suggest that these were probably parallel to the micro-faults measured in both the north and central parts of the basin i.e. striking NW-SE.

How then would faults orientated NW-SE be affected by a N-S orientated direction of compression? It is highly likely that N-S compression would have reactivated the extensional faults with a oblique reverse motion. The sense of shear theoretically in this case, should be dextral (Fig. 7.15), but it is interesting to note that all the slickensides found on the faults at the Akseki road locality on the northern margin of the Manavgat basin are reverse with a sinistral component. One feasible explanation of this (Fig. 7.15) is that an east-west compressional event followed a north-south directed one (exactly the opposite scenario to that suggested by

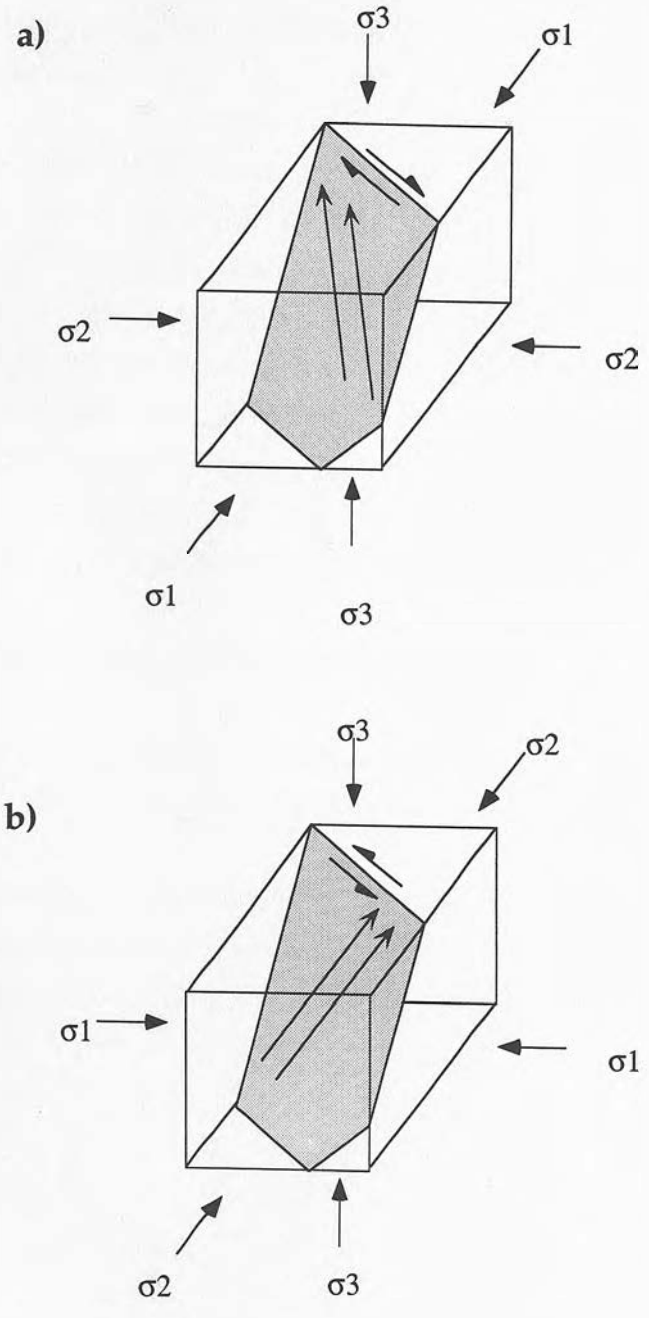

Figure 7.15 The theoretical orientation of slickensides produced on a NW-SE striking fault when a) σ1 is north-south and b) σ1 is east-west. Full arrows indicate the slickenside direction likely.

Frizon de Lamotte *et al.*, 1995). Equally probable however, is the possibility that the sinistral sense of shear is an expression of the dominance of an east-west component in a slightly north-south orientated $\sigma 1$ direction.

Reactivation of these NW-SE faults could well have produced the steeper dips associated with outcrop of the Oymapinar limestone particularly along the northern margin of the anticline producing the rather box-like shape of the fold. The relatively shallow dips of the Upper Miocene formations indicate gentle flexure over the top of this and it is possible that this fold structure, though prominent today, actually represents a very small amount of N-S compression. In other words, the folding of Upper Miocene sediments may be the expression of a small scale inversion structure of the underlying extensional faults (Fig. 7.16).

7.5.1.4 Interpretation and basin evolution

The evidence for the structural evolution of the Manavgat basin deduced from sedimentary and structural information is summarised in table 7.2.

It is not possible to preclude the possibility, that the fault along which the Alanya Massif was emplaced onto the Antalya Complex to the north of the Manavgat basin (Monod, 1977; Okay and Ozgül, 1984) was active during the Miocene and influenced the development of the structures (i.e. faulting and folding, see below) on its upper surface to the south. There is no evidence of foredeep-type sedimentation to the north of this fault however (Monod, 1977; Robertson, unpublished data), suggesting that, if active, it had minimal affect on Miocene sedimentation patterns.

The combination of sedimentary evidence in the form of fault-related facies and thickness variations across the basin with the observation of numerous micro-faults affecting the lower part of the Miocene succession has led to the suggestion that a distinct extensional faulting event occurred in the Manavgat basin at this time (section 3.8.1). This led to the generation of an asymmetrical half graben in the north of the basin and a further fault-generated deep to the south of the present-day southern limb of the anticline. The orientation of the extension direction, as

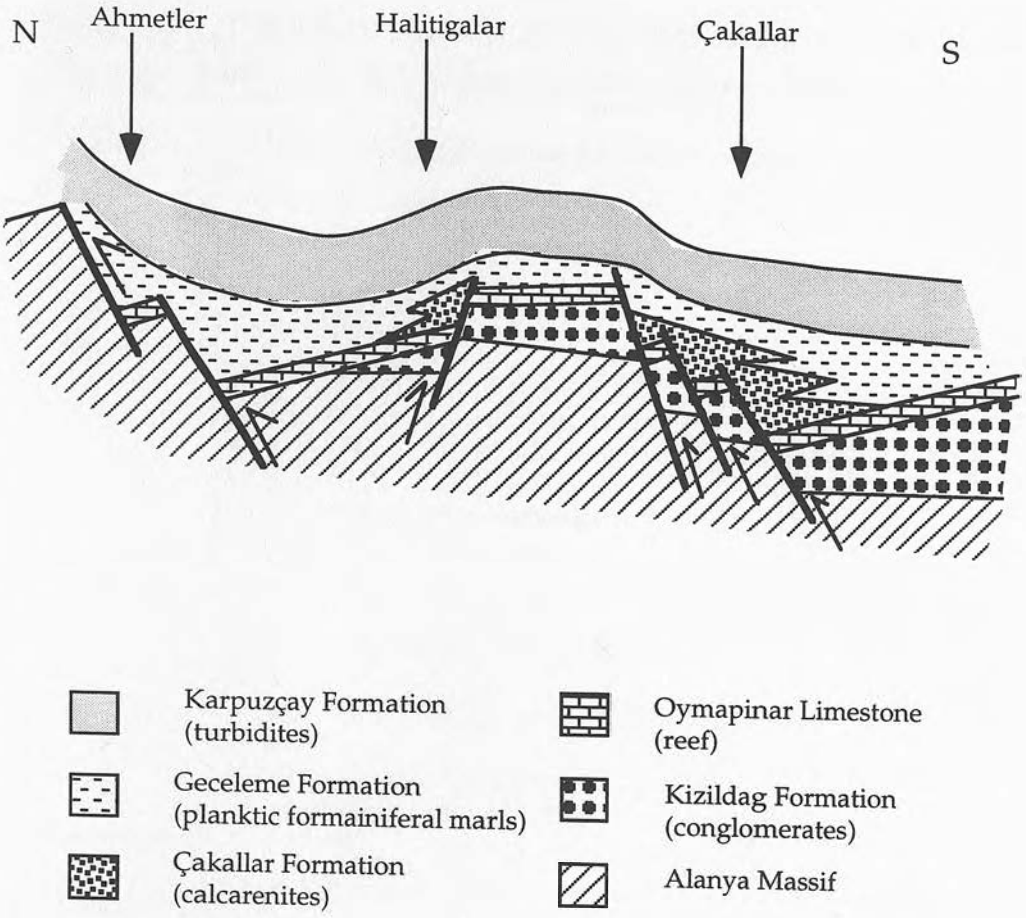

Figure 7.16 Schematic cross section across the Manavgat basin at the end of compressional event in the Latest Messinian-Early Pliocene. Lower Miocene extensional faults are suggested to have been reactivated, probably transpressionally. Overlying softer Geceleme and Karpuzçay Formations may not have been fully lithified, leading to more ductile behaviour. The rather box-fold like shape of the structure may have been inherited from the Lower Miocene horst-graben structure.

Table 7.2 Tabulation of the timing and tectonic events affecting the Manavgat basin. Evidence from the basin is also listed.

Time	Evidence from the Manavgat basin	Structural result	Tectonic event
Pre-Early Miocene?	i) Relationship with Antalya Complex (Monod, 1977; Okay and Ozgül, 1985)		Emplacement of the Alanya Massif
	i) Absence of material coming from the north, i.e. barrier to sediment from the Antalya Complex exposure to the north of the Alanya Massif ii) No conglomerate underneath the reefs on the northern margin	Generation of palaeo-topography?	
Burdigalian-Langhian boundary	i) Faults with normal offsets in the reefs; ii) Deposition of fault talus at Akseki road; iii) Extensional joint formation prior to complete lithification near Alarahan;		NNW-SSE extensional event
	i) Patchy distribution of Çakallar formation; ii) Thickness variations in the Geceleme formation; iii) Steep sides of later fold limbs may reflect the presence of faults	Asymmetrical half-graben in the north of the basin and fault-generated deep in the south.	
Late Messinian-Early Pliocene	i) Transpressional slickensides at Akseki on older normal faults;	Reverse faulting	Aksu Phase of east-west compression (Poisson, 1977;)
	i) Gentle folding of Miocene sediments with points of inflexion on the limbs concentrated along earlier graben faults;	Fold generation	Susuz Dag Phase of north-south compression (Frizon de Lamotte *et al.*, 1995)
Plio-Quaternary	i) high angle normal offset faults in Late Miocene sediments	Extensional faulting and graben formation	Extension

deduced from the faults was NE-SW, approximately parallel to the strike of the boundary between the Alanya Massif and the Antalya Complex to the north. However, extensional jointing in sequences not directly influenced by the fabric of the Alanya Massif, suggest that in some places, at a particular time, the extension direction was closer to east-west. Although the joint orientation may have been controlled by local stress patterns over a relatively short period, it is possible that the overall NW-SE trend to the strike of the faults at this time relates to reactivation of older weaknesses in the Alanya Massif basement orientated in a similar direction and possibly generated during northward emplacement.

Figure 7.17 shows the subsidence curve for the Ahmetler section in the Manavgat basin. Fitted to it is a theoretical, uniform stretching subsidence curve with a stretching factor (β) = 1.08 (Condon, 1988). The data from the Manavgat basin appears to be consistent with a short pulse of extension between 16-17Ma followed by gentle thermal subsidence (J. Turner, pers. com. 1995).

The full discussion of the Aksu Phase and its relationship to the Susuz Dag Phase can be found in section 7.6.2 and 3. In the Manavgat basin however, the following evidence can be used in the discussion:

- Folding occurred after the deposition of the Miocene sequence;
- Transpressional reactivation of faults also occurred after deposition of the Miocene succession although some syn-sedimentary activity cannot be altogether ruled out;
- E-W striking folding indicates a component of north-south compression;
- Slickensides on reactivated extensional faults are sinistral, suggesting that the largest component of compressional stress is likely to have been orientated east-west;

In summary, there is no clear evidence from the data in the Manavgat basin alone that the Aksu Phase and the Susuz Dag Phase can be separated and chronologically ordered (section 7.3; Frizon de Lamotte, *et al.*, 1995).

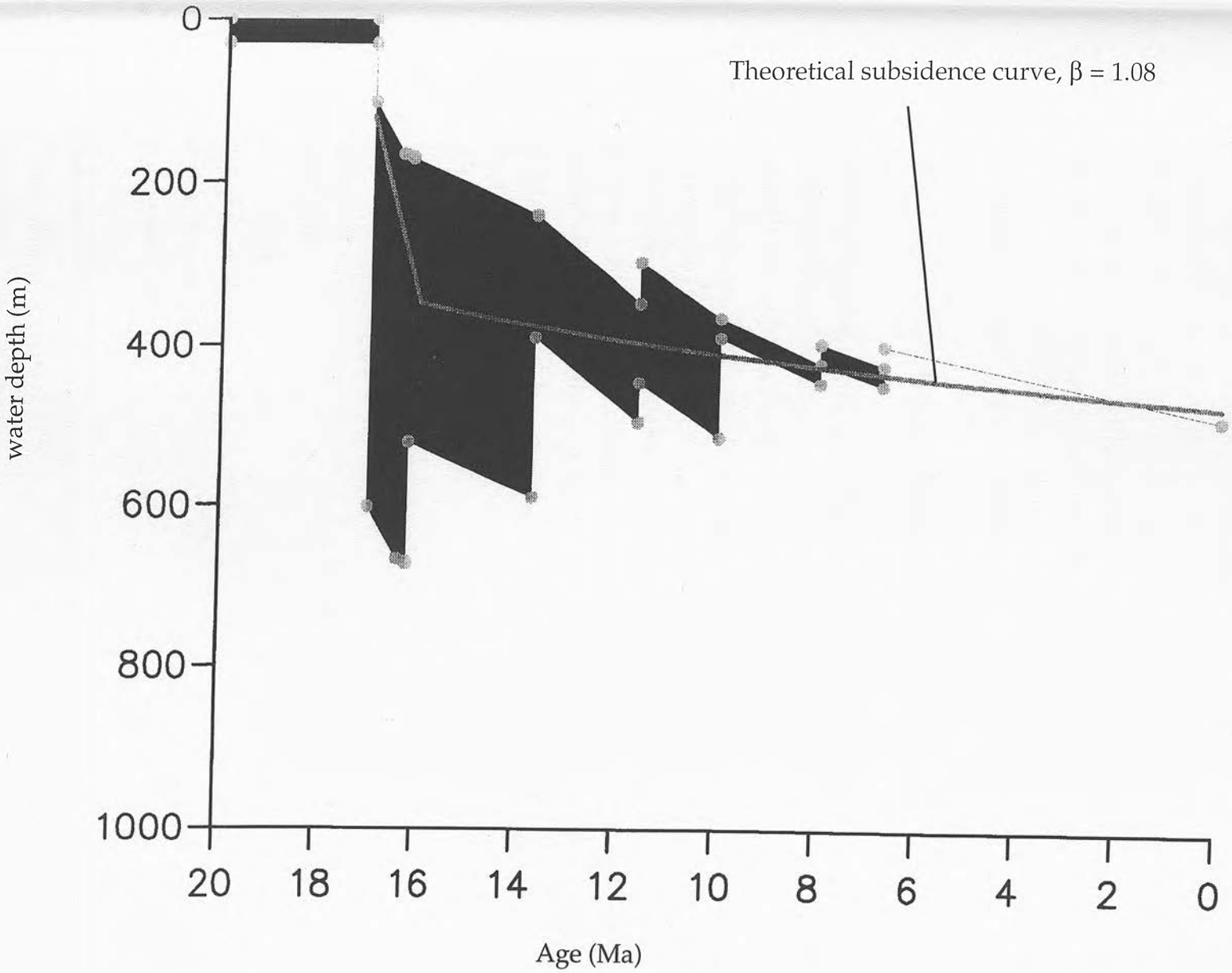

Figure 7.17 Subsidence curve for the Ahmetler section of the Manavgat basin with a theoretical (uniform stretching) subsidence curve (β = 1.08) fitted to it (Condon, 1988). Diagram constructed using software written by J. Turner (see Appendix 6).

7.5.2 *The Köprü and Aksu basins*

The structural evolution of these two basins is far more difficult to assess than that of the Manavgat basin. In part this is because the stratigraphy is less clear (conglomerates are in general difficult to date), but the main reason is that a continuous succession through from basement to Upper Miocene sediments is not exposed, as it is in the Manavgat basin. The two north-south orientated basins (Aksu and Köprü) are discussed together here, because it seems inefficient to deal with them separately, when, in all probability, they were responding to similarly orientated contemporaneous tectonic stress.

7.5.2.1 Basement and basal Miocene structures

The basement surrounding the Aksu and Köprü basins is heterogeneous in terms of its age and rock types. It can be divided into three broad formations: the Bey Daglari Mesozoic limestone, which forms most of the western margin of the Aksu basin; the Antalya Complex which consists of Triassic- Palaeocene deep-sea carbonates, radiolarites and basalts and forms most of the basement promontory dividing the Aksu and Köprü basins; and the Anamas-Akseki platform, which is dominantly Triassic shales and carbonate and forms the eastern border of the Köprü basin (Figs. 7.1b, and 7.2). It was beyond the scope of this project on the Miocene sediments to study in detail the structural features of the basement on which they are found. However, the satellite image of the area (Fig. 1.4) shows clearly the strong north-south grain of the fabric in the basement around the Miocene basins. The age of this grain is difficult to assess given the duration of time over which it may have occurred, but it is thought to have originated during Triassic rifting (Robertson and Woodcock, 1980; 1982; section 7.4). The study of the overlying Miocene sediments suggests that the prominent N-S grain in these younger rocks is the product of reactivation of older weaknesses (Flecker *et al*,. 1995; this study, see below).

Miocene sediments directly overlying basement rocks are only exposed in a few places in the Aksu and Köprü basin area. At one of these, on the Mesozoic "promontory" which divides the two basins (Fig. 7.5) small

pockets of reddened, channelised and imbricated conglomerates directly overlie basement carbonate, basalt and radiolarite (Fig. 5.5, chapter 5 section 5.5.1.2). Dating of these thin sequences has not been attempted during this study, but Akay and Uysal (1985) identified them as Miocene because of their similarity to the Miocene continental successions seen elsewhere in the area (e.g. Kargi and Aspendos; Fig. 5.6). It is possible however, that these conglomerates are Pliocene in age.

Figure 7.18 is a geological map based on that drawn by Akay and Uysal (1985), centred on the southern part of the Mesozoic "promontory" between the Aksu and Köprü basins. Two small linear conglomerate-filled sub-basins can be seen overlying Mesozoic basement, both with a prominent west-verging north-south striking thrusts along their eastern margins. In detail, these Miocene exposures contain abundant micro-faults. The dominant normal-fault orientation is shown in figure 7.19a and strikes NE-SW, at variance with the orientation of both the micro-normal faults and the extensional joints in the Manavgat basin (see section 7.5.1.2 above). It is not possible to be absolutely certain that these faults are Miocene in age, but their association with the preservation of small sub-basins suggest that they may be related to their genesis.

Reverse faults within these Miocene sediments are also found, often in greater abundance than the normal faults. These reverse faults also show a greater scatter of orientations than the normal faults (Fig. 7.19b), but it is interesting to note how few of them are orientated north-south, parallel to the strike of the east-bounding fault. The dip of this bounding fault is difficult to estimate, but there is little evidence of any that the reverse faults in the study area are low angle and it is therefore assumed, in the absence of any contradictory evidence, that these bounding faults are also relatively high angle.

7.5.2.2 Basin bounding faults and faults within Miocene sediments

Large scale, north-south, high-angle faults dominate Miocene exposures in the Aksu and Köprü basins. This fault trend has previously been documented by Poisson (1977) and Akay and Uysal (1985). The basin margin faults (Kirkkavak Fault, Pinargözü fault zone, and Aksu Thrust

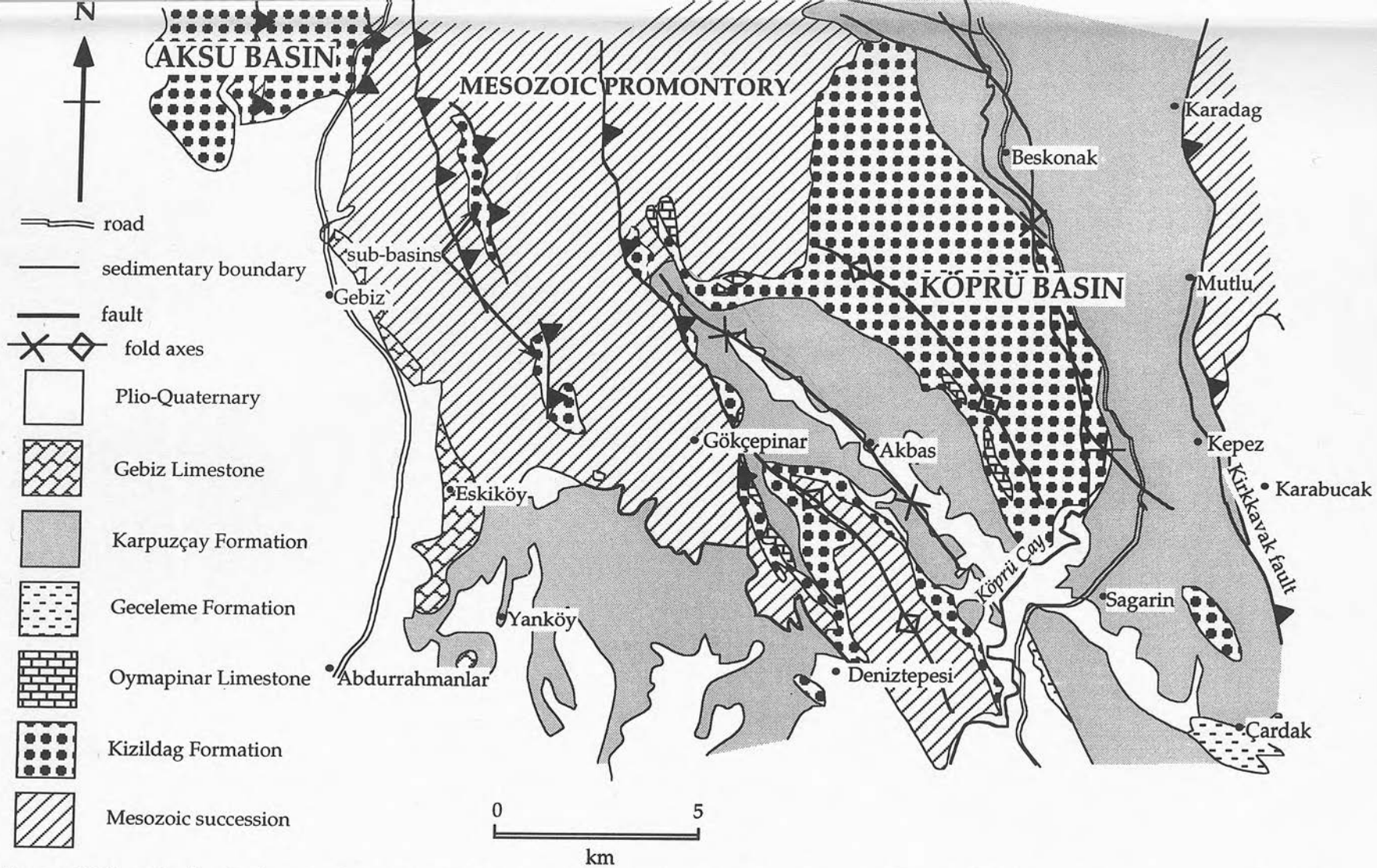

Figure 7.18 Geological map of the central region of the study area after Akay and Uysal (1985). The map is centred on the Mesozoic "promontory" which divides the Aksu from the Köprü basin. Note the development of small N-S orientated linear outcrops of conglomerate on top of the basement and the thrusts that mark their eastern boundaries. Characteristically, the strong N-S orientated fabric of the faults is untraceable throught Pliocene or Quaternary sediments, indicating that the age of formation of these faults (the Aksu Phase, Poisson, 1977) is likely to have been at the Miocene-Pliocene boundary.

a)

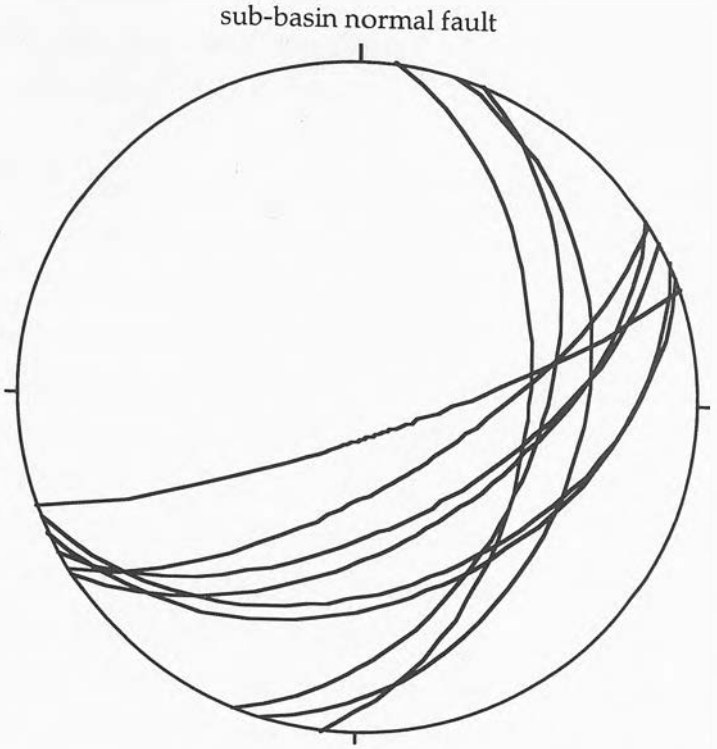

Normal faults n=9

b)

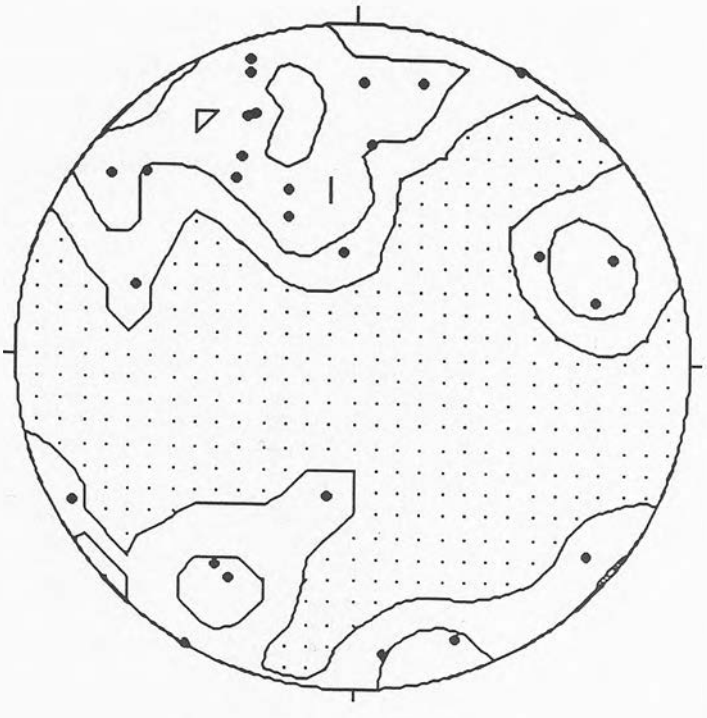

Reverse faults n=26

Figure 7.19 Stereonet projections of faults measured from the sub-basins on top of the Mesozoic "promontory" which divides the Aksu and Köprü basins: a) normal faults striking NE-SW; b) reverse faults with a variety of orientations, very few of which are north-south, parallel to the basin bounding thrust.

(Fig 7.5) are mirrored by faults within the basins which have smaller offsets (e.g. Kargi Fault).

The Kirkkavak fault on the eastern margin of the Köprü basin has intrigued geologists over several decades. Today it rises steeply from the basin floor, but as already discussed in chapter 4 (see section 4.6.2.4), palaeocurrent data indicate that during the Miocene it probably had little or no topographic expression, such that there is no evidence of it having been a source of material for turbidite deposition. Its lack of topography in the south of the Köprü basin is thought to be the cause of overfilling in this area. Dumont and Kerey (1975) studied the Kirkkavak fault and identified two periods of movement on it during the Miocene. The first was post-Burdigalian dextral strike-slip movement identified near Burmahan. This was followed by post-Tortonian east-west compression, resulting in high angle reverse movement. Active talus fans obscure much of the accessible face of the fault and its relationship with Miocene sediments, but these fans indicate that it has been reactivated more recently than the Late Miocene, probably as part of the Plio-Quaternary extensional events (Glover, 1995). The southern end of the Kirkkavak fault bifurcates close to the most northern tip of the Manavgat basin and then disappears underneath Miocene sediment close to the village of Çardak. Folding in the area south of the most southerly exposure of the Kirkkavak fault may well indicate that it has subsurface expression as a blind fault.

The eastern margins of both Aksu and Köprü basins are generally less clearly delineated than the western margins. The western margin of the Köprü basin for instance is faulted, but not as a single concentrated fault zone like the Kirkkavak fault. The western margin of the Aksu basin is largely unfaulted with sedimentary evidence suggesting a steep, but passive contact between the Miocene and Mesozoic (see chapter 5, section 5.6.4.2). The eastern margin of the Aksu basin however, like the Kirkkavak fault, is a well defined fault lineament striking north-south, which, like others parallel to it, disappear without trace under Pliocene sediment (Fig 7.18, north-western corner). A few kilometres further south, Antalya Complex rocks are overlain by a shallow-water carbonate called the Gebiz limestone (Akay and Uysal, 1985; Akay *et al.*, 1985). The

age of this limestone is crucial to the accurate termination age of the Aksu Phase of deformation, but it remains tantalisingly difficult to date and its age cannot be pinned down closer than Late Messinian to Early Pliocene (Poisson, pers. com. 1994).

Strike-slip faulting in both the Aksu and Köprü basins is common although the sense of movement on these faults varies from place to place. Figure 7.20a shows the distribution of poles to planes for strike-slip faults from Serravallian conglomerates (Poisson, 1977) near the village of Kargi in the Aksu basin and from the Karpuzçay Formation in the eastern half of the Köprü basin. There is a clear north-south trend in the orientation of the planes. The Kargi measurements come from a well delineated north-south striking fault zone, which though it appears to have little stratigraphic offset (Poisson pers. com., 1994) has 2-300m of topographic expression just to the east of the village of Kargi. Frizon de Lamotte *et al.* (1995) also collected fault data from this area with differing results (Fig 7.21). In contrast to the clear delineation of the Kargi fault zone, the Köprü basin measurements were taken along cross-sections from the eastern margin bounding Kirkkavak fault to the centre of the basin. The faults were therefore much more dispersed over an area outside the clearly defined Kirkkavak fault zone.

Figure 7.20b is a stereonet projection of poles to normal faults measured in the area to the west of the Kirkkavak fault. From the limited data available, these faults appear to have a bimodal distribution with one set of planes orientated approximately north-south parallel to the strike-slip faults, and another possibly more dominant set striking NE-SW. It is interesting to note the similarity in the strike of these normal faults and those seen affecting the pockets of Miocene conglomerate overlying the Mesozoic promontory displayed in figure 7.19a (section 7.5.2.1 above). The reverse faults also show this same bimodal pattern of distribution (Fig. 7.20c).

The Pinargözü fault zone which marks the western margin of the Köprü basin is, like the other fault zones in the area orientated north-south (Fig. 7.5). Measurements on faults within this zone also have a strong north-south trend (Fig. 7.21a, and b). From the generations of slickensides

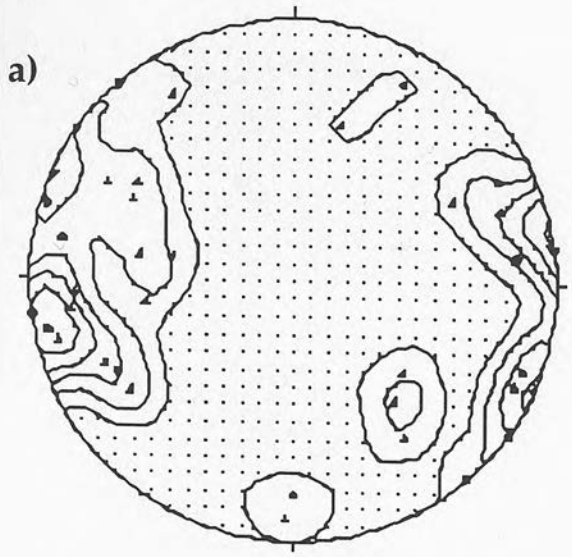

Strike slips faults from the Aksu and Köprü basins

● Köprü basin a mixture of sinistral and dextral

▲ Aksu basin, mostly dextral

n = 35

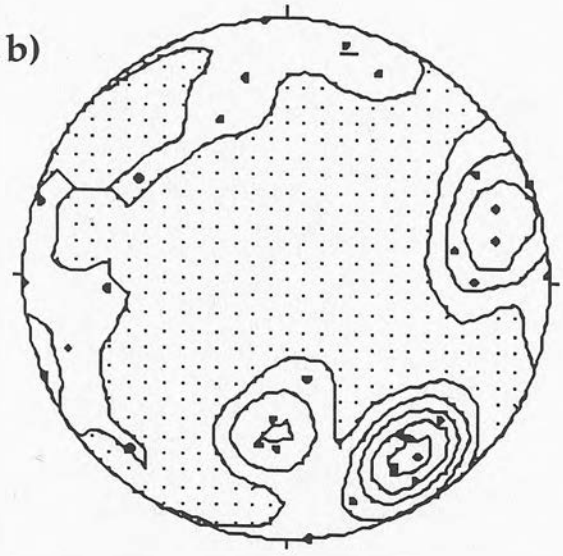

Normal faults from the Köprü basin

n = 28

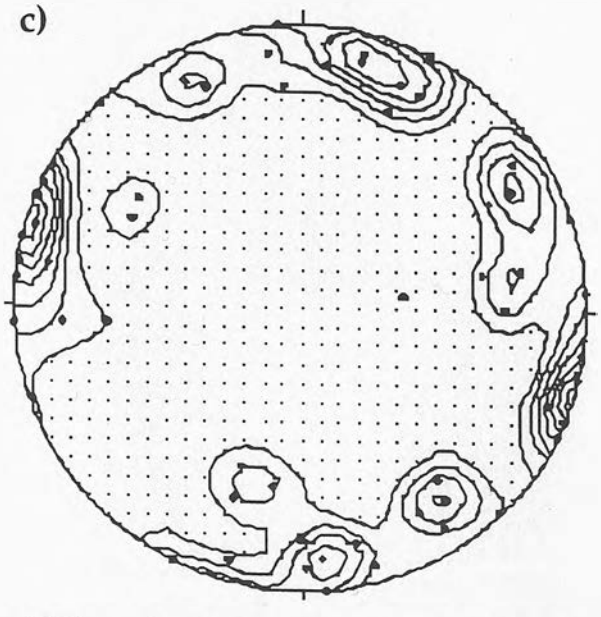

Reverse faults and those with unspecified sense of movement

n = 79

Figure 7.20 Stereoplots of fault data from the Aksu and Köprü basins.
a) Strike slip faults with a dominantly north-south strike, parallel to the basin bounding faults and the structural grain of the basement; b) normal faults from the eastern side of the Köprü basin showing a bimodal distribution pattern, broadly north-south striking and a set striking NE-SW; c) Reverse faults and those whose sense of movement was not discerned also showing a similar distribution pattern to that of the normal faults in the Köprü basin.

a)

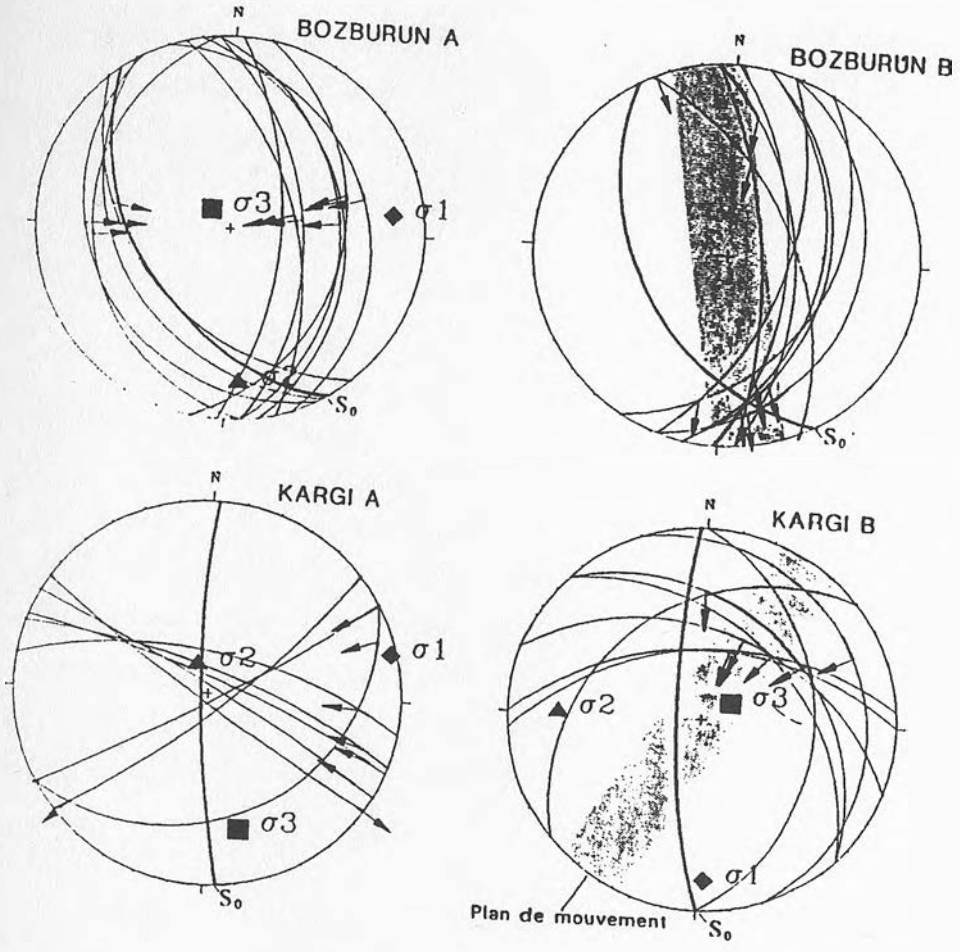

b)

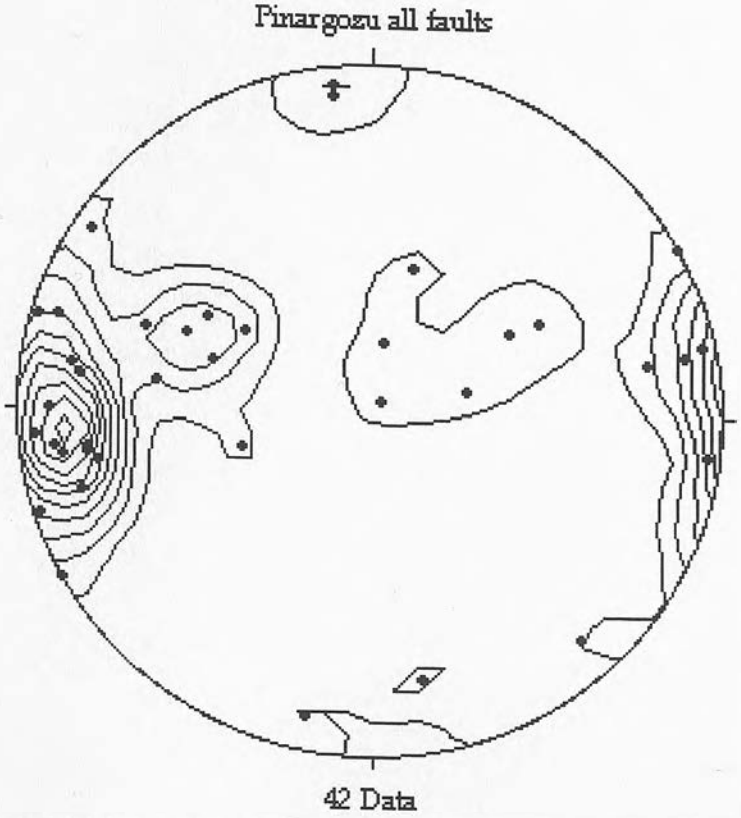

Figure 7.21 a) Stereonet projections of fault plane data from Kargi and Pinargözü from Frizon de Lamotte *et al.* (1995); b) Stereonet projections from the Pinargözü fault zone collected during this study.

collected from these faults, Frizon de Lamotte *et al.* (1995) suggest that the compressional system forming these north-south faults can be divided into two distinct events, the first caused by east-west compression they called the Aksu Phase (Poisson, 1977), the second caused by north-south compression, they called the Susuz Dag Phase. Based on the small data set of sequential slickenside generations on a single fault plane, this study cannot conclusively confirm or disprove this hypothesis. However, given that the data set presented in their paper (Frizon de Lamotte *et al.*, 1995) for the Pinargözü fault zone was itself small (n = 11, Aksu Phase; n = 8, Susuz Dag Phase) it is perhaps justified to mention that the data set generated during this study (n = 12) suggests that the final movement on faults with more than one generation of slickensides is almost always reverse. On north-south orientated faults this indicates that east-west compression is required. This observation does not preclude there having been a later south directed compressional event as most of the evidence comes from the Bey Daglari, but no evidence can be presented here to support this concept.

7.5.2.3 Folding of Miocene sediments

Frizon de Lamotte *et al.* (1995) suggest in their paper that the Miocene conglomerates found at the top of Bozburun Dag, the 2500m peak between Pinargözü and Ballibucak (Fig. 7.5) on the western margin of the Köprü basin is part of a west-vergent recumbent fold which also folds Mesozoic basement beneath Miocene cover (cross-section in figure 7.22b). Looking east from the Pinargözü pass, it is possible to observe the change in the dips of the Miocene conglomerate over the fold nose in agreement with this hypothesis (Fig. 7.23). The cross-section taken from the Frizon de Lamotte *et al.* (1995) paper is unfortunately difficult to correlate with the map from which it was supposedly drawn (Fig. 7.22). Note that to the west of Bozburun, the area of Bey Daglari carbonate is not shown on the cross-section and the missing fault from this area is assumed to be that which on the map divides this carbonate from the Antalya Complex further to the west.

Although these are relatively minor errors, even when drawn correctly, this cross-section does not, in detail fit the field evidence from the

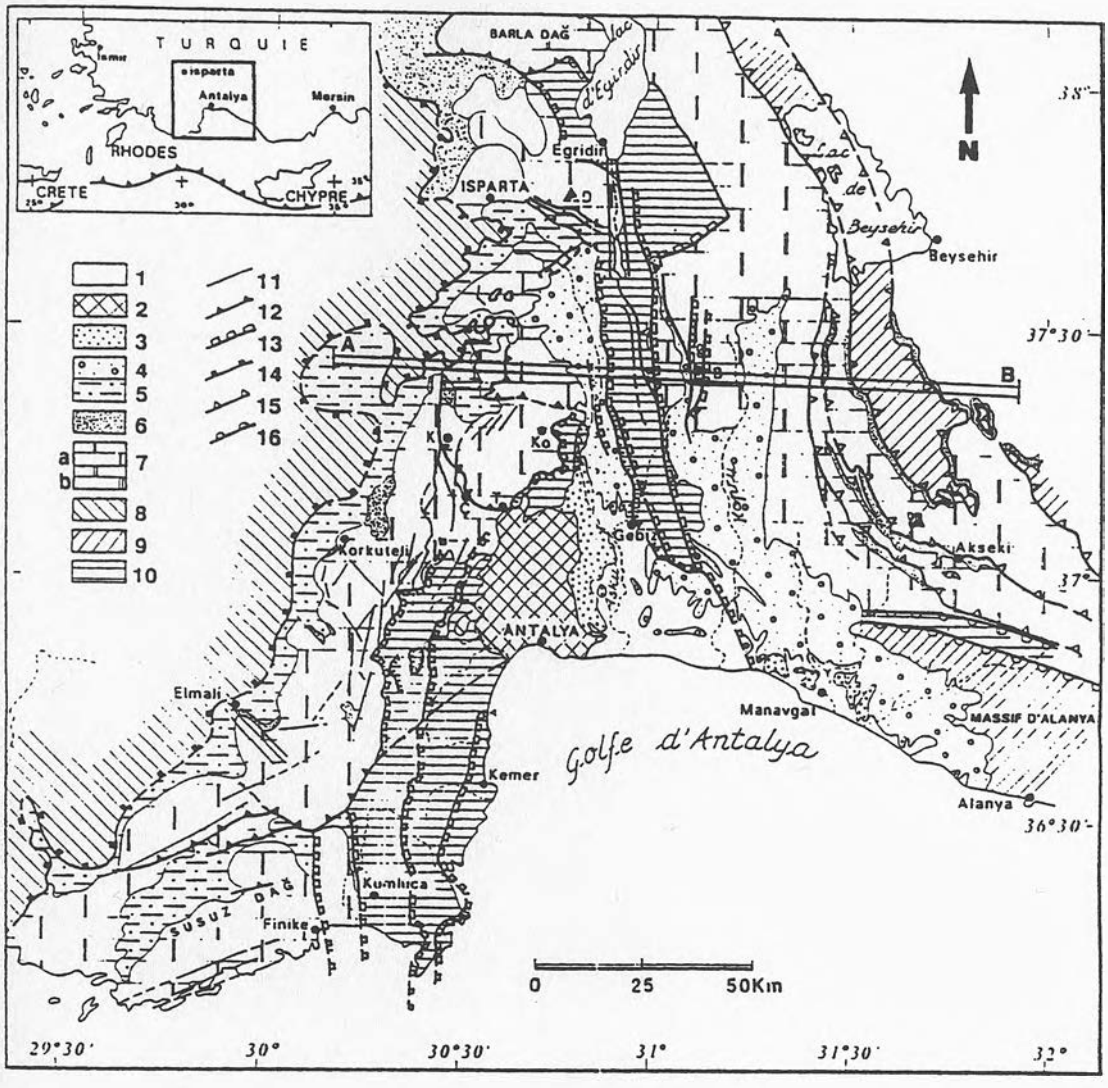

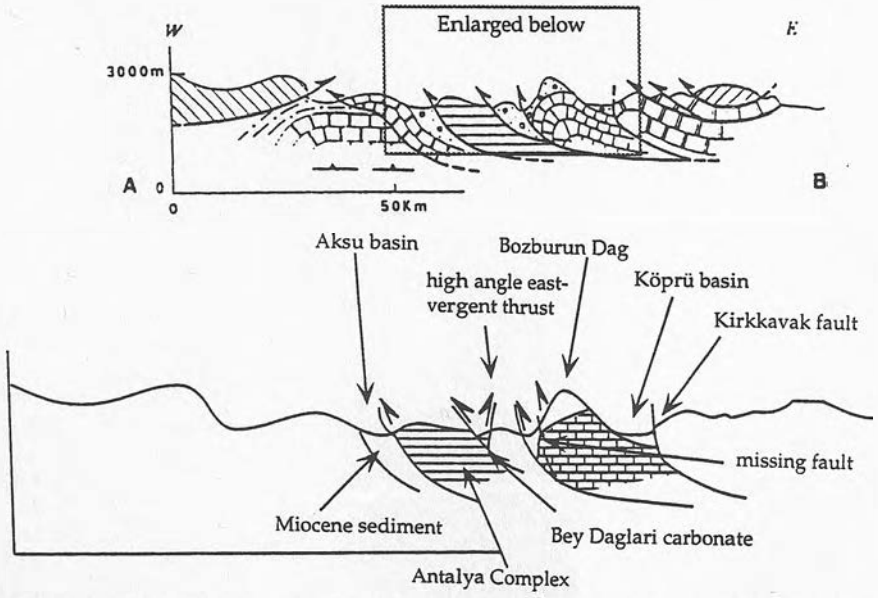

Figure 7.22 a) map of the structural configuration in and around the Isparta Angle from Frizon de Lamotte et al. (1995); b) cross-section drawn from the map by Frizon de Lamotte et al.; c) cross-section correcting minor mistakes on cross-section b and adding the east-vergent high angle reverse fault which can be observed in the field.

Figure 7.23 Photograph of the nose of the Bozburun Dag (Fig. 7.5) recumbent fold looking east.

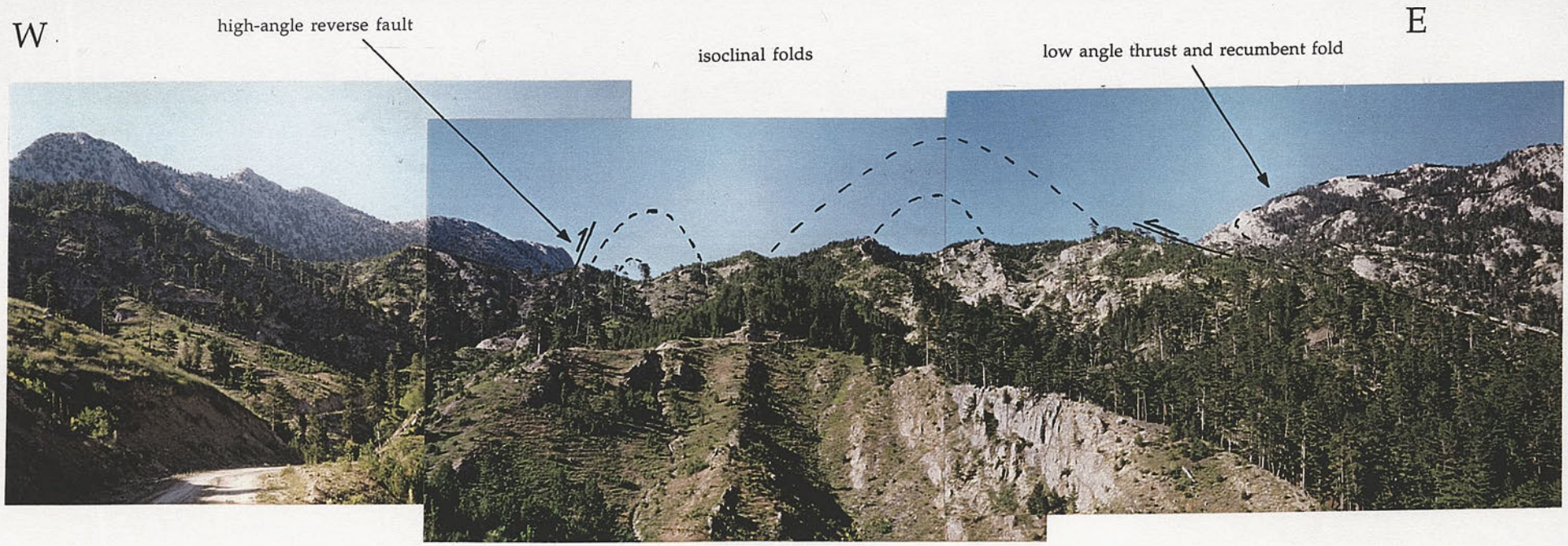

Figure 7.24 Photo-montage looking north from the Pinargözü pass showing the thick pile of conglomerates of the Bozburun Dag fold to the east jamming up against isoclinally folded conglomerates and marls (centre, foreground). In the west the Mesozoic carbonate interpreted as part of Bey Daglari carbonate platform has been thrust eastwards over the isoclinally folded conglomerates.

Pinargözü area. Figure 7.24 is a photomontage and interpretative sketch looking north from the Pinargözü pass, showing that between the thick pile of conglomerates making up the nose of the Bozburun Dag fold and the Bey Daglari carbonate in the west, conglomerates and marls have been deformed into upright isoclinal folds. The boundary between the Bey Daglari carbonates and conglomerates can be observed in a steep gully just beyond the bridge going up towards the pass from Pinargözü. It is clearly exposed as a high angle reverse fault, placing Mesozoic carbonate eastward on top of Miocene conglomerates.

The Bozburun Dag nappe is not the only large scale recumbent fold in the study area. In the south-west of the Köprü basin near Gökçepinar and Akbas (Fig. 7.5) an east verging recumbent fold with a core of Mesozoic limestone can be seen (Fig. 7.25). Akay and Uysal (1985) marked the boundary between this limestone and the Miocene sediments as a fault and it is quite possible that slip did occur along this horizon.

Smaller-scale folding similar to the isoclinal folds is seen elsewhere in the basin, generally associated with well defined fault zones like that at Pinargözü. Figure 7.26b indicates that the folds found in these situations have axial planes that strike parallel to the north-south trend of the fault zone. The turbidites in the eastern half of the Köprü basin are folded in a different style, generally much more openly and often with an overturned limb. The orientation of the axial planes of these folds is shown in figure 7.26a which suggests that they trend NW-SE.

7.5.2.4 Interpretation

Interpretation of the Aksu and Köprü basin structural data is much more difficult than that of the Manavgat basin primarily because the stratigraphy is far less well exposed and dated. It is not possible, for instance to clearly identify an Early Miocene extensional event like that discussed in section 7.5.1.2 above. Because of the almost complete absence of Pliocene sediment in all but the far south of the Aksu basin, only the large north-south trending faults can be seen to have a clear pre-Pliocene age. The micro-faults are almost impossible to date. However, assuming that a tectonic event affecting Miocene sediments in the Manavgat basin

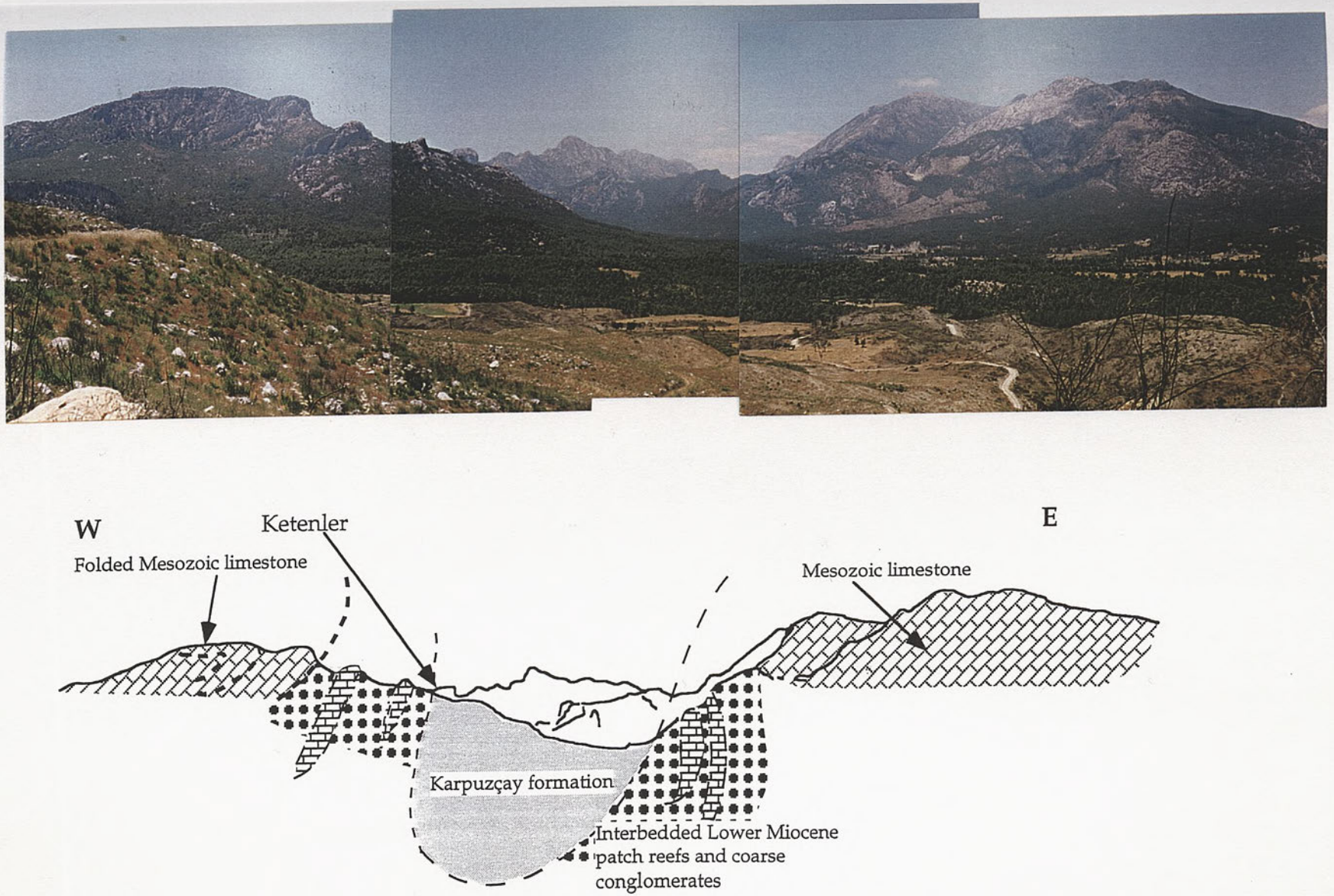

Figure 7.25 Photo-montage and sketch of the east-vergent recumbent fold structure near Akbas, SW Köprü basin

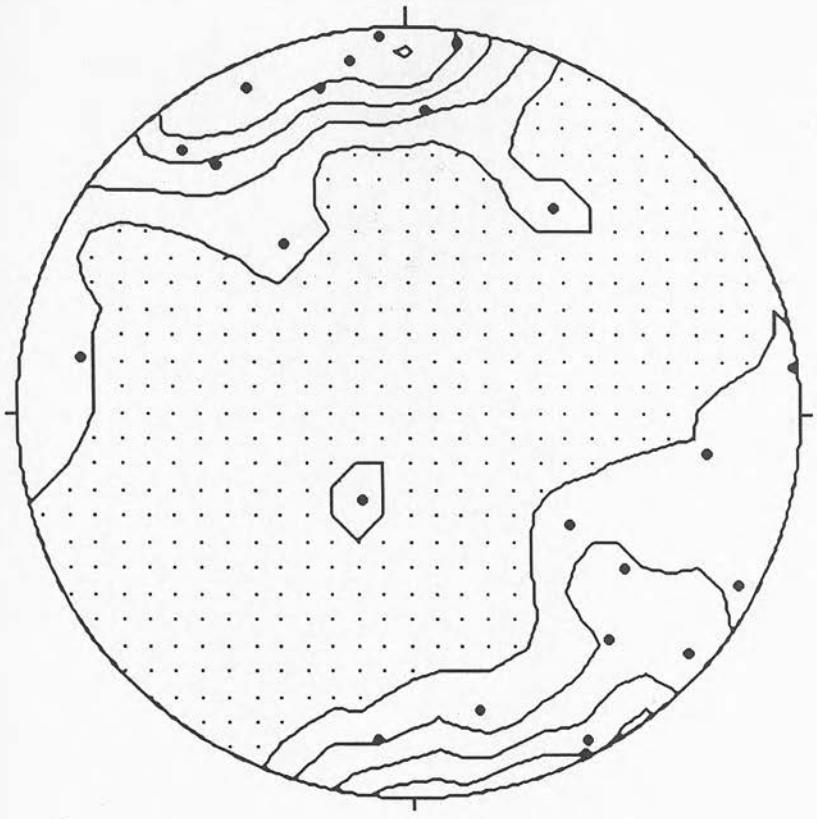

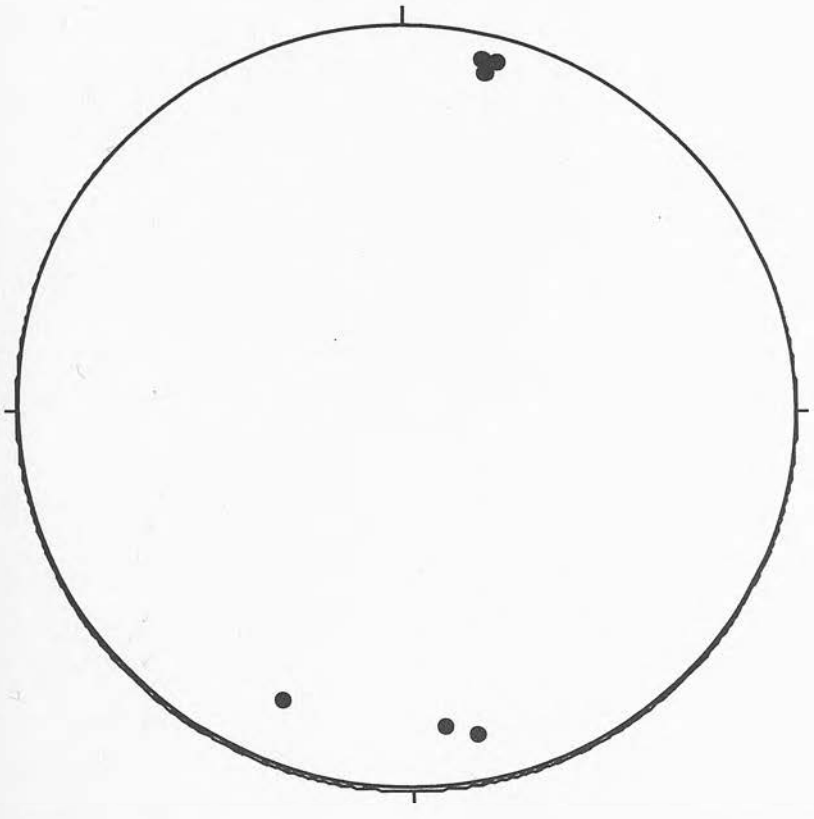

Figure 7.26 Stereonet projections of fold axes from a) the eastern side of the Köprü basin in the Karpuzçay turbidites, and b) from close to well defined north-south striking fault zones at Pinargözü and Kargi.

is likely to have had some expression in the Aksu and Köprü successions it is possible to put together a tentative structural history.

There is no conclusive evidence to suggest that the micro-scale normal faults in the Aksu and Köprü basins and on top of the Mesozoic promontory which divides them are not Plio-Quaternary. However, if they did form during the Miocene, one possibility is that their dominant NE-SW orientation was generated during formation of a pull-apart basin in relation to strike-slip faulting along north-south lineaments such as the Kirkkavak fault. Dumont and Kerey (1975) suggest that the Kirkkavak fault moved dextrally in post-Burdigalian times and this would fit with a theoretical model of the Aksu and Köprü basin area behaving as a pull-apart system. Note that even outside the well defined fault zones most of the micro-scale strike-slip faults trend north-south, parallel to the basin bounding faults (Fig. 7.20a). These may or may not be connected to faults at depth generated by the earlier fabric of the basement and thus these faults may not represent failure in a stress field free from direct basement influence. They do however indicate that most of the strike-slip movement visible on faults post-Early Miocene is taken up on north-south striking fractures.

Dumont and Kerey (1975) suggest that the Post-Tortonian movement on the Kirkkavak fault resulted in high angle reverse faulting due to east-west compression (later named the Aksu Phase; Poisson, 1977). It has never been quite clear how much compression this event actually resulted in. Poisson *et al.* (1984) suggested that a minimum of 50% shortening had occurred and certainly the formation of large scale recumbent folds, such as the Bozburun Dag fold, would support significant shortening. However, most authors have viewed the results of the east-west compressional event purely in terms of westward transport (e.g. Poisson, 1977; Poisson *et al.*, 1984). This study presents evidence that eastward transport in some areas was by no means insignificant leading to the formation of east-verging recumbent folds (e.g. at Akbas) and high angle east-directed reverse faults (at Pinargözü). This east-directed faulting may well be a back-thrust within a westward transporting system (Fig. 7.22c). The east-vergent fold is not so easily explained however and may suggest that rather than a simple westward

transport system, the Isparta Angle was being tightened by the movement of both arms. Palaeomagnetic studies of Miocene sediments on top of the Bey Daglari on the eastern margin of the Aksu basin indicate a Post-Langhian anticlockwise rotation of 30° (Kissel and Poisson, 1986). Kissel and Poisson (1987) suggested that this rotation was taken up on a décollement beneath the Neogene basins in order to explain the absence of a rotation signature in the post-Langhian sediments (Kissel and Poisson, 1987). It is possible, however, that some of the east-vergent compression resulting from this rotation might have produced the east-vergent structures observed in the field.

7.6 Tectonic context

7.6.1 Formation of the Miocene basins

7.6.1.1 Post-Langhian anticlockwise rotation of the Bey Daglari and extension in the Manavgat basin.

The orientation of the extensional faults in the Manavgat basin (NW-SE, Fig. 7.6) are, on the surface, an unlikely direct result of anticlockwise rotation of the Bey Daglari. The cause of this rotation however is perhaps more worth considering. Both Kissel and Poisson (1987), Kissel *et al.* (1993) and Morris and Robertson (1993) suggest that south-eastward movement of the Lycian Nappes played an important rôle in the recording of the palaeomagnetic signature in the western arm of the Isparta Angle either as the origin of orogenic fluids which caused widespread remagnetisation throughout the permeable rocks of the basement at this time (Morris and Robertson, 1993), and/or as a mechanism for inducing rotation (Fig. 7.3, Kissel *et al.*, 1993). Can then the Lycian Nappes be viewed as an encroaching load causing flexure and faulting in the foreland much like the model put forward for the evolution of the Adana basin to the east (see below, Williams and Unlügenç, 1992; Gürbüz, 1993)? Once again the orientation of the faults in the Manavgat basin are difficult to reconcile with generation during a south-eastward transport of the Lycian Nappes. However, Flecker *et al.* (1995) suggested that rather than generating new faults related to flexure, Lycian loading of the lithosphere might have induced block faulting in

the foreland which exploited pre-existing lines of basement weakness. There are various pieces of evidence which support this hypothesis:

- There is a west to east diachroneity of basin formation (e.g. the Kas-Dariören flexural basin (Fig. 7.2) contains Aquitanian transgressive limestone; the thick pile of Lower Miocene conglomerates in the Aksu and Köprü basin is certainly Burdigalian in age, although it could be older.; the Manavgat basin contains a thinner succession of probably Upper Burdigalian conglomerates. This diachroneity could have been caused by an encroaching nappe pile from the NW;
- The orientation of the extensional faults within the Manavgat basin mirrors the northerly bounding fault with the Antalya Complex suggesting that these faults may have reactivated older weaknesses within the Alanya Massif. This is supported by the evidence that extensional fracture (e.g. localised jointing), when unconnected to basement, is orientated at a different angle (section 7.5.1.2; Fig. 7.11);
- Evidence of recurrent reactivation of N-S faults in the Aksu and Köprü basins from Early Mesozoic to recent times (Robertson *et al.*, 1991; Robertson, 1991).

Fault-defined blocks in the Isparta Angle area may have behaved in a similar style to the broken slat model (Taymaz *et al.*, 1991; Fig. 7.27) This model was originally put forward to explain Quaternary N-S extension along the Aegean coast of western Turkey in the context of a westward moving Anatolia. The Isparta Angle lies along the transition zone where in the model Taymaz *et al.*, (1991) indicate that pinning of the slats to the Anatolian block occurs. Taymaz *et al.*, (1991) did not really consider deformation in this region, but their model predicts dextral strike-slip between individual ENE-WSW trending individual slats (Fig. 7.27). This is not observed today in this transition zone (Price and Scott, 1994). These authors proposed that the boundary between the slats and Anatolia was accommodated by a N-S trending deforming zone across which dextral displacement occurs and within which NE-SW trending fault blocks rotate clockwise (Fig. 7.28).

It is suggested that during the Early Miocene, a not dissimilar tectonic scenario could have been active. Figure 7.29 is a schematic representation of the region from Burdigalian to Tortonian times, when Lycian Nappe emplacement to the SE is thought to have caused the rotation of the Bey Daglari (Kissel et al., 1993; Morris and Robertson, 1993). Kissel and

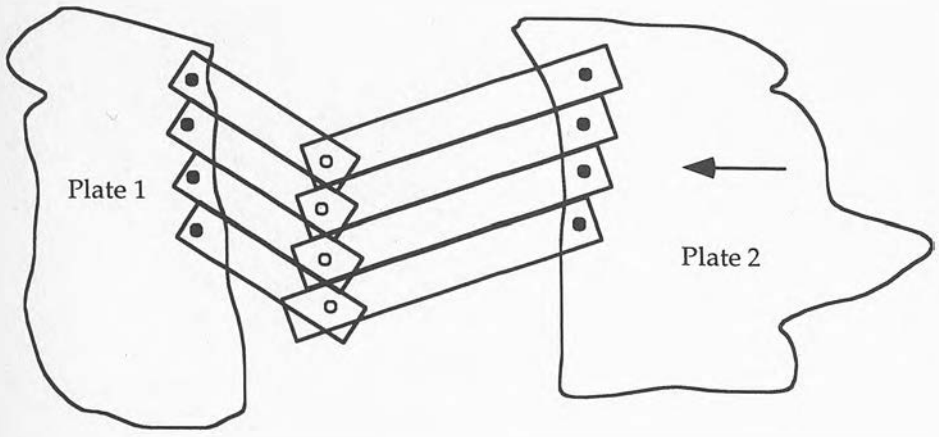

Figure 7.27 Model of broken rotating slats. Filled circles are screws that attach the slats to the margins of plates 1 and 2. Open circles are the screws which join only the two arms of each broken slat (from Taymaz *et al.*, 1991).

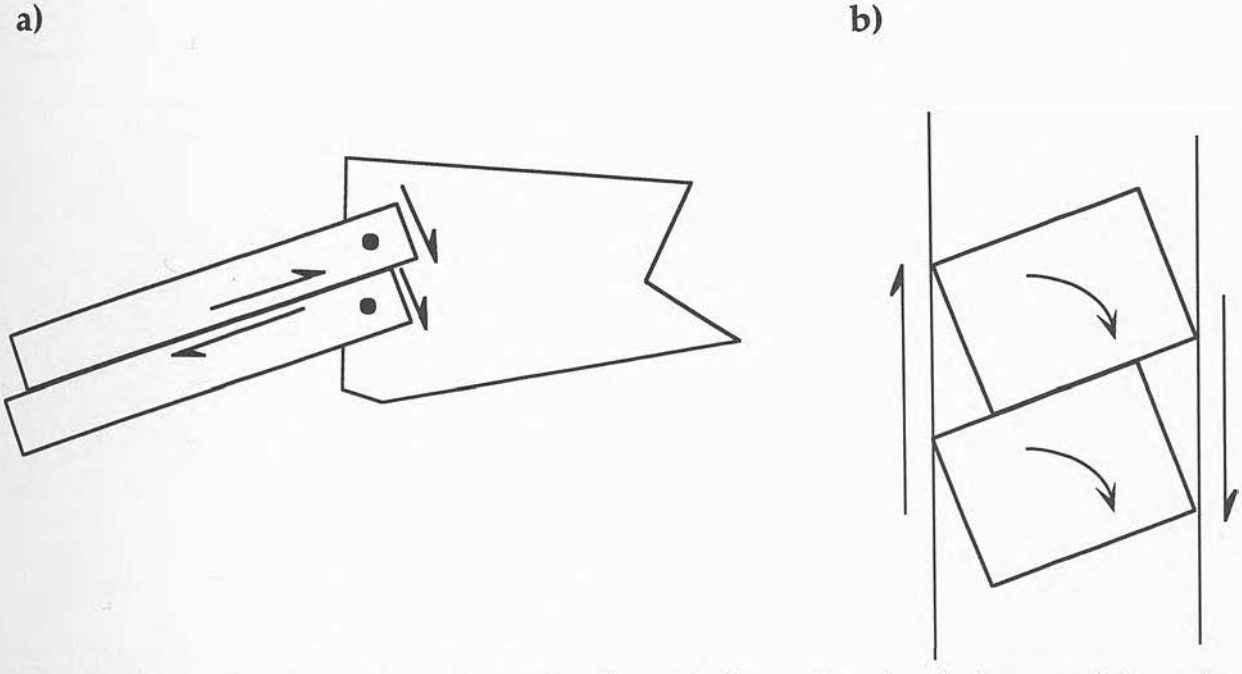

Figure 7.28 a) close up view of the dextral shear direction between slats and between the slat and the plate to which it is attached. b) Modification of the eastern margin of the model by Taymaz *et al.* (1991) to accommodate the structures observed in the Burdur region. The region of attachement is suggested to be an approximately N-S deforming zone across which dextral shear is taken up and in which NE-SW trending faults rotate.

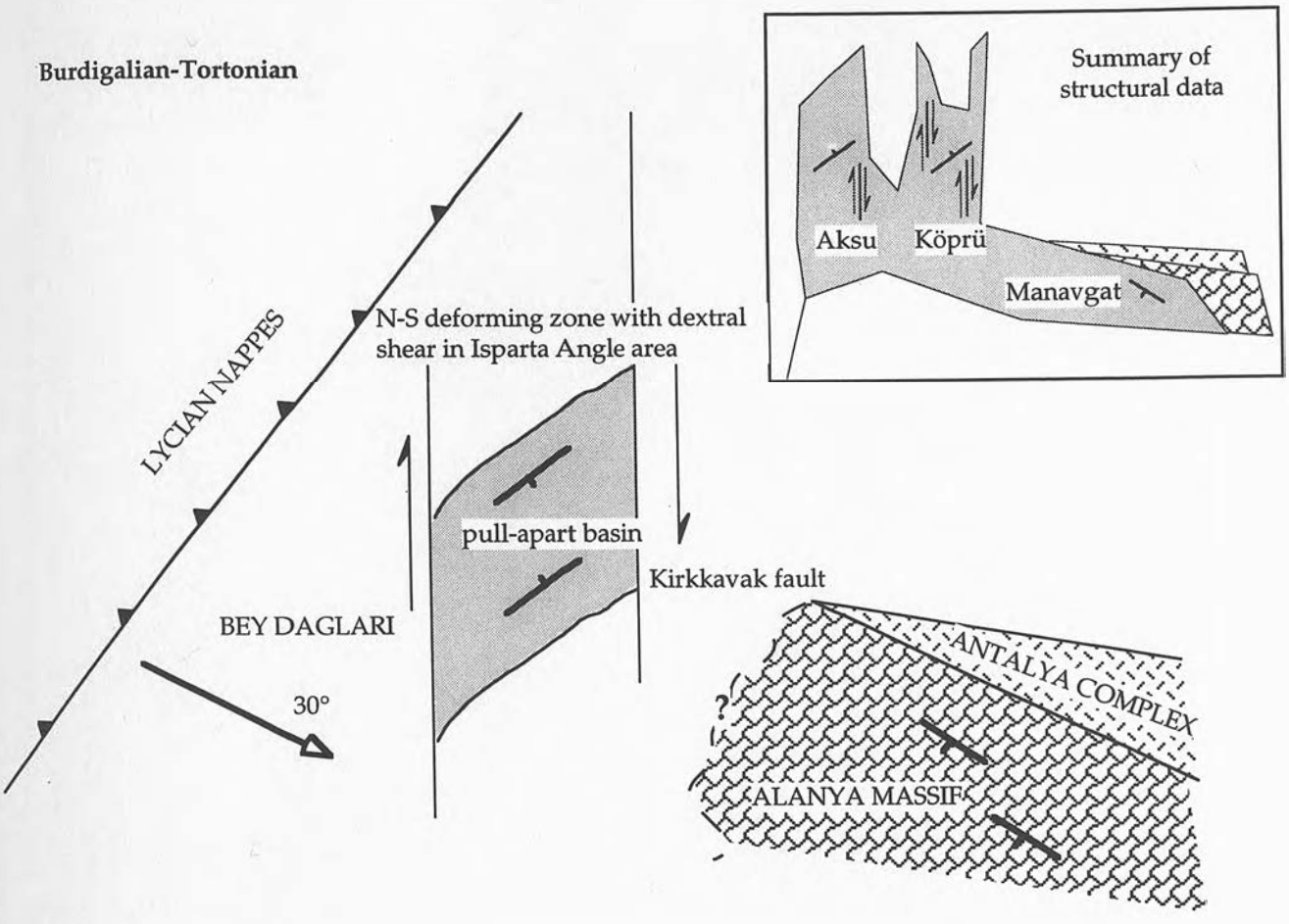

Figure 7.29 Model of the development of extension in the study area during the Lower-Middle Miocene invoking the formation of a pull-apart basin driven by the rotation of the Bey Daglari and the emplacement of the Lycian Nappes.

Poisson (1987) suggested that this rotation was accommodated by a deep décollement at the base of the Antalya Complex in order to explain the absence of rotation in post-Burdigalian sediments. It is suggested however, that some of the rotation might have been taken up by dextral strike-slip along N-S orientated old lineaments. This strike-slip appears to have been focused within the Isparta Angle as a north-south deforming zone, like that envisaged by Price and Scott (1994) for the Quaternary. Within this dextral shear zone the formation of one or several, small, pull-apart basins potentially explains the formation of accommodation space (e.g. ~1.5km of Lower Miocene conglomerate (Kizildag Formation) in the Köprü basin) within a compressional regime at this time, something that the décollement hypothesis of Kissel and Poisson, (1987) fails to generate.

The Manavgat basin behaved differently from the Aksu and Köprü basins (Fig. 7.29 inset). It is suggested that the orientation of the NW-SE trending normal faults which developed at this time in the Manavgat basin (section 7.5.1.2) are controlled by basement weaknesses in the Alanya Massif trending parallel to its boundary with the Antalya Complex. Dextral shear on the eastern bounding fault of the N-S deforming zone (i.e. the Kirkkavak fault) might be expected to reactivate these. There is little evidence to suggest that the motion on these NW-SE faults was purely normal and significant oblique slip could have occurred whilst still producing the horst-graben structure deduced from the sediment facies and thickness variations.

7.6.1.2 Subduction related extension on the upper plate of the Hellenic-Cyprus system

Another possible cause for extension in the study area is tectonic activity along the Hellenic Arc south of Cyprus. The timing of initiation of northward subduction along this system has long been a matter for debate (e.g. Crete: McKenzie, 1978; Le Pichon and Angelier, 1979; Meulenkamp *et al.*, 1988; Cyprus: Kempler and Ben Avraham, 1987; Eaton and Robertson, 1993). However, the agreement between most recent authors lends credence to an Oligo-Miocene time of initiation (Meulenkamp *et al.*, 1988; Eaton and Robertson, 1993). Robertson and Woodcock (1986)

suggested that the Kyrenia Range in northern Cyprus subsided allowing the transgressive deposition of the Kithrea Flysch at this time. This subsidence can be explained (Robertson and Woodcock, 1986) by extension on the upper plate of a recently initiated northward-dipping (Jackson and McKenzie, 1984; Kempler and Ben Avraham, 1987) subduction zone to the south of Cyprus. The extension of the northern Cyprus Miocene basin across the Cilicia Basin (Fig. 7.1) to Adana is well established (e.g. Evans, 1978; Robertson and Woodcock, 1986; Ünlügenç *et al.*, 1990) and it seems probable that the Antalya area was part of the same system. However, extensional faulting in the Manavgat basin occurs significantly later (e.g. 10 Ma later) than the collapse of the Kyrenia Range and workers in the Adana basin suggest that Early Miocene extensional faults formed in relation to load-induced flexure resulting from renewed thrusting in the Taurides to the north rather than due to supra-subduction zone extension.

Another possibility stems from a suggestion by Poisson (1984) that the Hellenic arc could have extended onto land along the front of the Lycian Nappe system (Fig. 7.30). In connecting with the Cyprean arc, this would place the Isparta Angle in the position of a transform fault along which dextral shear would be predicted (Fig 7.31). Within this context, (i.e. the close connection of the two subduction systems) the supra-subduction zone extension in the Cilician basin assumes a much more credible position in the formation of the Manavgat basin, which represents the northern margin of Cilicia during the Miocene.

7.6.2 *Emplacement of the Lycian Nappes and the Aksu Phase*

In their model, Kissel *et al.* (1993) suggest that the north-south Aksu thrust on the eastern margin of the Aksu basin, used by Poisson to date the phase of compression at the end of the Miocene (the Aksu Phase) was generated during the rotation of the Bey Daglari (Fig. 7.3). There is no clear evidence to suggest that compressional activity could not have begun significantly earlier that the Latest Miocene in some areas. In fact the thick successions of coarse grained conglomerates and sandstones deposited in the basin despite a rising sea level (section 5.10) during the whole of the Tortonian suggest that active uplift and erosion of the

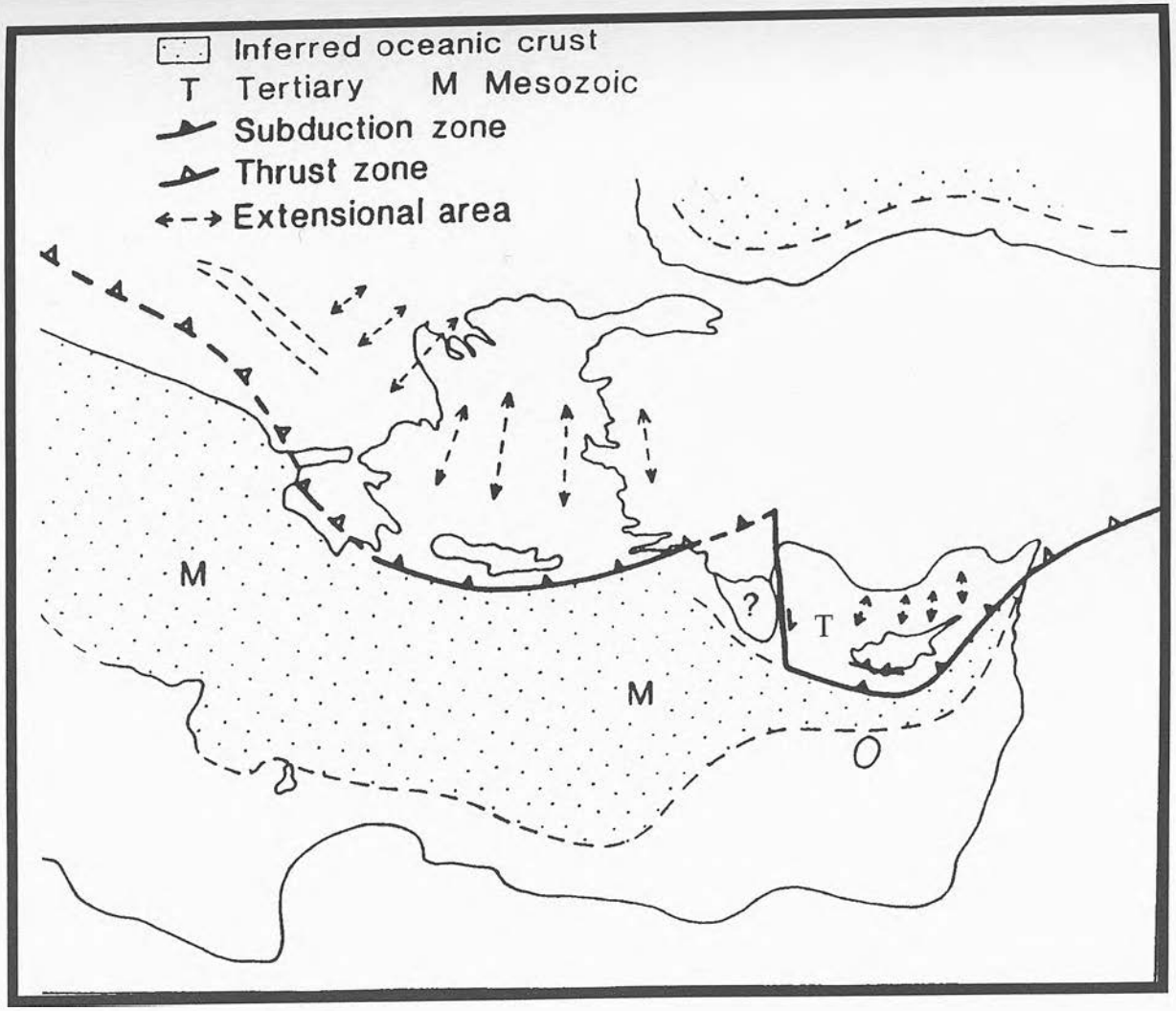

Figure 7.30 Early Miocene plate tectonic reconstruction of the connection between the Aegean and Cyprus subduction systems along the Lycian Front (Poisson, 1984). (Diagram from Robertson and Grasso, in press.)

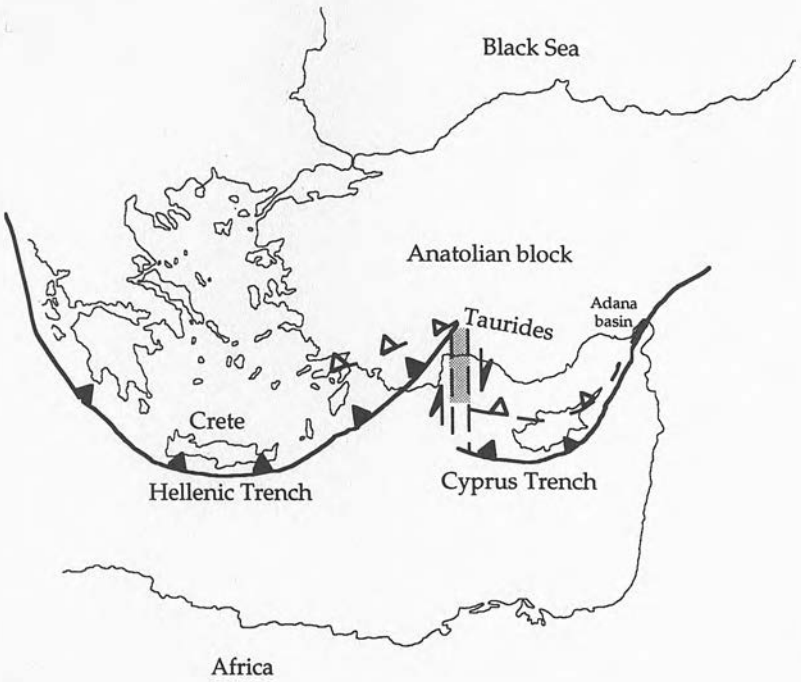

Figure 7.31 Model of the possible rôle of the Isparta Angle as a transform zone linking the Hellenic and Cyprus arcuate subduction systems during the Miocene. Dashed lines with open triangles on them indicate the location and orientation of these systems at the Oligo-Miocene boundary. See text for further explanation.

hinterland of the basins was occurring at this time (chapter 8 for full discussion), alongside subsidence due to pull-apart formation within the Isparta Angle (Fig. 7.29). The Aksu Phase has previously been envisaged as a product of the westward escape of Anatolia and it was for this reason that the dominance of west-vergent structures was explained. The presence of some quite large scale east-vergent systems (e.g. the Akbas syncline, Fig 7.25) supports the idea that the western arm of the Isparta Angle was not entirely passive at this time. The relative dominance of the west-vergent structures over the east-vergent structures may suggest the complex interplay between the initiation and strengthening rôle of westward escape of the Anatolian block during the final phases of Lycian emplacement to the SE and anticlockwise rotation of the Bey Daglari.

Also important, however, is the recognition that at least 30° of the curvature on the Lycian front would have been produced during the Miocene. Using the reconstruction of the pre-rotation front from either Poisson (1984; Fig. 7.30) or Kissel *et al.*, (1993; Fig. 7.3) it seems reasonable to suggest that the thrust direction at the beginning of the Middle Miocene was south or SSE directed rather than the SE thrusting direction which might be deduced from the curvature of Lycian front today. The change in thrusting direction during the Miocene due to rotation of the Lycian front may therefore have been fundamental in changing the orientation of the stress direction acting on a N-S zone of faults within the Isparta Angle. A more southerly directed thrusting direction during the Middle Miocene would initiate strike-slip movement on a N-S suture, while a larger component of eastward compression, likely to have occurred towards the end of the Miocene, would result in less transpression and more orthogonal compression along N-S orientated faults.

7.6.3 Evidence for a later Susuz Dag Phase of southward transport

Although there is clear evidence that a component of the compression at the end of the Miocene was orientated towards the south, none of the data presented here gives unqualified support to the idea that this southward-directed transport event was separate from the east-west compressional event as envisaged by Frizon de Lamotte *et al.* (1995). The

folding of Upper Miocene sediments in the Manavgat basin is the clearest indication that north-south compression was important at this time, but it is suggested here that this deformation may represent very minor shortening over an already faulted Lower and Middle Miocene succession. The N-S structural grain of the Köprü and Aksu basins may perhaps obscure any E-W orientated structures present in the Miocene succession. Equally, it is possible that southward transport was taken up along a décollement beneath the basins parallel to the Florence Rise as suggested by Frizon de Lamotte *et al.*, (1995) although more recent investigations of the Florence Rise suggest that a simple thrust-front interpretation is problematic. Southward transport along north-south fault zones such as that at Pinargözü has been measured, but the data set did not indicate that the southward movement was either separate from, or later than east-west compressional structures. It is suggested rather that the combination of lessening Lycian movement towards the south-east and strengthening westward movement due to the initiation of expulsion of the Anatolian block (Sengör *et al.*, 1985) resulted yet again in the partitioning of obliquely orientated stress directions causing the reactivation of older weaknesses (Fig. 7.32).

7.7 Conclusions

- There is clear evidence of a previously unidentified extensional faulting event in the Late Burdigalian-Langhian which resulted in the development of a horst-graben system in the Manavgat basin;

- A theoretical (uniform stretching) subsidence curve fitted to the data in the Ahmetler section suggests that a short period of low-magnitude (β = 1.08) extensional rifting occurred between 16-17Ma, close to the Burdigalian-Langhian boundary;

- Subsequent reactivation of extensional faults in a transpressional (sinistral) sense may have been caused by a dominantly east-west compressional system.

- A component of north-south compression must have affected the area in post-Miocene times to form the open folds in the east of the

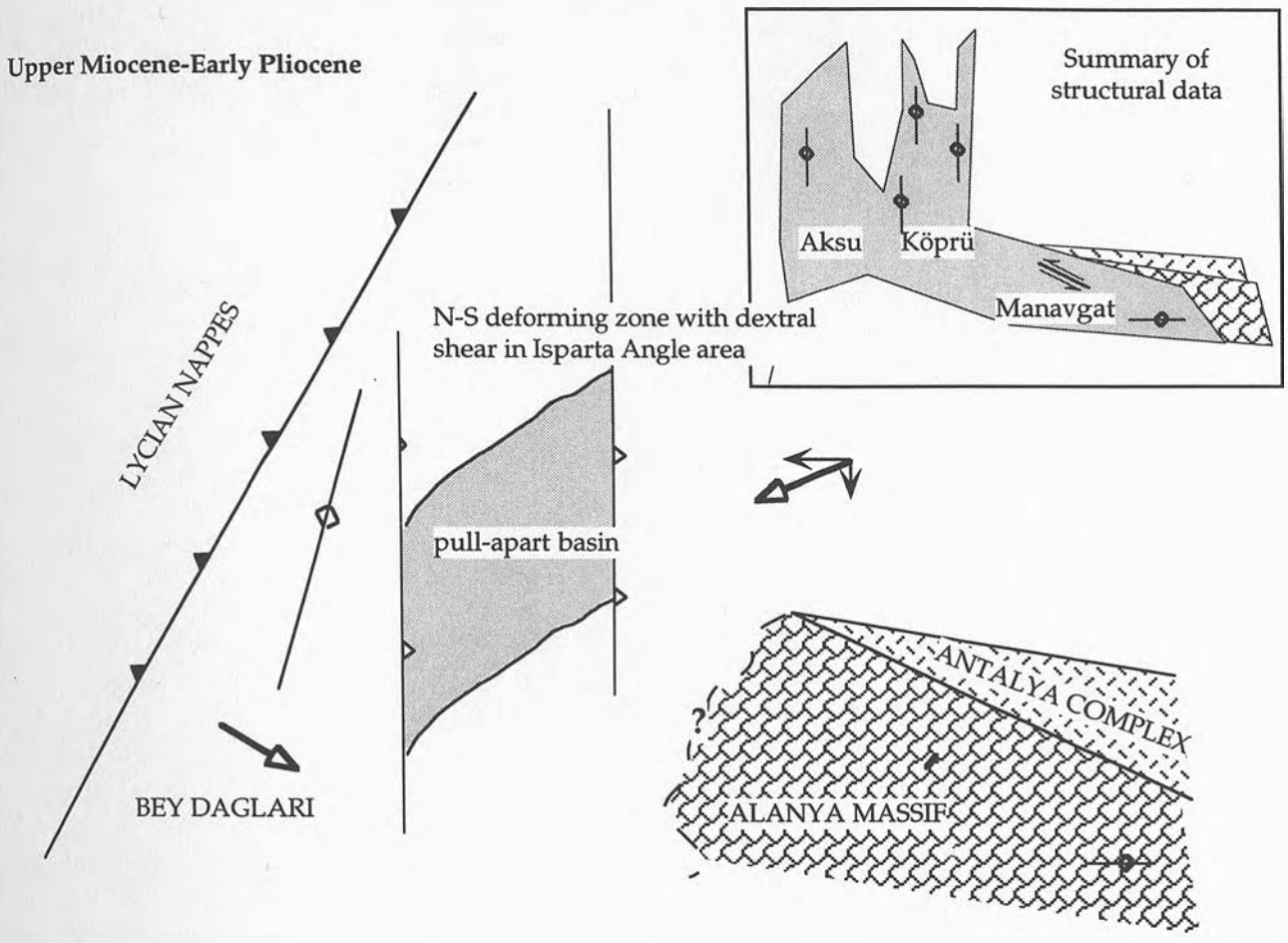

Figure 7.32 Schematic model of the development of the Late Miocene-Pliocene deformation. Because of the close proximity of the Lycian Nappes, further emplacement tectonics is likely to have affected the study area. Westward expulsion of Anatolia is also thought to have had a more regional effect. All deformation however, is accommodated along older lineaments.

Manavgat basin. It is not thought however, that very much compression is required to bring about this folding, particularly if reactivation of underlying faults also occurred at this time.

- A model has been put forward for the evolution of the Miocene basins suggesting that:
  - Rotation of the Bey Daglari was taken up by strike-slip motion on N-S orientated faults during Mid-Late Miocene times rather than on a décollement horizon at the base of the Antalya Nappes;
  - Narrow, deep (~1.5km) sediment depocentres in the Aksu and Köprü basins areas were created by pull-apart formation in a north-south orientated deforming zone undergoing dextral shear;
  - Dominantly west-vergent compressional structures were formed due to initiation of westward transport related to the expulsion of the Anatolian block at the end of the Miocene;
  - More rare eastward-vergent structures may suggest that Lycian emplacement and rotation of the Bey Daglari were still active at the end of the Miocene.

- There is no clear evidence for a separate, north-south compressional event (the Susuz Dag Phase) after the Aksu Phase at the end of the Miocene in the Miocene sediments of the Aksu, Köprü and Manavgat basins.

Chapter 8

REGIONAL COMPARISONS AND CONCLUSIONS

8.1 Introduction

The Miocene sedimentary rocks of the Aksu, Köprü and Manavgat basins have been described in preceding chapters. The reader is referred to table 8.1, which is a summary chart of the information derived from this study. Chapter 7 examined the structural evidence for the initiation and development of basins within the Isparta Angle during the Miocene and placed them in a tentative tectonic context of Eastern Mediterranean evolution. This chapter compares the evolution of the Isparta Angle with other Eastern Mediterranean Miocene basins and then examines the relative rôles of the fundamental processes of tectonics and eustacy in basin development and the controls on their sedimentary fill and architecture.

8.2 Regional comparisons

8.2.1 Kas basin, outboard of the Lycian Nappes, SW Turkey

A Miocene stratigraphy is preserved to the west of the Aksu basin mainly in a narrow NE-SW orientated basin along the Lycian thrust front which runs from Isparta in the north (Dariören basin) to Kas on the south Turkish coast (Figs. 7.1 and 7.2). A transgressive shallow-water limestone (the Karabayir Formation, Poisson and Poignant, 1974) of Aquitanian age is known also as "la barre Aquitanien" because of its strongly linear outcrop pattern along the south-eastern margin of the basin. It is overlain by a thick succession of Burdigalian-Langhian turbidites (Hayward, 1982; Gutnic *et al.*, 1979), which are themselves overlain by Serravallian-Tortonian fan-delta conglomerates in the south (Hayward, 1982). Hayward (1982) interpreted the development of the Dariören-Kas basin succession as being controlled by movement of the Lycian Nappes located directly to the NW. He suggested that the basin formed by flexural

Table 8.1 Summary of sedimentation information from previous chapters.

Age	Formation	Köprü and Aksu facies	Manavgat facies	Implications
Tortonian-Messinian	Aksu Formation	Continental, shoreline and shelf conglomerates, sandstones and patch reefs		Relative rising sea level
	Karpuzçay formation		Corridor of very coarse sub-marine debris flows containing large detached blocks. Background sedimentation of sandy turbidites and planktic foraminiferal marls	Shallowing of the basin due to infill. Sedimentation rate increases dramatically here with no evidence of increased subsidence.
Serravallian-Tortonian		Sand and silt turbidites.		Base of formation abrupt marking a rapid relative sea level rise
Langhian-Serravallian	Geceleme formation		Planktic foraminiferal marls	Low energy environment of deposition in relatively deep water. Base marks rapid sea level rise.
Langhian	Çakallar formation		Calcarenites containing shallow-water debris and locally derived basement	Likely to have been fault generated
Burdigalian-Langhian	Oymapinar limestone	Patch reef facies often associated with conglomerates	Patch and fringing reef facies	Diachronous transgression from south to north visible in Manavgat basin
?-Burdigalian	Kizildag Formation	Continental-coastal conglomerates	Continental-coastal conglomerates	Relative sea level rise

loading of the lithosphere (Fig. 8.1), allowing Aquitanian transgression followed by passive turbiditic fill. The subsequent transition to fan-delta sedimentation indicates further advance of the nappes (Hayward, 1982). This also led to deformation of the Lower Miocene sequences, particularly clearly visible in the north of the Aksu basin (Gutnic et al., 1987). Hayward (1982) suggested that this later advance of the Lycian Nappes occurred at the Langhian-Serravallian boundary and this is in good agreement with palaeomagnetic evidence (Morris and Robertson, 1993; section 7.4). The time also coincides with the abrupt rapid relative sea level rise, thought to have been controlled by extensional faulting in the Manavgat basin and in the south of the Aksu and Köprü basins.

On the south eastern margin of the Bey Daglari (Fig. 7.2) a small Lower Miocene succession is preserved. This documents regional subsidence of the Bey Daglari in the Oligocene tentatively linked to initial emplacement of the Lycian Nappes to the NW (Hayward and Robertson, 1982). During the Early Miocene, the Antalya Complex to the east formed an elevated landmass from which sediments were shed westwards into a relatively deep water (~500m), narrow, north-south trending basin on the eastern flank of the Bey Daglari (Fig. 8.2; Hayward, 1982; Hayward and Robertson, 1982). The Antalya Complex landmass was rapidly eroded with rivers supplying coarse conglomerates to fan-deltas, which in turn fed a series of small submarine fans. At the same time, fault dissection of the Bey Daglari produced considerable volumes of carbonate clastics (Hayward and Robertson, 1982). The boundary between the Antalya Complex and the Bey Daglari was active during Eocene times when the Antalya Complex underwent extensive strike-slip faulting (Robertson and Woodcock, 1980a). In the Late Miocene sedimentation was abruptly terminated by a phase of westward thrusting of the Antalya Complex into its present position. During this deformation, the Antalya Complex, overrode earlier Miocene sediments forming a basal tectonic melange (Hayward and Robertson, 1982).

Synchronous deepening in the Aksu-Köprü-Manavgat basins with shallowing in the basins on the Bey Daglari can be explained in part by the behaviour of the Lycian Nappes. Hayward tentatively linked changes in sedimentation to periods of emplacement of the nappes (e.g. in the

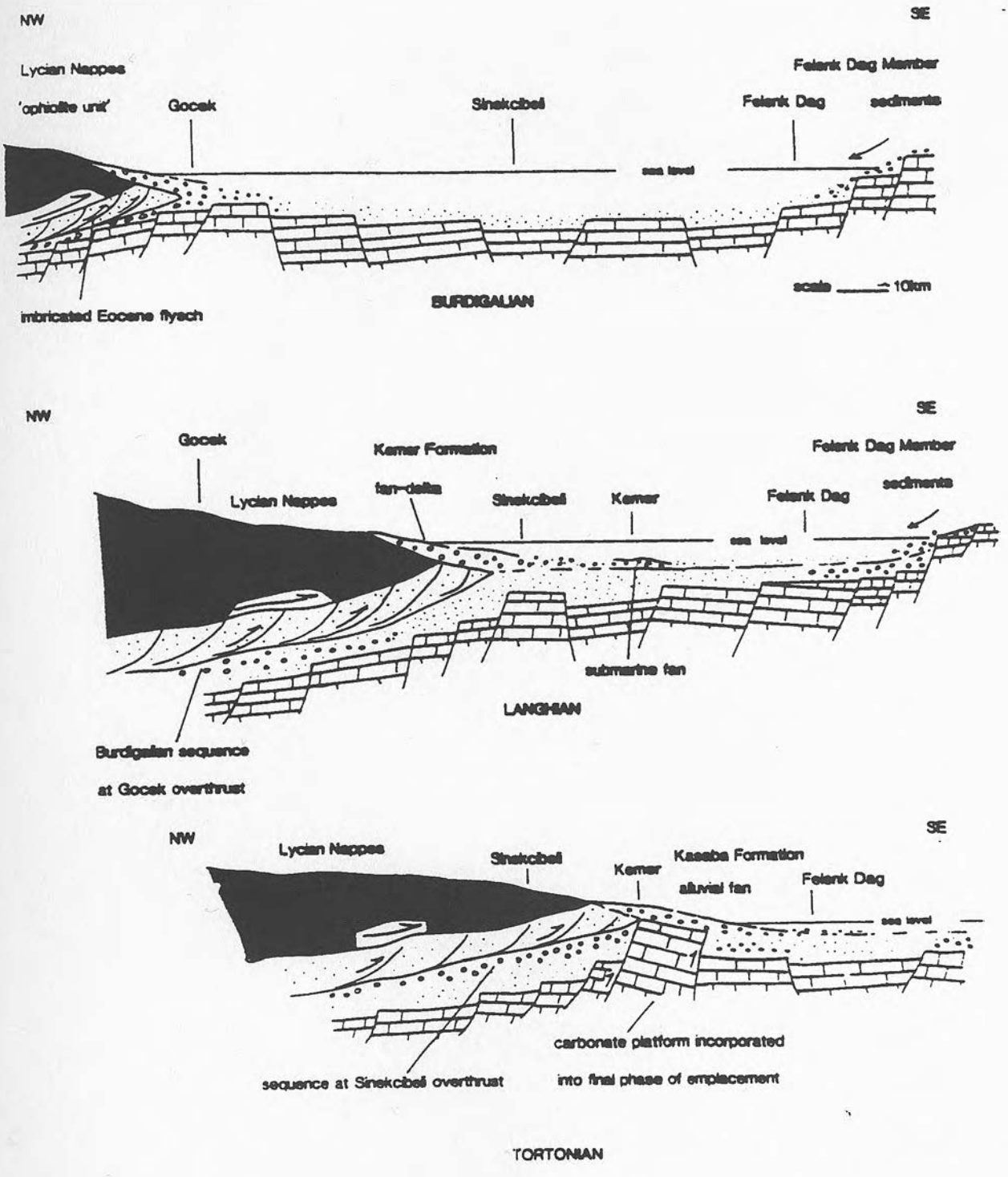

Figure 8.1 Model of the Miocene emplacement of the Lycian Nappes with respect to the Dariören-Kas flexural basin on the west flank of the Bey Daglari (Hayward, 1982).

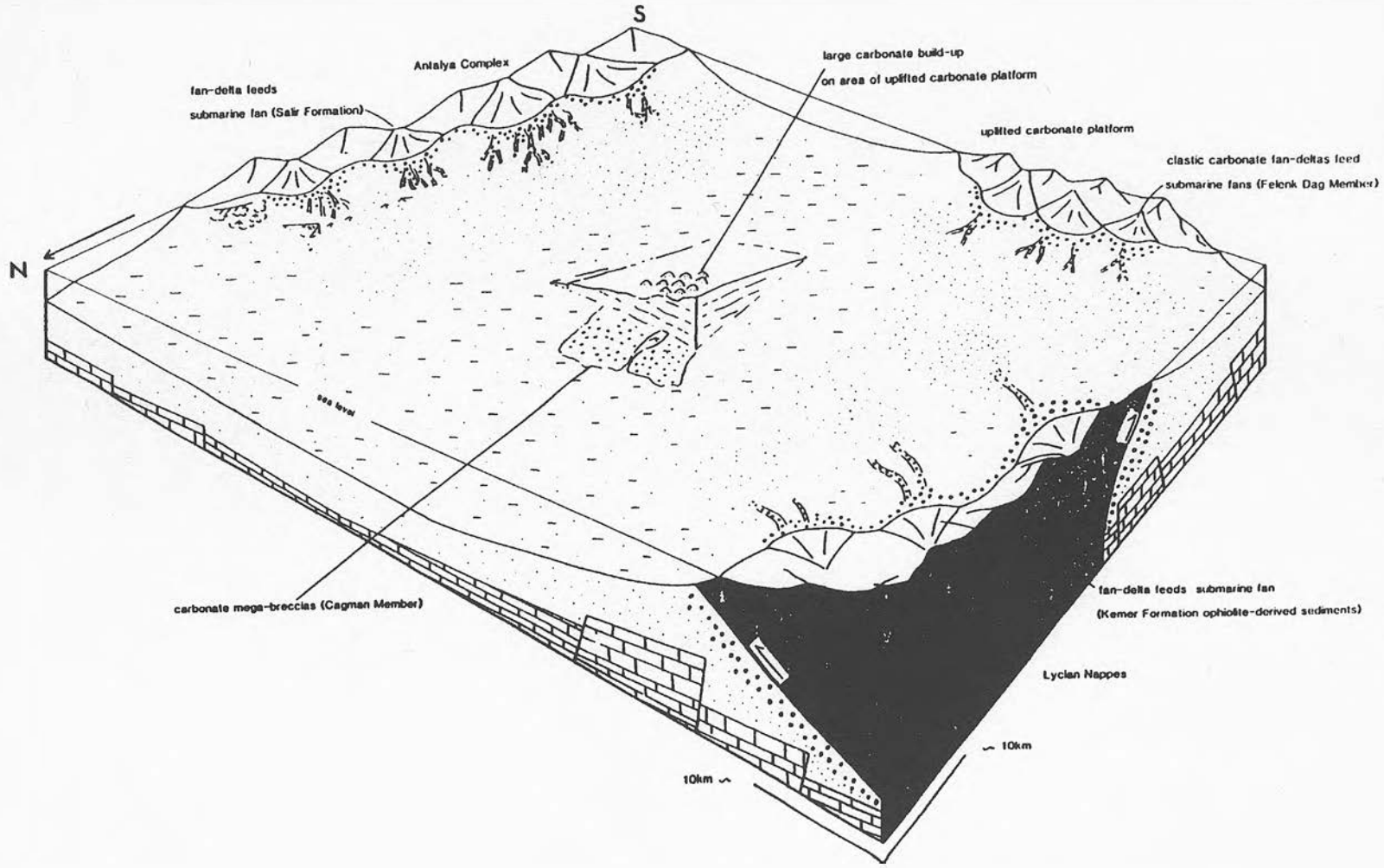

Figure 8.2 Palaeogeographic model of the Lower Miocene sedimentary basins on top of the Bey Daglari with the Antalya Complex to the east and the Lycian Nappes to the west (Hayward, 1982)

Oligocene and Late Miocene). It is possible that loading of the lithosphere induced block faulting in the Aksu-Köprü-Manavgat basins and allowed the accumulation of the thick succession of Burdigalian (or older) conglomerates (~1.5km of Kizildag Formation). Some of the east-vergent structures in the study area (chapter 7; section 7.5.2.3) may be attributed to Late Miocene movement on the Lycian Nappes and this may also have contributed to the uplift and erosion which formed the Mio-Pliocene unconformity. It is not clear how, or if the Mid-Miocene eastward thrusting of the Antalya Complex onto the Bey Daglari affected sedimentation in the Aksu-Köprü-Manavgat area. Note however, that it coincides with a period of uplift which causes shallowing in the Manavgat basin and a transition from turbiditic sedimentation to continental conglomerates and shallow-marine reef carbonates in the Aksu and Köprü basins.

8.2.2 Adana basin, north-east corner of Mediterranean, SE Turkey

A similar stratigraphy to that in the Lower-Middle Miocene of the Manavgat basin developed 400km to the east in the Adana basin at the same time. Gürbüz (1993) has shown that transgressive patch reefs characterise the Aquitanian-Burdigalian, slightly earlier than the south to north transgression seen in the Manavgat basin (Burdigalian-Langhian; Fig. 8.3). Williams and Unlügenç (1992) suggest that the marine transgression leading to the formation of patch reefs in the Adana basin was due to extensional faulting, in response to load-induced flexure resulting from thrusting in the Taurides to the north. In the Isparta Angle by contrast, there is very little evidence to suggest tectonic activity within the basin at the time of transgression although there is clear evidence for strong relative sea level rise. It is difficult to exclude the possibility that the Aquitanian-Burdigalian extensional event in the Adana basin masks a regional sea level rise at a slightly later date correlating with that seen in the Antalya area to the west. However, further clarification from the Adana and Mut (situated between Antalya and Adana) basins and in off-shore sediments along the south Turkish coast, would be required to assert this hypothesis more strongly.

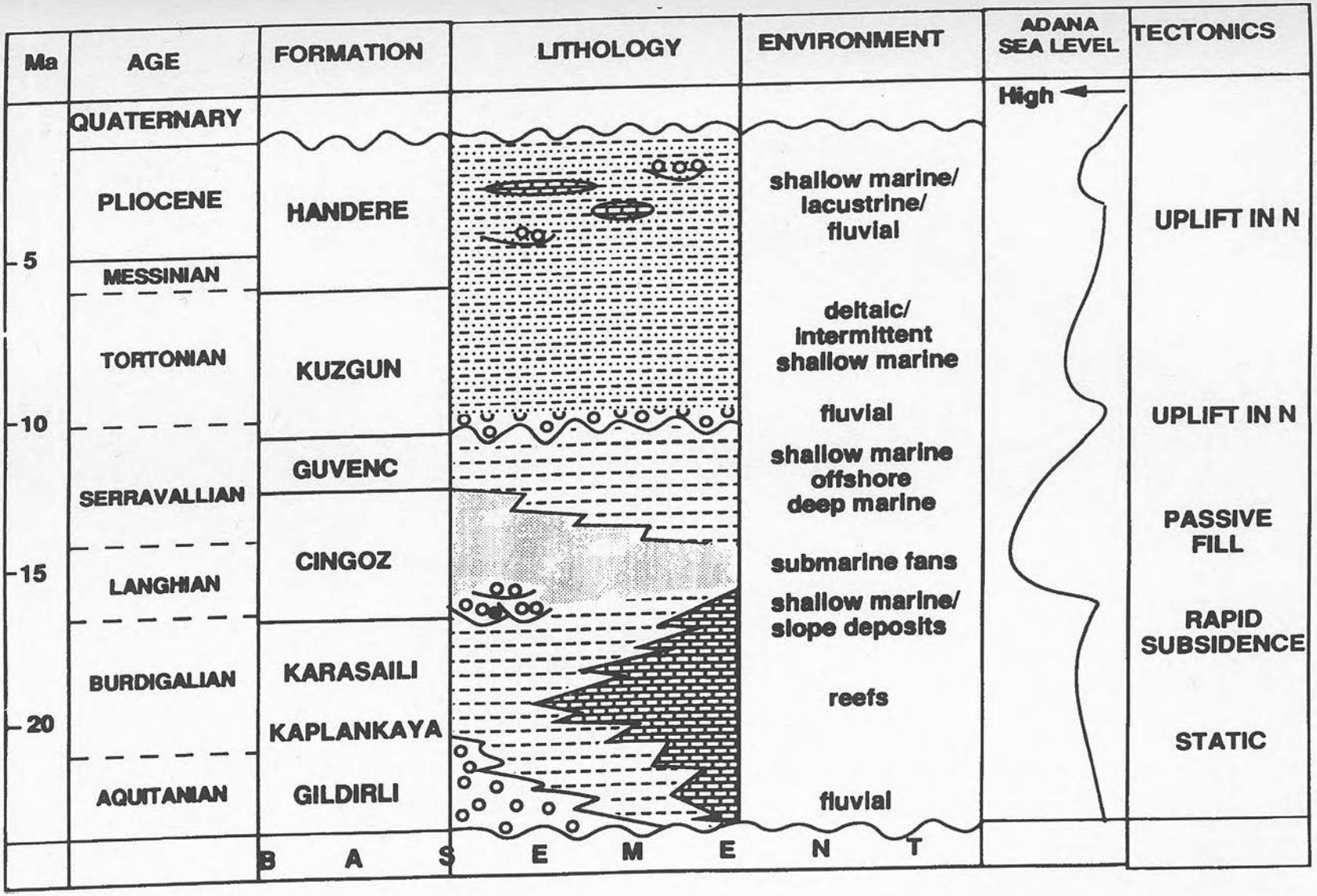

Figure 8.3 Stratigraphy, sea level and tectonic interpretation of the Miocene sediments of the Adana basin (after Gürbüz, 1993; G. Williams pers. com., 1993).

Shallow-water carbonates in the Adana basin were drowned in Late Burdigalian-Early Langhian times, causing a sharp transition to deep-marine turbidites in the Adana basin, as seen in the Manavgat basin and in the south of the Aksu and Köprü basins. This rapid relative sea level rise in the Adana area is attributed to tectonically induced subsidence forming a deep, underfilled, flexural foreland basin caused by continued thrusting in the Taurides to the north (Williams and Unlügenç, 1992, Gürbüz, 1993). A serious difficulty arises in the direct application of this model to the evolution of the Isparta Angle, in that there is no evidence of thrusting of the Taurides in the area at this time. Flecker *et al.* (1995) suggested that in a broader sense however, this model may be relevant to the development of the Isparta Angle in the Miocene. As described in section 7.6.1, the Lycian Nappes on the western limb of the Isparta Angle are thought to have been active at this time (Kissel and Poisson, 1987; Kissel *et al.*, 1993; Hayward, 1980; Morris and Robertson, 1993). Flexural loading from the north-east may therefore have induced block faulting of the foreland which, in turn, exploited pre-existing lines of basement weakness and resulted in rapid relative sea level rise. It is not clear if thrusting in the Taurides north of Adana is genetically related to thrusting of the Lycian Nappes to the north-west of the Isparta Angle, within a regional tectonic context.

Seismic reflection profiles across the Adana basin have been interpreted to indicate that little or no syn-sedimentary faulting occurred during subsequent infilling and shoaling during Langhian and Serravallian times (Williams and Ünlügenç, 1992). This shallowing ultimately led to the deposition of deltaic sequences in the Tortonian and Messinian in the Adana basin (Fig. 8.3). Shallowing in the Manavgat basin, in contrast, was not sufficient to allow deposition of anything other than fully marine sediments. The apparently passive post-rift fill of the Adana sequence is however, mirrored by the deposition of fine grained Karpuzçay Formation in the Aksu and Köprü basins and the planktic foraminiferal marls of the Geceleme Formation in the Manavgat basin.

The Misis Complex to the east of the Adana basin (Fig. 8.4) is an accumulation of Late Oligocene to Early Miocene olistostromes which were emplaced onto Early Miocene-Pliocene sediments (Kelling *et*

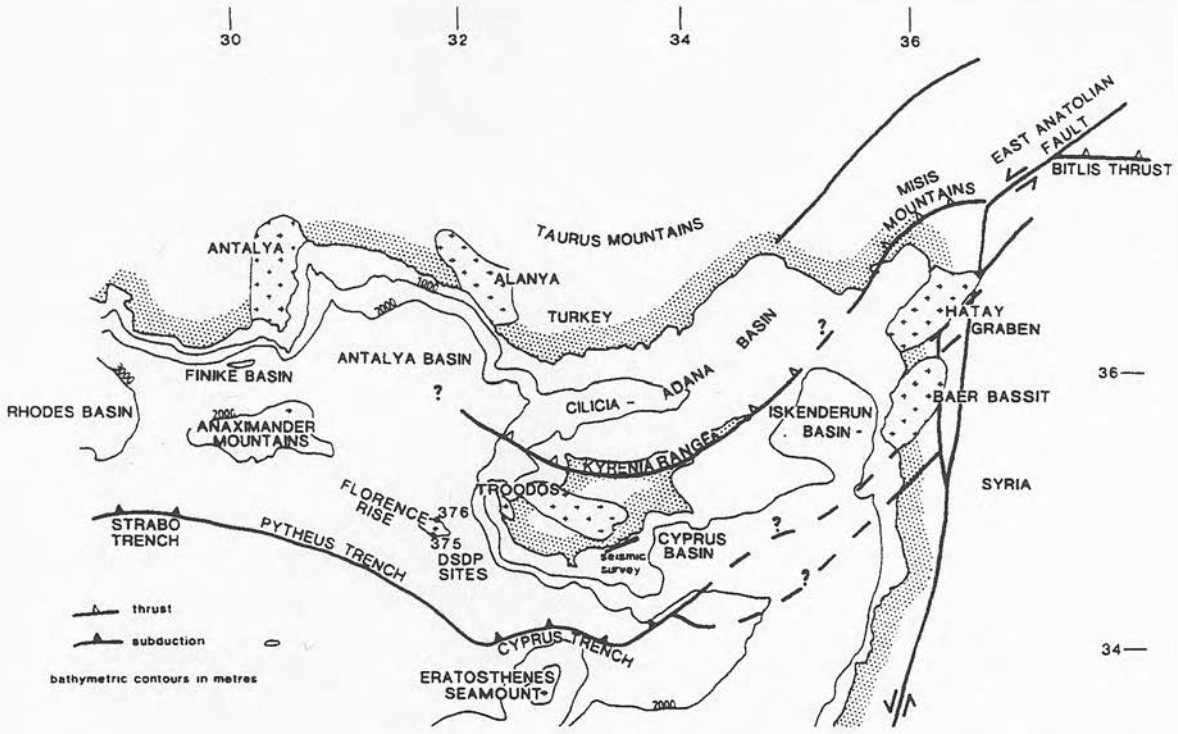

Figure 8.4 Map of Cyprus and the surrounding area showing tectonic units referred to in the text.

al.,1987). A combination of thrusting and strike-slip movement, not dissimilar from the emplacement tectonics of the Antalya Complex (Robertson and Woodcock, 1980a) is envisaged for the Misis Complex during the Late Miocene to Early Pliocene deformation (Kelling *et al.*,1987). To the north-east, close to the junction between the East Anatolian Fault and the Bitlis thrust (Fig. 8.4), a flexural (Çüngüs-Lice) basin formed during the Miocene (Aktas and Robertson, 1985). Kelling *et al.* (1987) suggest that overall transpression characterises the Adana area (i.e. the north-eastern segment of the Bitlis-Cyprus sector; Fig. 8.4) during the Neogene-Holocene, whilst, transtension affected the Cyprus area to the south-west. The oblique orientation of the tectonic stress thought to be active in this system accord well with observations of both transpression and transtension in the Isparta Angle area at this time (chapter 7).

8.2.3 Northern Cyprus

In northern Cyprus, patchy lacustrine limestone and lime mud (Flecker *et al.*, 1995) and Upper Oligocene conglomerates are exposed adjacent to the Kyrenia Range (Fig. 8.4), interpreted as a palaeo-subduction zone (Robertson and Woodcock, 1986). These were the first sediments to accumulate after a phase of thrusting (Baroz, 1979). The conglomerates have been interpreted as alluvial fans derived from the future Adana basin to the north-east, that prograded across a broad alluvial plain, now covered by the sea dividing Cyprus from Turkey, the Cilicia basin (Robertson and Woodcock, 1986). A thick succession of turbidites, known as the Kithrea flysch, overlies these conglomerates and palaeocurrent directions also indicate that these were derived from the Adana basin to the north-east (Robertson and Woodcock, 1986; Kelling *et al.*, 1987). The alluvial plain linking Turkey and Cyprus is thought to have collapsed around the Oligo-Miocene boundary leading to a rapid transition to marine turbidites. Dewey *et al.* (1986) interpreted the Adana-Cilicia basin as a triple-junction incompatibility feature generated by westward expulsion of Turkey (Sengör *et al.*, 1985). Robertson and Woodcock (1986) however, interpreted the cessation of thrusting and collapse of the Kyrenia Range as being due to a jump in the location of subduction from the Kyrenia lineament to near the present-day Cyprus trench, located just

south of Cyprus. Relative to this new, northward-dipping subduction zone, the Kyrenia Range is situated on the upper plate of the subduction zone and thus the subsidence seen in northern Cyprus and the Cilicia basin could be explained by supra-subduction zone extension (Robertson and Woodcock 1986). Anastasakis and Kelling (1991) however, suggest that initiation of the subduction zone south of Cyprus did not occur until the Mid-Miocene. These authors also note evidence of extensional block faulting which is thought to have occurred after the Mid-Miocene thrusting of this area.

The relevance of supra-subduction zone extension in generating subsidence in the Isparta Angle generally and more particularly the Manavgat basin, which was the northern margin of the Cilicia basin during the Miocene has been touched on briefly in chapter 7 (section 7.6.1) is discussed further below in the light of information from Crete (section 8.2.5). Further clarification of the age of faulting of the Misis-Kyrenia thrust belt north-west of Cyprus is important in understanding whether the north and south margins of the Cilicia basin were acting in tandem or were subject to more local tectonic stress patterns.

8.2.4 Southern Cyprus

A significantly different stratigraphy is preserved in southern Cyprus where Oligocene (and older) deep-water pelagic chalks and marls of the Lefkara Formation are overlain by more localised, shallower-water, Miocene pelagic chalks, marls, calcarenites and conglomerates of the Pakhna Formation (Robertson *et al.*, 1991). Eaton and Robertson (1993) argue that this change at the Oligo-Miocene boundary, was caused by uplift related to the initiation of subduction along the Cyprus trench, following the termination of thrusting along the Kyrenia Range to the north.

In addition, reefs developed in the Burdigalian and Tortonian (Follows and Robertson 1990; Follows, 1992; Eaton and Robertson, 1993) in southern Cyprus with a similar Mid-Miocene hiatus of reef growth to that of the Isparta Angle area (section 3.8.1). Follows (1990) tentatively

suggested that this was a result of eustatic sea level rise. Although eustacy may contribute a component of the relative sea level rise associated with drowning of Lower Miocene reefs in the Isparta Angle, the evidence of fault related subsidence at this time is too strong to allow the suggestion that eustatic processes may have completely controlled vertical facies change.

Payne and Robertson (1995) also suggest that the cause of extensional faulting and deepening of the Polis graben, Western Cyprus during the Tortonian might be due to "roll-back" of the Cyprus trench. "Roll-back" (i.e. the downward and backward migration of the subducting slab, which can result in extension in the upper plate; Dewey *et al.*, 1980) as a process controlling extensional faulting and subsidence on the upper plate is discussed further in the light of evidence from Crete (8.2.5).

8.2.5 Crete, north of the Hellenic trench

Middle to Late Miocene basins on the island of Crete have been linked to activity along the Hellenic trench for over 20 years. Early work on Cretan exposures and on the mantle structure beneath the island suggested that basin generation occurred as a result of initiation of subduction along the Hellenic arc (e.g. McKenzie, 1978; Le Pichon and Angelier, 1979). More recently however, Meulenkamp *et al.* (1988) suggested that the initiation of subduction occurred approximately 26Ma ago, at the Oligo-Miocene boundary, over 10 million years earlier than the age of the oldest sediments in the basins on Crete itself. They suggested therefore, that Late Serravallian to Early Tortonian inception of "roll-back" within the South Aegean subduction system changed the tectonic stress regime and caused the fragmentation of Crete into a series of transtensional basins. In the Late Miocene and continuing throughout the Pliocene-Quaternary, uplift of the Cretan area occurred. This is thought to be related to outward gravity collapse away from the locus of crustal thinning in the Sea of Crete (Meulenkamp *et al.*, 1994).

As argued by Flecker *et al.* (1995) and in section 7.6.1 the agreement between Meulenkamp *et al.* (1988) and Eaton and Robertson (1993) in Crete and Cyprus, respectively, lends credence to an Oligo-Miocene time

of initiation of subduction of the South Aegean and Cyprus segments of the active margin, although evidence exists for the initiation of the NW Hellenic segment of the trench around 6Ma (Underhill, 1989). The formation of the Cilicia basin has been credited to supra-subduction extension relating to the initiation of the active margin south of Cyprus. However, the transgression and rapid relative sea level rise in the Burdigalian and Langhian of the Isparta Angle, the northern margin of the Cilicia basin, post-dates this initiation event possibly by as much as 10 million years.

Another possibility suggested by Flecker *et al.* (1995), however, is that the previously subducted slab underneath the Kyrenia lineament, located by earthquake foci beneath northern Cyprus (Kempler and Ben-Avraham, 1987) may also have had a rôle. Once the compressional forces of the Africa-Eurasia collisional system have been relieved in the Kyrenia area by active subduction to the south of Cyprus, a slab lying beneath, but still attached along the Kyrenia lineament, might have been gravitationally unstable causing "roll-back" and extension of the upper plate. The 10 million year diachroneity between initiation of extension south and north of the Cilicia basin remains a problem however.

Equally, the timing of the inferred inception of "roll-back" for both the Cyprus (Payne and Robertson, 1995) and South Aegean (Meulenkamp *et al.*, 1988) sections of the trench system, causing extension-related subsidence, appears to coincide around the Serravallian-Tortonian boundary, synchronous with the input of coarse clastic material into the Manavgat basin, the initiation of continental and coastal deposition in the north of the Aksu and Köprü basins and the sub-deltaic sequence boundary in the Adana basin (Williams *et al.*, 1993). It is possible that the uplift to the north of the Isparta Angle, postulated as having caused the change in depositional mode in southern Turkey, could have resulted from marginal uplift related to the initiation of "roll-back". If this was the case however, "roll-back" on the Cyprus trench would have been behaving effectively synchronously across Cyprus and the Cilicia basin, in contrast with the diachroneity across the Cilicia basin inferred for extension related to the sinking of a slab beneath the Kyrenia Range 5-15 million years earlier.

Evidence to support marginal uplift around the Isparta Angle during the Burdigalian-Langhian extensional event is easily found in the form of thick (i.e. up to 1.5km) Burdigalian conglomerate successions. This strongly suggests hinterland uplift and erosion as well as the generation of accommodation space. These deposits have previously been attributed to uplift of the hinterland caused by flexural upwarp of the foreland outboard of the advancing Lycian Nappes.

How likely is "roll-back"-generated extension to have affected the Isparta Angle and have caused the 10Ma diachroneity from south to north? Within such an asymmetrical system as a subduction zone, it is perhaps unreasonable to expect related extensional stress to cause symmetrical rifting. There is little evidence however, of the character of the Pre-Messinian subsidence of the Cilicia basin (Evans *et al.*, 1978). Symmetrical extension-related subsidence is inherently difficult to fit with a picture of diachronous subsidence away from the subduction zone. Asymmetrical stretching models appear more relevant, but are also difficult to apply simply in a meaningful way. Figure 8.5 is a grossly simplified model of the generation of the Cilicia basin due to "roll-back" on the Kyrenia slab. In an asymmetrical model where the effects of extension migrate out from the point of initiation, the application of average rates of "roll-back" from the present day Aegean system (Chase, 1978; Minster and Jordan, 1978) and probable angle of slab descent (Jarrard, 1986) suggest that the effects of extension might be expected to be seen in the south of the Isparta Angle around 10Ma after initiation. Note however, that this system cannot be treated meaningfully in this simple way, as there is no clear information on the type of rifting active at this time. For instance, the Kyrenia lineament itself is thought to have been arcuate (Fig. 8.2) so that alterations in the stress patterns along its length would be expected. Also, heterogeneities in the lithosphere around the Isparta Angle itself are clearly fundamental in controlling the structural development of the area and without considerably more knowledge of the basement beneath the Cilicia basin it would be unwise to go any further than pointing out that "roll-back" on the Kyrenia suture zone may have played a part in evolution of the Isparta Angle.

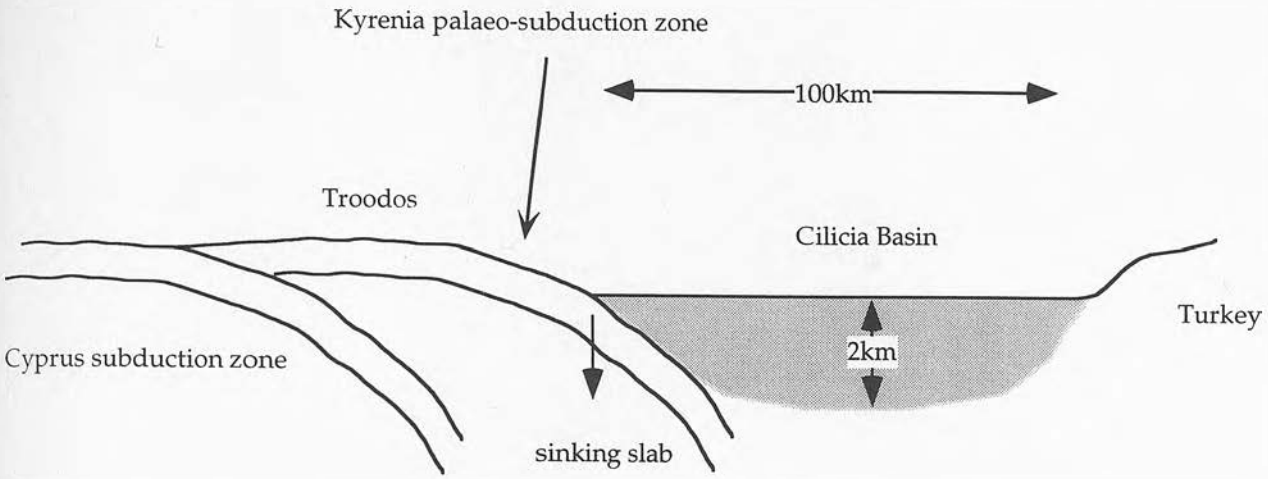

Assumptions: slab remains attached

*dip of slab is 45°

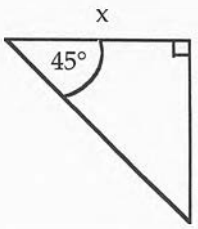

y = x

Slab sinking rate** approximately 1cm/yr

= 10m/1000yrs

= 100km/10Ma

Sedimentation rate of Kithrea Flysch approximately 2km/20Ma

= 10cm/1000yrs

Rate of sinking > Sedimentation rate **= UNDERFILLED BASIN**

As horizontal (x) and vertical (y) displacements are equal, this model predicts subsidence 100km away occurs 10Ma after initiation of "roll-back"

* Angle of descent of slabs undergoing "roll-back" is between the angle of the slab dip and vertical (Jarrard, 1986). This is in agreement with predictive models of "roll-back" of Dewey (1980) and Molnar and Atwater (1978). Slab of present Aegean subduction system dips at 20-40°.

** Rate of horizontal component of "roll-back" of the Aegean system today is between 2cm\yr (Chase, 1978) and 2.9cm\yr (Minster and Jordan, 1978). Other subductions thought to be undergoing "roll-back" generally have a smaller rate (Jarrard, 1986).

Figure 8.5 Tentative assessment of the ability of "roll-back" on the Kyrenia lineament to create subsidence in the Cilicia basin area.

8.3 The relative importance of tectonics (local and regional) versus eustacy in controlling sedimentation

Figure 8.6 shows the sea level curves generated by sedimentation in the Manavgat and a combined curve for the Aksu and Köprü basins taking sedimentation rate into account, but assuming no tectonic activity. These can be compared with the sea level curve for the Adana basin (Gürbüz, 1993) and a composite curve for Cyprus (Robertson *et al.*, 1991) and the eustatic sea level curve generated by Haq *et al.* (1988) in figure 8.7. In very broad terms the following points concerning the similarities and discrepancies between the relative sea level curves and the eustatic curve can be discerned.

Similarities

- Burdigalian-Langhian transgression in the Isparta Angle, Cyprus and Adana correlates with the eustatic curve. The Langhian is recognised as a period of high sea level throughout the Eastern Mediterranean (e.g. Cyprus, Follows, 1990; Sardinia, Cocozza and Javobacci, 1975);
- The shape of the eustatic curve suggesting a regression throughout the Serravallian fits with foraminiferal evidence from the Manavgat basin, but the shallowing deduced from this data could be entirely accounted for by infill at the calculated sedimentation rates. This has been taken into account in the drawing of the curves for both the Manavgat and combined Aksu and Köprü basins and results in the curve appearing flat at this time. Gürbüz took sedimentary fill into account when drawing the curve for the Adana basin; Robertson *et al.*, (1991) did not;
- Evidence for relative sea level rise during the Tortonian in the north of the Köprü and Aksu basins correlates with a eustatic rise in sea level. There is also some evidence of a short period of transgression at the beginning of the Tortonian in the Adana basin and in northern Cyprus;

Differences

- Oscillation of the eustatic curve during the Langhian cannot be recognised in the sedimentary record of the Isparta Angle. This may be due to unobserved hiatuses in the record;
- The eustatic curve does not indicate the major relative sea level rise deduced for the Isparta Angle, Adana and Cyprus areas around the Langhian-Serravallian boundary.

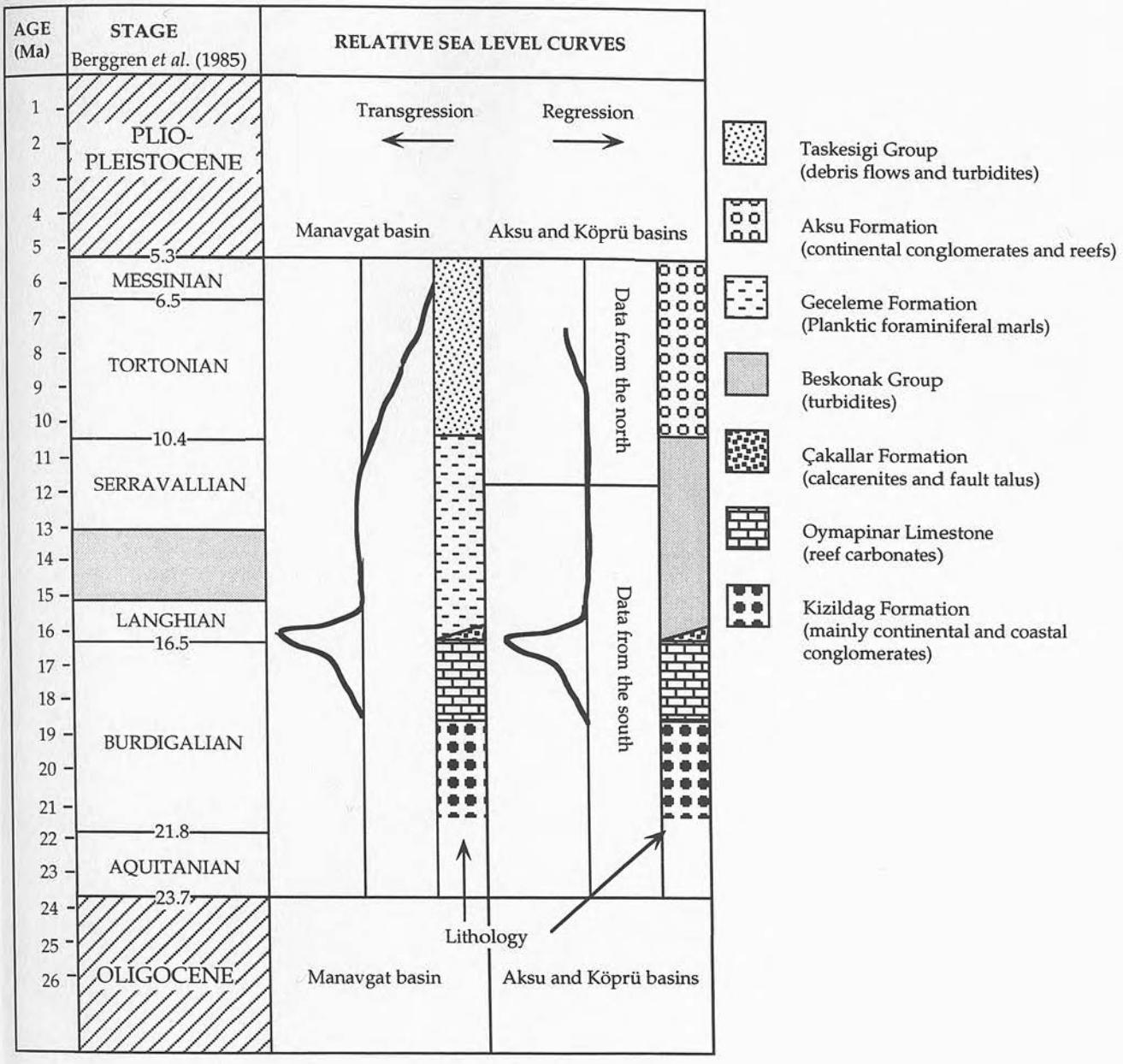

Figure 8.6 Relative sea level curves for the Manavgat basin and a composite for the Köprü and Aksu basins derived from separate successions in the north and south of the area. The curves have been drawn taking into account the sedimentation rate, the subsidence induced by the sediment pile and the compaction associated. The curve represents changes in relative sea level which cannot be accounted for by these processes.

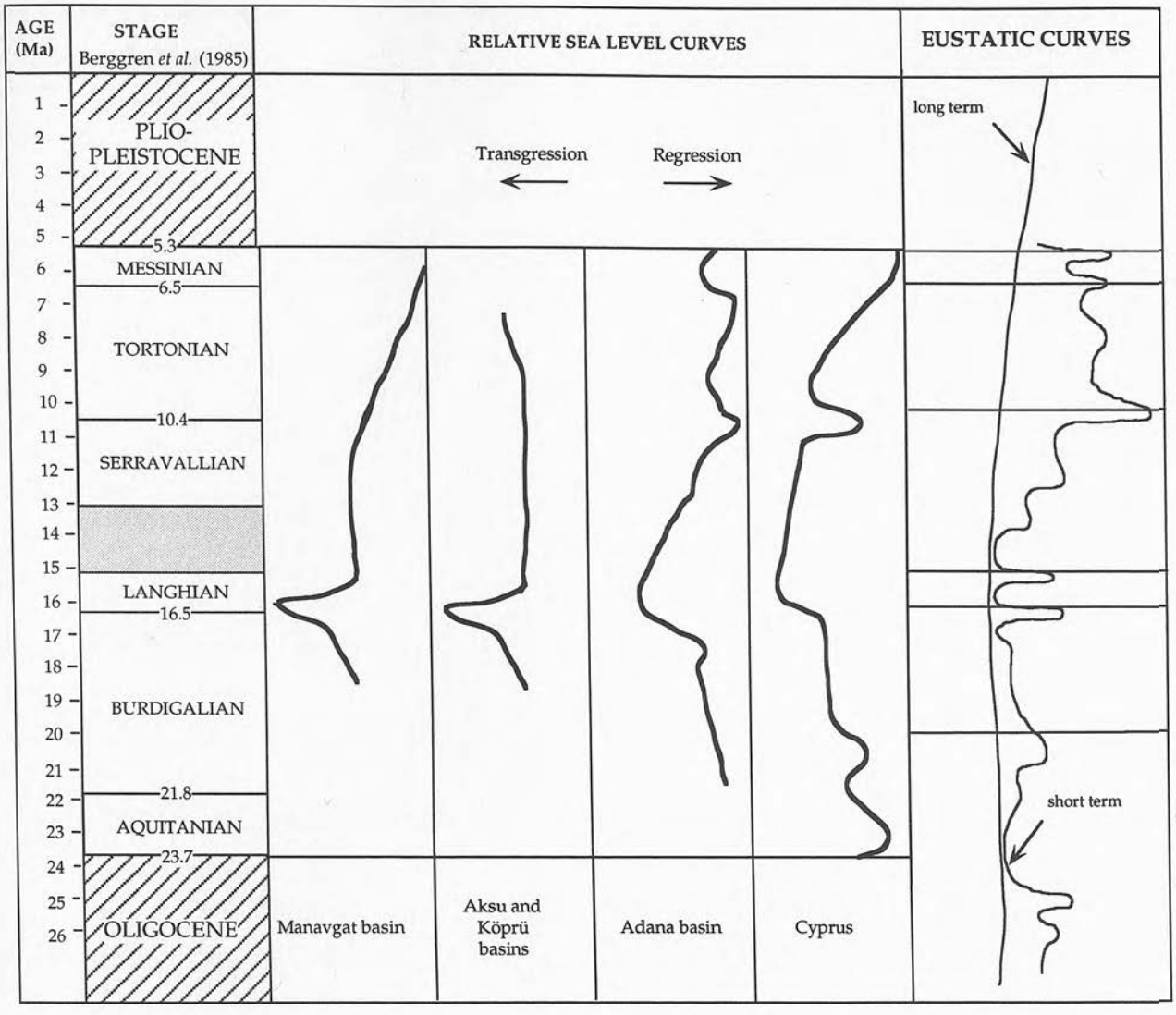

Figure 8.7 Relative sea level curves for the Manavgat basin and a composite for the Köprü and Aksu basins compared with the curves for the Adana basin (Gürbüz, 1993) and Cyprus (Robertson *et al.*, 1991) and the eustatic sea level curve of Haq *et al.* (1988). The curves are not drawn to the same horizontal scale. The horizontal lines on the eustatic curve indicate the position of stage boundaries. Not all of these are in agreement with those defined by Berggren *et al.* (1985; see Figure 2.2).

- In the Manavgat basin, foraminiferal evidence suggests that shallowing of the basin continued throughout the Serravallian, Tortonian and Messinian. A similar trend can be seen both in the Adana basin and in Cyprus, but it contrasts with evidence from the northern parts of the Aksu and Köprü basins and the eustatic curve;
- The erosion associated with the Mio-Pliocene boundary is not associated with a regression on the eustatic curve. The Messinian drawdown (Hsü *et al.*, 1973) of the Mediterranean is well documented through out the region and resulted from the isolation of the Mediterranean from the Atlantic.

Only the Lower Miocene transgression and the Serravallian regression can therefore be directly and consistently linked with the eustatic curve produced by Haq *et al.* (1988). Where a direct correlation cannot be made, there is, in all cases, evidence of local tectonic activity (e.g. the Burdigalian-Langhian faulting event; the Tortonian dissimilarity of sea level curves between north and south of the Isparta Angle suggesting independent movement of small blocks).

8.3.1 Closure of Neotethys

The Mediterranean Sea is the last remaining remnant of a Neotethyan Ocean which opened behind rifted fragments of Africa and caused the closure of Paleaotethys during the Late Palaeozoic and Early Mesozoic (e.g. Sengör et al., 1984; Robertson and Dixon, 1984; Üstaömer and Robertson, 1994; Pickett, 1994). Subsequent northward movement of Africa relative to Eurasia resulted in near complete closure of Neotethys. Miocene sediments throughout the Mediterranean document a crucial period in this closure, from a narrow ocean fully integrated with global circulation to a marginal basin periodically closed at both ends. This closure has implications not only for the tectonic style of oceanic subduction and continental collision, but also for the palaeoceanographic regime. In terms of the marine sediments preserved in the Isparta Angle, the dwindling coral diversity supports similar evidence from elsewhere in the Mediterranean (e.g. Cyprus, (Follows, 1989; Spain, Martin *et al.*, 1989; Southern France, Chevalier, 1961) which documents the termination of the seaway connecting it to the Indian Ocean (chapter 3; Chevalier, 1977) as Arabian Margin collided with the Eurasian plate (Angelier *et al.*, 1982).

The development of a mud-dominated acretionary prism (Mediterranean Ridge; Limanov and Ivanov, 1994), active arc volcanism and back-arc extension in the Aegean area contrasts with the limited subduction which occurred along the Cyprus segment (see Robertson and Grasso, in press for review). The Isparta Angle lies at the boundary between these two systems and may well have played a vital rôle in accommodating the tectonic disparity between the two systems (Fig 7.31). The marked change in convergence direction of Africa and Eurasia around 9Ma influenced the kinematics of the tectonic systems in both the Eastern and Western Mediterranean basins (Dewey *et al.*, 1989). The Tortonian uplift of the Isparta Angle and the deformation which characterised the Latest Messinian (Aksu Phase) can, and should be viewed within this context taking into account the effects of other, more local units, also reacting to this change in tectonic stress.

As far as the applicability of the eustatic sea level curve is concerned there is no evidence that the Mediterranean became isolated from the global oceans prior to the Messinian salinity crisis although the exact timing of this is not well documented (Müller *et al.*, 1990; section 6.5.2.2). More important is the effect that closure of an ocean has upon the marginal regions affected by subduction. Within the context of such active tectonics, can the concept of eustacy have any relevance to the Mediterranean? The correlation, albeit inconclusive, of the eustatic and locally derived curves suggests that eustacy probably contributed to the sea level changes documented by the sedimentation, but are only visible when tectonic quiescence can be demonstrated.

CONCLUSIONS

1. Prior to the earliest deposition of continental conglomerates a marked and uneven palaeotopography had been developed. In the Manavgat basin the northern margin of the Alanya Massif formed a high which funnelled sediment westward in the south and along the Antalya Complex (a relative palaeotopographic low) to the north (section 5.7.1). Palaeotopographic features are localised along older sutures which have been interpreted as zones along which closure of Tethyan ocean basins took place (i.e. Antalya Complex-Alanya Massif boundary). This suggests that reactivation of these lineaments may have, at least in part, generated and controlled drainage during and prior to Miocene deposition (table 7.2).

2. Preservation of thick successions of continental fan-delta conglomerates and sandstones throughout the basin (e.g. ~1.5km in the Köprü basin, section 5.9.2; several hundred metres in the north-west of the Manavgat basin, figure 4.24) underlines the initial presence of palaeotopography, but also suggests that relative uplift of the hinterland is occurring to provide the quantity of coarse clastic material deposited (section 5.10). This uplift and the generation of accommodation space within the Isparta Angle at this time has been tentatively linked with south to south-eastward movement of the Lycian Nappe system to the north-west of the area (7.6.1), causing block faulting, pull-apart basin formation within a north-south striking zone.

3. Rising relative sea level during the Burdigalian and Langhian resulted in a clear diachronous transgression from south to north in the Manavgat basin (sections 4.7 and 6.5.2). This relative rise in sea level also affected the Aksu and Köprü basins in areas already undergoing active deposition (i.e. in central and southern parts of both basins; figure 5.31). Fan-delta sedimentation continued unabated on previously established fans, but the successions preserved reflect the relative sea level rise by a transition from purely continental deposits to coastal fan-delta successions (figure 5.31). Patch-reefs developed within these successions

on coarse conglomerate horizons similar to those described from the present day Red Sea (Hayward, 1982b), and the Miocene of southern Spain (Martin *et al.*, 1989) and the Kas basin, to the south-west of the study area (Hayward, 1982a and b). The interaction of rising relative sea level and rapid, episodic sediment influx is clearly documented by the growth of individual corals up through successive clastic horizons (section 5.6.3.2, figure 5.21). Overall, study of these sensitive coastal sediments suggests that the dominant control on sedimentation at this time was relative sea level rise, despite the rapid sedimentation rate (section 5.9.2 and 5.10).

4. A previously unidentified extensional faulting event occurred in Late Langhian-Serravallian times. In the Manavgat basin this is most pronounced in the south-eastern part of the basin where Miocene sediments overlie Alanya Massif basement. Here, NW-SE trending normal faults developed at this time and resulted in the formation of an asymmetrical horst-graben system (section 7.5.1.2). These micro-faults affecting Lower-Middle Miocene sediments, parallel older structural trends within the Alanya Massif and probably represent reactivation along such weaknesses (section 7.5.1.4).

5. Extension-related deepening resulted in the abrupt transition from shallow-water carbonates (Oymapinar Limestone) to planktic foraminiferal marls (Geceleme Formation) in the Manavgat basin. This boundary is marked by localised deposition of fault generated-talus and calcirudites (Çakallar Formation; sections 7.5.1.2 and 4.7). In the Aksu and Köprü basins a similar transition occurred, where shallow water-carbonates were overlain by deeper-water fine-grained turbidites (Karpuzçay Formation). In some places (e.g. Deniztepesi) this boundary is also marked by a coarse talus horizon (section 3.6.2.3 and figure 4.24) indicating that faulting was not restricted to the Manavgat basin at this time.

6. After a short (1Ma) period of extension-generated faulting the Manavgat basin underwent a period of tectonic quiescence which allowed the accumulation of several hundred metres of planktic foraminiferal marls (Geceleme Formation; figure 4.22) as post-rift fill (section 7.1.5.2). In the Aksu and Köprü basins, turbidites sourced from the north flowed

south along north-south orientated older lineaments at this time (figure 4.11). Evidence from the south of the Köprü basin suggests that these lineaments, though focusing sediment dispersal patterns, may not have had a strong topographic relief during turbidite deposition (Flecker *et al.*, 1995; section 4.6.2.4).

7. The Serravallian-Tortonian boundary is marked throughout the Isparta Angle by a change in sedimentation. The hinterland to the Manavgat basin was extended and uplifted dramatically at this time resulting in the deposition of conglomerates, debris flow, sandstones and siltstones (4.6.3.3). There is no correlative signature of tectonic intra-basinal subsidence which continued to shallow with time throughout the Tortonian to Middle Messinian. In the north of the Köprü and Aksu basins the Tortonian and Lower Messinian were characterised by continental and coastal conglomerate deposition (section 5.7.2). Once again, reef carbonate colonisation of conglomerate horizons suggests that rising relative sea level was a dominant control on sedimentation over and above high sediment influx (section 5.9.2). The different behaviour of the north and south of the Isparta Angle is evidence for the block faulted nature of the controlling basement.

8. A period of compression which terminated in the Lower-most Pliocene (the Aksu Phase) produced many of its characteristic west-vergent structures in the Latest Miocene (Poisson, 1977) and formed the angular unconformity which separates the Miocene from the Pliocene successions in the area. Previously unrecognised east-vergent structures can also be found affecting Miocene sediments and underlying Mesozoic basement (e.g. Akbas syncline, section 7.5.2.3). In addition there is evidence of minor folding related to inversion of the horst-graben system in the Manavgat basin at this time (section 7.5.1.3). Earlier interpretations argued that westward escape of the Anatolian block was fundamental in forming the westward transport signature during the Late Miocene (Poisson, 1984; Sengör *et al.*, 1986). It is suggested here (section 7.6.2) however that movement of the Lycian Nappes orientated obliquely to north-south trending lineaments may have dominated the area close to the thrust front, including the Isparta Angle and resulted in some of the apparently east-west compression.

9. Facies models have been constructed for the Miocene sediments within the Isparta Angle. These indicate that the area was dominated by coarse (sandstone-conglomerate) clastic input throughout the Miocene. Deposition of these clastics occurred in a variety of environments from continental, to coastal to shelfal marine. Reef carbonates were deposited in coastal environments when environmental factors including sediment influx and relative sea level rise were favourable for coral colonisation.

10. Increased biostratigraphic and isotopic age resolution has allowed the correlation of Miocene sections across the Isparta Angle (Fig. 4.32). This has led to the modification of the existing stratigraphic framework (Akay and Uysal, 1985).

A final comment

The most important conclusion to come out of this study is that the fundamental control over the evolution of the Isparta Angle during the Miocene was the strong north-south structural grain of the heterogeneous basement. Stress, orientated in various directions, affected this long lived suture zone, but the structural features within it relate first and foremost to basement fabric. This conclusion severely limits the amount of direct interpretation that can be put on microstructural features in terms of the stresses affecting the Isparta Angle as a whole (e.g. Hague, 1993). The placing of the evolution of the three basins studied into the context of the development of the Eastern Mediterranean can therefore only be done in a tentative manner relying heavily on the temporal and spatial correlation of tectonic events outwith the Isparta Angle to those identified from within it. In doing so, a valuable perspective on the size and style of deformation that tectonic processes have on pre-existing suture zones is gained. More study of transitional areas between those which respond in an orthogonal manner to tectonic stress and those which develop oblique structures is required before the less tentative statements can be made.

References

Acevedo, R., Morelock, J., & Olivieri, R. A. (1989). Modification of coral reef zonation by terrigenous sediment stress. Palaios, 4, 92-100.

Aigner, T., & Reineck, H. (1982). Proximality trends in modern storm sands from the Helegoland Bight (North Sea) and their implications for basin analysis. Senckenbergiana marit., 14, 183-215.

Akay, E., & Uysal, S. (1985). Orta toroslarin batisindaki (Antalya) Neojen çökellerinin stratigrafisis, sedimentolojisi ve yapisal jeolojisi No. M.T.A report.

Akay, E., Uysal, S., Poisson, A., Cravatte, J., & Müller, C. (1985). Stratigraphy of the Antalya Neogene Basin. Bull. Geol. Soc. Turkey,, 28, 105-119.

Akbulut, A. (1977) Etude géologique d'une partie du Taurus occidentale au siud d'Egirdir (Turquie). Thèse Univ. Paris-Sud, Orsay.

Aktas, G., & Robertson, A. H. F. (1985). The Maden Complex, SE Turkey: evolution of a Neotethyan active margin. In J. E. Dixon & A. H. F. Robertson (Eds.), The Geological Evolution of the Eastern Mediterranean (pp. 375-401). Oxford: Blackwell Scientific Publications.

Albarede, F., & Michard, A. (1987). Evidence for slowly changing 87Sr/86Sr in runoff from freshwater limestones of southern France. Chemical Geology, 64, 55-65.

Allen, J. R. L. (1970). The angle of intial yield of haphazard assemblages of equal spheres in bulk. Geol. Mijnb., 49, 13-22.

Allen, J. R. L. (1974). Studies in fluviatile sedimentation: implications of pedogenic carbonate units, Lower Old Red Sandstone, Anglo-Welsh outcrop. Geol. J., 9, 181-208.

Anastasakis, G., & Kelling, G. (1991). Tectonic connection of the Hellenic and Cyprus arcs and related geotectonic elements. Marine Geology, 97, 261-277.

Angelier, J., Dumont, J. F., Karamanderesi, H., Poisson, A., Simsik, S., & Uysal, S. (1981). Analyses of fault mechanisms and expansion of southwestern Anatolia since the Late Miocene. Tectonophysics, 75, T1-T9.

Angelier, J., Lyberis, N., Le Pichon, X., Barrier, E., & Huchon, P. (1982). The tectonic development of the Hellenic arc and the Sea of Crete: a sythesis. Tectonophysics, 86(159-196).

Arche, A. (1983). Coarse-grained meander lobe deposites in the Jarama River, madrid, spain. In J. D. Collinson & J. Lewin (Eds.), Modern and ancient alluvial systems (pp. 313-321). Int. Ass. Sed. Spec. Publ.

Barnes, R. S. K., & Hughes, R. N. (1982). An introduction to Marine Ecology. Oxford: Blackwells.

Baroz, F., Bernoulli, D., Biju-Duval, B., Bizon, G., Bizon, J. J., & Letouzey, J. (1978). Initial Rep. D.S.D.P., 42 (903-906).

Baroz, F. (1979) Etude geologique dans le Pentadaktylos and Mesaoria (Chypre septentrionale). PhD, Nancy.

Barrier, P. (1984) Evolution téctono-sédimentaire Pliocene et Pléistocene du Détroit de Messine (Italie). Doctoral dissertation, Marseille, France.

Beets, C. J., & De Ruig, M. J. (1992). 87Sr/86Sr dating of coralline algal limestones and its implications for the tectonostratigraphic evolution of the eastern Prebetic (Spain). Sedimentary Geology, 78(3/4), 233-250.

Beets, C. J., & Ruig, M. J. (1992). Calibration of marine 87Sr/86sr-isotope variations and chronostratigraphy during the past 13 Ma. In C. J. Beets (Eds.), Calibration of late Cenozoic strontium isotope variations and its chronostratigaphic and geochemical applications (pp. 7-37). Amsterdam:

Berggren, W. A., Kent, D. V., & van Couvering, J. A. (1985). The Neogene: Part 2. Neogene geochronology and chronostratigraphy. In Snelling (Eds.), The Chronology of the Geological Record (pp. 211-260). Blackwell Scientific publications.

Birck, J. L. (1986). Precision K-Rb-Sr isotopic analysis: application to Rb-Sr chronology. Chemical Geology, 56, 73-84.

Bizon, G., Biju-duval, B., Letouzay, J., Monod, O., Poisson, A., Ozer, B., & Oztumer, E. (1974). Nouvelles précisions stratigraphiques concernant les bassins tertiaires du sud de la Turquie (Antalya, Mut, Adana). Rev. Inst. Fr. Petrole, Paris, 29, 305 - 320.

Blumenthal, M. (1947). Geologie der Taurusketten im Hinterland von Seydsehir und Beysehir (Series D No. 2). M.T.A report.

Blumenthal, M. (1951). Recherches géologiques dans le Taurus occidental dans l'arrière-pays d'Alanya No. D. 5 p134). M.T.A., Ankara.

Blumenthal, M. (1963). Le système structural du Taurus sud-Anatolien. In Livre à la mémoire du Professeur Paul Fallot (pp. 611-662). Mém. hors-série Soc. géol. Fr.

Boltovsky, & Wright, R. (1976). Recent Foraminifera. .

Bouma, A. H. (1962). Sedimentology of some flysch deposits: a graphic approach to facies interpretation. Amsterdam: Elsevier.

Braga, J. C., & Martin, J. M. (1988). Neogene coralline-algal growth-forms and their palaeoenvironments in the Almanzora river valley (Almeria, S. E. Spain). Palaeogeography, Palaeoclimatology, Palaeoecology, 67, 285-303.

Brass, G. W. (1976). The variation of the marine 87Sr/86Sr ratio during Phanerozoic time: Interpretation using a flux model. Geochim. Cosmochim, Acta, 40, 721-730.

Bridge, J. S. (1985). Palaeochannel pattern inferred frm alluvial deposits: a critical evaluation. Journal of Sedimentary Petrology, 55, 579-589.

Brunn, J. H., Dumont, J. F., Graciansky, P. C. d., Gutnic, M., Juteau, T., Marcoux, J., Monod, O., & Poisson, A. (1971). Outline of the Geology of the Western Taurides. In A. S. Campbell (Eds.), Geology and History of Turkey (pp. 225 - 255). Tripoli: Petrol. Explor. Soc. of Libya.

Brunn, J. H. (1974). Le problème de l'origine des nappes et leurs translations dans les Taurides occidentales. Bull. Soc. Géol. Fr., 16, 101-106.

Bull (1977). Geological Society of America, Bulletin, 88.

Burke, W. H., Denison, R. E., Hetherington, E. A., Koepnick, R. B., Nelson, H. F., & Otto, J. B. (1982). Variation of seawater 87Sr/86Sr throughout Phanerozoic time. Geology, 10, 516-519.

Butzer, K. W. (1964). Climatic-geomorphic interpretations of Pleistocene sediments in the Eurafrican sub-tropics. In F. C. Howell & F. Bourliere (Eds.), African Ecology and Human evolution (pp. 1-25). London: Methuen.

Caen, L., & al, e. (1988). .

Calvert, S. E. (1987). Oceanographic controls on the accumulation of organic matter in marine sediments. In J. Brooks & A. J. Fleet (Eds.), Marine Petroleum Source Rocks (pp. 137-151). Geological Society of London Special Publication.

Carpenter, S. J., Lohmann, K. C., Holden, P., Walter, L. M., Huston, T. J., & Halliday, A. N. (1991). d18O values and 87Sr/86Sr and Sr/Mg ratios of Late Devonian abiotic marine calcite: Implications for the composition of ancient seawater. Geochemica et Cosmochimica Acta, 55, 1991-2010.

Chamberlain, C. K. (1978). Recognition of trace fossils in cores. In P. B. Basan (Eds.), Trace fossil concepts. SEPM short course. (pp. 119 -167). Oklahoma: Society of Economic Palaeontologists and Mineralogists.

Chase, C. G. (1978). Plate kinematics: The Americas, East Africa and the rest of the world. Earth Planet. Sci. Let., 37, 355-368.

Chevalier, J. P. (1961). Recherches sur les Madréporaires et les formations récifales Miocene de la Méditerranée occidentale. Mémoir de la Société Géologique de France, 40/93 (pp 562)

Chevalier, J. P. (1977). Aperçu sur la faune coralliene récifale du Néogene. Mémoires du Bureau de Recherches Géologiques et Minieres, 89, 359-366.

Church, M., & Gilbert, R. (1975). Proglacial fluvial and lacustrine environments. In A. V. Jopling & B. C. McDonald (Eds.), Glaciofluvial and Glaciolacustrine sedimentation (pp. 22-100). Society of Economic Paleontologists and Mineralogists Special Publication.

Cocozza, T., & Jacobacci, A. (1975). Geological outline of Sardinia. In C. Squyres (Eds.), Geology of Italy (pp. 49-81). Tripoli: Earth Sciences of the Lybian Arab Republic.

Colella, A., De Boer, P. L., & Nio, S. D. (1987). Sedimentology of a marine intermontane Pleistocene Gilbert-type fan-delta complex in the Crati Basin, Calabria, southern Italy. Sedimentology, 34, 721-736.

Colella, A., & Prior, D. B. (1990). Preface. In A. Colella & D. B. Prior (Eds.), Coarse-Grained Deltas Oxford: Blackwell.

Collinson, J. D. (1986). Alluvial Sediments. In H. G. Reading (Eds.), Sedimentary Environments and Facies (2nd edition) (pp. 20-62). Oxford: Blackwell Scientific Publications.

Condon, P. J. (1988) Seismic stratigraphy and distribution of Palaeogene sediments west and east of Shetland. Ph.D., Edinburgh.

Degirmenci, M. (1992). Karstification at the Beskonak dam site and reservoir area. 1st International Symposium on Eastern Mediterranean Geology., Proceedings and abstracts, 255 - 268.

DePaolo, D. J., & Ingram, B. L. (1985). High-resolution stratigraphy with strontium isotopes. Science, 227, 938-941.

DePaolo, D. J. (1986). Detailed record of the neogene Sr isotopic evoltion of seawter from DSDP site 590B. Geology, 14, 103-106.

Dewey, J. F., & Sengor, A. M. C. (1979). Aegean and surrounding regions: complex multiplate and continuum tectonics in a convergent zone. Geological Society of America Bulletin, 90(Part 1), 84-92.

Dewey, J. F. (1980). Episodicity, sequence and style at convergent plate boundaries. In The continental crust and its mineral deposites (pp. 553-573). Spec. Pap. Geol. Assoc. Can.

Dewey, J. F., Hempton, M. R., Kidd, W. S. F., Sarglu, F., & Sengor, A. C. M. (1986). Shortening of continental lithosphere: the neotectonics of Anatolia - a young collisional zone. In M. P. Coward & A. C. Ries (Eds.), Collision Tectonics (pp. 3-36). Special Publ. Geol. Soc. London.

Dewey, J. F., Helman, M. L., Turco, E., Hutton, D. H. W., & Nott, S. D. (1989). Kinematics of the western Mediterranean. In M. P. Coward, D. Dietrich, & R. G. Park (Eds.), Alpine Tectonics (pp. 265-283). Spec. Publ. Geol. Soc. Lond.

Dott, R. H. J., & Bourgeois, J. (1982). Hummocky stratification: significance of its variable bedding sequences. Bull. geol. Soc. Am., 93, 663-680.

Dumont, J.-F., Gutnic, M., Marcoux, J., Monod, O., & Poisson, A. (1972). Definition du bassin pamphylien: Un nouveau domain a ophiolites a la marge extrene de la chaine taurique. Z. Dtsch. Geol. Ges., 123, 385-409.

Dumont (1974) Etudes géologique dans les Taurides occidentales les formations Paleozoiques et Mézozoiques de la coupole de Karacahisar (Isparta, Turquie). PhD, L'Université de Paris Sud "Centre d'Orsay".

Dumont, J.-F., & Kerey, E. (1975). L'accident de Kirkkavak, un décrochement majeur dans le Taurus occidental (Turquie). Bull. Géol. Soc. Fr., 7, XVII(6).

Dunham, R. J. (1962). Classification of carbonate rocks according to depostional texture. In W. E. Ham (Eds.), Classification of carbonate rocks (pp. 108-121). American Association of Petroleum Geologists Memoir.

Dunham, R. J. (1962). Classification of carbonate rocks according to depostional texture. In W. E. Ham (Eds.), Classification of carbonate rocks (pp. 108-121). American Association of Petroleum Geologists Memoir, 1 (108-121).

Dunne, L. A., & Hempton, M. R. (1984). Strike-slip basin sedimentation at Lake Hazar (Eastern Taurus Mountains). In O. Tekili & M. C. Goncuoglu (Eds.), Geology of the Taurus Belt Proceedings of the International Symposium in Ankara.

Dupoux, B. (1983) Etude comparée de ma tectonique néogène des bassins du sud de Chypre et du bassin d'Antalya (Turquie). PhD, Paris-Sud "Centre Orsay".

Dzulynski, S., & Saunders, J. E. (1962). Current marks on firm mud bottoms. Trans. Conneticut Acad. Arts amd Sciences, 42, 57-96.

Eaton, S. (1987) The sedimentology of Mid to Late Miocese carbonates and evaporites in Southern Cyprus. Unpublished thesis, Edinburgh.

Eaton, S., & Roberton, A. (1993). The Miocene Pakhna Formation, southern Cyprus and its relationship to the Neogene tectonic evolution of the Eastern Mediterranean. Sedimentary Geology, 86, 273 - 296.

Elderfield, & Geiskes (1982). Sr isotopes ininterstitial waters of marine sediments from Deep Sea Drilling Project cores. Nature, 300, 493-497.

Elderfield, H. (1986). Sr isotope stratigraphy. Palaeogeography, Palaeoclimatology, Palaeoecology, 57, 71-90.

Elderfield, H. (1994). Recent trends in Strontium isotope stratigraphy. Terra Nova, 6(4), 331-358.

Elliott, T. (1986). Deltas. In H. G. Reading (Eds.), Sedimentary Environments and Facies (pp. 113-154). Oxford: Blackwell.

Embry, A. F., & Klovan, J. E. (1971). A late Devonian reef tract on northeastern Banks Islnd Northwest Territories. Bulletin of Canadian Petroleum Geologists, 19, 730-781.

Enos, P. (1977). Flow regimes in debris flow. Sedimentology, 24.

Esteban, M. (1979). Significance of the Upper Miocene coral reefs of the Western Mediterranean. Palaeogeography, Palaeoclimatology, Palaeoecology, 29, 169-188.

Etheridge, F. G., & Westcott, W. A. (1984). Tectonic setting, recognition and hydrocarbon reservoir potential of fan-delta deposits. In E. H. Koster & R. J. Steel (Eds.), Sedimentology of Gravels and Conglomerates (pp. 217-235). Calgary: Mem. Can. Soc. Petrol. Geol.

Evans, G., Morgan, P., Evans, W. E., Evans, T. R., & Woodside, J. M. (1978). Faulting and halokinetics in the Northeastern Meditertranean between Cyprus and Turkey. Geology, 6, 392 - 396.

Flecker, R., Robertson, A. H. F., Poisson, A., & Müller, C. (1995). Facies and Tectonic significance of two contrasting Miocene basins in south coastal Turkey. Terra Nova, 7, 221-232.

Folk, R. L. (1959). Practical petrographic classification of limestones. Bull. Am. Ass. Petrol. Geol., 43, 1-38.

Folk, R. L. (1962). Spectral subdivision of limestone types. In W. E. Ham (Eds.), Classification of carbonate rocks (pp. 62-84). Mem. Am. Ass. Petrol. Geol.

Follows, E. J., & Robertson, A. H. F. (1990). Sedimentology and structural setting of Miocene reefal limestones in Cyprus. In J. Malpas, E. M. Moores, A. Panayiotou, & C. Xenophontos (Ed.), Ophiolites Oceanic Crustal Analogues. Proc. Symp. "Troodos 1987", (pp. 207-216). Nicosia: Geol. Surv. Dept.

Fraser, G. S., & Suttner, L. (1986). Alluvial fans and fan deltas. A guide to exploration for oil and gas. Boston: International Human Resources Development Corporation.

Frizon de Lamotte, D., Andrieux, J., & Guezou, J. C. (1991). Cinématique des chevauchements néogènes dans l'Arc bético-rifain: discussion sur les modèles géodynamiques. Bull. Geol. Soc. Fr., 162, 661-626.

Frizon de Lamotte, D., Poisson, A., Aubourg, C., & Temiz, H. (1995). Chevauchments Post-Tortoniens vers l'ouest puis vers le sud au coeur de l'Angle d'Isparta (Taurus, Turquie). Conséquences géodynamiques. Bull. Soc. Géol. France.

Frizon de Lamotte, D., Averbuch, O., & Guezou, J.-C. (in press). Distinguishing lateral folds in thrust systems. J. Struct. Geol.

Frost, S. H. (1977). Ecological controls of Caribbean and Mediterranean Oligocene reef coral communities. In D. L. Taylor (Ed.), Proceedings of the Third Internationl Coral Reef Symposium, 2 (pp. 367-373).

Frost, S. H., & Weiss, M. P. (1979). Patch-reef communities and succession in the Oligocene of Antigua, West Indies: Summary. Geological Society of America Bulletin, 90, 612-616.

Frost, S. (1981). Eocene, Oligocene and Miocene reef corals, meditteranean area. Unpublished manuscript in the Natural History Museum, London.

Garrison, R. E. (1981). Diagenesis of oceanic carbonate sediments: A review of the DSDP perspective. In The Deep Sea Drilling Project: A decade of progress (pp. 181-207). SEPM Spec. Publ.

Geister, J. (1983). Kolozane westindische Korallenriffe: Geomorphologie, Okologie und Fazies. Facies, 9, 173-284.

Gloppen, T. G., & Steel, R. J. (1981). The deposits, internal structure and geometry in six alluvial fan-fan delta bodies (Devonian, Norway) - a study in the significance of bedding sequences in conglomerates. In F. G. Etheridge & R. M. Flores (Eds.), Recent and Ancient Non-marine Depositional Environments: Models for Exploration (pp. 49-69). Society of Economic Paleontologists and Meralogists Special Publication, 31.

Glover, C. P. (1995) ? Ph. D., Edinburgh.

Graciansky (1972) Recherches géologiques dans le Taurus lycien occidental. Thèse doct. d'état, Univ. Paris Sud (Orsay).

Gurbuz, K. (1993) Identification and Evolution of Miocene Submarine Fans, in the Adana Basin, Turkey,. PhD, Keele.

Gutnic, M., Monod, O., Poisson, A., & Dumont, J.-D. (1979). Géologie des Taurides occidentales (Turquie). Mém. Soc. Géol. Fr., 58(no 137), 112p.

Gwirtzmann, G., & Buchbinder, B. (1978). Recent and Peistocene coral reefs and coastal sediments of the Gulf of Elat. In Post-Congress Guidebook, Tenth International Congress on Sedimentology (pp. 163-189). Jerusalem:

Hague, P. (1993) The structural and volcanic evolution of Tertiary basins along the southern margin of the Rhodope Massif, northeastern Greece. Ph.D., Southampton.

Hague, P. (1993) The structural and volcanic evolution of Tertiary basins along the southern margin of the Rhodope Massif, northeastern Greece. Ph.D., Southampton.

Haq, B. U., Hardenbol, J., & Vail, P. R. (1988). Mesozoic and Cenozoic chronostratigraphy and eustatic cycles. In C. K. Wilgus, B. S. Hastings, C. G. S. C. Kendall, H. Posamentier, C. A. Ross, & J. Van Wagoner (Eds.), Sea-level changes: an integrated approach (pp. 71-108). Society of Ecconomic Palaeontologists and Mineralogists, Special Publication no 42.

Harms, J. C., & Fahnestock, R. K. (1965). Stratification, bed forms and flow phenomena (with an example from the Rio Grande). In G. V. Middleton (Eds.), Primary sedimentary structures and their hydrodynamic interpretation. (pp. 84-115). Soc. Econ. Paleont. Mineral. Spec. Publ.

Harvey, A. M. (1984). Debris flows and fluvial deposits in Spanish Quaternary alluvial fans: implications for fan morphology. In E. H. Koster & R. J. Steel (Eds.), Sedimentology of gravels and conglomerates (pp. 123-132). Canadian Society of Petroleum Geologists.

Hayward, A. B. (1982a). Reefs in coarse clastic sedimentary environments. Jornal of coral reefs, 1, 109-114.

Hayward, A. B. (1982b) Tertiary ophiolite-related sedimentation in S. W. Turkey. Ph.D., University of Edinburgh.

Hayward, A. B., & Robertson, A. H. F. (1982). Direction of ophiolite emplacement inferred from Cretaceous and Tertiary sediments of an adjacent autochthon, the Bey Daglari, southwest Turkey. Bull. Geol. Soc. Am., 93, 68-75.

Hayward, A. B. (1984). Miocene clastic sedimentation related to the emplacement of the Lycian Nappes and the Antalya Complex, SW Turkey. In J. E. Dixon & A. H. F. Robertson (Eds.), The geological evolution of the Eastern Mediterranean Geol. Soc. London.

Hein, F. J., & Walker, R. G. (1977). Bar evolution and development of stratification in the gravelly, braided Kicking Horse River, British Columbia. Canadian Journal of Earth Sciences, 14(562-570).

Hein, F. J. (1984). Deep-sea and fluvial braided channel conglomerates: a comparison of two case studies. In E. H. Koster & R. J. Steel (Eds.), Sedimentology of gravels and conglomerates (pp. 33-49). Canadian Society of Petroleum geologists.

Hess, J., Bender, M. L., & Schilling, J. (1986). Evolution of the ratio of Strontium-87 to Strontium-86 in seawater from the Cretaceous to the present. Science, 231, 979-984.

Hiscott, R. N., & Middleton, G. V. (1979). Depositional mechanics of thick-bedded sandstones at the base of a submarine slope, Tourelle Formation (Lower Ordivician), Quebec, Canada. In L. J. Doyle & O. H. Pilkey (Eds.), Geology of continental slopes (pp. 307-326). Soc. Econ. Paleont. Minarl. Spec. Publ.

Hiscott, R. N., & Middleton, G. V. (1980). Fabric of coarse eep-water sandstones, Tourelle Formation, Quebec, Canada. J. Sed. Petrol., 50, 703-722.

Hodell, D. A., Muella, P. A., & Garrido, J. R. (1991). Variations in the strontium isotopic compoition of seawater during the Neogene. Geology, 19, 24-27.

Hodell, D. A., & Woodruff, F. (1994). Variations in the strontium isotopic ratio of seawater during the Miocene: Stratigraphic and geochemical implications. Paleoceonography, 9(3), 405-426.

Hodell, D. A. (1994). Editorial: Progress and paradox in strontium isotope stratigraphy. Paleoceonagraphy, 9(3), 395-398.

Holmes, A. (1965). Principles of Physical Geology (2nd ed.). London: Thomas Nelson.

Hooke, R. L. (1967). Processes on arid region alluvial fans. Journal of Geology, 75, 438-460.

Hsü, J. K., Ryan, W. B. F., & Cita, M. B. (1973). Late Miocene dessication of the Mediterranean. Nature, 242, 240-244.

Hubert, J. F., & Hide, M. G. (1982). Sheet flow depostis of graded beds and mudstones on an alluvial sandflat-playa system: Upper Truassic Blomidin redbeds, St mary's bay, Nova Scotia. Sedimentology, 29, 457-474.

Jackson, R. G. (1978). Preliminary evaluation of lithofacies models for meandering alluvial streams. In A. D. Miall (Eds.), Fluvial Sedimentlogy (pp. 543-576). Canadian Society Petroleum Geologists, Memoir.

Jackson, J., & Mckenzie, D. P. (1984). Active tectonics of the Alpine-Himalayan Belt between western Turkey and Pakistan. Geophysical Journal of the RoyAl Astronomical Society, 77, 185 - 264.

Jarrard, R. D. (1985). Relations among subduction parameters. Rev. Geophysics, 24, 217-284.

Johnson, D. P., Belperio, A. P., & Hop;ey, D. (1986). A field guide to mixed terrigenous-carbonate sedimentation in the Central Great Barrier Reef Province, Australia.

Jolivet, L., Brun, J.-P., Gautier, P., Lallemant, S., & Patriat, M. (1994). 3D0-kinematics of extension in the Aegean region from the early Miocene to the Present, insights from the ductile crust. Bull. Soc. géol France, 165(3), 195-209.

Jones, C. E., Jenkyns, H. C., & Hesselbo, S. P. (1994). Strontium isotopes in Early Jurassic seawater. Geochimica et Cosmochimica Acta, 58(4), 1285-1301.

Kelling, G., & Holroyd, J. (1978). Clast size, shape and composition in some ancient and modern fan gravels. In D. J. Stanley & G. Kelling (Eds.), Sedimentation in Submarine Canyons, Fans and Trenches (pp. 136-159). Stroudsburg, Pennsylvania: Dowden, Hutchinson and Ross.

Kelling, G., Gokcen, S. L., Floyd, P. A., & Gokcen, N. (1987). Neogene Tectonics and plate convergence in the Eastern Mediterranean: New data from southern Turkey. Geology, 15, 425 - 429.

Kempler, D., & Ben-Avraham, Z. (1987). The tectonic evolution of the Cyprean Arc. Annales Tectonicae, 1(1), 58 - 71.

Kempler, D. (1994) Tectonic patterns in the easternmost Mediterranean. Ph. D., Hebrew University of Jerusalem.

Kissel, C., & Poisson, A. (1986). Etude paléomagnétique préliminaire des formations néogenes du bassin d'Antalya (Taurides occidentales, Turquie). C. R. Acad. Sc. Paris, t 302(10), 711-716.

Kissel, C., & Poisson, A. (1987). Etude paléomagnétique préliminaire des formations cénozoiques des Bey Daglari (Taurides occidentales, Turquie). C. R. Acad. Sc. Paris, 304(Séris II), 343 - 348.

Kissel, C., Averbunch, O., Frizon de Lamotte, D., Monod, O., & Allerton, S. (1993). First palaeomagnetic evidence for a post-Eocene clockwize rotation of the Western Taurides thrust belt east of the Isparta reentrant (Southwestern Turkey). Earth and Planetary Science Letters, 117, 1-14.

Klapper, C. F. (1980). Rhizoliths in terrestrial carbonates: classification, recognition, genesis and significance. Sedimentology, 27, 613-629.

Koepnick, R. B., Burke, W. H., Denison, R. E., Hetherington, E. A., Nelson, H. F., Otto, J. B., & Waite, L. E. (1985). Construction of the seawater 87Sr/86Sr curve for the Cenozoic and Cretaceous: Supporting data. Chemical Geology, 58, 55-81.

Koepnick, R. B., Denison, R. E., & Dahl, D. A. (1988). The Cenozoic seawater 87Sr/86Sr curve: Data review and implications for correlations of marine strata. Palaeoceanography, 3, 743-756.

Kraus, M. J. (1984). Sedimentology and tectonic setting of Early Tertiary Quartzite conglomerates, Northwest Wyoming. In E. H. Koster & R. J. Steel (Eds.), Sedimentology of Gravels and Conglomerates (pp. 203-216). Calgary: Canadian Society of Petroleum Geologists.

Larsen, V., & Steel, R. J. (1978). The sedimentary history of a debris flow-dominated alluvial fan: a study of textural inversion. Sedimentology, 25, 37-59.

Le Pichon, X., & Anglier, J. (1979). The Hellenic Arc and trench system: a key to the evolution of the Eastern Mediterranean area. Tectonophysics, 60, 1 - 42.

Le Pichon, X., & Anglier, J. (1981). The Aegean Sea. Phil. Trans. Roy. Soc. London, A300, 357-372.

Le Pichon, X., & Gaulier, J.-M. (1988). The rotation of Arabia and the Levant fault system. Tectonophysics, 153, 271-294.

Le Pichon, X., Chamot-Rooke, N., Huchon, P., & Luxey, P. (1993). Implications of new Space Geodesy measurements in Greece qnd Turkey upon the lateral extrustion of Anatolia and Agea. Comptes Rendus Acadamie de Sciences, Paris, 316(2), 983-990.

Leeder, M. R. (1975). Pedogenic carbonate and flood sediment accretion rates: a quantitative model for alluvial, arid-zone lithofacies. Geol. Mag., 112, 257-270.

Lefevre, R. (1967). Un nouvel élément de la géologie du Taurus Lycien : les nappes d'Antalya (Turquie). C.R. Acad. Sc., Paris, 263, 1029-1032.

Lefevre, C., Bellon, H., & Poisson, A. (1983). Volcanologie - Présence de leucitites dans le volcanisme pliocene de la région d'Isparta (Taurides occidentales, Turquie). C. R. Acad. Sc. Paris, t. 297(II), 367-372.

Limanov, A., & Ivanov, M. (1994). Mud volcanism in the Mediterranean and Black Seas and shallow structure of the Eratosthenes Seamount,Initial results of the 'Training through Research' Cruise of RV Gelendzhik. UNESCO.

Lowe, D. R. (1976). Subaqueous liquified and fluidized sediment flows and their deposits. Sedimentology, 22, 157-204.

Lowe, D. R. (1979). Sediment gravity flows: their classification and some problems of application to natural flows and deposits. In L. J. Doyle & O. H. Pilkey (Eds.), Geology of continental slopes (pp. 75-82). Society of Economic Paleontologists and Mineralogists Special Publication.

Lowe, D. R. (1982). Depositional models with special reference to the deposits of high density turbidity currents. Journal of Sedimentary Petrology, 52(1), 279-297.

Lucchi, R., Pott, M., Nieto, E., Ivanova, E., Lototskaya, A., Glover, C., Flecker, R., Basov, E., Kidd, R., & Robertson, A. H. F. (1994). Bottom sampling. In A. F. Limonov, J. M. Woodside, & M. K. Ivanov (Eds.), Initial results of the goelogical and geophysical investigations during the Third UNESCO-ESF "Training-through-Research" Cruise of RV Gelendzhik (June-July 1993) (pp. 134-145). UNESCO reports in marine science.

Lucchi, R., Pott, M., Nieto, E., Ivanova, E., Lototskaya, A., Glover, C., Flecker, R., Basov, E., Kidd, R., & Robertson, A. H. F. (1994). Bottom sampling. In A. F. Limonov, J. M. Woodside, & M. K. Ivanov (Eds.), Initial results of the goelogical and geophysical investigations during the Third UNESCO-ESF "Training-through-Research" Cruise of RV Gelendzhik (June-July 1993) (pp. 134-145). UNESCO reports in marine science.

Luyendyk, B. P., Forsyth, D., & Phillips, J. D. (1972). Experimental approach to paleocirculation of the oceanic surface waters. Geological Society of America Bulletin, 83, 2649-2664.

Maizels, J., & McBean, C. (1990). Cenozoic alluvial fan systems of interior Oman: palaeoenvironmental reconstruction based on discrimination of palaeochannels using remotely sensed data. In A. H. F. Robertson, S. M. P., & A. C. Reis (Eds.), The geology and tectonics of the Oman region (pp. 565-582). Special publication of the Geological Society.

Manton, S. M. (1935). Ecological surveys of coral reefs No. 3 273-312). Scientific reports of the Great Barrier Reef Expedition.

Manton, S. M. (1935). Ecological surveys of coral reefs No. 3 273-312). Scientific reports of the Great Barrier Reef Expedition.

Marcoux, J. (1976). Les séries triassiques des nappes à radiolarites et ophiolites d'Antalya (Turquie): homologies et signification probable. Bull. Soc. Géol. Fr., 18, 511-512.
Marcoux, J. (1976). Les séries triassiques des nappes à radiolarites et ophiolites d'Antalya (Turquie): homologies et signification probable. Bull. Soc. Géol. Fr., 18, 511-512.
Marcoux, J., Ricou, L. E., Burg, J. P., & Brun, J. P. (1989). Shear-sense criteria in the Alanya thrust system (southwestern Turkey); evidence for southward emplacement. Tectonophysics, 161, 81 -91.
Marshall, & Orr (1931). Sedimentation on Low Isles and its relation to coral growth No. 1 273-312). Scientific Reports of the Great Barrier Reef Expedition.
Marshall, & Orr (1931). Sedimentation on Low Isles and its relation to coral growth No. 1 273-312). Scientific Reports of the Great Barrier Reef Expedition.
Martin, J. M., Braga, J. C., & Rivas, P. (1989). Coral successions in Upper Tortonian Reefs in SE Spain. Lethaia, 22, 271-286.
Martin, J. M., Braga, J. C., & Rivas, P. (1989). Coral successions in Upper Tortonian Reefs in SE Spain. Lethaia, 22, 271-286.
Martin, J. M., & Braga, J. C. (1993). Eocene to Pliocene coralline algae in the Queensland Plateau (Northeastern Australia). In J. A. McKenzie, P. J. Davies, & A. Palmer-Julson (Eds.), Proceedings of the Ocean Drilling Program, Scientific results
Martin, J. M., & Braga, J. C. (1993). Eocene to Pliocene coralline algae in the Queensland Plateau (Northeastern Australia). In J. A. McKenzie, P. J. Davies, & A. Palmer-Julson (Eds.), Proceedings of the Ocean Drilling Program, Scientific results
McArthur (1994). Recent trends in strontium isotope stratigraphy. Terra Nova, 6(4), 331-358.
McCallum (1989) Sedimentation and tectonics of the Plio-Pleistocene of Cyprus. Ph.D., University of Edinburgh.
McCallum (1989) Sedimentation and tectonics of the Plio-Pleistocene of Cyprus. Ph.D., University of Edinburgh.
McCallum, J. E., & Robertson, A. H. F. (1990). Pulsed uplift of the Troodos Massif: evidence from the Plio-Pleistocene Mesaoria basin. In E. Moores, J. Malpas, & C. Xenophontas (Eds.), Ophiolites and Oceanic Lithosphere (pp. 2317-230). Nicosia, Cyprus: Ministry of Agriculture and Natural Resorces.
McCallum, J. E., & Robertson, A. H. F. (1990). Pulsed uplift of the Troodos Massif: evidence from the Plio-Pleistocene Mesaoria basin. In E. Moores, J. Malpas, & C. Xenophontas (Eds.), Ophiolites and Oceanic Lithosphere (pp. 2317-230). Nicosia, Cyprus: Ministry of Agriculture and Natural Resorces.
McCallum, J. E., Scrutton, R. A., Robertson, A. H. F., & Ferrari, W. (1992). Seismostratigraphy and Neogene-Recent depositional history of the south central continental margin of Cyprus. Marine and Petroleum Geology, 10, 426 - 438.
McCallum, J. E., Scrutton, R. A., Robertson, A. H. F., & Ferrari, W. (1992). Seismostratigraphy and Neogene-Recent depositional history of the south central continental margin of Cyprus. Marine and Petroleum Geology, 10, 426 - 438.
McCallum, J. E., & Robertson, A. H. F. (in press). Sedimentology of two fan-delta systems in the Plio-Pleistocene of the Mesaoria basin, Cyprus. .
McGowen, J. H. (1970). Gum Hollow fan delta, Nueces Bay Texas No. 69). Bureau of Economic Geology, Texas University.
McKenzie, D. (1972). Active tectonics ion the Meidterranean region. Geophys. J. R. ast. Soc., 30, 109-185.
McKenzie, D. P. (1978). Active tectonics of the Alpine-Himalayan belt: the Aegean Sea and surrounding regions. Geophysical Journal of the Royal Astronomical Society., 55, 217 - 254.
McKenzie, J. A., Hodell, D. A., Mueller, P. A., & Mueller, D. W. (1988). Application of strontium isotopes to late Miocene-early Pliocene stratigraphy. Geology, 16, 1022-1025.
Meulenkamp, J. E., Wortel, M. J. R., Van Wamel, W. A., Spakman, W., & Hoogerduyn Strating, E. (1988). On the Hellenic subduction zone and the geodynamic evolution of Crete since the late Middle Miocene. Tectonophysics, 146, 203 - 215.
Meulenkamp, J. E., van der Zwaan, G. L., & Van Wamel, W. A. (1994). On Late Miocene to Recent vertical movement on the Cretan segment of the Hellenic arc. Tectonophysics, 234, 53-72.
Middleton, G. V., & Hampton, M. A. (1973). Sediment gravity flows: mechanics of flow and deposition. In G. V. Middleton & A. H. Bouma (Eds.), Turbidites and deep water secimentation (pp. 1-38). Anaheim: SEPM Short Course.
Middleton, G. V., & Hampton, M. A. (1976). Subaqueous sediment transport and deposition by sediment gravity flows. In D. J. Stanley & D. J. P. Swift (Eds.), Marine sediment transport and environmental management (pp. 197-218). New York: Wiley-Interscience.

Miller, K. G., & Feigenson, M. D. (1991). Miocene isotope reference section, Deep Sea Drilling Project site 608: an evolution of isotope and biostratigaphic resolution. Paleoceaongraphy, 6(1), 33 - 52.

Minster, J. B., & Jordan, T. H. (1978). Present day plate motions. J. Geophys. Res., 83(5331-5354).

Monod, O. (1976). La 'courbure d'Isparta', une mosaïque de blocs autochtones surmontés des nappes composites à la jonction de l'arc hellénique et de l'arc taurique. Bull. Soc. géol. Fr., 18, 521-532.

Monod, O. (1977) Recherches géologiques dans le Taurus occidental au sud de Beysehir (Turquie). Thèse doct. d'état, Univ. Paris-Sud, "Centre d'Orsay".

Morris, A., & Robertson, A. H. F. (1993). Miocene remagnetisation of carbonate platform and Antalya Complex units within the Isparta Angle, SW Turkey. Tectonophysics, 220, 243 - 266.

Murray, J. (1973). Distribution and ecology of living benthic foraminiferids. .

Murray, J. W. (1991). Ecology and palaeoecology of Benthic Formainifera. New York: Longman Scientific and Technical.

Mutti, E., & Ricci Lucchi, F. (1972). Le torbiditi dell'Apennino settentrionale/ introduzione all'analisi di facies. Mem. Soc. Geol. Italy, 11, 161-199.

Mutti, E. (1992). Turbidite sandstones. Agip.

Müller, D. W., Mueller, P. A., & McKenzie, J. A. (1990). Strontium isotopic ratios as fluid tracers in Messinian evaporites of the Tyrrhenian sea (western Mediterranean sea). Proceedings of the Ocean Drilling Program, Scientific Results, 107, 603-614.

Nemec, W., & Steel, R. J. (1984). Alluvial and coastal conglomerates: their significant features and some comments on gravelly mass-flow deposits. In E. H. Koster & R. J. Steel (Eds.), Sedimentology of Gravels and Conglomerates (pp. 1-31). Canadian Society of Petroleum Geologiss.

Nemec, W., Steel, R. J., Johannessen, E., & Netland, A. (1984). Domba conglomerate, Devonian, Norway: Process and lateral variability in a mass flow-dominated lacustrine fan-delta. In E. H. Koster & R. J. Steel (Eds.), Sedimentology of gravels and conglomerates (pp. 295-320). Calcary: Canadian Society of Petroleum Geologists.

Nemec, W., & Steel, R. J. (1988). What is a fan delta and how do we recognise it? In W. Nemec & R. J. Steel (Eds.), Fan Deltas: Sedimentology and Tectonic Settings (pp. 3-13). Blackie and Son.

Nemec, W. (1990a). Deltas- remarks on terminology and classification. In A. Colella & D. B. Prior (Eds.), Coarse-Grained Deltas (pp. 3-12). Blackwells Scientific Publications.

Nemec, W. (1990b). Aspects of sediment movement on steep delta slopes. In A. Colella & D. B. Prior (Eds.), Coarse-Grained Deltas (pp. 29-74). Blackwells Scientific Publications.

Okay, A. I., & Özgül, N. (1982). Blueschist and eclogites from the Alanya Massif, Turkey. In The Geological Evolution of the Eastern Mediterranean, Abstract (pp. 82). Edinburgh:

Okay, & Ozgul (1984). HP/LT metamorphism and the structure of the Alansya Massif, southern Turkey: an allochthonous composite tectonic sheet. In J. E. Dixon & A. H. F. Robertson (Eds.), The Geological Evolution of the Eastern Mediterranean (pp. 429-439). Spec. Publ. Geol. Soc. London.

Orzag-Sperber, F., Poignant, A.-F., & Poisson, A. (1977). Palaeogeographic significance of rhodolites: some examples from the Miocene of France and Turkey. In E. Flugel (Eds.), Fosil algae, recent results and developments. (pp. 286-294).

Oslick, J. S., Miller, K. G., Feigenson, M. D., & Wright, J. D. (1994). Oligocene-Miocne strontium isotopes: Stratigraphic revisions and correlations to and inferred glacioeustatic record. Paleoceanography, 9(3), 427-443.

Özgül, N. (1983). Stratigraphy and tectonic evolution of the Central Taurides. In O. Tekeli & Göncüoglu (Eds.), International symposium on the geology of the Taurus belt (pp. 77 - 90). Ankara:

Palmer (1985). Sr isotope compositio of seawater over the past 75 Myr. Nature, 314, 526-528.

Palmer, M. R., & Edmond, J. M. (1989). The strontium isotope budget of the modern ocean. Earth and Planetary Science Letters, 92, 11-26.

Pantin, H. M. (1979). Interaction between velocity and effective density in turbidity flow: phase-plane analysis, with criteria for autosuspension. Marine Geology, 31, 59-99.

Payne, A. S., & Robertson, A. H. F. (1994). Neogene supra-subduction zone extension in the Polis graben system, West Cypus. Geological Society of London, 152, 613-628.

Pemberton, S. G. (1992). Application of Ichnology to Petroleum exploration. In SEPM core workshop (pp. 429). Calgary:

Peterman, Z. E., Hedge, C. E., & Toutelot, H. A. (1970). Isotopic composition of strontium in sea water throughout Phanerozoic time. Geochim. Cosmachim. Acta, 34, 105-120.

Pickering, K. T., Stow, D. A., Watson, M., & Hiscott, R. N. (1986). Deep-water facies, processes and models: a review and classification scheme for modern and ancient sediments. Earth Science Review, 22, 75-174.

Pickering, K. T., Hiscott, R. N., & Hein, F. J. (1989). Deep marine environments. London: Unwin Hyman Ltd.

Pickett, E. A. (1994) Tectonic Evolution of the Palaeotethyan ocean in NW Turkey. Ph.D., Edinburgh.

Plaziat, J.-C. (1984) Le domaine pyrénéen de la fin du Crétacé à la fin de l'Eocène. Stratigraphie, paléoenvironments et évolution paléogeographique. Thesis, multigr, no 2885, Université de Paris-Sud, Orsay.

Plaziat, J.-C. (1993). Modern and fossil Potamids (Gastropoda) in saline lakes. Journal of Paleolimnology, 8, 163-169.

Poisson, A., & Poignant, A. F. (1974). La formation de Karabayir, base de la transgression Miocène dans la région de Korkuteli (Antalya, Turquie). Lithothamnium pseudoramossissimum, nouvelle espèce d'Algue rouge de la formation de Karabayir. Bull. Min. Res. Expl. Inst. Turkey, Ankara, 82, 67 - 71.

Poisson, A. (1977a) Recherches geologiques dans le Taurus occidental, Turquie. Thèse d'état, Univ. Paris-Sud, (Orsay).

Poisson, A. (1977b). Evolution structurale des Taurides occidentales au cours du Mésozoïque et du Tertiaire. In Cong. CIESM, 24, 7a (pp. 175-176). Split: Rap. Com. Int. Mer Médit.

Poisson, A., Akay, E., Cravatte, J., Müller, C., & Uysal, S. (1983). Données nouvelles sur la chronologie de mise en place des nappe d'Antalya au centre de l'angle d'Isparta (Taurides occidentales, Turquie). C. R. Acad. Sc. Paris, t. 296, 923-925.

Poisson, A. (1984). The Isparta Angle: a Mesozoic palaeorift in the Western Taurides. In O. Tekeli & C. Goncuuoglu (Eds.), International symposium on the geology of the Taurus belt Ankara: Special Publication M. T. A.

Poisson, A., & Kissel, C. (1986). Etude paléomagnétique préliminaire des formations néog ènes du bassin d'Antalya (Taurides occidentales-Turquie). C. R. Acad. Sc. Paris, 302(Série II), 711 - 716.

Poisson, A., & Robertson, A. H. F. (1990). Field excursion B1, Western Taurides. In IESCA, 6 . Izmir, Turkey:

Poole, A. J. (1992) Sedimentology, neotectonics and geomorphology related to tectonic uplift and sea-level change: Quaternary of Cyprus. Ph.D., Edinburgh.

Postma, G. (1984). Mass-flow conglomerates in a submarine canyon: Abrioja fan-delta, Pliocene, Southeast Spain. In E. H. Koster & R. J. Steel (Eds.), Sedimentoliogy of gravels and conglomerates (pp. 237-258). Calgary: Canadian Society of Petroleum Geologists.

Postma, G., & Roep, T. B. (1985). Resedimented conglomerates in the bottomsets of Gilbert-type gravel deltas. Journal of sedimentary Petrology, 55, 874-995.

Postma, G. (1990). Depositional architecture and facies of river and fan deltas: a synthesis. In A. Colella & D. B. Prior (Eds.), Coarse-Grained Deltas (pp. 13-28). Blackwells Scientific Publications.

Price, S. P., & Scott, B. (1991). Pliocene Burdur basin, southwest Turkey: tectonic seismicity and sedimentation. Journal of the Geological Society of London, 148, 345-355.

Price, S. P., & Scott, B. (1994). Fault-block rotations at the edge of a zone of continental extension; southwest Turkey. Journal of Structural Geoogy, 16(3), 381-392.

Quinn, T. M., Lohmann, K. C., & Halliday, A. N. (1991). Sr isotopic variation in shallow water carbonate sequences: stratigraphic, chronostratigraphic and eustatic implications of the record at Enewetak Atoll. Paleoceongraphy, 6, 371-385.

Richter, F. M., & DePaolo, D. J. (1988). Diagenesis and strontium isotope evolution of sea water using data from DSDP 590B and 575. Earth. Planet. Sci. Lett., 90, 382-394.

Richter, F. M., & Liang, Y. (1993). The rate and consequences of Sr diagenesis in deep-sea carbonates. Earth and Planetary Science Letters, 117, 553-565.

Ricou, L.-E., Argyriadis, I., & Lefevre, R. (1974). Proposition d'une origine interne pour les nappes d'Antalya et le massif d'Antalya (Taurides occidentales, Turquie). Bull. Soc. géol. Fr., 16, 107-111.

Ricou, L.-E., Argyriadis, I., & Marcoux, J. (1975). L'axe calcaire dy Taurus, un alignement de fenêtres arabo-africaines sous des nappes radiolaritiques, ophiolitiques et métamorphiques. Bull. Soc. géol. Fr., 17, 1024-1044.

Ricou, L.-E., Marcoux, J., & Poisson, A. (1979). L'allochtonie des Bey Daglari orientaux. Reconstruction palinspastique des Taurides occidentales. Bull. Soc. géol. France, 7(2), 125-133.

Ricou, L. E., Marcoux, J., & Whitechurch, H. (1984). The Mesozoic organisation of the Taurides: one or several oceanic basins. In J. E. Dixon & A. H. F. Robertson (Eds.), The Geological Evolution of the Eastern Mediterranean (pp. 349-359). Oxford: Spec. Publ. Geol. Soc. London.

Robertson, A. H. F., & Woodcock, N. H. (1979). Tectonic setting of the Troodos massif in the east Mediterranean. In A. Panayiotou (Eds.), Ophiolites (pp. 36-49). Ministry of Agriculture and Natural Resources, Geological Dept., Cyprus.

Robertson, A. H. F., & Woodcock, N. H. (1980). Strike-slip related sedimentation on the Antalya Complex, SW Turkey. In Spec. Publ. Int. Ass. Sediment. (pp. 127-145).

Robertson, A. H. F., & Woodcock, N. H. (1982). Sedimentary history of the south-western segment of the Mesozoic-Tertiary Antalya continental margin, south-western Turkey. Ecolgae Geol. Helv., 75, 517-562.

Robertson, A. H. F., & Dixon, J. E. (1984). Introduction: aspects of geological evolution of the Eastern Mediterranean. In J. E. Dixon & A. H. F. Robertson (Eds.), The Geological Evolution of the Eastern Mediterranean (pp. 1-74). Oxford: Blackwell Scientific publications.

Robertson, A. H. F., & Woodcock, N. H. (1984). The SW segment of the Antalya Complex, Turkey as a Mesozoic-Tertiary Tethyan continental margin. In J. Dixon E. & a. H. F. Robertson (Eds.), The Geological Evolution of the Eastern Mediterranean (pp. 251-271). Gel. Soc. London Spec. Publ.

Robertson, A. H. F., & Woodcock, N. H. (1986). The Geological evolution of the Kyrenia Range, a critical lineament in the Eastern Mediterranean. In

Robertson, A. H. F., & Woodcock, N. H. (1986). The role of the Kyrenia Range Lineament, Cyprus, in the Geological evolution of the Eastern Mediterranean. In J. Watson., H. G. Reading, & S. H. White (Eds.), Major crustal lineaments and their influence on the geological history of continental lithosphere (pp. 141-178). Proceedings of Royal Society Discussion Meeting, Royal Society London.

Robertson, A. H. F., Eaton, S., Follows, E. J., & McCallum, J. E. (1991a). The role of local tectonics versus global sea-level change in the Neogene evolution of the Cyprus active margin. Special Publication of the International Association of Sedimentologists., 12, 331 - 369.

Robertson, A. H. F., Clift, P. D., Degnan, P. J., & Jones, G. (1991b). Palaeogeographic and palaeotectonic evolution of the Eastern Mediterranean Neotethys. Palaeogeography, Palaeoclimatology, Palaeoecology, 87, 289 - 343.

Robertson, A. H. F. (1993). Mesozoic-Tertiary sedimentary and tectonic evolution of Neotethyan carbonate platforms, margins and small ocean basins in the Antalya Complex, of Southwest Turkey. In (pp. 415 - 465). Special Publication of the International Association of Sedimentologists.

Robertson, A. H. F., Eaton, S., Follows, E. J., & Payne, A. J. (in press). Depositional processes and basin analysis of Messinian evaporites in Cyprus. .

Robertson, A. H. F., & Grasso, M. (in press). Overview of the Late Tertiary tectonic and palaeo-environmental development of the Mediterranean region. Terra Nova.

Rodine, J. D., & Johnson, A. M. (1976). The ability of debris, heavily freighted with coarse clastic materials, to flow on gentle slopes. Sedimentology, 23, 213-234.

Rust, B. R. (1975). Fabric and structure in glaciofluvial gravels. In A. V. Jopling & B. C. McDonald (Eds.), Glaciofluvial and Glaciolacustrine Sedimentation (pp. 238-248). Society of Economic Paleontologists and Mineralogists Special Publication.

Rust, B. R. (1979). Facies models 2: Coarse alluvial deposits. In R. G. Walker (Eds.), Facies Models (pp. 9-23). Geoscience Canada Reprint.

Ryan, W. B. F., & Cita, M. B. (1977). Ignorance concerning episodes of ocean-wide stagnation. Marine Geology, 23, 197-215.

Sage, L., & Letouzey, J. (1990). Convergence of the African and Eurasian plates in the Eastern Mediterranean. In J. Letouzey (Eds.), Petroleum and tectonics in mobile belts (pp. 49-68). Ed. Technip Paris.

Samuel, M. A. (1994) The structural and stratigraphic evolution of islands at the active margin of the Sumatra forearc, Indonesia. Ph. D., University of London.

Scoffin, T. P. (1972). The fossilization of Bermuda patch reefs. Science, 178, 1280-1282.

Scoffin, T. P., & Stoddart, D. R. (1978). The nature and significance of microatolls. Philosophical Transactions of the Royal Society of London, B 284, 99-122.

Scoffin, T. P. (1987). An introduction to carbonate sediments and rocks. Glasgow: Blackie and Son Ltd.

Sengor, A. M. C., Yalçin, N., & Cantiez, N. (1980). The origin of the Adana/Cilicia basin. An incompatibility structure arising at the common termination of the East Anatolian and Dead Sea transform faults. In Sedimentary basins of Mediterranean margins, Abstract (pp. 45-46).

Sengor, A. M. C., & Yilmaz, Y. (1981). Tethyan evolution in Turkey: A plate tectonic approach. Tectonophysics, 75, 181 - 241.
Sengor, A. M. C. (1984). The Cimmeride orogenic system and the tectonics of Asia. Geol. Soc. Am., 195(Special Paper), 82 pp.
Sengor, A. M. C., Gorur, N., & Saroglu, F. (1985). Strike-slip faulting and relating basin formation in zones of tectonic escape: Turkey as a case in study. In K. T. Biddle & N. Christie-Blick (Eds.), Strike-slip deformation, basin formation and sedimentation. (pp. 227 - 264). Society of Ecconomic Palaeontologists and Mineralogists Special publication.
Steel, R. J., & Wilson (1975). Sedimentation and tectonism (?Permo-Triassic) on the margin of the North Minch Basin, Lewis. Journal of the Geological society, 183-200.
Steel, R., & Aasheim, S. M. (1978). Alluvial sand depostion in a rapidly subsiding basin (Devonian, Norway). In A. D. Miall (Eds.), Fluvial Sedimentology Calgary: Mem. Can. Soc. Petrol. Geol.
Stoddart, D. R., McLean, R. F., Scoffin, T. P., Thom, B. G., & Hopley, D. (1978). Evolution of reefs amd ioslands, northern Great Barrier Reef: synthesis and interpretaion. Philosophical Transactions of the Royal Society of London, B284, 149-159.
Stow, D. A. V., & Bowen, A. J. (1980). A physical model for the transport and sorting of fine-grained sediments by turbidity currents. Sedimentology, 27, 31-46.
Stow, D. A. V. (1984). Turbidite facies associations and sequences in the southeastern Angola Basin. In W. W. Hay, J. C. Sibuet, & e. al. (Eds.), Initial Reports Deep Sea Drilling Project (pp. 785-799). Washington: US Gouvernment Printing Office.
Tandon, S. K., & Narayan, D. (1981). Calcrete conglomerate, case-hardended conglomerate and cornstone - a comparative account of pedogenic and non-pedogenic carbonates from the continental Siwalik Group, Punjab, India. Sedimentology, 28, 353-367.
Taymaz, T., Jackson, J. A., & McKenzie, D. P. (1991). Active tectonics of the North and central Aegean Sea. Geophys. J. Int., 106, 433-490.
Taymaz, T., & Price, s. P. (1992). Burdur earthquake sequence: A synthesis of seismological and geological observations. Geophys. J. Int, 108, 589-603.
Tucker, M. E. (1981). Sedimentary Petrology An Introduction. Blackwell Scientific Publications.
Tunbridge, I. P. (1981). Sandy high-energy flood sedimentation - some criteria for recognition, with an example from the Devonian of S. W. England. Sedimentary Gology, 28, 79-95.
Turner, J. (1996). The subsidence of sedimentary basins. Ph.D., Edinburgh
Underhill, J. R. (1989). Late Cenozoic deformationof the Hellenic foreland, western Greece. Bull. Geol. Soc. Am., 101, 613-634
Ünlugenc, U. C., Kelling, G., & Demirkol, C. (1993). Aspects of basin evolution in the Neogene Adana basin, SE Turkey. International Earth Sciences Congress on the Aegean region.
Üstaömer, T. (1993) Paleotethyan evolution of the Central Pontides, Turkey. Ph.D., Edinburgh.
Üstaömer, T., & Robertson, A. H. F. (1994). Late Palaeozoic marginal basin and subduction-acretion: the Palaeotethyan Küre Complex, Cnetral Pontidies, northern Turkey. J. Geol. Soc., London, 151, 291-305.
Veizer, J., & Compston, W. (1974). Sr 87/Sr86 composition of seawater during the Phanerozoic. Geochim. Cosmochim. Acta, 38, 1461-1484.
Waldron, J. W. F. (1981) Mesozoic sedimentary and tectonic evolution of the northeast, Antalya Complex, Egirdir, S. W. Turkey. Ph.D., University of Edinburgh.
Waldron, J. W. F. (1984a). Structural history of the Antalya Complex in the 'Isparta Angle', southwest Turkey. In J. E. Dixon & A. H. F. Robertson (Eds.), The geological evolution of the Eastern Mediterranean Geological Society of London.
Waldron, J. W. F. (1984b). Evolution of carbonate platforms on a margin of the Neotethys ocean: Isparta angle, southwestern Turkey. Ecolgae Geol. Helv., 77, 553-582.
Waldron, J. W. F. (1984). Structural history of the Antalya Complex in the 'Isparta Angle', southwest Turkey. In J. E. Dixon & A. H. F. Robertson (Eds.), The geological evolution of the Eastern Mediterranean, Geological Society of London Sp. Publ.
Walker, R. G. (1965). The origin and significance of the internal sedimentary structures of turbidites. Proc. Yorkshire Geol. Soc., 35, 1-32.
Walker, R. G. (1975). Generalized facies models for resedimented conglomerates of turbidite association. Geological Society of America Bulletin, 86, 737-748.
Walker, R. G. (1984). Preface. In E. H. Koster & R. J. Stell (Eds.), Sedimentology of gravels and conglomerates Calgary: Canadian Society of Petroleum Geologists.
Walton, E. K. (1967). The sequence of internal structures in turbidites. Scottish J. Geology, 3, 306-317.
Wells, J. W. (1954). Recent corals of the Marshall Islands. United States Geological Survey Professional Papers, 260(I), 385-486.

Wescott, W. A., & Ethridge, F. A. (1980). Fan-delta sedimentology and tectonic settings - Yallahs Fan-delta. Bulletin of the American Association of Petroleum Geologists, 64, 374-399.
Wickman, F. W. (1948). Isotope ratios - A clue to the age of certain marine sediments. Journal of Geology, 56, 61-66.
Williams, G. D., Unlugenç, U. C., Kelling, G., & Demirkol, C. (1993). Structural controls on stratigraphic evolution of the Adana basin, Turkey.
Wilson, J. W. (1993) The origin and tectono-stratigraphic evolution of the Meso-Hellenic Trough, northern Greece and Albania. Ph.D., Edinburgh University.
Winn, R. D., Jr., & Dott, R. H., Jr. (1977). Large scale traction-produced structures in deep-water fan-channel conglomerates in southern Chile. Geology, 5, 41-44.
Woodcock, N. H., & Robertson, A. H. F. (1977a). Origins of some ophiolite-related metamorphic rocks of the 'Tethyan' belt. Geology, 3, 373-376.
Woodcock, N. H., & Robertson, A. H. F. (1977b). Imbricate thrust belt tectonics and sedimentation as a guide to emplacement of part of the Antlaya Complex, S. W. Turkey. In E. Izdar & E. Nakoman (Ed.), Sixth Coloquium on the Geology of the Aegean Region, no 2 (pp. 661-670). International Contribution Series, Publ.
Woodcock, N. H., & Robertson, A. H. F. (1981). Wrench-related thrusting along a Mesozoic-Cenozoic continetnal margin, Antlay Complex, S. W. Turkey. In K. R. McClay & N. J. Price (Eds.), Thrust and nappe tectonics (pp. 359-362). Geol. Soc. London. Special. Publ.
Woodcock, N. H., & Robertson, A. H. F. (1981b). Imbricate thrusting and wrench tectonics in the Antalya Complex, S. W. Turkey. Journal Geol. Soc., London.
Woodcock, N. H., & Robertson, A. H. F. (1982). Wrench and thrust tectonics along a Mesozoic-Cenozoic continental margin: Antalya Complex, SW Turkey. Journal of the Geological Society of London, 139, 147-163.
Woodside, J., & Ivanov, M. (1992). Geological and geophysical investigations in the Mediterranean and Black Seas. Unesco reports in marine science, 56.
Zanchi, A., Kissel, C., & Tapirdamaz, C. (1993). Late Cenozoic and Quaternary brittle continental deformation in western Turkey. Bull. Soc. géol France, 164(4), 507-517.

APPENDIX 1
XRD analysis on coral samples from the Köprü and Manavgat basins

XRD no	sample no	area	% Aragonite	Low Mg Calcite	High Mg Calcite	Quartz
RA1	27j.Yes.5	Yesilbag		yes		yes
RA2	10j.Alar.3	Alarahan		yes		
RA3	26j.399.3	Kesme		yes		
RA4	14J.144.3b	Beskonak	50-55	yes		
RA5	16J.168.1/2	Balibucak	65	yes		
RA6	26J.217.4c	Karapinar		yes		yes
RA7	26J.217.4a	Karapinar	55	yes		yes
RA8	22M.406.2	Dumanli	90	yes		yes

APPENDIX 2
Strontium dating table (see chapter 6)

Section name	Sample no	Fossil type	weight (g)	barrel no	2(S.D.)	Dynamic 86/87	norm Miller	Errors Miller	25.1-14.7 Miller	14.6-8.3 Miller	norm Hodell	Errors Hodell	Hodell 5th polynomial
Alarahan	4j.Alarahan.1	coral	0.01961	4	26	0.708357	0.708372	9.20884E-06	22.433		0.708355	9.20862E-06	20.886
	4j.Alarahan.2	porites	0.05552	3	26	0.70835	0.708365	9.20875E-06	22.550		0.708348	9.20852E-06	21.011
	4j.Alarahan.3	porites	0.20565	2	24	0.7083648	0.7083798	8.50056E-06	22.302		0.7083628	8.50035E-06	20.751
	4j.Alarahan.4	coral	0.10258	3	24	0.7086134	0.7086284	8.50354E-06	18.131		0.7086114	8.50334E-06	17.587
	10j. Alarahan.5	*Operculina*	0.00558	4	22	0.7085766	0.7085916	7.79451E-06	18.748		0.7085746	7.79432E-06	18.028
	8O.Alarahan.1	forams	0.00948	3	26	0.7087022	0.7087172	9.21332E-06	16.641		0.7087002	9.2131E-06	16.457
	8O. Alarahan.2	forams	0.00395	4	22	0.7087106	0.7087256	7.79598E-06	16.500		0.7087086	7.79579E-06	16.347
	8O. Alarahan.3	forams	0.00425	4	22	0.708767	0.708782	7.7966E-06	15.554		0.708765	7.79642E-06	15.281
Ahmetler	12j.Ahmetler.1	algae	0.01016	3	26	0.708736	0.708751	9.21376E-06	16.074		0.708734	9.21354E-06	15.911
	16S.313.6	algae	0.01401	2	26	0.708662	0.708677	9.2128E-06	17.315		0.70866	9.21258E-06	16.991
	12j.Ahmetler.2	algae	0.00581	4	22	0.708728	0.708743	7.79617E-06	16.208		0.708726	7.79599E-06	16.052
	16S.313.7	algae	0.00343	3	26	0.708688	0.708703	9.21314E-06	16.879		0.708686	9.21292E-06	16.654
	16S.341.6	forams	0.02622	4	26	0.708726	0.708741	9.21363E-06	16.242		0.708724	9.21341E-06	16.087
Yaylaalan	14j.290.2	echinoid	0.00680	3	24	0.708661	0.708676	8.50411E-06	17.332		0.708659	8.50391E-06	17.004
	14j.290.5	algae	0.00626	4	22	0.7087287	0.7087437	7.79618E-06	16.196		0.7087267	7.79599E-06	16.040
	14j.290.6	forams	0.00316	2	24	0.708803	0.708818	8.50582E-06	14.950		0.708801	8.50561E-06	13.555
	14j.290.7	forams	0.00353	4	22	0.708794	0.708809	7.7969E-06	15.101		0.708792	7.79671E-06	14.366
Oymapinar	13j.Oymapinar.4	echinoid	0.02398	3	22	0.708702	0.708717	7.79589E-06	16.644		0.7087	7.7957E-06	16.464
	13j.Oymapinar.7	forams	0.00437	2	22	0.70877	0.708785	7.79664E-06	15.504		0.708768	7.79645E-06	15.208
	13j.Oymapinar.8	forams	0.00329	3	24	0.7087735	0.7087885	8.50546E-06	15.445		0.7087715	8.50526E-06	15.108
Saburlar	11j.295-6.1	*Operculina*	0.00849	2	26	0.708536	0.708551	9.21116E-06	19.429		0.708534	9.21094E-06	18.477
	11j.295-6.2	algae	0.00859	2	32	0.708568	0.708583	1.13373E-05	18.893		0.708566	1.13371E-05	18.114
	11j.295-6.3	porites	0.01830	2	26	0.708551	0.708566	9.21136E-06	19.178		0.708549	9.21114E-06	18.302
	30A.296.3	forams	0.00240	2	28	0.708568	0.708583	9.92016E-06	18.893		0.708566	9.91992E-06	18.114
Deniztepesi	25S.373.6	algae	0.00283	2	22	0.708621	0.708636	7.795E-06	18.003		0.708619	7.79481E-06	17.495
	25S.373.3	oyster	0.01165	1	FAILED	FAILED						0	
	16J.373.2	forams	0.00391	3	30	0.708721	0.708736	1.0631E-05	16.326		0.708719	1.06308E-05	16.175
	16j.373.1	forams	0.00391	4	24	0.708695	0.70871	8.50452E-06	16.762		0.708693	8.50432E-06	16.559
Bucakköyü	17J.416.6	forams	0.00259	3	26	0.708631	0.708646	9.2124E-06	17.836		0.708629	9.21218E-06	17.377
	18j.417.4	algae	0.00565	1	24	0.708529	0.708544	8.50253E-06	19.547		0.708527	8.50232E-06	18.556
	18j.417.2	algae	0.07234	3	22	0.708601	0.708616	7.79478E-06	18.339		0.708599	7.79459E-06	17.732
	18J.417.5	forams	0.00092	1	FAILED	FAILED						0	

Section name	Sample no	Fossil type	weight (g)	barrel no	2(S.D.)	Dynamic 86/87	norm Miller	Errors Miller	25.1-14.7	14.6-8.3	norm Hodell	Errors Hodell	Hodell 5th
	18J.417.6	forams	0.00106	2	FAILED	FAILED					0.710263	0	
Aspendos	17j.415.1	echinoid	0.08422	1	22	0.708667	0.708682	7.7955E-06	17.232		0.708665	7.79532E-06	16.926
	17j.415.2	shell	0.01861	1	24	0.708654	0.708669	8.50403E-06	17.450		0.708652	8.50382E-06	17.094
	17j.415.3a-c	gastropod	0.09450	2	24	0.708671	0.708686	8.50423E-06	17.165		0.708669	8.50403E-06	16.887
	17j.415.4	forams	0.00318	1	40	0.708753	0.708768	1.41754E-05	15.789		708753	14.17506	15.572
Altinkaya	19J.181.2	oyster	0.10750	2	FAILED	FAILED (Rb)						0	
	19J.181,1a	oyster	0.01786	1	26	0.708723	0.708738	9.21359E-06	16.292		0.708721	9.21337E-06	16.140
	19J.180.2	algae	0.03721	2	24	0.708581	0.708596	8.50315E-06	18.674		0.708579	8.50295E-06	17.970
Ballibucak	16J.163.3	algae	0.01355	1	22	0.708657	0.708672	7.79539E-06	17.399		0.786568	8.65225E-06	17.043
	16J.164.2	oyster	0.00510	1	64	0.7087172	0.7087322	2.26794E-05	16.389		0.7087152	2.26789E-05	16.241
Kesme	26j.399.1b	oyster	0.08408	1	24	0.709015	0.70903	8.50836E-06			0.709013	8.50816E-06	9.978
Yesilbag	27j.Yesil.3	algae	0.04427	1	22	0.708742	0.708757	7.79633E-06	15.973		0.70874	7.79614E-06	15.806
	27j.Yesil.9	oyster	0.02301	2	24	0.708721	0.708736	8.50483E-06	16.326		0.708719	8.50463E-06	16.175
Dumanli	22m.407.1	forams	0.00170	1	FAILED	FAILED						0	
	22m.404.3	oyster	0.29865	1	64	0.708735	0.70875	0.00002268	16.091		0.708733	2.26795E-05	15.930
Cetmi	20j.421.1	algae	0.00600	2	FAILED	FAILED						0	
Kargi baraj	15M.1	oyster	0.03302	3	26	0.708727	0.708742	9.21365E-06	16.225		0.708725	9.21343E-06	16.069
	15M.3	oyster	0.03535	4	20	0.708848	0.708863	7.08863E-06		13.104	0.708846	7.08846E-06	11.163
	15M.5	oyster	0.00879	4	24	0.708722	0.708737	8.50484E-06	16.309		0.70872	8.50464E-06	16.157
Sipahiler	30J.236.8	algae	0.00413	4	24	0.708881	0.708896	8.50675E-06		10.487	0.708879	8.50655E-06	10.794
	Standard NBS987			1	26			9.23315E-06					
	Standard NBS987			1	24			8.52262E-06					
	Standard NBS987			1	24			8.52295E-06					
	Standard NBS987			1	28			9.94388E-06					
	Standard NBS987			3	26			9.2333E-06					
	Standard NBS987			3	30			1.06536E-05					
	Standard NBS987			4	28			9.94353E-06					
	Standard NBS987			4	24			8.52294E-06					
	mean of all 987	0.710237											
	2SD	0.000026											
	mean of my 987	0.710239											
	2SD	0.00003											
	E & A			2	24			8.49593E-06					
	E & A			2	26			9.20416E-06					

APPENDIX 3.A.1
Nannoplankton from the Ahmetler Section samples, Manavgat basin

Sample number	NN number	Age	Species present	Abundance
16S.341.2	NN4	Upper Burdigalian	*Helicosphaera carteri*	abundant
16S.341.3	NN4	Upper Burdigalian	*Helicosphaera ampliaperta*	abundant
16S.341.5	NN4	Upper Burdigalian	*Reticulofenestra pseudoumbilica*	abundant
16S.341.6	NN4	Upper Burdigalian	*Sphenolithus abies*	abundant
			Sphenolithus heteromophus	abundant
			Coccolithus pelagicus	abundant
			Cyclicargolithus floridanus	abundant
			Discoaster deflandrei	abundant
17S.343.1	NN5	Langhian	*Cyclicargolithus abisectus*	common
17S.343.2	NN5	Langhian	*Cyclicargolithus floridanus*	common
17S.343.3	NN5	Langhian	*Sphenolithus abies*	common
17S.343.4	NN5	Langhian	*Sphenolithus heteromophus*	common
17S.343.5	NN5	Langhian	*Helicosphaera carteri*	common
17S.343.6	NN5	Langhian	*Helicosphaera perch-nielseniae*	common
17S.343.8	NN5	Langhian	*Reticulofenestra pseudoumbilica*	common
17S.343.9	NN5	Langhian	*Micrantholithus vesper*	common
17S.343.10	NN5	Langhian	*Coccolithus pelagicus*	common
17S.343.12	NN5	Langhian	*Cyclicargolithus cf. macintyrei*	common
17S.343.13	NN5	Langhian	*Discoaster deflandrei*	common
17S.343.14	NN5	Langhian		
17S.343.15	NN5	Langhian		
17S.343.16	NN5	Langhian		
17S.343.19	NN5	Langhian		
17S.316.1	NN5	Langhian		
17S.316.2	NN6	Serravallian	*Cyclicargolithus floridanus*	abundant
17S.316.3	NN6	Serravallian	*Cyclicargolithus rotula*	abundant
17S.316.4	NN6	Serravallian	*Rhabdosphaera stylifer*	abundant
17S.316.5	NN6	Serravallian	*Helicosphaera carteri*	abundant
17S.316.6	NN6	Serravallian	*Reticulofenestra pseudoumbilica*	abundant
17S.316.8	NN6	Serravallian	*Coccolithus miopelagicus*	abundant
17S.316.9	NN6	Serravallian	*Discoaster deflandrei*	abundant
17S.316.11	NN6	Serravallian	*Discoaster exilis*	abundant
17S.316.12	NN6	Serravallian		
17S.316.13	NN6	Serravallian		
18S.344.1		Middle Miocene	*Nannoplancton markers absent*	
18S.344.2		Middle Miocene	*Nannoplancton markers absent*	
18S.344.3		Middle Miocene	*Nannoplancton markers absent*	

Sample number	NN number	Age	Species present	Abundance
18S.344.5		Middle Miocene	*Nannoplancton markers absent*	
18S.344.6		Middle Miocene	*Nannoplancton markers absent*	
18S.344.7		Middle Miocene	*Nannoplancton markers absent*	
18S.308.2		Middle Miocene	*Nannoplancton markers absent*	
18S.308.4	NN9	Tortonian	*Discoaster hamatus*	common
18S.327.1	NN9	Tortonian		
18S.327.2	NN9	Tortonian		
19S.328.1	NN11a	Tortonian	*Discoaster quinqueramus*	common
19S.328.3	NN11a	Tortonian	*Discoaster pentaridiatus*	common
19S.328.4	NN11a	Tortonian		
19S.328.5	NN11a	Tortonian		
19S.328.6	NN11a	Tortonian		
19S.329.1	NN11a	Tortonian		
19S.329.2	NN11a	Tortonian		
19S.329.3	NN11a	Tortonian		
19S.329.4	NN11b	Messinian	*Discoaster quinqueramus*	less
19S.330.1	NN11b	Messinian	*Triquetrorhabdulus rugosus*	less
19S.330.2	NN11b	Messinian	*Ceratolithus acutus*	less
19S.345.1	NN11b	Messinian		

APPENDIX 3.A.2

Nannoplankton from the Aksu, Köprü and Manavgat basins (with the exception of the Ahmetler section). See Appendix 5.2 for stratigraphic logs.

Name of section	Locality	Basin/area	Sample number	NN number	Age	Species present	Abundance
Kargi baraj	Karagi baraj	Central Aksu	24J.384.1				no fauna
Kargi baraj	Karagi baraj	Central Aksu	24J.384.2	NN11-12	Messinian-Lower Pliocene	*Amaurolithus delicatus*	common
						Sphenolithus abies	common
						Sphenolithus heteromophus	common
Aspendos	Aspendos	South Köprü	17j.415.4		Serravallian	*Cyclococcolithus miopelagicus*	rare
Aspendos	Aspendos	South Köprü	17j.415.5		Serravallian	*Helicosphaera carteri*	very rare
Aspendos	Aspendos	South Köprü	17j.415.6		Serravallian	*Discoaster exilis*	
						Cyclicargolithus macintyrei	
Aspendos	Aspendos	South Köprü	17j.415.1	?	?		very rare
373 Deniztepesi	Deniztepesi	South Köprü	16J.373.2	NN5	Langhian	*Sphenolithus heteromophus*	common
						Helicosphaera carteri	common
						Cyclococcolithus abisectus	common
373 Deniztepesi	Deniztepesi	South Köprü	16J.373.1	NN5	Langhian	*Sphenolithus heteromophus*	common
						Helicosphaera carteri	common
						Cyclococcolithus abisectus	common
373 Deniztepesi	Deniztepesi	South Köprü	25S.373.1	NN5	Langhian	*Sphenolithus heteromophus*	

Name of section	Locality	Basin/area	Sample number	NN number	Age	Species present	Abundance
Bucakköyü B	Bucakköyü	South Köprü	18j.417.5		Serravallian	*Discoaster exilis* *Cyclococcolithus abisectus*	rare
Bucakköyü B	Bucakköyü	South Köprü	18j.417.6		Serravallian	*Cyclococcolithus miopelagicus*	rare
180 Altinkaya	Altinkaya	South Köprü	19J.181.1	?	?		very rare
180 Altinkaya	Altinkaya	South Köprü	19J.180.1	?	?		very rare
163 and 164 Ballibucak	Ballibucak	Central Köprü	16J.164.3	NN5?	Langhian?	*Sphenolithus heteromophus*	very rare
236B Sipahiler	Sipahiler	North Köprü	30J.236.4				No fauna
236B Sipahiler	Sipahiler	North Köprü	30J.236.2				No fauna
236B Sipahiler	Sipahiler	North Köprü	30J.236.3	?	?		very rare
Dumanli	Dumanli	North Köprü	22M.407.2		Middle Miocene, Serravallian?		
		North Köprü	22M.407.1		Middle Miocene, Serravallian?		
Yaylaalan	Yaylaalan	North Manavgat	14j.290.5		Serravallian		
Yaylaalan	Yaylaalan	North Manavgat	14j.290.6	NN6-7	Serravallian	*Cyclicargolithus macintyrei*	common
						Discoaster exilis	common
						Reticulofenestra pseudoumbilica	common
Yaylaalan	Yaylaalan	North Manavgat	14j.290.7		Serravallian		
Saburlar	Saburlar	South Manavgat	30A.296.3				

Name of section	Locality	Basin/area	Sample number	NN number	Age	Species present	Abundance
Alarahan	Alarahan	South Manavgat	80. Alarahan. 1	NN4	Burdigalian	*Helicosphaera ampliaperta*	common
						Sphenolithus heteromophus	common
Alarahan	Alarahan	South Manavgat	80. Alarahan. 2	NN4	Burdigalian	*Helicosphaera ampliaperta*	common
						Sphenolithus heteromophus	common
Alarahan	Alarahan	South Manavgat	80. Alarahan. 3	NN6?	Serravallian	*Cyclicargolithus macintyrei*	common

APPENDIX 3.B
Counts of benthic and planktic foraminifer from the Ahmetler section, Manavgat basin

Sample	Planktic no	Planktic %	Benthic no	Benthic %	Total	P/B ratio
16S.314.6	206	94.46	12	5.54	218	17.17
16S.341.3	256	93.09	19	6.91	275	13.47
16S.341.5	376	89.74	43	10.26	419	8.74
16S.341.6	206	94.50	12	5.50	218	17.17
16S.342.1	590	92.48	48	7.52	638	12.29
17S.343.1	326	92.09	28	7.91	354	11.64
17S.343.4	300	99.34	2	0.66	302	150.00
17S.343.6	335	94.63	19	5.37	354	17.63
17S.343.8	234	98.73	3	1.27	237	78.00
17S.343.10	385	98.97	4	1.03	389	96.25
17S.343.13	382	86.04	62	13.96	444	6.16
17S.343.14	317	95.48	15	4.52	332	21.13
17S.343.15	294	96.71	10	3.29	304	29.40
17S.343.16	303	94.69	17	5.31	320	17.82
17S.316.2	273	89.51	32	10.49	305	8.53
17S.316.3	310	92.81	24	7.19	334	12.92
17S.316.4	300	87.21	44	12.79	344	6.82
17S.316.11a	393	91.82	35	8.18	428	11.23
17S.316.12	310	91.99	27	8.01	337	11.48
17S.316.13	325	90.53	34	9.74	359	9.56
18S.344.1	297	79.62	76	20.38	373	3.91
18S.344.3	288	93.20	21	6.80	309	13.71
18S.344.7	303	86.32	48	13.68	351	6.31
18S.308.2	247	78.41	68	21.59	315	3.63
18S.308.3	297	90.27	32	9.73	329	9.28
18S.327.2	206	69.36	91	30.64	297	2.26
19S.328.1	268	82.21	58	17.79	326	4.62
19S.328.5	306	89.47	36	10.53	342	8.50
19S.328.6	226	77.13	67	22.87	293	3.37
19S.329.1	234	75.00	78	25.00	312	3.00
19S.329.2	233	77.93	66	22.07	299	3.53
19S.329.4	240	78.69	65	21.31	305	3.69
19S.330.1	198	81.15	46	18.85	244	4.30
19S.330.2	198	66.22	101	33.78	299	1.96
19S.345.1	71	78.89	19	21.11	90	3.74
19S.346.1	235	77.56	68	22.44	303	3.46
19S.347.1	183	79.91	46	20.09	229	3.98
19S.348.1	215	68.47	99	31.53	314	2.17

APPENDIX 3.C
Coral identification

Locality	Sample number	Coral	Age range
Gökçepinar	26J.217.4a	*Heliastrea oligophylla*	Early-Mid Miocene
Gökçepinar	26&.217.4b	*Favites neglecta*	Aquitanian-Tortonian
Gökçepinar	26J.217.4c	*Favites neglecta*	Aquitanian-Tortonian
Gökçepinar	26J.217.4d	*Tarbellastrea carryensis/ellisiana*	Aquitanian-Burdigalian
Gökçepinar	26J. 217.4f	*Caulastria matheroni*	Aquitanian-Burdigalian
Beskonak	14J.144.3a	*Heliastrea (aatiguacensis?)*	Mid-Vindobonian
Beskonak	14J.144.3b	*Porites (collegiana?)*	Aquitanian
Ballibucak	16J.168.2/1	*Stylophora reussiana*	Middle Miocene
Aspendos	26S.335.1	*Tarbellastrea ellisiana*	Aquitanian-Burdigalian
Aspendos	23S.332.2b	*Tarbellastrea caryensis*	Aquitanian-Burdigalian
Aspendos	23S.332.6	*Porites (collegiana?)*	Aquitanian
Aspendos		*Favites neglecta*	Aquitanian-Tortonian

APPENDIX 4.A.1
Conglomerate analyses from the Kizildag Formation in the Manavgat basin

Clast type	Akbas 310	Akdam 94	Alarahan 94	Guneyci k 304	Guneyci k 94	Kepezbelenli	Yaylaalan 94a	Yaylaalan 94b	Yaylaalan 94c	Alanya 310	Yaylaalan 289	Yaylaalan 287	Kizildag 284	Guneyci k 304	Alarahan a	Alarahan b	Alarahan c	Alarahan d	Saburlar 295	Saburlar 94
Grey limestone							6		39	13				48						
Chert	4	6	7	13	15	14	40	19	28	4	11	11	5	13	61	16	9	1		
Calcarenite	1		38		35	35			20	1	7	1							16	17
Brown silt and sandstone	16			13						16			21		19	21	49	7	3	
Grit																				
Igneous		1			1		10	13	10		20	29							14	53
Mud																				
Algal lms																				
Oolitic lms									2								2			
Nummulitic lms																				
Dark grey lms	55	60	50		31		14	2			14	11	40							
Green silt						3														
Brown breccia														15	4	4		26	53	16
Fawn lms	10			15			3	2		10										
White vien lms				11						4	70			11						
Lms congl									1			3								
Siderite silt																			1	
Carbonate sand												13								
Nummulitic e																				
Fawn lithified silt																				
silt					2		9													
White	4	4	8		29		49	57	48											
yellow silt								11												
carbonate silt	8			13						8			6	13	3	6				
diagenetic chert				12	2	16			10			4		12		2	1			
microfossil-rich lms									12			10								7
fawn calcarenite																				
yellow sandstone												10								
red limestone	3	20			1	14			1											
Sandstone					8	12			3											

Clast type	Akbas 310	Akdam 94	Alarahan 94	Guneyci k 304	Guneyci k 94	Kepezbelenli	Yaylaalan 94a	Yaylaalan 94b	Yaylaalan 94c	Alanya 310	Yaylaalan 289	Yaylaalan 287	Kizildag 284	Guneyci k 304	Alarahan a	Alarahan b	Alarahan c	Alarahan d	Saburlar 295	Saburlar 94
Gastropod												2	1							
pink calcarenite							3	4												
red quartzite																				
mustard sst																				
Phyllite		2															2			
Orange silt																				
red silt																				
red felsite																				
schist		12						1												
calcite			2																	
Granodiorite																				
Alanya Massif	13			48	5	22				58					55	65	50	81		
limestone																	5			
Mustard carbonate													51							
Light grey limestone												1							5	
coraline lms												3							4	
coral																				

APPENDIX 4.A.2
Conglomerate analyses from the Kizildag Formation and the Aksu Formation in the Köprü basin

	Aspendos 94	Bozbarun 94	Bucakkoyu 94	Deniztepesi 374	Deniztepesi 368	Dumanli channel a	Dumanli channel b	Dumanli reef	Kasimlar a	Kasimlar b	Kasimlar c	Kasimlar d	Kasimlar e	Tasagil 334	Yesilbaga
Grey limestone	8	0	0	44	0	38	27	31	22	34	32	36	36	36	31
Chert	16	15	6	30	3	4	1	0	9	12	12	8	12	12	8
Calcarenite	7	9	10	0	0	9	10	13	7	2	2	14	11	11	19
Brown silt and sandstone	0	0	0	0	0	0	0	0	0	0	0	0	15	15	12
Grit	0	0	0	2	2	0	0	0	0	0	0	0	0	0	0
Igneous	8	3	1	7	10	3	15	0	0	0	6	8	3	3	4
Mud	0	0	0	0	0	0	0	0	0	0	0	0	0	0	0
Algal lms	0	0	0	0	0	0	0	3	0	0	0	0	0	0	0
Oolitic lms	0	0	0	0	0	11	0	0	0	0	5	0	1	1	0
Nummulitic lms	0	0	3	0	0	0	0	0	0	0	0	0	0	0	0
Dark grey lms	4	5	13	0	0	0	16	6	15	8	17	1	5	5	2
Green silt	0	0	0	0	0	2	0	0	1	0	8	0	0	0	1
Brown breccia	0	0	0	0	0	0	0	0	0	0	0	0	0	0	0
Fawn lms	16	23	0	0	0	0	0	0	0	0	0	0	0	0	0
White vien lms	0	0	0	0	0	0	0	0	0	0	0	0	0	0	0
Lms congl	0	0	0	0	7	0	0	0	0	0	2	0	1	1	0
Siderite silt	0	0	0	0	0	0	0	0	0	0	0	0	0	0	0
Carbonate sand	0	0	0	0	0	0	0	0	0	0	0	0	0	0	0
Nummulitic e	7	0	0	0	0	0	0	0	0	0	0	0	0	0	0
Fawn lithified silt	0	0	0	0	0	0	0	0	0	0	0	0	0	0	0
silt	0	0	0	0	0	0	1	3	0	0	0	0	0	0	1
White limestone	31	24	21	0	34	18	9	40	7	8	8	8	9	9	11
Yellow silt	1	0	0	0	0	0	0	0	0	0	0	0	0	0	0
carbonate silt	0	0	0	0	0	0	0	0	0	0	0	0	0	0	0
diagenetic chert	0	17	13	12	30	0	0	0	2	8	0	3	0	0	3
microfossil-rich lms	0	0	25	0	0	0	14	0	0	0	0	0	0	0	0

	Aspendos 94	Bozbarun 94	Bucakkoyu 94	Deniztepesi 374	Deniztepesi 368	Dumanli channel a	Dumanli channel b	Dumanli reef	Kasimlar a	Kasimlar b	Kasimlar c	Kasimlar d	Kasimlar e	Tasagil 334	Yesilbaga
fawn calcarenite	0	0	0	0	0	0	0	0	0	0	0	0	0	0	0
yellow sandstone	0	0	0	0	0	0	0	0	0	26	7	8	0	0	0
red limestone	0	0	0	0	0	0	0	4	0	2	0	0	0	0	1
Sandstone	0	2	3	5	14	12	5	0	0	0	0	0	0	0	0
Dark grey sst	2	0	5	0	0	0	0	0	12	0	0	12	0	0	0
Gastropod	0	0	0	0	0	0	0	0	0	0	0	0	0	0	0
pink calcarenite	0	0	0	0	0	0	0	0	0	0	0	0	0	0	0
red quartzite	0	0	0	0	0	0	0	0	4	0	2	0	0	0	0
mustard sst	0	0	0	0	0	0	0	0	20	0	0	0	0	0	0
Phyllite	0	0	0	0	0	0	0	0	1	0	0	1	3	3	6
Orange silt	0	0	0	0	0	1	3	0	1	0	0	1	3	3	0
red silt	0	0	0	0	0	4	0			0	0	1	0	0	0
red felsite	0	0	0	0	0	0	0			0	0	1	1	1	0
schist	0	0	0	0	0	1	0								

APPENDIX 4.B.1
Typical values of point couted marls from the Manavgat and Köprü basins

sample	locality	carbonate	composite grains	quartz	organics	mica	heavy minerals	planktic forams	benthic forams	shell fragments	spicules	TOTAL
20S.348.3	Ahmetler	274	0	76	42	4	0	1	3	0	0	400
16S.341.3	Ahmetler	534	0	0	36	0	0	23	7	0	0	600
16S.341.6	Ahmetler	371	0	0	19	0	0	9	1	0	0	400
17S.343.8	Ahmetler	350	0	0	20	0	0	25	5	0	0	400
17S.343.14	Ahmetler	274	0	0	13	0	0	12	1	0	0	300
17S.316.2	Ahmetler	390	0	0	3	0	0	5	2	0	0	400
17S.316.13	Ahmetler	363	0	2	19	0	0	14	2	0	0	400
18S.344.1	Ahmetler	266	0	2	5	0	0	20	7	0	0	300
18S.344.3	Ahmetler	788	0	2	14	0	0	84	12	0	0	900
18S.344.7	Ahmetler	212	0	6	10	1	0	65	7	0	0	300
19S.348.1	Ahmetler	254	0	17	24	0	1	4	0	0	0	300
19S.328.5	Ahmetler	278	0	5	12	0	1	4	0	0	0	300
19S.329.1	Ahmetler	290	0	3	2	0	2	2	1	0	0	300
26J.217.1	Karapinar	241	0	59	18	0	2	0	0	0	0	79
26J.217.2	Karapinar	240	0	14	31	0	0	3	0	1	0	49
26J.217.9	Karapinar	139	169	20	0	2	0	0	1	2	1	195
26J.217.11	Karapinar	230	0	39	34	0	1	0	2	1	0	77

APPENDIX 4.B.2

Typical point counts from the Karpuzçay Formation sandstones of the Köprü, Aksu and Manavgat basins

Sample	1S.301.2	1S.301.3	17S.343.11	17S.343.18	18J.174.2	18J.174.3	22A.255.3	22A.255.1 (%)	22A.257.1 (%)
quartz	2.5	4.5	5	0	128	42	25	8.2	31.4
carbonate	29.6	31.5	55	62	64	98	91	41.1	22.4
mica	0	0	0	0	5	4	0	0.3	0.9
organic	10	8.1	18	4	24	17	27	3.2	5.1
chert	4.5	0.4	0	0	7	48	6	8.2	5.1
pyroxene	0	0	0	0	0	0	0	0	0
sutured qz	0	0	1	0	48	10	0	3.2	11.8
micrite	25.4	23.8	171	138	36	67	94	28.9	11.8
opaque	0	0	0	5	4	3	3	0.3	0.9
plagioclase	0	0	0	0	3	1	1	0.3	0.6
feldspar	0	0	0	0	3	1	0	0	0.9
chlorite	0	0	0	0	3	3	0	0	0
igneous	0.3	4	6	1	0	0	8	4.9	8.3
shell frags	9.6	4.9	7	10	0	6	49	0.9	0.3
Planktic foraminifera	11.2	15.7	33	5					
Benthic foraminifera	3.2	6.3	19	26					
corals			0	1					
bivalve			1	1					
algae	3.2	0.4	69	64					
brachiopods			8	6					
echinoid spines			2	0					
Total count	310	304	395	318	325	300	304	99.5	99.5

APPENDIX 5.1

Akseki Road Section

Key

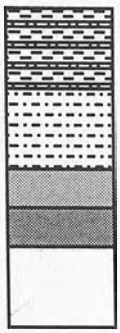

Marl

Siltstone

Sandstone

Conglomerate

Lithology also denodes grain size

Sample numbers are coded in the following way:

Date (i.e. 25S = 25th September) . Site number (i.e. 348) . Sample number (i.e. 2)

25S.348.2

The section was logged from bottom to top and the dates therefore follow this trend.

Samples are refered to extensively in Chapter 4 and 6 and in Appendix 2.

Top of log

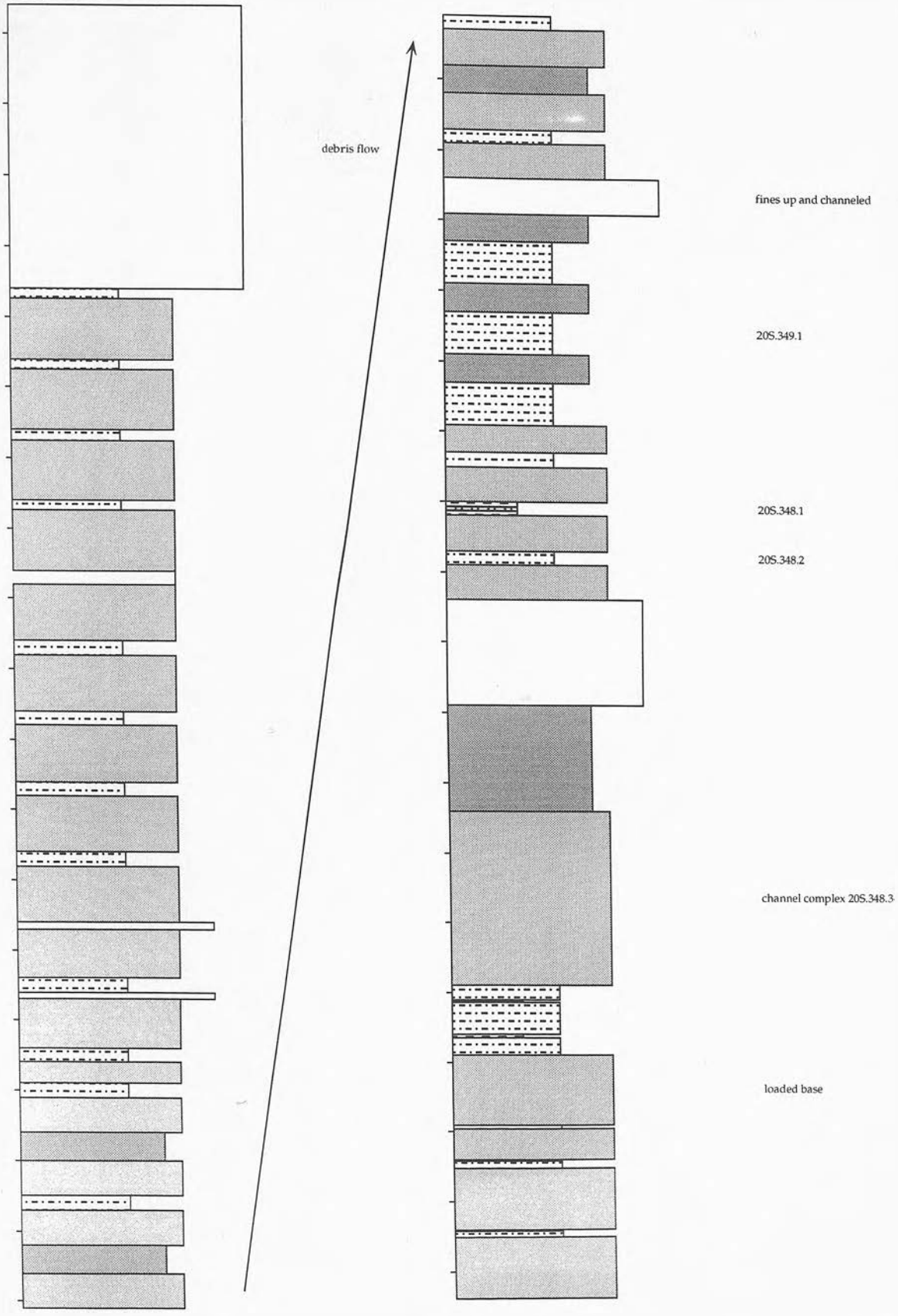
debris flow
fines up and channeled
20S.349.1
20S.348.1
20S.348.2
channel complex 20S.348.3
loaded base

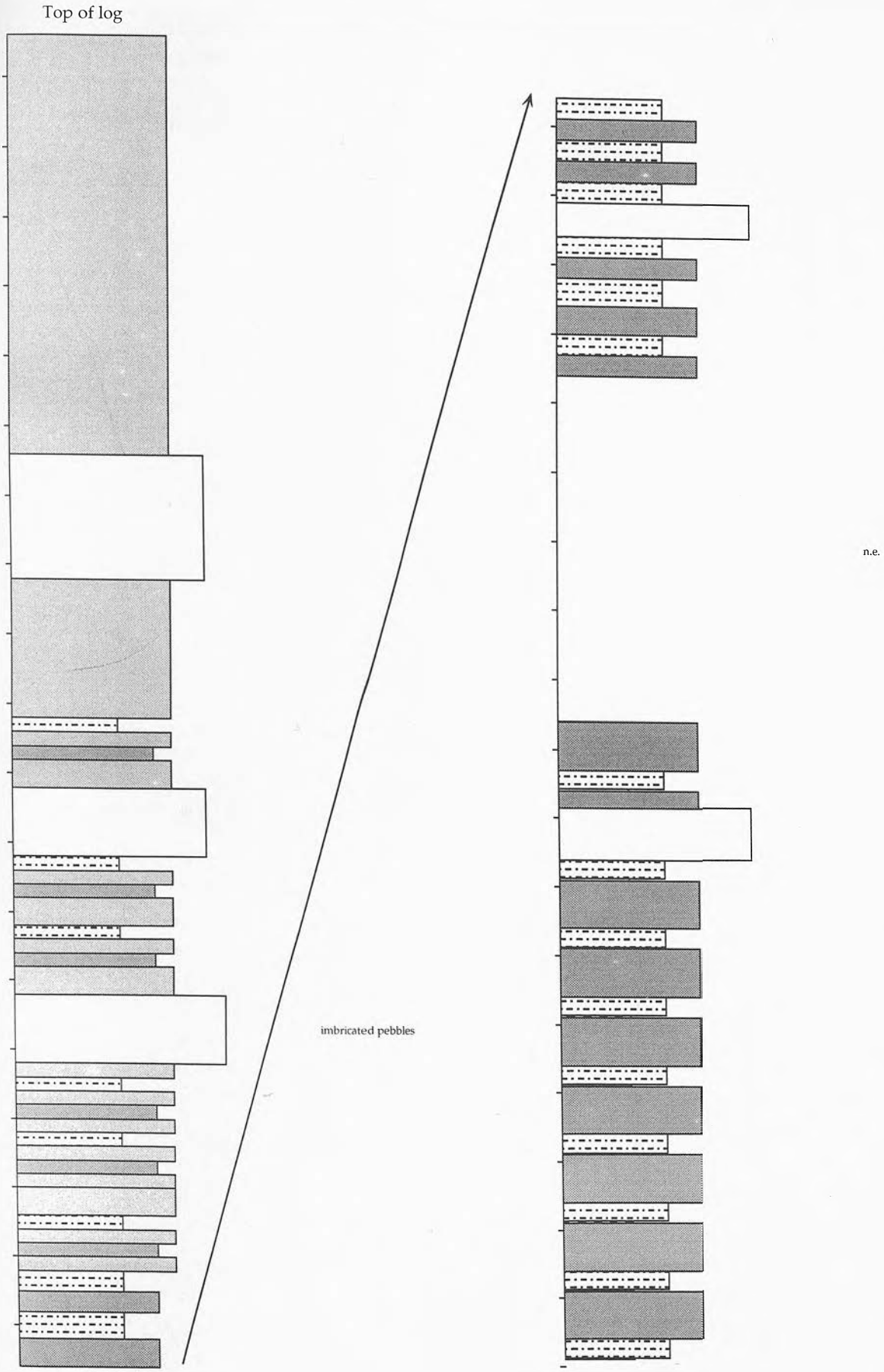
Top of log
imbricated pebbles
n.e.

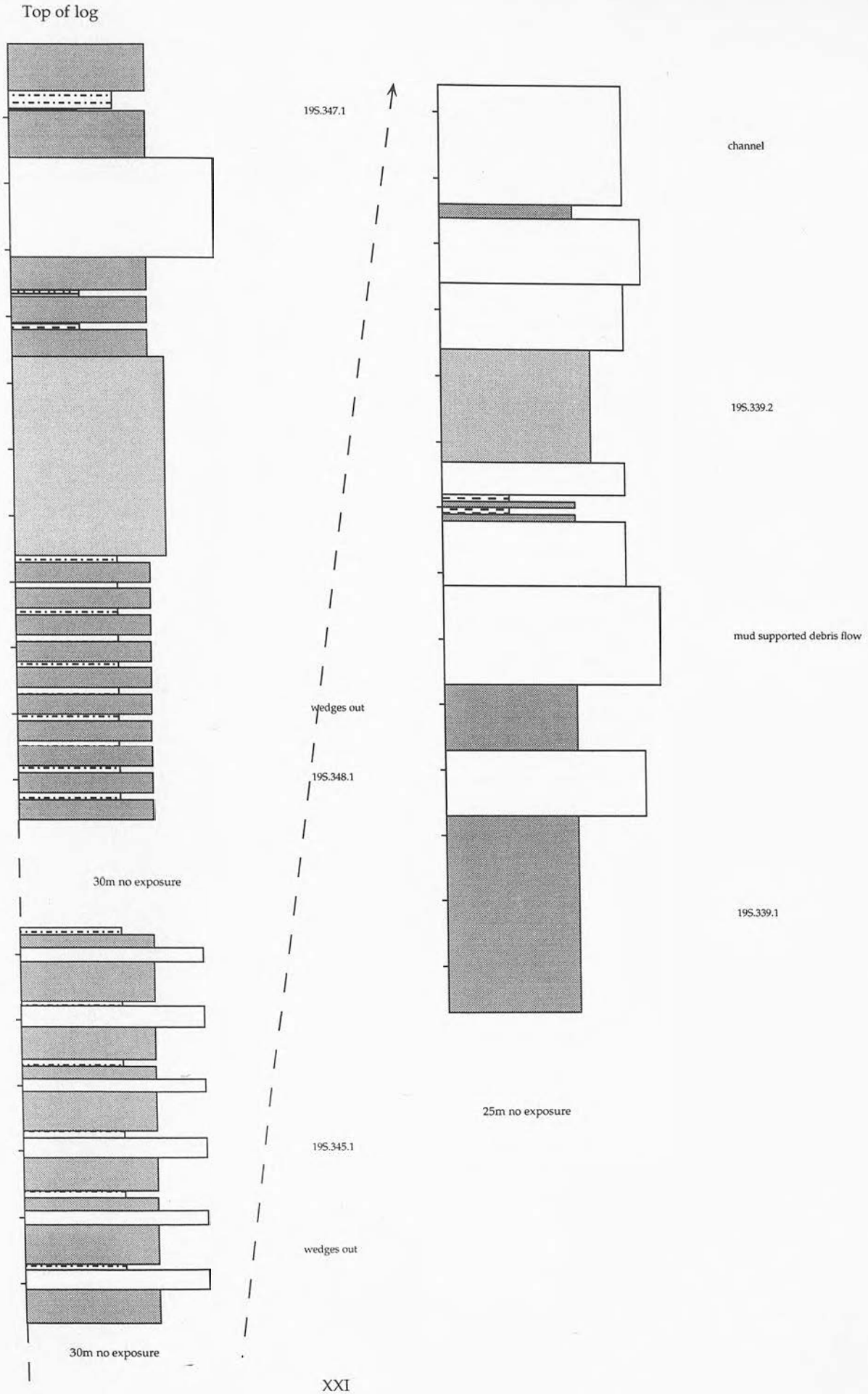
Top of log
19S.347.1
channel
19S.339.2
mud supported debris flow
wedges out
19S.348.1
30m no exposure
19S.339.1
25m no exposure
19S.345.1
wedges out
30m no exposure

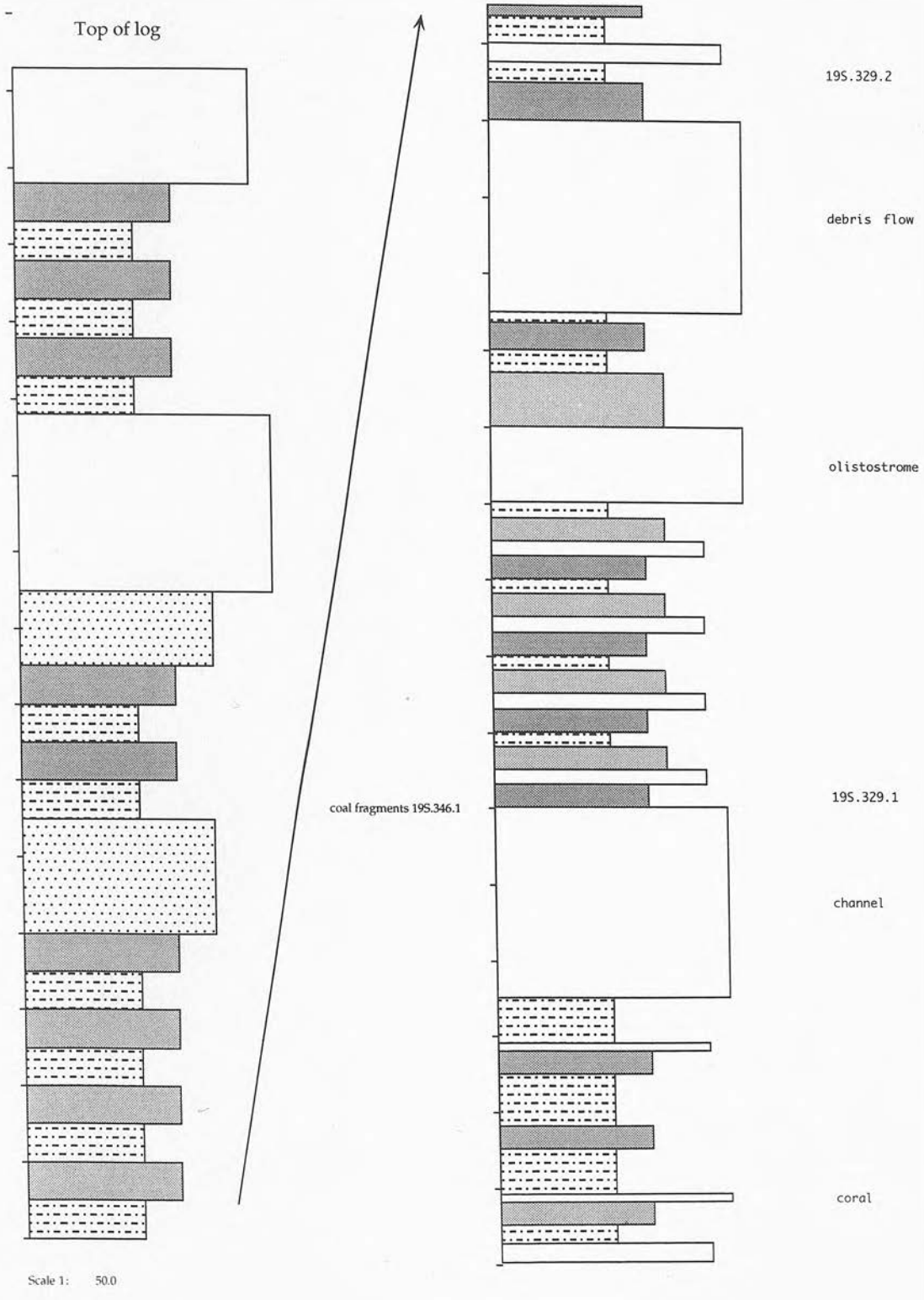
Top of log
coal fragments 19S.346.1
19S.329.2
debris flow
olistostrome
19S.329.1
channel
coral
Scale 1: 50.0

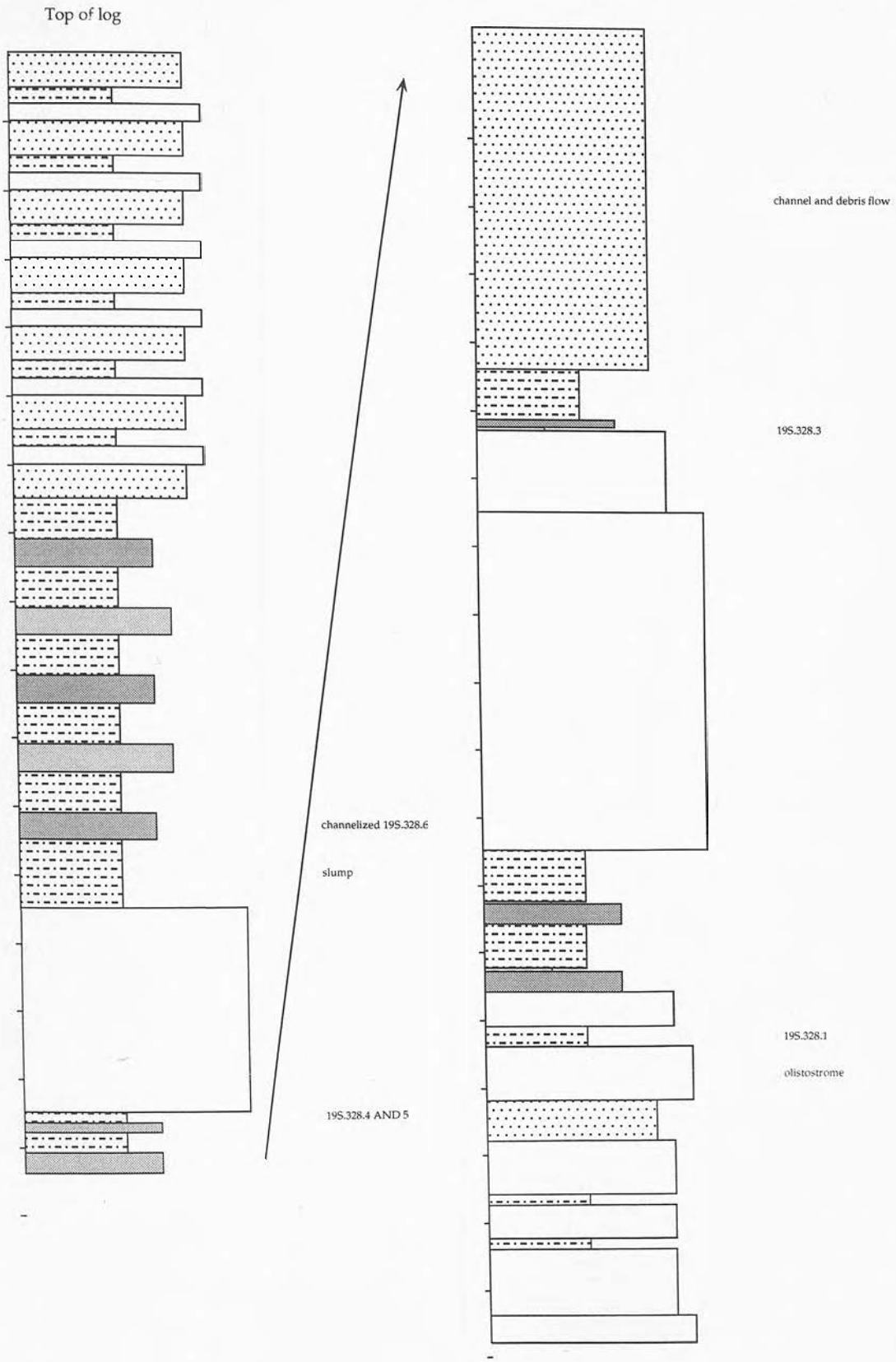
Top of log
channelized 19S.328.6
slump
19S.328.4 AND 5
channel and debris flow
19S.328.3
19S.328.1
olistostrome

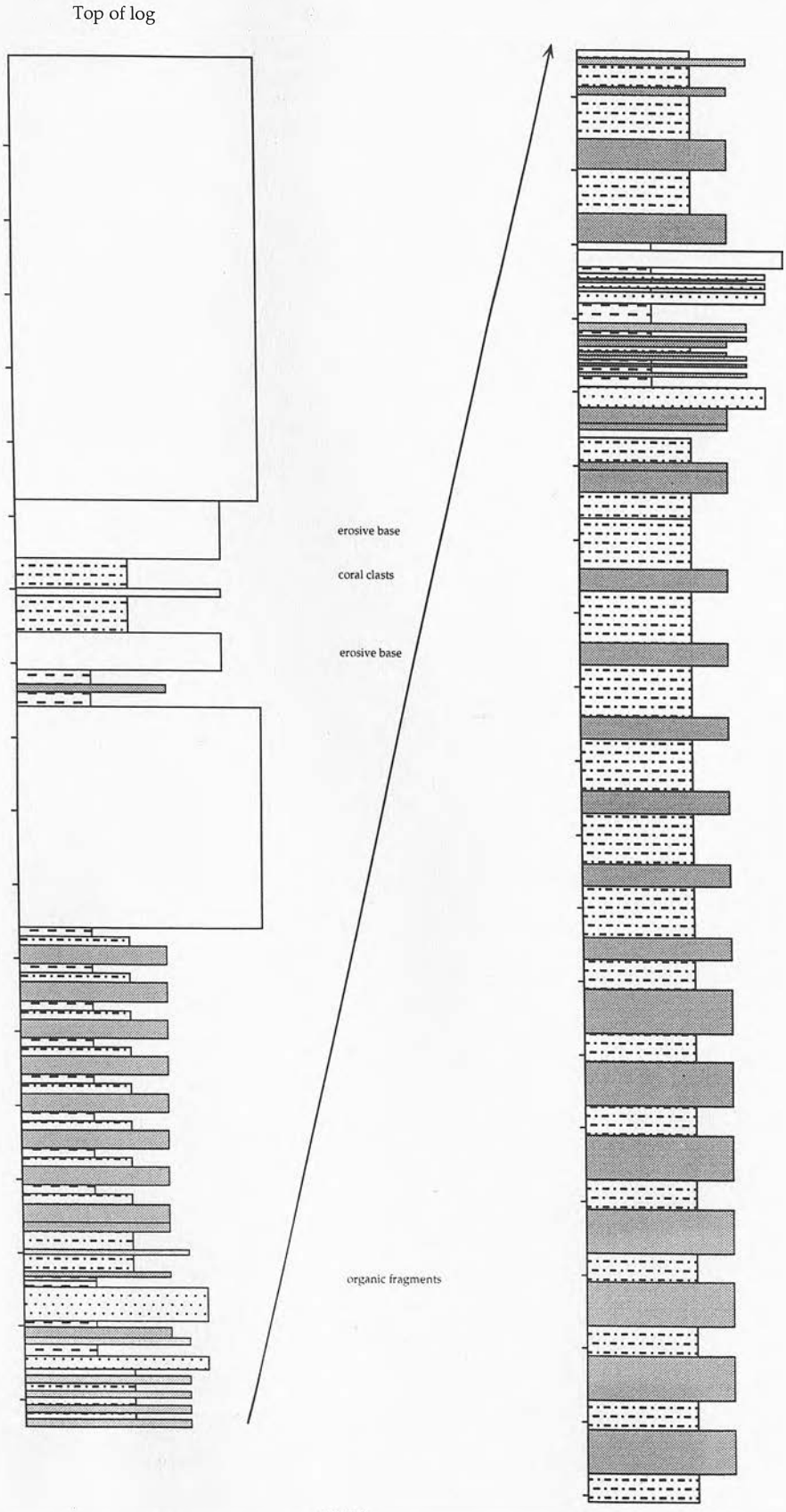
Top of log
erosive base
coral clasts
erosive base
organic fragments
rippled
Fe rich

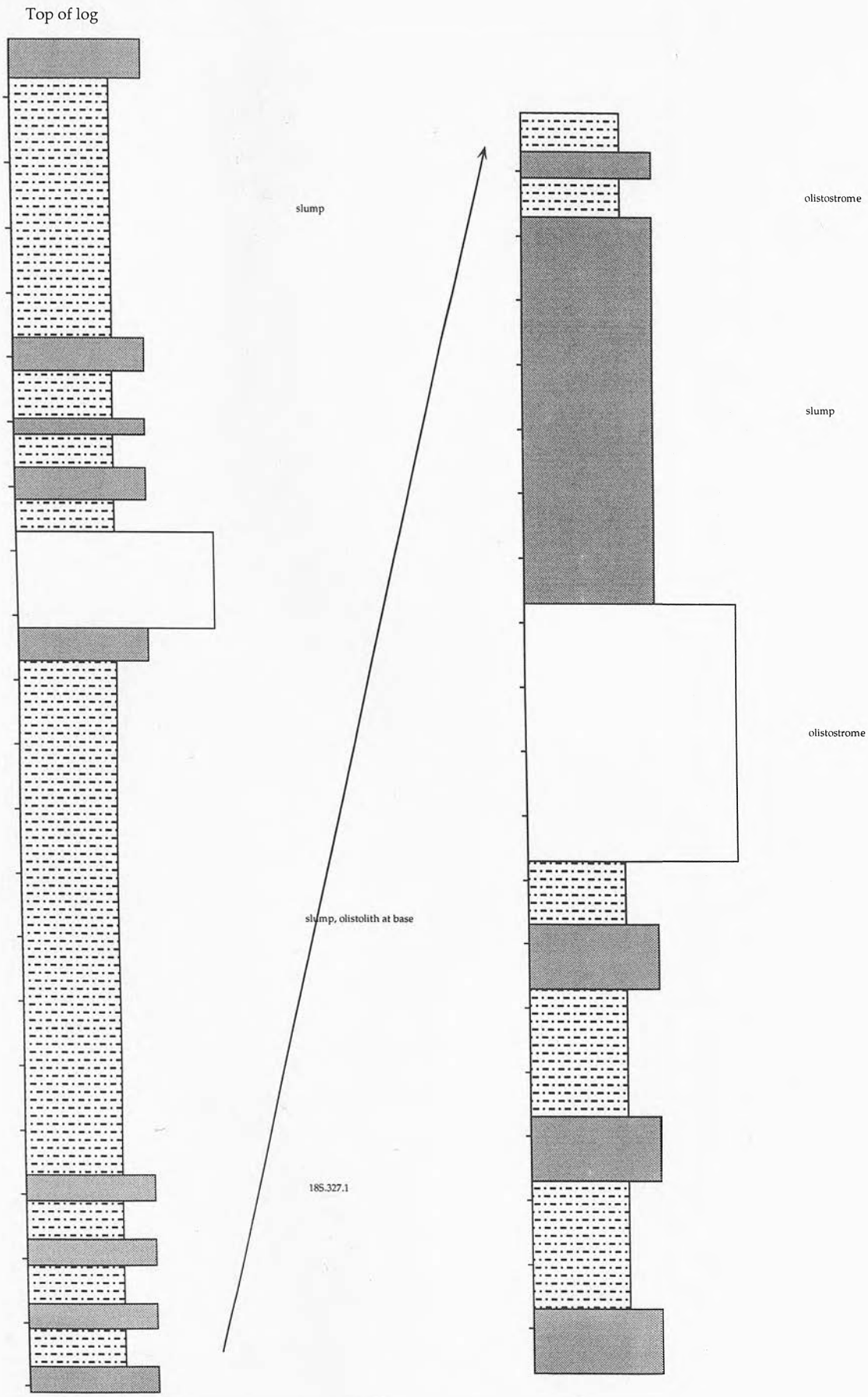
Top of log
slump
olistostrome
slump
olistostrome
slump, olistolith at base
185.327.1

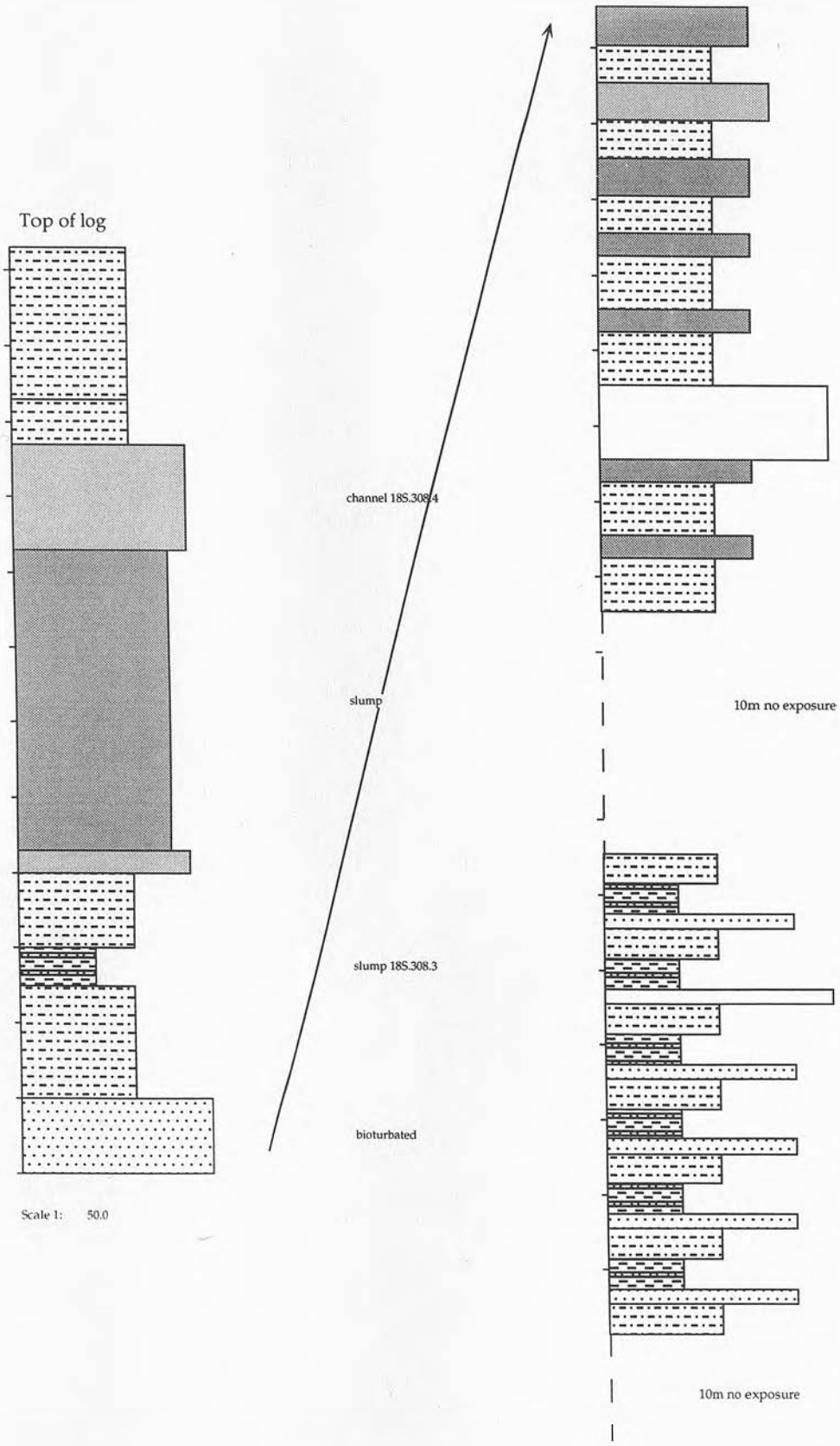
Top of log
channel 18S.308.4
slump
slump 18S.308.3
bioturbated
10m no exposure
10m no exposure
Scale 1: 50.0

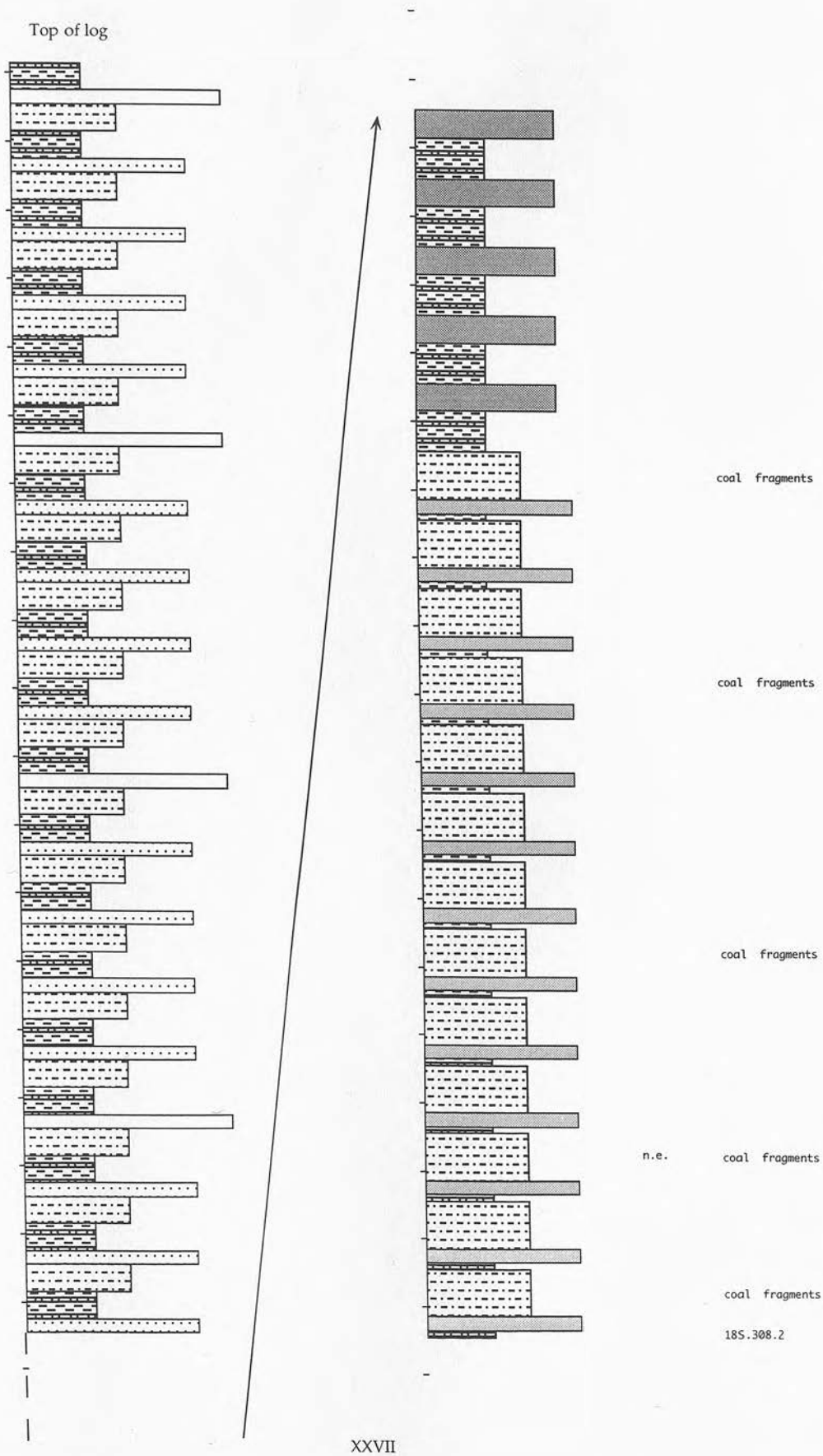
Top of log
coal fragments
coal fragments
coal fragments
n.e.
coal fragments
coal fragments
18S.308.2

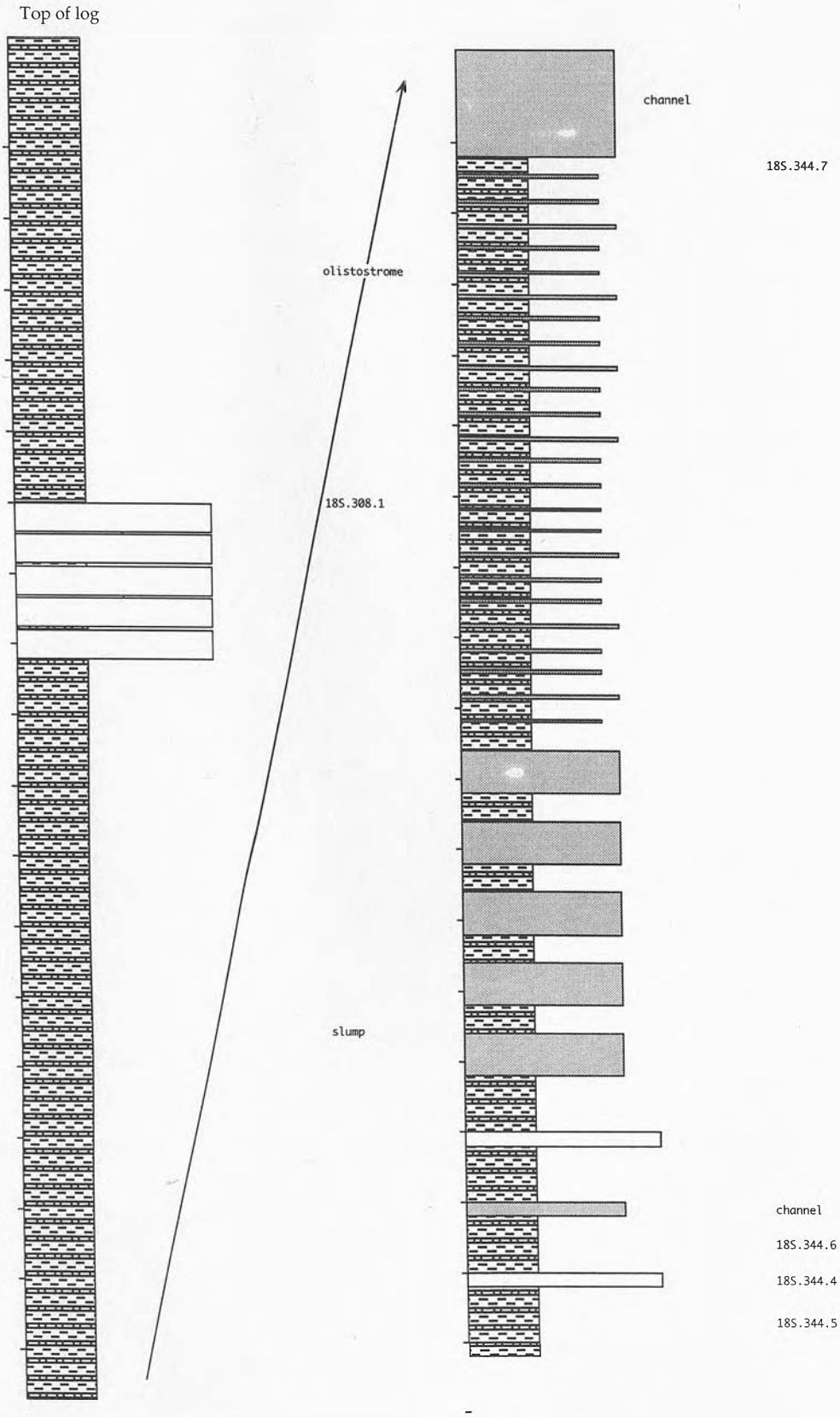
Top of log
channel
18S.344.7
olistostrome
18S.308.1
slump
channel
18S.344.6
18S.344.4
18S.344.5

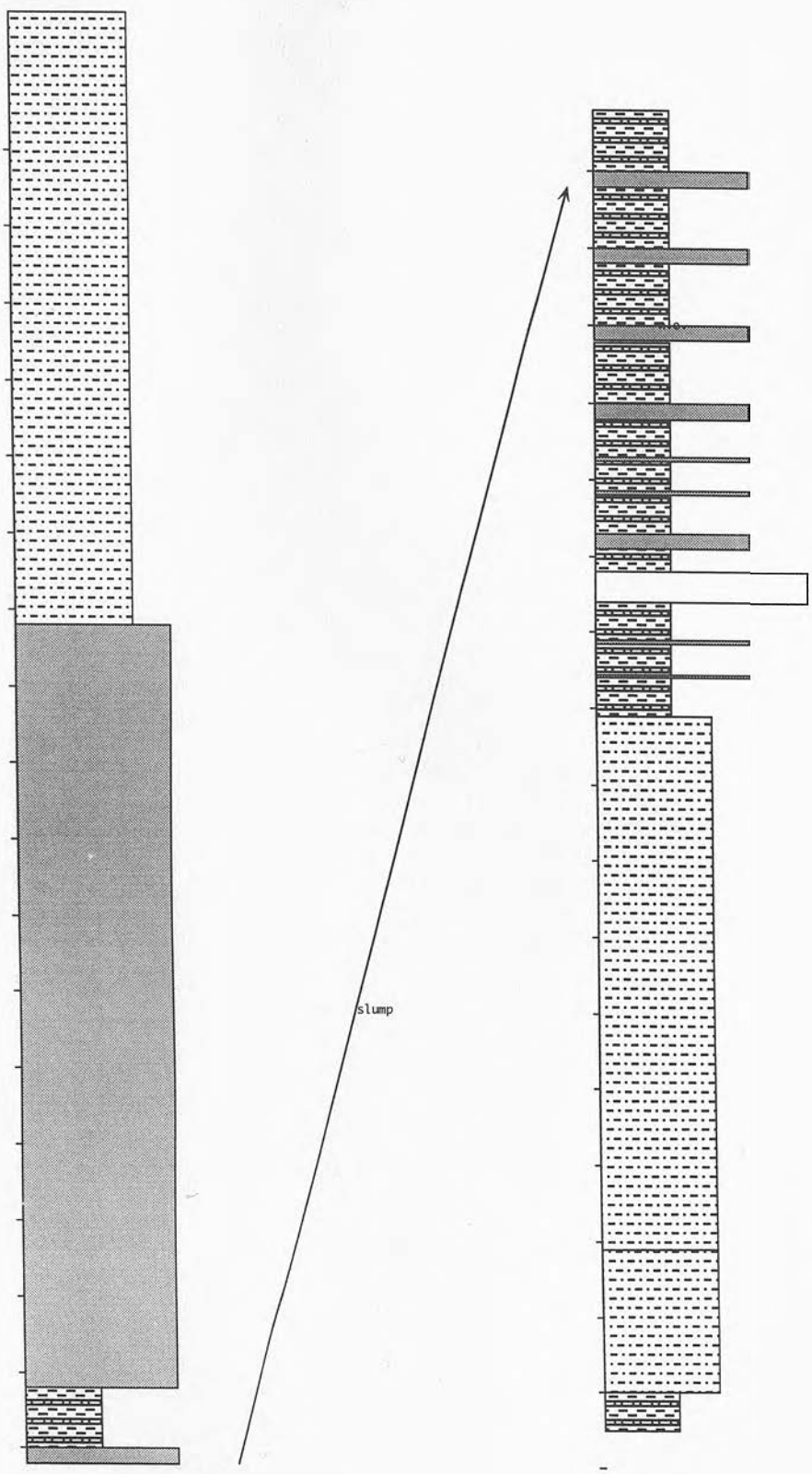
Top of log
slump

Top of log

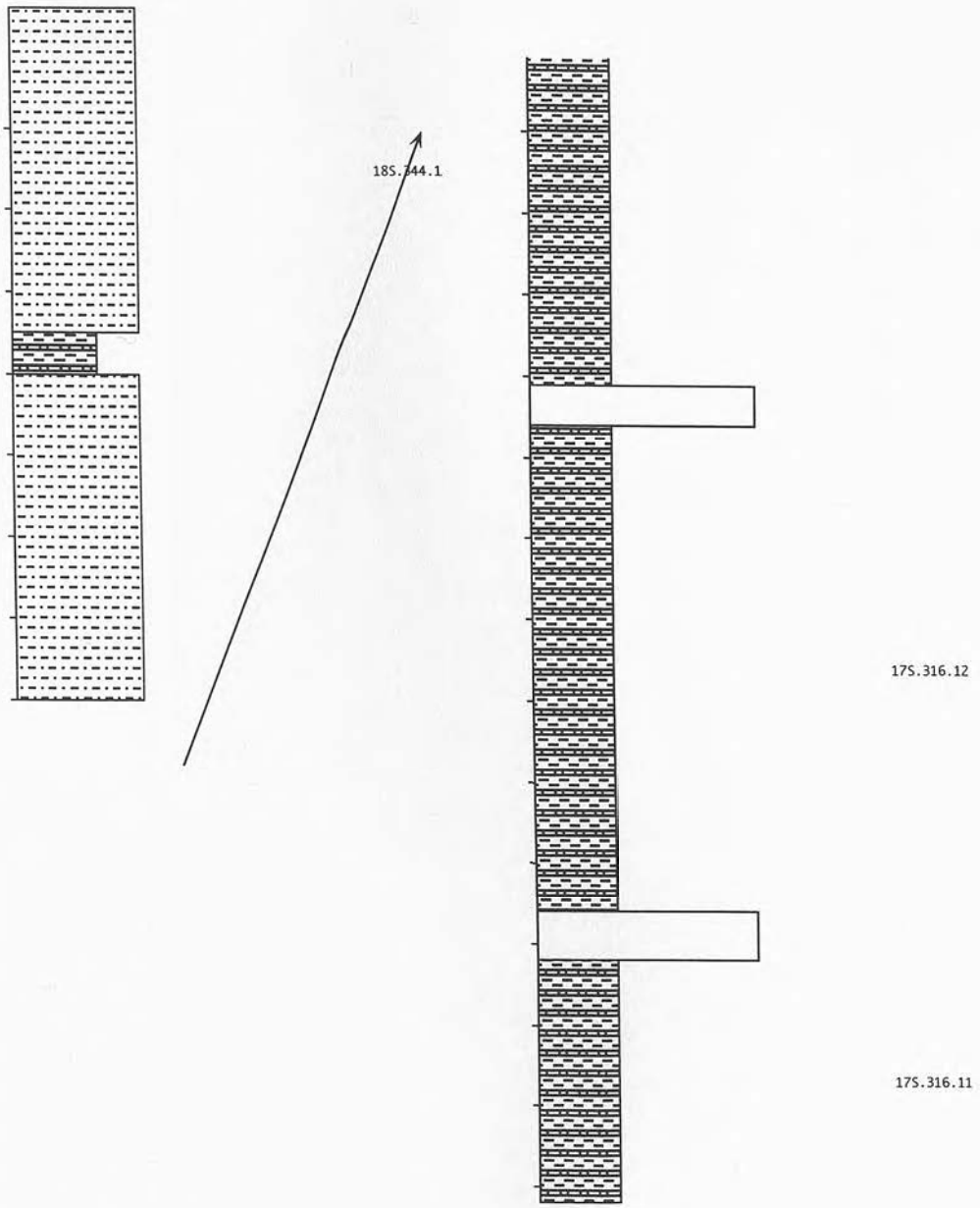

XXX

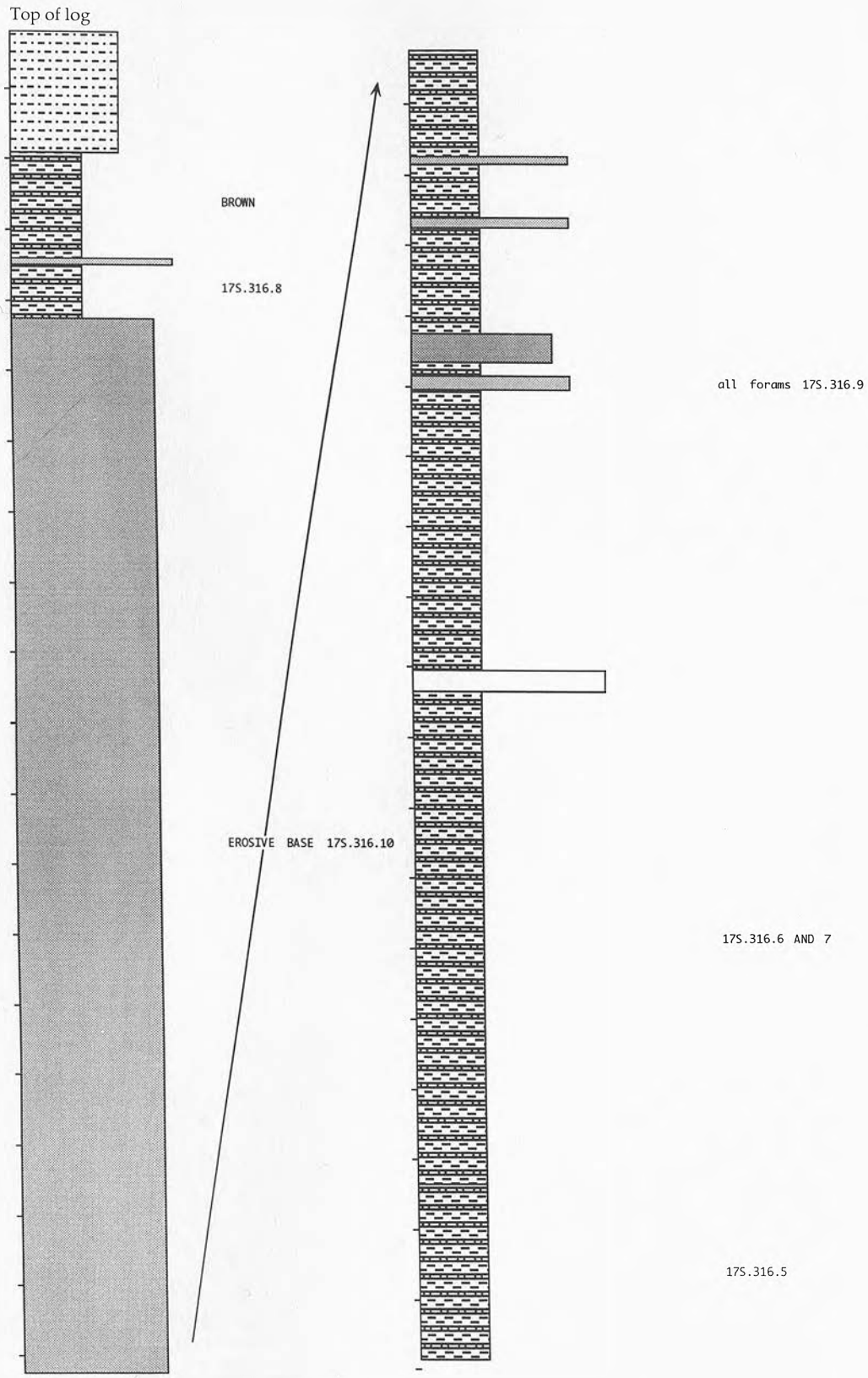
Top of log
BROWN
17S.316.8
all forams 17S.316.9
EROSIVE BASE 17S.316.10
17S.316.6 AND 7
17S.316.5

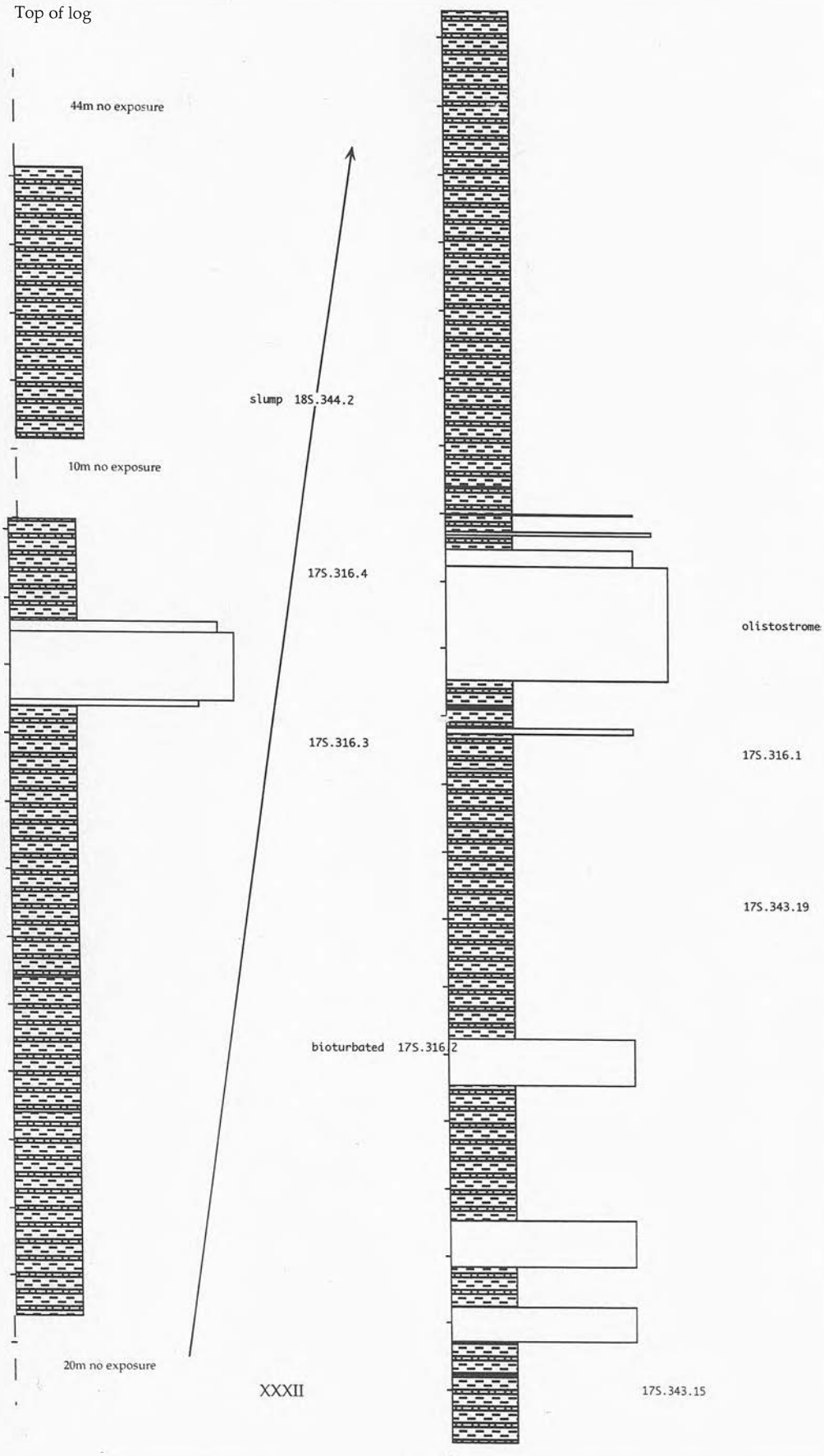
Top of log
44m no exposure
slump 18S.344.2
10m no exposure
17S.316.4
olistostrome
17S.316.3
17S.316.1
17S.343.19
bioturbated 17S.316.2
20m no exposure
XXXII
17S.343.15

Top of log

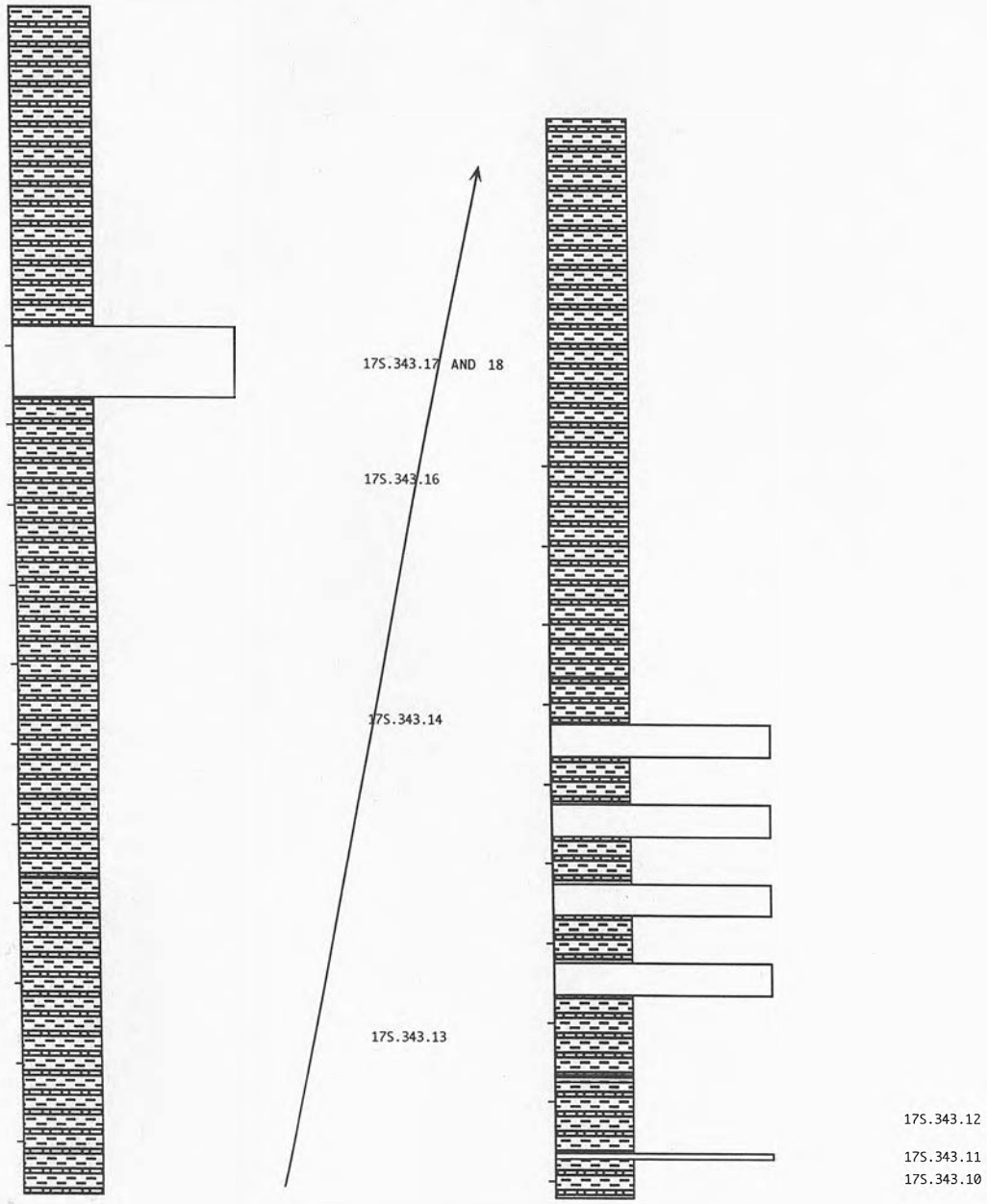
17S.343.17 AND 18
17S.343.16
17S.343.14
17S.343.13
17S.343.12
17S.343.11
17S.343.10

Top of log

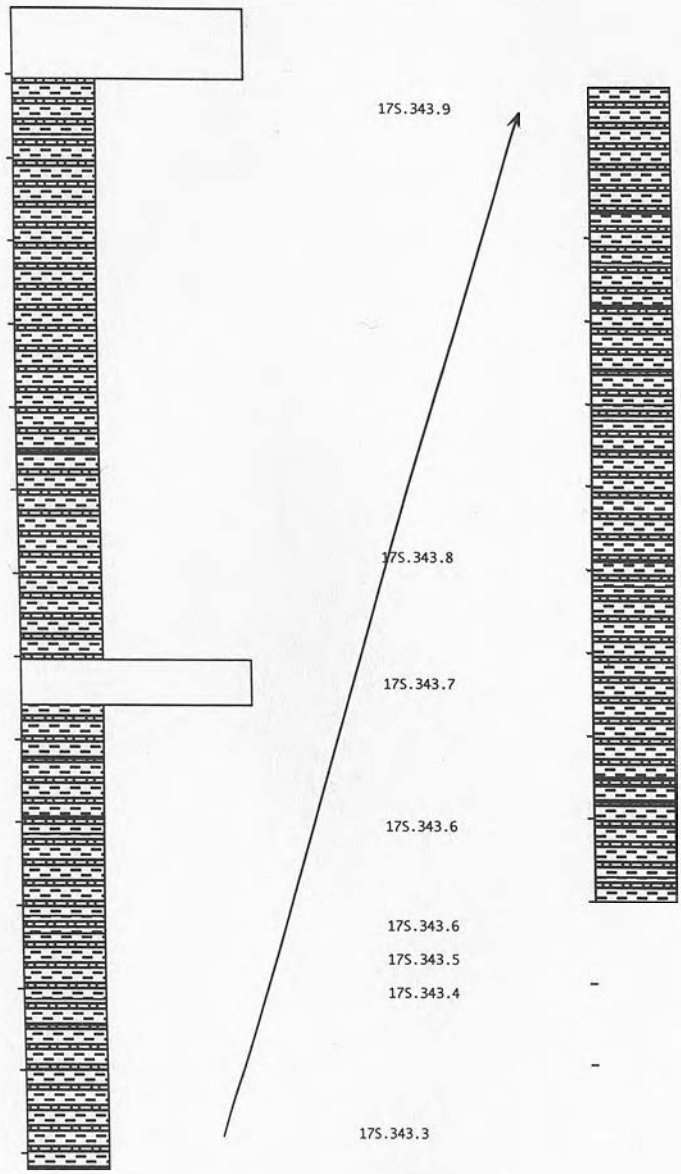
17S.343.9
17S.343.8
17S.343.7
17S.343.6
17S.343.6
17S.343.5
17S.343.4
17S.343.3
17S.343.2
17S.343.1
16S.341.6
16S.341.5
16S.341.4
16S.341.3
16S.341.2

APPENDIX 5.2

Stratigraphic location of samples used for nannoplankton analyses and Sr dataing (Appendix 2)

For location of sections, see figure 3.1. For key, see figures 3.3 and 3.4.

KARGI BARAJ

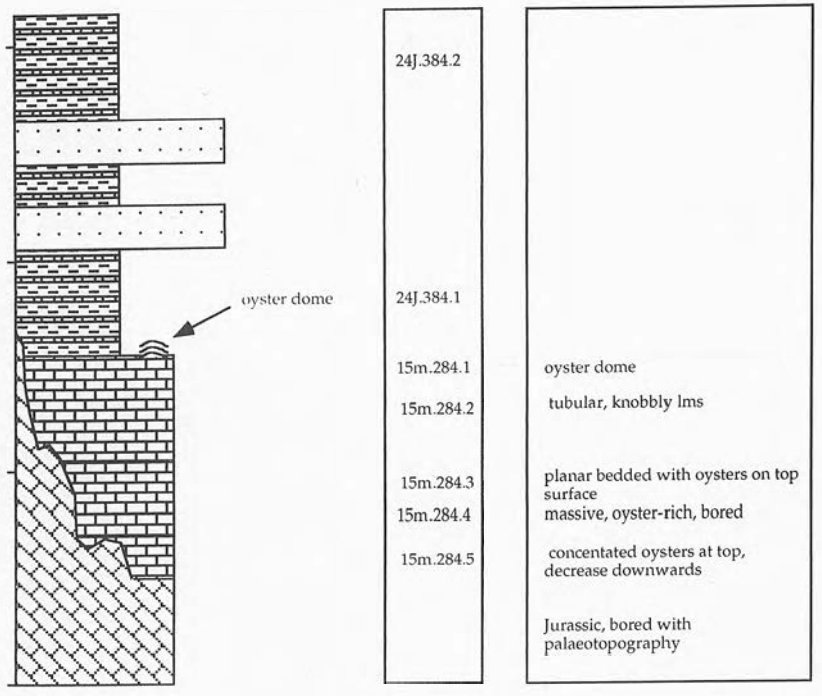

Kargi baraj section
Scale 1: 25.0

ASPENDOS

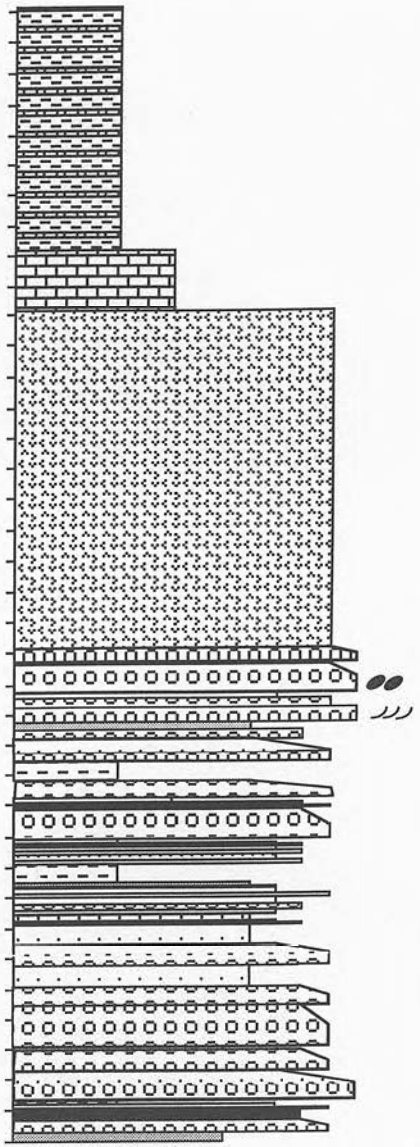

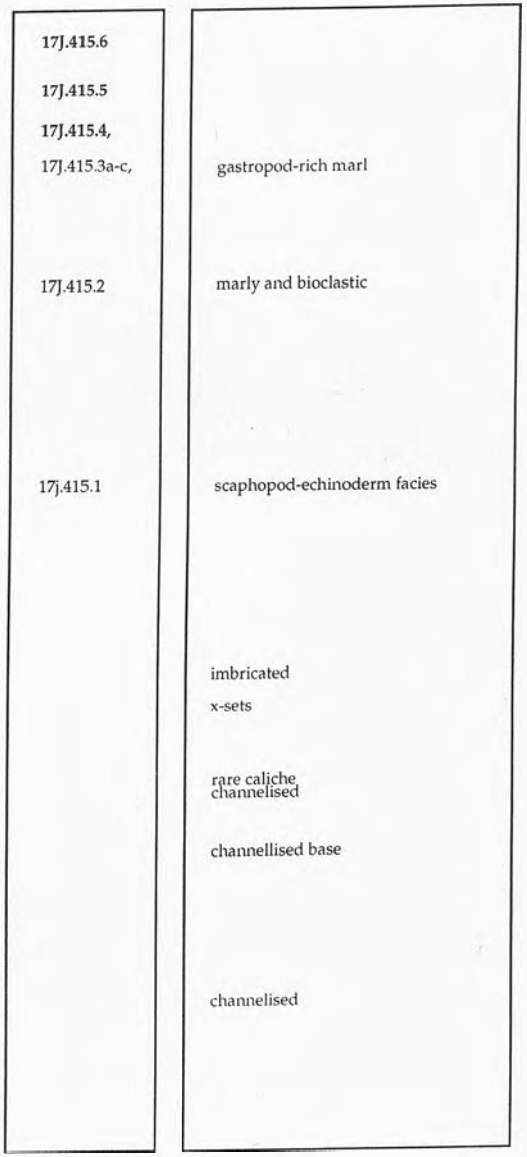

Aspendos section
Scale 1: 175.0

DENIZTEPESI

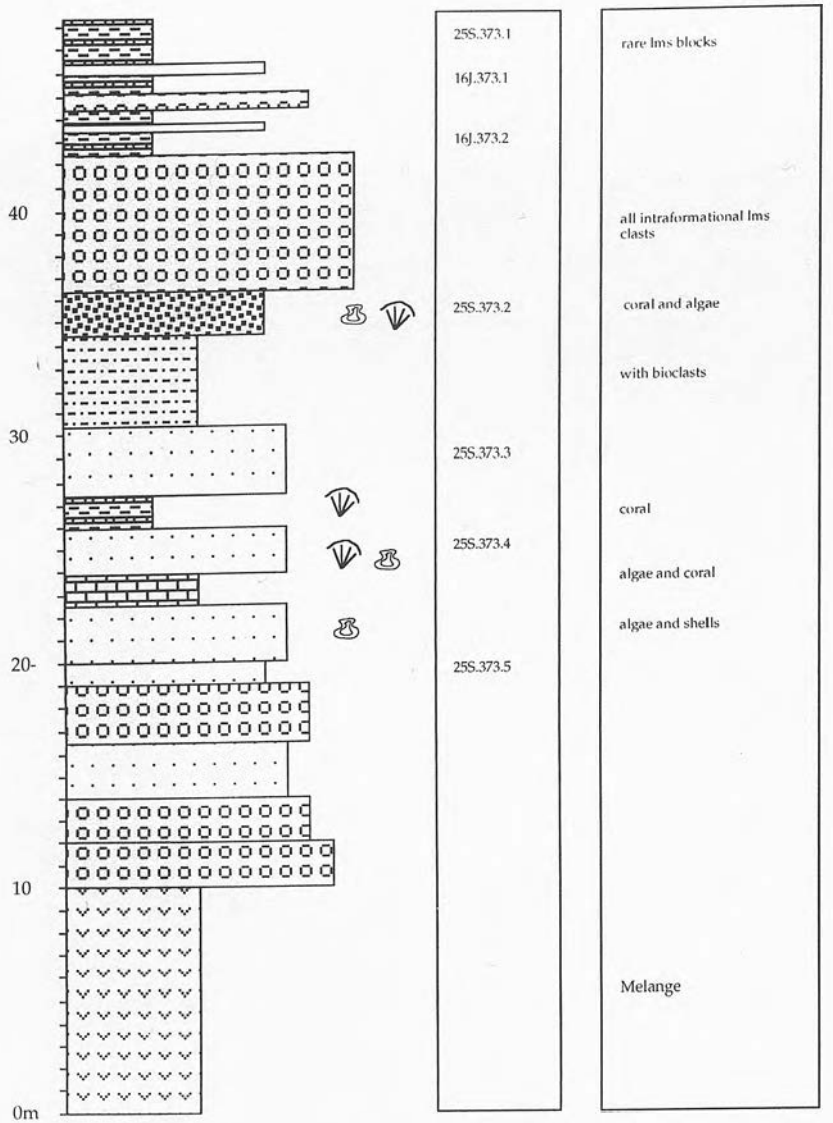

SECTION 373 Deniztepesi
Scale 1: 200.0

BUCAKKÖYÜ

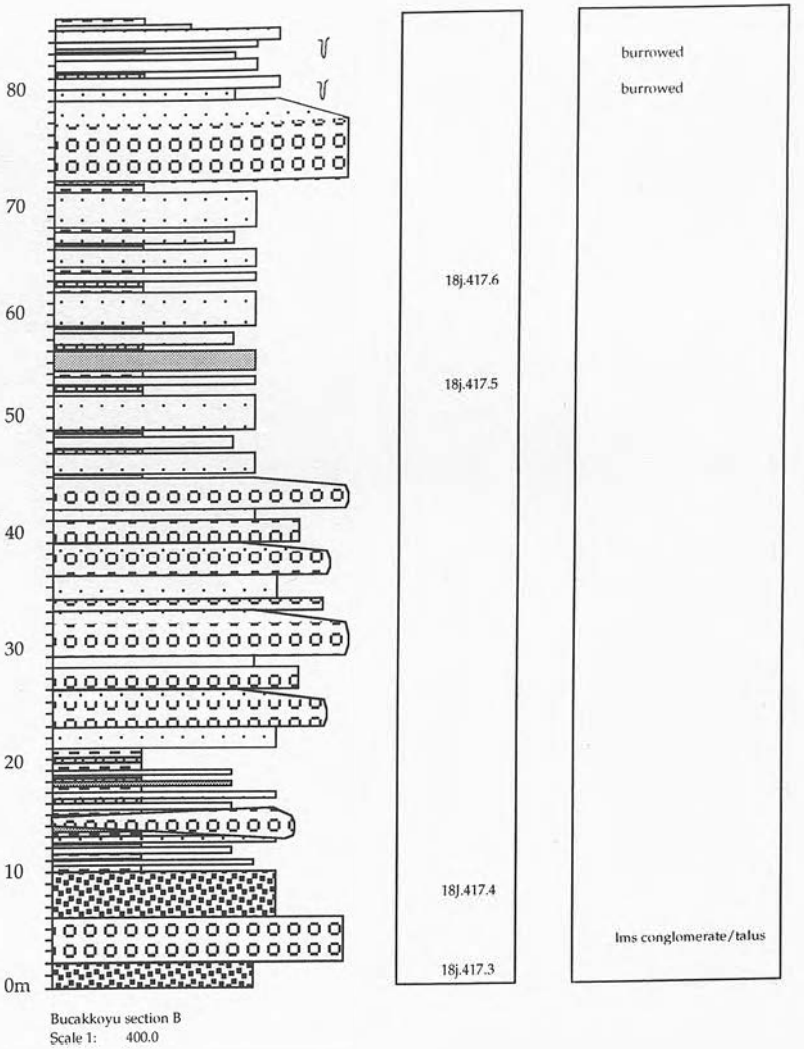

Bucakkoyu section B
Scale 1: 400.0

ALTINKAYA

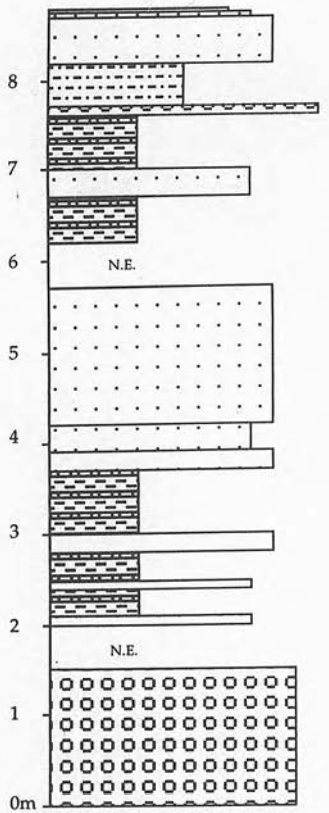

19J.180.5	bivalves and gastropods
19J.180.4	large corals, oysters and algae
19J.180.2	abundant small coral
19J.180.3 19J.180.6	shells and coral fragments in sandy matrix
19J.180.1	fossil-rich, planar bedded
	fossil rich
19J.181.2 19J.181.1	wood, oysters and whole bivalves
	clasts of nummulite-rich lms

SECTION 180 Altinkaya
Scale 1: 50.0

BALLIBUCAK

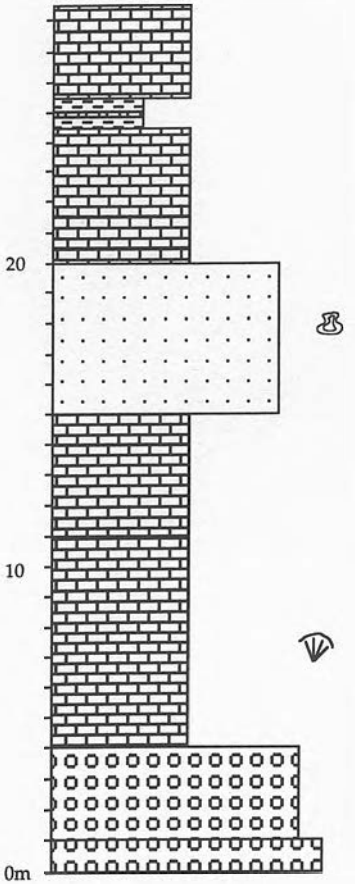

16J.164.4	
16J.164.3	bivalves and gastropods
16J.164.2	
16J.164.1	echinoderms
	oysters, gastropods, bivalves and algae
16J.163.1	bivalves, gastropods and wood
16J.163.2	abundant shells
16J.163.3	
16J.163.4	with shells
16J.163.5	

SECTION 163 and 164 Ballibucak
Scale 1: 150.0

SIPAHILER

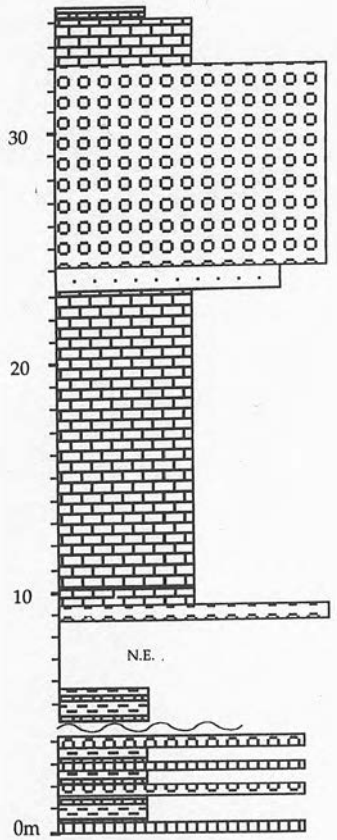

SECTION 236 B Sipahiler
Scale 1: 200.0

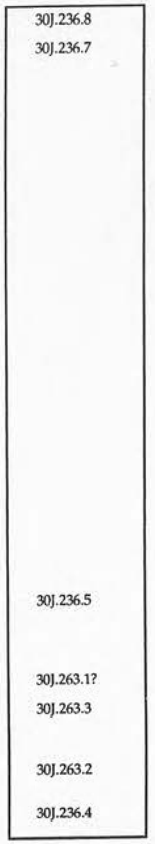

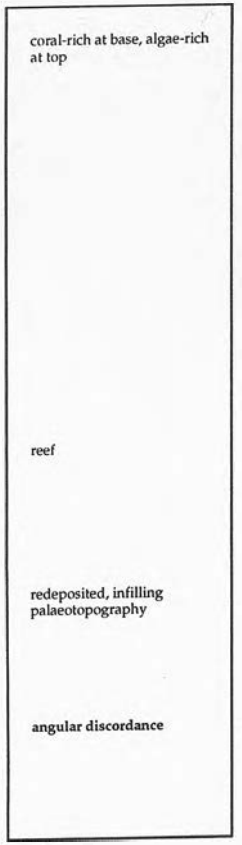

DUMANLI

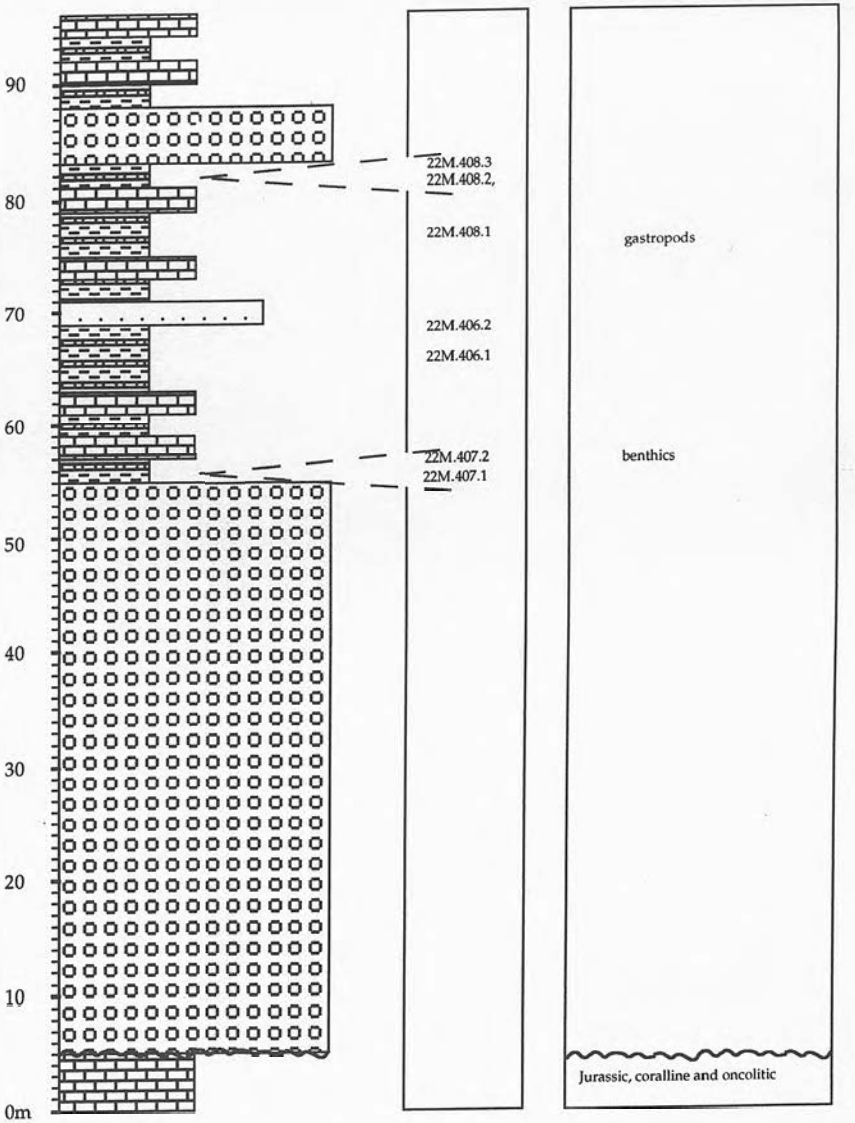

Dumanli section
Scale 1: 400.0

YAYLAALAN

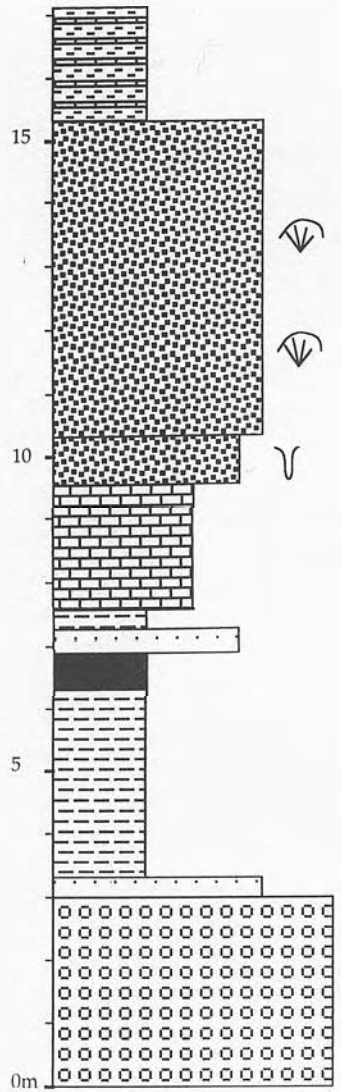

Yaylaalan Section
Scale 1: 75.0

samples	comments
14j.290.7	
14j.290.6	
14j.290.5	
14j.290.4	well bedded, oysters and echinoids, poritds and algae
14j.290.3	
14j.290.2	burrowed layer
14j.290.1	deformed, laminated algal?
29A.290.3	
29A.290.4	green, sticky
29A.290.5	
29A.290.2	
29A.290.6	green, sticky
	yellow

SABURLAR

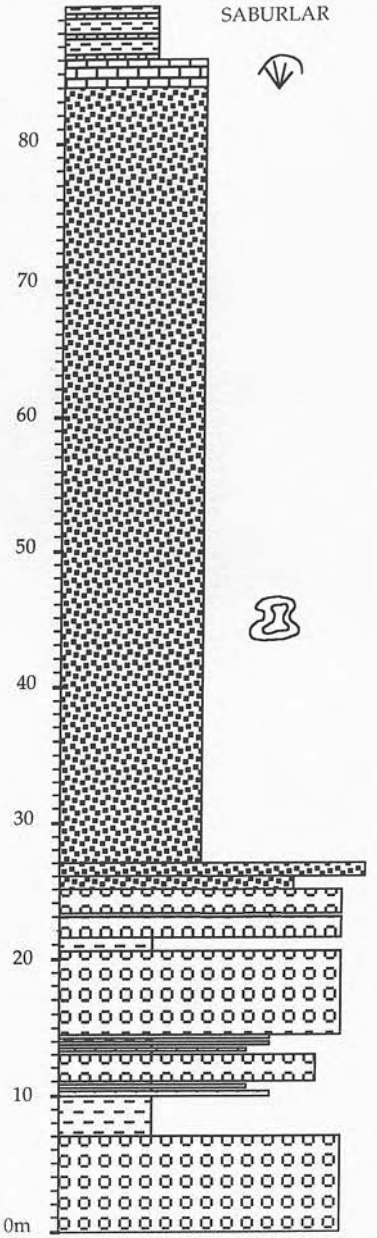

Saburlar section
Scale 1: 350.0

30A.296.3	
11j.295-6.3	domal coral
11j.295-6.2	rhodolithic
11J.295-6.1	operculina and echinoids

ALARAHAN

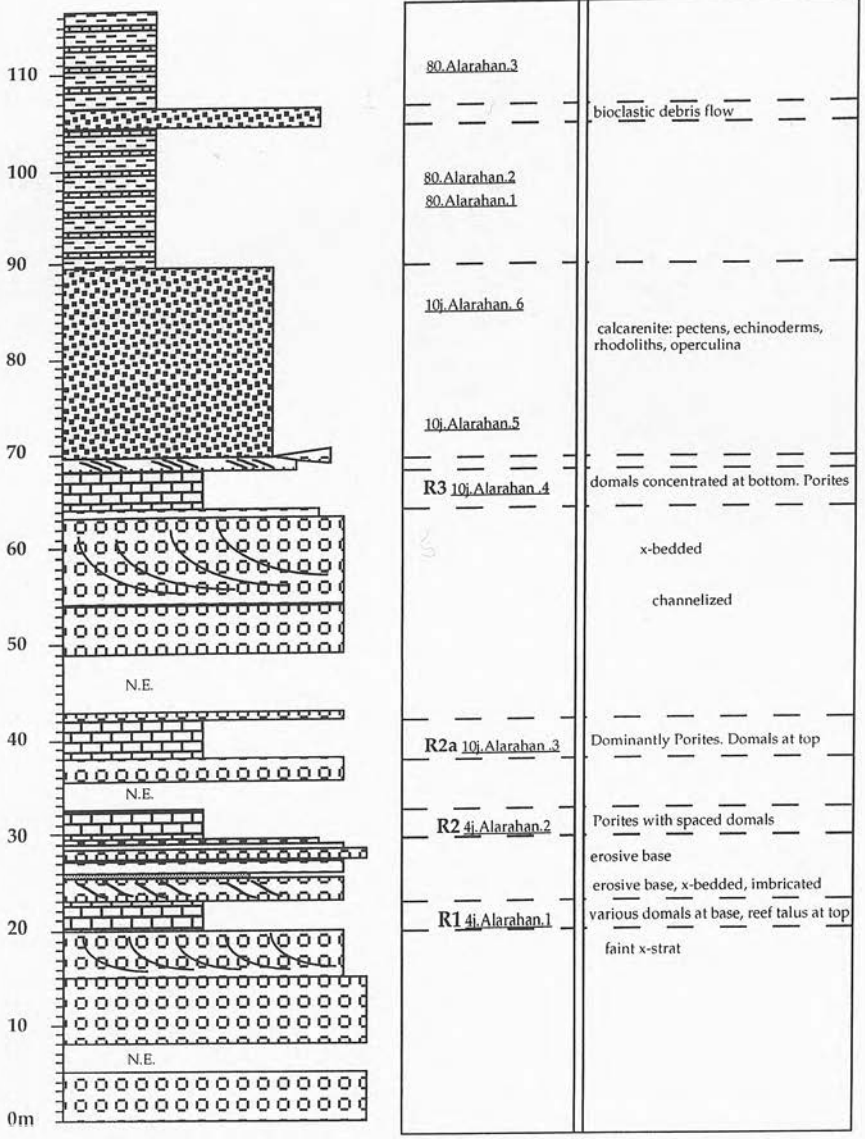

Alarahan SECTION
Scale 1: 500.0

R2 = reef number
10j.Alarahan.2 = sample number

Appendix 6

BACKSTRIPPING

The procedure followed in backstripping is outlined below and illustrated using a fictional well, Well X (Figure A6.1).

Data Preparation

First the well to be backstripped is split up into a number of layers, the tops of which can be dated. Each layer is assigned a bulk lithology and the water depth of deposition for sediments at the top and bottom of the layer is estimated (Figure A6.1). Unconformities are treated as periods of zero deposition, and assigned a nominal thickness of 0.1 metres, unless independent estimates for the amount of erosion associated with the unconformity are available. The age, depth and water depth of deposition of the oldest sediments on basement are also required (Figure A6.1).

These layers are then removed, one by one and youngest first, (back stripped) to reconstruct the subsidence history of the well site being investigated.

Decompaction

The simple calculation described above assumes that each layer has remained the same thickness through time. This is clearly not the case. Sedimentary rocks can be thought of as being composed of two parts: solid grains and the void spaces between these grains which are normally filled with water. Porosity is a measure of the proportion of the total rock volume made up of void spaces and is found to vary with depth of burial. For example, the porosity of newly deposited marine muds is typically around 65% whilst the present day porosity of Jurassic Heather Formation marine shales at depths of 4 km in the North Sea is closer to 10%. This reduction in porosity (volume) since deposition represents a decrease in layer thickness of more than 60%. The empirical relationship observed between porosity and depth of burial (Figure A6.2) has led to the general belief that mechanical compaction, due to the weight of the overlying sediments, is the

This appendix is provided by J. Turner as part of his thesis work (Turner, 1996).

major control on porosity reduction. Correcting for the effects of compaction is a major part of backstripping and geohistory calculations.

This observed relationship between porosity and depth of burial, which varies between lithologies (Figure A6.2), is used to correct for the effects of compaction. As each layer is removed the porosity, and so thickness (Figure A6.3a), of each of the remaining layers is recalculated by moving the layer back up the appropriate porosity/depth function (Figure A6.2). This increases the thickness of all the remaining layers (Figure A6.3a). On a plot of depth to basement against time (Figure A6.3b) decompaction increases the amount of basement subsidence calculated for the early part of the basin's subsidence history. The amount of subsidence calculated for later, nearer to the present day, is reduced by a commensurate amount due to the fact that space for sediments being deposited is being generated, in part, by the compaction of the existing sediment pile rather than any additional basement subsidence.

Compaction also has a major impact on calculated sedimentation rates (Figure A6.3c). Sedimentation rates uncorrected for compaction are simply calculated by dividing the observed sediment layer thickness by the length of time it took for that layer to be deposited. Sedimentation rates corrected for compaction, assuming a simple exponential porosity/depth function, can be calculated using the equation:

$$R = \frac{L(1-\phi)}{T(1-\phi_0)} \qquad \text{(van Hinte 1978)}$$

R - Sedimentation Rate (mMa^{-1})
L - Layer Thickness (m)
T - Time taken for layer to be deposited
$\emptyset$ - Present Day Porosity
$\emptyset_0$ - Depositional Porosity

This correction increases calculated sedimentation rates over the entire period of deposition (Figure A6.3c) although again these effects are greatest for the most deeply buried sediments. Sediments rates calculated in this way are plotted on Figures 4.28 and 4.23.

This appendix is provided by J. Turner as part of his thesis work (Turner, 1996).

Sediment Unloading

By making corrections for the effects of sediment compaction and changing water depths, a picture of the actual subsidence history of well X has been reconstructed (Figure A6.3 a&b). Total subsidence is plotted in Figure 4.33. For tectonic subsidence to be calculated an additional step in the backstripping calculations is necessary.

A number of different forces and processes control basin basement subsidence and the way in which it is recorded in the basin's sedimentary fill. Apart from tectonic subsidence, the main cause of basin basement subsidence is sediment loading. To calculate tectonic subsidence the effect of sediment loading is removed by isostatically unloading the remaining sediment column from the basement (Figure A6.4) as each layer is removed. The resulting plot of water loaded depth to basement against time can then be compared to the predicted tectonic subsidence curves generated by theoretical models. Tectonic subsidence has been calculated for the Ahmetler section and is shown fitted to a theoretical subsidence curve in figure 7.17.

By convention, tectonic subsidence curves are presented as plots of water loaded, rather than completely unloaded, depth to basement. For comparison with theoretical subsidence curves the most important consideration is that both sets of curves are unloaded in the same way. In this study, as has been the practice in most previous studies using well data, Airy (local) isostasy is assumed. Flexural backstripping, which is more realistic mechanically and so desirable, requires additional information concerning variations in the two dimensional structure of the sediment load and the mechanical properties of the lithosphere through time.

Decompaction of Lithologically Mixed layers

Five lithology types have been used for the decompaction calculations in this study. Each layer is only assigned one of these lithology types. Clearly many layers will be mixtures of grain size (sand, silt, shale) and/or composition (clastic, carbonate, volcanic). The most rigorous method for dealing with this would be to treat each stratigraphically dated layer as a composite, made up of

several separate layers of different compositions. This approach would, however, be very time consuming, both in breaking down the preserved sedimentary section and in computer time for the calculations, and would probably not produce any great change in the calculated subsidence history. A simplifying approach taken in this study was to define each layer's lithology on the basis of the percentage of each lithology type present. This was only possible for clastic units. Where units were a mixture of clastics, carbonates or volcanics the dominant lithology type was used.

3.6.2 Non-mechanical Compaction

The vast majority of decompaction models are based upon the premise that mechanical compaction due to overburden pressure is the only form of porosity reduction. This is not the case as cementation and dissolution can have an important impact on porosity, and therefore compaction, throughout a sediment unit's burial history. For example, an early phase of cementation may bind together individual sediment grains, strengthening the sediment and so retarding mechanical compaction. In these circumstances the present day thickness of that unit will be greater than it would have been had there been no cementation, and the decompacted sediment thickness will be overestimated.

The degree to which mechanical compaction may have been retarded, or enhanced, by cementation or dissolution cannot be assessed without detailed petrological information and, as a result, is almost impossible to estimate in most wells. Although some workers have attempted to introduce mathematical terms into their decompaction calculations to make an allowance for these effects (e.g. Thorne & Watts 1989) these corrections are almost impossible to verify. For this reason, and because mechanical compaction is still the dominant factor in porosity reduction, we have elected to leave them out of our calculations rather than introduce additional complexities.

This appendix is provided by J. Turner as part of his thesis work (Turner, 1996).

Non-exponential porosity-depth Functions

In this study the exponential porosity/depth functions of Sclater & Christie (1980) have been used for the decompaction calculations. These corrections have become the standards which many workers have used in previous studies of basins worldwide.

Their applicability has been challenged on a number of grounds, as has the validity of an exponential rather than linear porosity/depth relationship. Compared to a linear relationship an exponential porosity/depth function will overestimate the amount of porosity reduction, and so compaction, in the early part of a well's burial history. A number of studies have also suggested that the effects of variations in factors like sediment composition or fluid flow mean that porosity/depth relationships for specific lithologies in each basin are different. Furthermore, part of the area over which Sclater & Christie (1980) took their data may have been affected by Cenozoic erosion and overpressure development.

A full assessment of the likely effects of the many different published porosity/depth functions and compaction corrections is beyond the scope of this study. However, since all of the wells in this study have been backstripped and decompacted using identical corrections, any trends in subsidence behaviour through time around the basin will not be the result of inadequacies in the compaction correction.

Overpressure

Overpresssure development may lead to localised anomalies in calculated subsidence patterns. Where shales, in particular, are deposited and then buried very rapidly water is trapped and the intraformational pore pressure increases to levels above normal hydrostatic pressure. In these circumstances the pore pressure profile, rather than increasing steadily downhole, proceeds in steps with zones of anomalously high pore pressure corresponding to overpressured shale units. In these units water is unable to escape. This keeps the shale unit's porosity higher than normal, and so retards compaction.

This appendix is provided by J. Turner as part of his thesis work (Turner, 1996).

The present day thickness of an overpressured shale unit will be thicker than it would be under normally pressured conditions because of the presence of the trapped water. If this present day thickness is decompacted using a normal porosity/depth function its depositional thickness will be overestimated. As with most of these possible sources of error, the magnitude of its effect is likely to be relatively minor.

Water Depth Estimates

Changes in water depth as well as sediment accumulation preserve the record of basin basement subsidence. Changes in water depth through time can be assessed from a variety of sources of geological information. They are notoriously difficult to assess accurately and uncertainties and errors in water depth estimates are likely to be the largest single source of error in any subsidence analysis study.

Probably the only diagnostic paleobathymetric markers are coals (Bertram & Milton 1989) which are indicative of terrestrial environments. Other sedimentary facies like red beds (non-marine), coarsening upward pure sands (shoreface) and turbidites (deep marine) are strongly indicative of, but not conclusive proof for, particular depositional environments and more importantly water depths. Even evidence from sedimentary structures, of processes like wave or storm action, can be misleading when attempting to determine a particular depth, since the depth to which the processes reach is strongly dependent upon the strength of the tide and prevailing winds. Fossils, macrofossils and particularly microfossils, are particularly useful environmental indicators. Ratios of planktic to benthic and particular assemblages of benthic foraminifera can, by reference to present day faunal distributions, be used to assess paleowater depths.

Often, however, particularly for ?deep water sediments or where microfossil preservation is poor, water depths are very hard to assess confidently. Good examples fof this come from the Kimmeridge Clay of the Late Jurassic and the Lower Cretaceous in the North Sea. The Kimmeridge Clay Formation is a laminated organic mudstone apart from parallel laminations it contains no sedimentary structures but frequently contains mass flow sands with a

characteristic blocky log character. This is characteristic of fairly deep water, certainly deeper than a shallow shelf, whilst the poorly preserved microfauna support this interpretation. Whether the Kimmeridge Clay represents an outer shelf (175-500 metres), upper bathyal (500-1000 metres) or even lower bathyal/slope (>1000 metres) is far less clear as are the likely variations in water depth it reflects throughout the area.

This appendix is provided by J. Turner as part of his thesis work (Turner, 1996).

Figure A6.1 Backstripping - Data Preparation

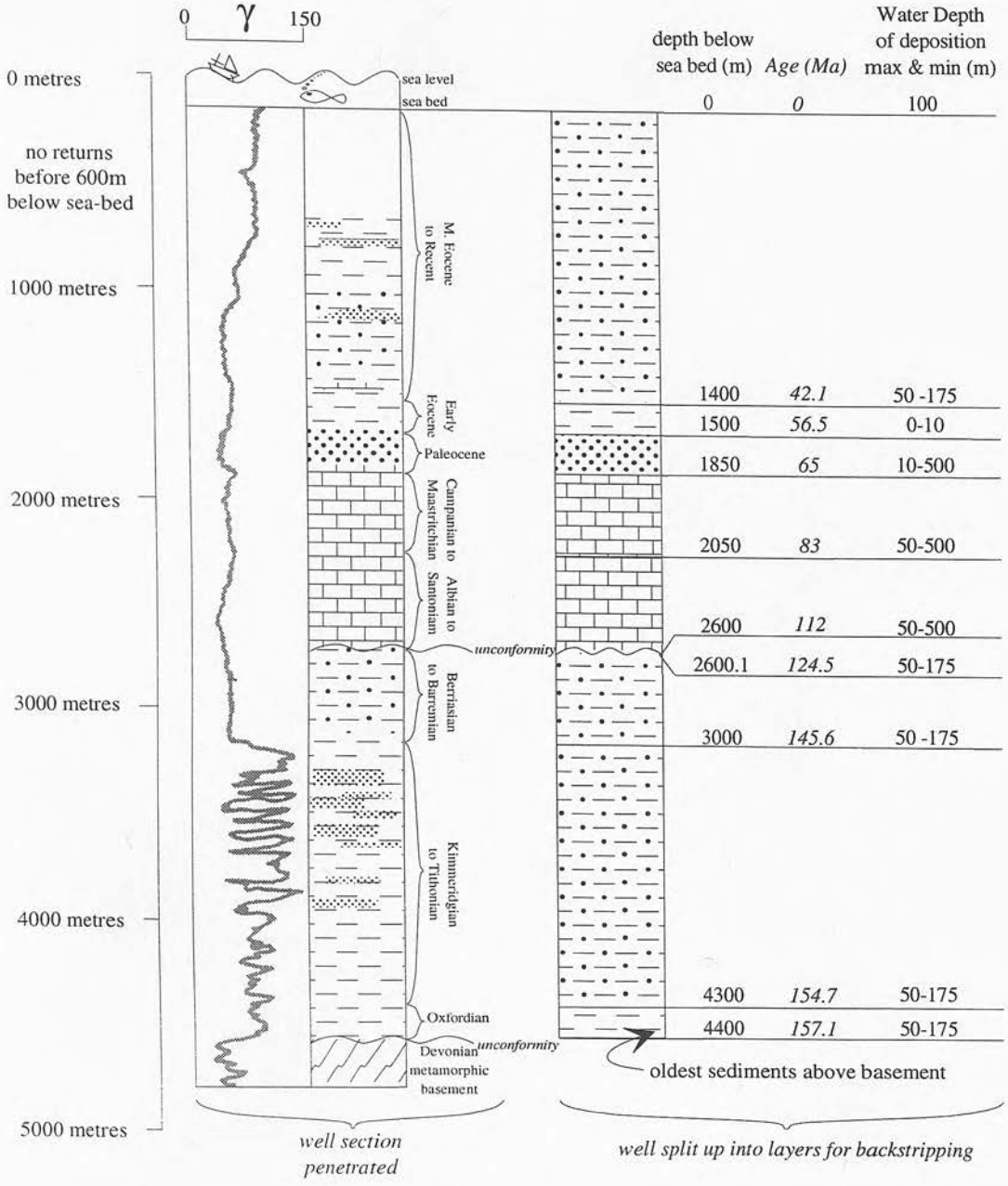

Well X - somewhere in the North Sea

Lithologies

	sand
	silt
	shale
	limestone/chalk

Before a well can be backstripped the preserved stratigraphic succession must be simplified and split up into a number of layers ready for input to the backstripping calculations. The age, depth below sea-bed (or an alternative datum level) and water depth of deposition for the top of each layer are assessed and each layer is assigned a bulk lithology. Although not shown in the diagram above, in this study the water depth of deposition for the base of each layer is also included. The age, depth below sea-bed and water depth of deposition of the oldest sediments sitting on basement are also required.

Jon Turner, University of Edinburgh (1995)

Figure A6.2 Porosity/Depth Relationships

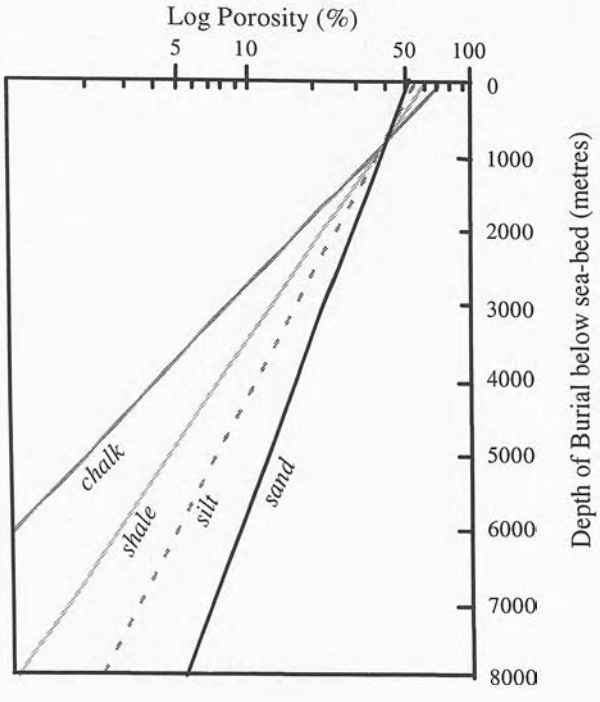

lithology	ϕ_0	c ($*10^5 cm^{-1}$)
shale	0.63	0.51
sand	0.49	0.27
chalk	0.70	0.71
silt	0.56	0.39

$$\phi = \phi_0 e^{-cz}$$

ϕ - porosity
ϕ_0 - porosity at depth = 0
c - porosity constant
z - depth

from Sclater & Christie (1980)

Plots of log porosity against depth for the four most common lithologies in wells from the Central North Sea (Sclater & Christie 1980). These functions are used in the decompaction calculations that generated the curves shown in Figures 3.4 and 3.5 . Mechanical compaction is most intense during the early portion of burial. The effects of compaction vary between lithologies. Although chalk and shale have higher depositional porosities (depth = 0) than sand they rapidly loose this porosity on burial. Sand, on the other hand, retains relatively high porosities until it has been very deeply buried.

Jon Turner, University of Edinburgh (1995)

Figure A6.3 Decompaction

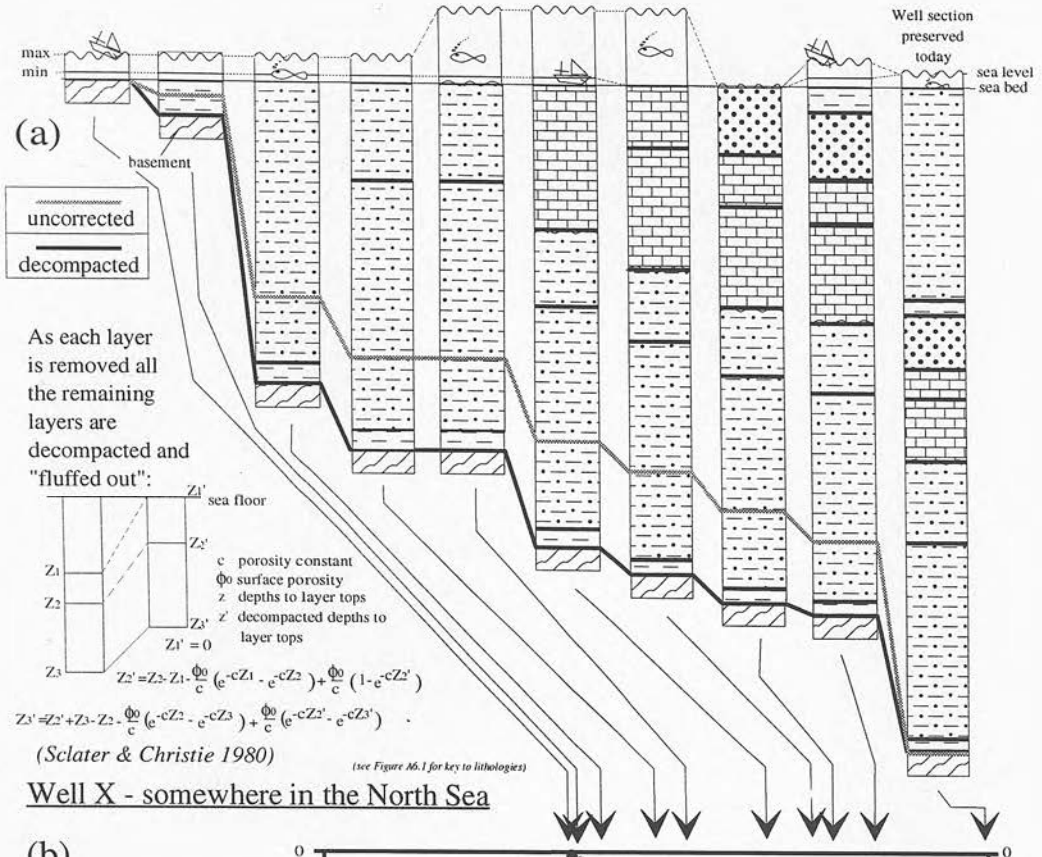

Well X - somewhere in the North Sea

(b)

Plot of depth to basement against time, uncorrected and decompacted, with minimum and maximum likely water depth estimates. The actual position of the basement at any time should be somewhere in the shaded area between these estimates.

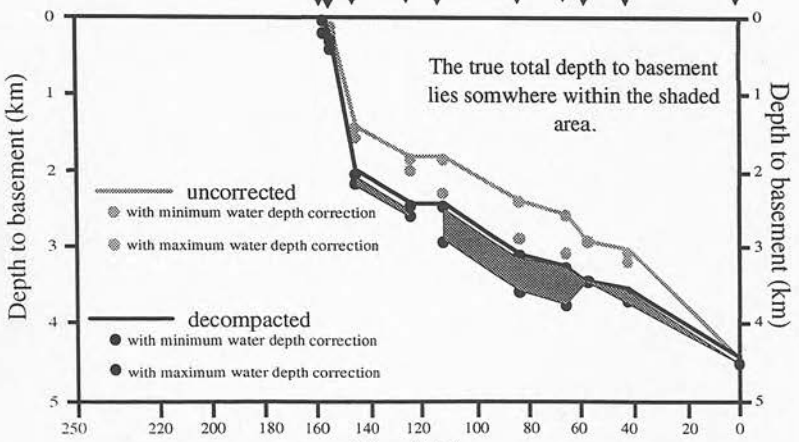

(c)

Plot of sedimentation rate against time, corrected and uncorrected for the effects of compaction.

Correcting for the effects of compaction increases the calculated sedimentation rates.

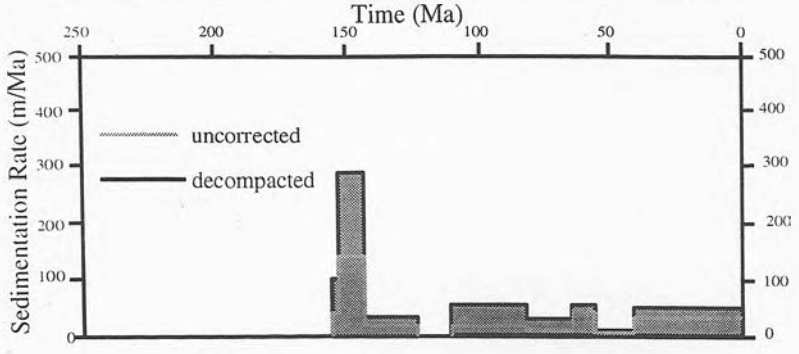

Jon Turner, University of Edinburgh (1995)

Figure A6.4

Sediment Unloading - Tectonic Subsidence

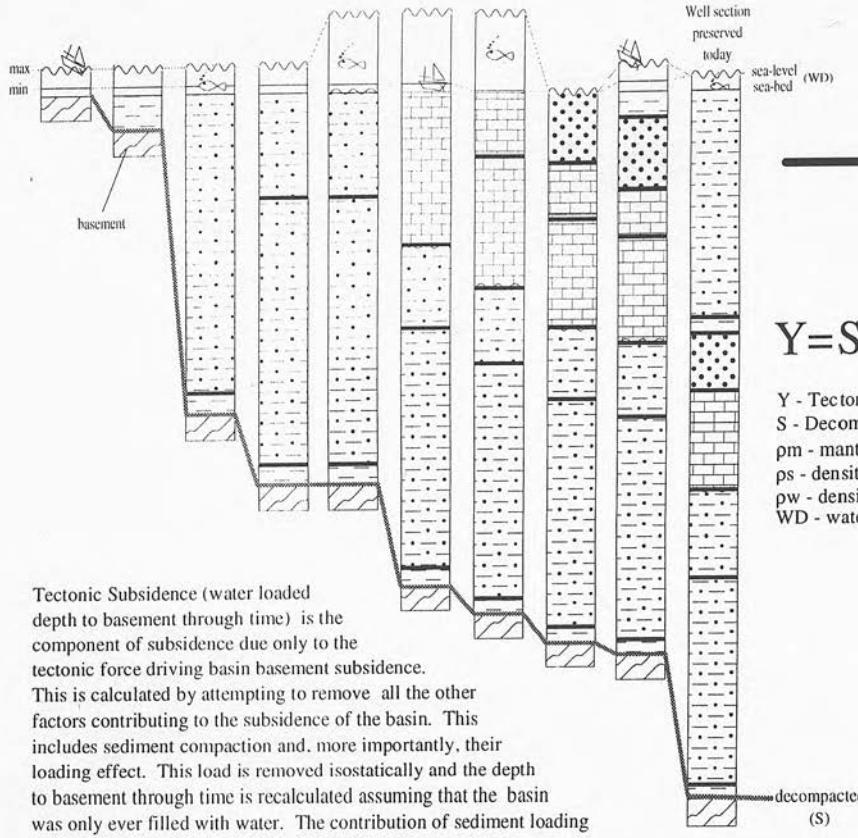

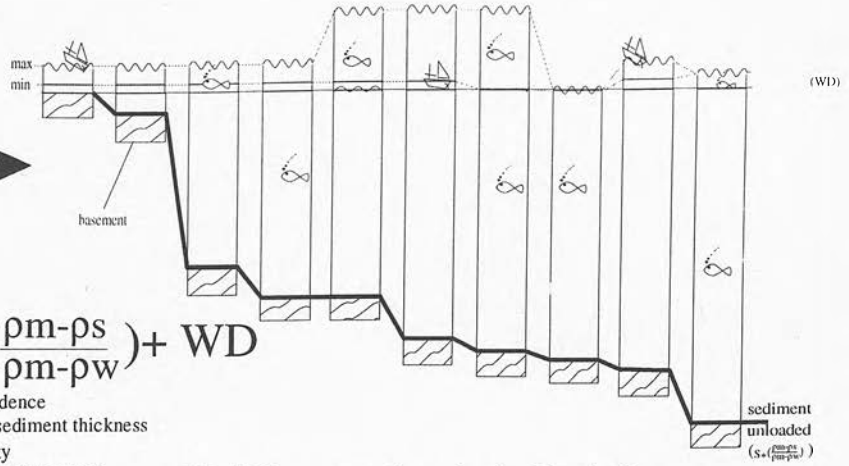

$$Y = S * \left(\frac{\rho m - \rho s}{\rho m - \rho w}\right) + WD$$

Y - Tectonic subsidence
S - Decompacted sediment thickness
ρm - mantle density
ρs - density of sediment column
ρw - density of water
WD - water depth of deposition

Tectonic Subsidence (water loaded depth to basement through time) is the component of subsidence due only to the tectonic force driving basin basement subsidence. This is calculated by attempting to remove all the other factors contributing to the subsidence of the basin. This includes sediment compaction and, more importantly, their loading effect. This load is removed isostatically and the depth to basement through time is recalculated assuming that the basin was only ever filled with water. The contribution of sediment loading to total subsidence increases through time as the basin fills, so that the amount of tectonic subsidence is much less than the total subsidence later in the basins history.

Well X - somewhere in the North Sea